Nonlinear Dynamical Systems Modelling for Environmental Sustainability

A thesis submitted to the University of Sheffield for the degree of Doctor of Philosophy

Angesh Anupam

Department of Automatic Control and Systems Engineering

December 2018

To Mother Earth

Acknowledgements

I would like to convey my sincere thanks to Prof Visakan Kadirkamanathan for offering me this PhD opportunity and supervising this research through his invaluable experience. He has been a natural support system during the entire course of this project.

I am thankful to the Grantham Centre for Sustainable Futures (GCSF) for funding this research and giving me an opportunity to contribute towards a sustainable world in the form of this research work. My co-supervisors, Prof David J Beerling and Prof Steven Banwart supported me through their domain knowledge and resources relevant to this project. I am thankful to them. Dr Manoj Menon provided his guidance during the entire project despite not being formally attached to this work. I am deeply thankful to him. Dr Sean Anderson gave some useful feedbacks and ideas on a few occasions and they turned out to be the turning points in this project. I thank him a lot.

In addition to the above mentioned supervisory team, postdoctoral research staffs − David W, Lyla, Euripides, Yang, Andrew, and Parham have supported me in form of some useful discussions. I thank Prof Colin Osborne, associate director of the GCSF for helping me with his feedbacks during the internal seminar sessions. I would also like to thank the administrative support staffs Deborah, Eva, Renata, and Matthew for helping me with scholarship and administration related queries.

Friends and colleagues in the Sir Henry Stephenson Building have witnessed the full course of this project − my anxieties, my frustrations, and my happiness. Many thanks to them for providing me a socio-work-ecosystem, where I could accomplish my project. I am thankful to Grantham friends, Nick, James T, James L, Emanga, Fiona, Hannah, Cecilie, and Monica for the cheerful social sessions. Apart from these sustainability themed networking, I am heartily thankful to Gautam and Nitanshu for providing me a 'home' like ambience and discussing the multiple germane issues over countless social events!

Lastly, it's time to thank the people who have supported me in all the phases of my life. I profoundly thank my parents, Mrs Vimla Verma and Mr S K Verma for supporting me throughout my life. This project officially started in 2014 but the foundation of this milestone was in process since a long time ago. I sincerely thank my siblings − Astha Anupam , Ankesh Anupam and my sister-in-law, Smita Anupam for supporting me during the tough phases of my life.

Abstract

Increasing global human population coupled with the climate change pose serious threats on the basic needs of society. The coming decades will witness the challenges associated with the food security, land availability, clean water availability, and energy security. These issues directly or indirectly affect the various components of the Earth's Critical Zone (ECZ). Our natural resources are finite and hence a policy framework is urgently required to deal with the growing demand in food, clean energy, and water in sustainable ways. This work characterises some key components of the ECZ such as wetlands, through modelling and computational simulation approaches. A data-driven methodology known as the system identification is used to devise a nonlinear dynamic model of the tropical wetlands. The dataset used in the study corresponds to a Global Inundation Extent from Multi-Satellites. The model gives some useful insights about the dynamics of tropical wetlands and the possible effects of climate change on wetlands. The prediction power of this model is shown to be superior than the competing analytical models representing the inundation dynamics. This work also contributes towards the theoretical advancements in the nonlinear system identification method by proposing a new algorithm capable of performing the model structure selection in the NARMAX model class under the Approximate Bayesian Computation (ABC) framework. In addition to the data-driven approach, this thesis also switches to analytical modelling framework for investigating the sustainable ways of food production and climate change mitigation through a Negative Emission Technology (NET) known as enhanced weathering. The recent reports of Intergovernmental Panel on Climate Change have highlighted the need of an NET to meet the ambitious targets of lowering the global temperature. A process-based model representing the enhanced weathering of a mineral is developed and integrated with standard soil, vegetation process models. The integrated model is termed as the Integrated Enhanced Weathering Critical Zone Model, which is used to analyse the potentials of enhanced weathering in the UK conditions. The simulation results indicate that with the implementation of enhanced weathering in the UK farmlands, we can reduce the atmospheric carbon through sequestration as well as increase the crop yield substantially. In another words, food security and climate change mitigation can be addressed simultaneously. In a nutshell, the simulation results and analyses of this thesis can be used to design further experiments for investigating the ECZ processes like inundation dynamics and enhanced weathering. The results can also act as guidelines for framing the relevant policies towards environmental and food sustainability.

Contents

List of Figures

List of Tables

Chapter 1

Introduction

1.1 Background and motivation

The global human population is expected to cross 9 billion by 2050 [1]. This projected figure depicts an increase of about 1.5 billion people in the next thirty years, which will eventually increase the demand for food [2], clean water [3], and energy [4] dramatically in the coming decades. The exploitation of the Earth's natural resources in various forms, such as, intense farming and unsustainable land use [5] appears inevitable for catering these basic needs of people. The climate change [6] and its effects on the ecosystem services further complicates the matter. Clearly, there is a need to adopt holistic approaches in dealing with these imminent societal crisis. This thesis has touched the 'holistic' criteria while addressing some crucial aspects of environmental and food sustainability issues. In a nutshell, this work comprises of modelling and analysing some key nonlinear dynamical processes pertinent to the biogeochemical cycles of the Earth's Critical Zone (ECZ).

The ECZ is a region between top of the vegetation canopy and the base of drinking water aquifers. Formally, the ECZ can be defined as the "heterogeneous, near-surface environment in which complex interactions involving rock, soil, water, air, and living organisms regulate the natural habitat and determine the availability of life-sustaining resources" [7, 8]. Most of the world's crucial problems such as, growing population, food security, water security, energy security, climate change, and extreme poverty are interlinked in some ways [9] and lead to the milking of the ECZ resources. In the purview of sustainable usage of the natural resources, the international organisations such as, the World Bank (WB) and the United Nations (UN) have reformed their policy frameworks substantially in the last two decades. The UN Sustainable Development Goals (SDGs) proposed in

2015 is a set of seventeen goals to transform the world for a sustainable future. The goals specified in the SDGs encapsulate all the major societal challenges as outlined in the beginning. The noteworthy point in the SDGs is the linkage among all the goals. The message is loud and clear that an integrated approach is required while dealing with most of the problems relevant to the domain of sustainability. A holistic or integrated viewpoint should be embedded at all the levels, from the scratch idea stage to the policy making and implementation stage.

From an engineering point of view, the ECZ can be perceived like a system having several subsystems. The ECZ system can be represented with the chosen level of abstraction. Which simply means that irrespective of the complexities possessed by the ECZ, it can be represented as a combination of some key subsystems. The characteristics and significance of these subsystems will get unfolded in the later parts of this section.

The motivation of this work relates to some sort of common solutions towards the climate change mitigation and food security. The recent Intergovernmental Panel on Climate Change (IPCC) reports have concluded that the ambitious targets of lowering the global mean temperature cannot be achieved solely by cutting down the greenhouse gas emission. The additional techniques capable of sequestering the anthropogenic carbon, known as Negative Emission Technology (NET) must come into play by the later half of this century [10]. One of such NETs known as, Enhanced Weathering (EW) can potentially absorb the carbons and also improve the crop production when applied in the farmland. The net effects of the carbon sequestration on the ECZ can only be assessed properly when all the biogeochemical cycles factors are taken into account. A wetland defined as an inundated land surface plays major roles in the absorption of carbon and emission of methane gas. Hence, wetlands are important factors in accounting the biogeochemical cycles of the ECZ. The extent of wetland exhibits seasonal variations and depend a lot upon the local climate. The analysis of wetland extent dynamics and EW potentials emerged as the core areas of investigation in this thesis and their significance in the ECZ system will be more apparent in the forthcoming chapters.

A mathematical model is a simple representation of some complex physical processes. This thesis has analysed some key processes of the ECZ, such as, weathering, vegetation, and inundation through modelling and computational simulation techniques. The interlinking of the SDGs particularly 'zero hunger', and 'climate action' has been at the heart of this thesis and therefore the modelling and simulation analysis in this work are inspired from the 'systems thinking' [11]. Herein, the system of interest encapsulates the models representing soil processes, vegetation processes, weathering processes, and inundation process. The system

approach in modelling supported the requirements collation and incorporation of all the processes accordingly with the desired level of abstraction. Some of the components such as, soil and vegetation processes [12–14] have previously been modelled and these models demonstrate the reasonable amount of fidelities as well. Therefore, these standard models have been adopted in this thesis. For the remaining components of the system, either a data-driven or analytical types of modelling take the centre stage. The nonlinear system identification methodology forms the basis of wetland modelling in this thesis, whereas, the enhanced weathering part is modelled using a process based modelling approach.

1.2 Aims and objectives

This thesis aims to model and perform the computational simulations of the essential ECZ processes for evaluating the various scenarios relevant to environmental sustainability and food security. During the course of modelling, the thesis also aims to bring out some methodological advancements in the Model Structure Selection (MSS) step, mainly in a System Identification (SID) context. For the sake clarity, the objectives corresponding to the aims of this thesis are placed under three different categories: wetland modelling objectives, enhanced weathering modelling objectives, and SID methodological advancement objectives.

1.2.1 Wetland modelling objectives

- Develop an Approximate Bayesian Computation (ABC) based identification procedure for wetland dynamics.
- Devise a single model structure capable of explaining the dynamics of entire tropical wetland sites.
- Estimation of model parameters across all the tropical wetlands sites and in turn capture the site specific topographic details in model.
- Show spatial variability of tropical wetland dynamics through model simulations.

1.2.2 Enhanced weathering modelling objectives

- Develop and implement a mathematical model representing the enhanced weathering of a rock using a shrinking sphere modelling methodology.

- Integrate the developed EW model with the existing ECZ process models. The integrated model will be termed as the Integrated Enhanced Weathering Critical Zone Model (IEWCZM).
- Calibrate and validate the IEWCZM using an actual field level experiment.
- Perform the sensitivity analyses to assess the sensitivity of weathering rate on the variables like soil pore water pH, temperature, and mass of the weathering mineral.
- Perform a case study for assessing the effects of EW on crop yield.
- Collect the key input data of a recent soil-vegetation process from the University of Leeds farm and parametrise the IEWCZM to represent all the key ECZ processes of the farm through the IEWCZM.
- Design a simulation experiment for winter wheat farming on the Leeds farm site. Thereafter, simulate the one off addition of basalt in Leeds farm for a period of three years and compare the effects of basalt addition with the baseline conditions for all the key soil-vegetation variables. Extend the simulation to the yearly addition of basalt in Leeds farm until the year 2099.
- Divide the entire UK land area into grid cells separated by 0.5×0.5 degree geographically. Parameterise the IEWCZM for all the sites while keeping the soil-vegetation parameters unchanged for the sake of simplicity. Which means, only climatic parameters will vary among these sites. Calculate the net CO_2 absorbed by the entire UK crop land by this century end.

1.2.3 SID methodological advancement

- Develop a novel algorithm known as the ABC-NARX-MSS using ABC and inspired by the Sequential Importance Sampling (SIS).
- Compare the performance of the ABC-NARX-MSS with the Forward Regression Orthogonal Least Square (FROLS) using a known example system.
- Perform a full nonlinear SID steps using the ABC-NARX-MSS on an unknown environmental system and eventually propose the ABC-NAR-MSS as an efficient algorithm capable of selecting an optimal model structure in a nonlinear SID.

1.3 Overview of the thesis

In the purview of above discussions, this thesis has been organised into three parts. The first part presents a novel algorithm for MSS in nonlinear SID. This contribution chapter appears after the chapters on theory, applications and literature surveys in SID and ABC. The second part contains a novel contribution in the form of a data-driven wetlands modelling. Similar to the previous part, a chapter highlighting the significance of wetlands and the current states of wetland models is placed in a preceding position. The final part of the thesis contains two contributions, firstly the development of a calibrated EW model using analytical approaches and the simulation analysis of EW in the UK conditions. Both of these chapters are positioned after a literature survey on enhanced weathering theory, its potentials and challenges.

1.3.1 Part I (System identification methodologies)

This part begins with the Chapter 2, titled as 'System identification theory and applications'. In this chapter, all the key steps in a typical SID are succinctly presented. The second part as said above contains a data-driven modelling of wetlands, a highly nonlinear system. Hence in the Chapter 2, nonlinear SID and its model class are emphasised more than linear SID. The modelling of wetlands comes under the ambit of applications of SID. So in this chapter, some recent literatures on the applications of SID particularly beyond a typical control application are provided. The first part of the thesis presents a novel algorithm on the structure detection in SID, therefore some existing methods on MSS are critically analysed here, to understand the research gaps as well as to highlight the thesis contribution.

The Chapter 3 starts with the motivations and theories associated with the ABC, which is a simulation based approach under the Bayesian framework. The MSS algorithm devised in this thesis is under the umbrella of the ABC framework as well as the parameter mapping of wetland sites in the next part is also guided by the Sequential Monte Carlo (SMC) version of ABC. Therefore, the Chapter 3 reviews the popular inference algorithms under ABC. In addition, this chapter also includes a survey about the theoretical advancements in ABC and the applications of ABC methodology in a wide range of disciplines.

The Chapter 4 is a novel contribution in the form of an MSS algorithm under the ABC framework. The SID methodology has surpassed the boundary of control applications and domain experts from other fields typically prefer a simple algorithm for SID steps. Existing algorithms on Nonlinear Autoregressive Exogenous

(NARX) MSS under a probabilistic framework are mathematically and computationally very complex. The algorithm referred as the 'ABC-NARX-MSS' in this chapter is a simple and easily adaptable in comparison to the competing methods. This algorithm mimics the Sequential Importance Sampling (SIS) and exploits the latest computing facilities under the umbrella of the ABC. The ABC-NARX-MSS is tested with a numerical example and its performance is also compared with the standard FROLS. A full cycle of the SID on an unknown environmental system is included in this chapter to highlight the performance of the ABC-NARX-MSS algorithm. This novel method of MSS was devised in the final phase of the project and hence could not be applied in the Part II of the thesis. Nevertheless, the simulation results of an unknown environmental system suggests that this algorithm would be very effective with such kind of systems.

1.3.2 Part II (Data driven modelling of wetlands)

This part mainly contains the modelling of wetlands using nonlinear SID methods and starts with the Chapter 5. In this chapter, the definition, significance and challenges of wetland modelling are presented. The popular wetland models are reviewed to assess the gaps and the scope of improvement in the modelling of wetlands. A data-driven approach known as the Data Based Mechanistic (DBM) modelling relevant in hydrology is also discussed in this chapter. The idea behind including a survey of DBM approach is to demonstrate the significance of data availability in hydrology and a potential of data-driven modelling in a wetland system where hydrology plays important roles.

The Chapter 6 is a novel contribution of the thesis and contains the model development and simulations of the tropical wetlands. Existing literatures on wetland modelling suggest that so far only analytical modelling approaches have been employed. However, all such modelling attempts fail to represent the wetland distribution fairly. In this chapter, a novel data-driven approach in the form of SID is brought into picture. The dataset used in this project corresponds to a Global Inundation Extent from Multi-Satellites (GIEMS) and a Single Input Single Output (SISO) system approach has been employed. The project's aim required the selection of average temperature as an input and the wetland fraction as output so that the model could be employed for evaluating the various scenarios of the IPCC until the end of this century.

The entire tropical wetland modelling exercise is divided into two stages. In the first stage, only three wetland sites are included and the FROLS is used for the MSS as well as parameter estimation. In the next stage, all the available wetland sites form the part of modelling and a single model representing the dynamics

of the tropical wetlands is obtained. The model is parameterised for all the sites separately so that the topographical details for each site gets captured in the form of parameters. The analysis of parameters across all the tropical sites are in accordance with the expected characteristics of tropical wetlands. The simulation results for all the available wetland sites are compared with the observed data to ensure the fidelity of developed model.

1.3.3 Part III (Analytical modelling of enhanced weathering)

The Part III of this thesis is a shift towards the analytical modelling approach. It starts with the Chapter 7, where some basic theories behind enhanced weathering along with its potentials and challenges are elaborated. This chapter compares the available weathering models and emphasises the need for integrating the weathering processes with the soil-vegetation processes.

In the Chapter 8, a shrinking sphere type of weathering model is developed. Some literatures containing the modelling of rock weathering processes do exist but they do not consider all the essential ECZ processes relevant to weathering mechanism. To some extents these models also ignore the effects of weathering products on the ECZ processes. In reality, rock weathering is linked to the ECZ, particularly the soil-vegetation processes. Therefore, this chapter also shows the integration mechanism of weathering processes with the ECZ process models. The integrated model is referred to as the IEWCZM.

A weathering reaction rate is largely governed by the rate constant. The existing literatures on weathering models use the rate constant values from some standard sources, containing the theoretically or laboratory determined values. However, at least one recent study [15] highlights the problems associated with such kind of theoretical rate constant values in an olivine weathering reaction. Therefore, in this chapter the IEWCZM is calibrated with a field result and a case study has also been presented. The weathering process depends upon the variables like pH and temperature, hence sensitivity analyses have been included, which can be helpful in choosing the optimum sites for the implementation of enhanced weathering. The IEWCZM is passed through some validation tests by reproducing an actual olivine weathering reaction results.

The Chapter 9 provides the analysis of EW in the UK condition. As briefed in the previous section, EW is an NET which can sequester the anthropogenic carbon and in parallel also improves the crop yield. The EW being in a concept phase has not been implemented so far in a UK cropland. In the absence of a weathering model capable of simulating weathering as well as all the key ECZ processes simultaneously, any simulation study of EW in the UK condition was not performed

before this project. As a geo-engineering process, any actual implementation of EW will have to pass through rigorous evaluations and therefore computational simulation turns out to be a natural choice for analysing the various scenarios pertaining to the implementation of enhanced weathering in a farmland. This chapter simulates the one-off addition of silicate mineral as well as yearly addition of mineral until this century end is also provided. The amount of carbon sequestrated and growth in the crop yield by 2099 are presented with necessary details.

1.4 Research outputs

The materials from the Chapter 6 have been adopted for the following paper (published):

- A. Anupam, D.J. Wilton, S.R. Anderson, and V. Kadirkamanathan. A data-driven framework for identifying tropical wetland model. In 2018 UKACC 12th International Conference on Control (CONTROL), pages 242–247. IEEE, 2018.

The extended version of the tropical wetland modelling under the ABC framework will be presented in another paper (in preparation):

- A. Anupam, D.J. Wilton, S.R. Anderson, and V. Kadirkamanathan. Identification and parameter mapping of tropical wetland model using the ABC.

The materials from the Chapter 4 are being adapted for a paper (in preparation):

- A. Anupam, S.R. Anderson, and V. Kadirkamanathan. An ABC based algorithm for the model structure selection in nonlinear system identification.

1.5 Summary of contributions

In summary, the novel contributions of this thesis are documented in the following chapters:

1. Chapter 4, NARX model structure detection under ABC framework
2. Chapter 6, Tropical wetlands modelling
3. Chapter 8, Integrated enhanced weathering critical zone model
4. Chapter 9, Enhanced weathering in the UK conditions

Part I

System identification methodologies

Chapter 2

System identification theory and applications

2.1 Introduction

System identification (SID) is a method of identifying the mathematical representation of a system on the basis of observed data of the system. The 'system' in this definition can be any kind of system such as, power station, financial system, environmental system, biological system etc. Any envisioned system can be represented by a mathematical model, which can facilitate the simulation and analysis of the system prior to its implementation. Therefore, modelling is at the heart of any system design.

Analytical modelling of a system is not so straightforward on numerous occasions. The challenges associated with an analytical modelling are manifold and any change incurred at a subsystem level might propagate through the entire system and leave the model futile. SID deals with the input-output data and regards the system as a blackbox. The generation of outputs corresponding to some input is a relatively simple task for any process. The output data emerging out of a system encapsulate the hidden dynamics of the system in some forms. The SID follows a well structured methodology for retrieving those dynamics and presents a dynamic model, consisting of the time lagged versions of system input and outputs. A system can be linear or nonlinear and ideally a SID algorithm should be able to distinguish among these features. For instance, a nonlinear model for a linear system will only haze the analysis of the system and the underlying science may not divulge at all. A SID broadly consists of two main steps, model structure detection and parameter estimation.

In this thesis, SID occupies a very prominent position and touches at least

fifty percent portions of the entire thesis. As briefed in the introductory chapter, wetlands play very crucial roles in the Earth's Critical Zone. In the later part of the thesis, a dynamical wetland model corresponding to the tropics of the earth will be developed using SID. The forthcoming chapters will also highlight the significance of a data-driven approach in wetland modelling and the limitations of the process based models. Therefore, this chapter on SID will cover all the basic elements used for devising a tropical wetland model in this thesis. This aspect of the SID in the context of wetland modelling can be placed under the realm of SID applications. This thesis also contains a chapter on the methodical advancement in SID. The model structure detection is very crucial and often the most difficult task in a SID. This research has added a novel method of structure detection in SIDs. Therefore, it is imperative to discuss the gaps in the existing SID algorithms. This chapter will attempt to provide all the facets of SID succinctly while keeping the research contributions in view at the same time.

This chapter unfolds with a description about the model structures corresponding to both linear and nonlinear class of systems. The choice of model type is a key part because an inappropriate selection could make the identification process very difficult. Thereafter, parameter estimation methods common in SID will be covered. The model structure detection is the toughest step in a SID and still open for wide research despite the establishment of this methodology for more than three decades. This thesis will also address this aspect in the chapter 4 and hence a critical review of some popular methods in the model structure detection will be presented in a dedicated section. The SID as a method has crossed the boundary of a typical control theory application many years ago. In fact, this thesis too shows a new application area of SID while modelling wetlands. The application areas of SID therefore need to be reviewed in order to understand the motivations of applying it in this particular research. Finally, the chapter will end with some concluding remarks.

2.2 Model structure

A SID technique can be used to build up a 'relevant' model using the observed data. The 'relevant' keyword is to emphasise that, a model must be in accordance to the system type. For instance, discrete systems can be represented using the difference equations, whereas, an ordinary differential equation should be able to describe continuous-time system. All the models must also take into account the linearity or nonlinearity of the system. In this section, some standard model structures corresponding to linear and nonlinear models will be discussed. Nev-

ertheless, all of the model types presented here are not pertinent in this study, as the modelling in this thesis are mainly based around nonlinear systems.

2.2.1 Linear models

The general model class of finite order linear system is known as the Autoregressive Moving Average with Exogenous Input (ARMAX) and can be represented as [16–18]

$$A(z^{-1})y(k) = \frac{B(z^{-1})}{F(z^{-1})}u(k) - \frac{C(z^{-1})}{D(z^{-1})}\xi(k) \tag{2.1}$$

where

$$\begin{aligned} A(z^{-1}) &= 1 + a_1 z^{-1} + ... + a_{na} z^{-na} \\ B(z^{-1}) &= b_1 z^{-1} + ... + b_{nb} z^{-nb} \\ C(z^{-1}) &= 1 + c_1 z^{-1} + ... + c_{nc} z^{-nc} \\ D(z^{-1}) &= 1 + d_1 z^{-1} + ... + d_{nd} z^{-nd} \\ F(z^{-1}) &= 1 + f_1 z^{-1} + ... + f_{nf} z^{-nf} \end{aligned} \tag{2.2}$$

In the above representation of an ARMAX model, $u(k)$ and $y(k)$ stand for the system input and output respectively. The n_a, n_b, n_c, n_d, and n_f relate with the model orders. The $\xi(k)$ represents an independently and identically distributed noise sequence. The z^{-1} symbol acts as the backward shift operator in the expansion of the above model structure.

The ARMAX is a generalised model structure for the linear systems and a full ARMAX representation is not always essential. Sometimes, a linear model can be explained with a shorter representation such as, AR (B=0, C=D=1), MA (A=1, B=0, D=1), ARMA (B=0, D=1), and ARX (C=D=F=1).

2.2.2 Nonlinear models

Most of the real world systems exhibit some kind of nonlinearity. Sometimes, a nonlinear system can be approximated as linear particularly at the operating regions, but that comes at the loss of precision. A single model class encompassing a broad range of nonlinearities is not so easy. The Nonlinear Autoregressive Moving Average with Exogenous input (NARMAX) model, firstly introduced around three decades ago has emerged as a popular choice in a nonlinear SID. In fact, the broad features within a NARMAX model structure have shaped it like a philosophy of the nonlinear SID [18, 19].

A typical nonlinear SID or NARMAX approach consists of the following steps:

1. Nonlinear model structure detection
2. Parameter estimation
3. Model validation
4. Forecasting
5. System analysis

The formal definition of NARMAX model is [18]

$$\begin{aligned} y(k) =& F[y(k-1), y(k-2), ..., y(k-n_y), \\ & u(k-d), u(k-d-1), ..., u(k-d-n_u), \\ & e(k-1), e(k-2), ...e(k-n_e)] + e(k) \end{aligned} \tag{2.3}$$

where $y(k)$ is system output, $u(k)$ is system input, $e(k)$ is noise sequences, n_y is maximum lag for system output, n_u is maximum lag for system input, n_e is maximum lag for noise, F is a nonlinear function, and d is time delay. The moving average (MA) part is not considered on most occasions and hence the above NARMAX representation can be reduced to a simpler NARX model structure.

2.2.3 Miscellaneous models

In this section some miscellaneous model classes will be discussed briefly. Noteworthy point is that most of these model structures have been tried as a substitute of the standard NARMAX in past, but they have not been able to possess the generality and robustness of a NARMAX model.

One of such models is known as Piecewise Linear Model (PLM). In a PLM method, a nonlinear system is partitioned into the operating regions of interests. The basic idea is to harness the available methods of linear modelling along these operating regions and eventually glue these linear models together to somewhat mimic like a nonlinear model of the system. The approximation of nonlinear system by a chain of linear models can be performed in many ways. A few popular methods for performing the PLM are available in [20]. Some other methods under the ambit of PLM can also be accessed through [18].

The Volterra Series Models (VSM) is another popular model choice. A VSM can represent a system dynamics through lagged inputs. In a way it acts like a subset of NARMAX but the absence of lagged outputs make the VSM a clumsy representation especially in nonlinear cases. The detailed survey and the application areas of the VSM can be found in [18, 21].

Block-Structured Models (BSM) or Cascade models is a prominent class of nonlinear model. The simplistic representation of this model class has been exploited in many systems especially in Biology. Fundamentally it is built through a cascading between linear dynamic blocks and static nonlinear blocks. Most common BSM types are Hammerstein and Wiener models. In Hammerstein models, static nonlinearity, $g(.)$, precedes the linear dynamics, $H(z^{-1})$, whereas, this order gets reversed in a Wiener model. The BSM can be generalised by considering the Hammerstein and Wiener models as special cases and loosely called as a sandwich model because $g(.)$ is sandwiched between two blocks of $H(z^{-1})$ [18, 21–23].

In addition to the model types discussed above, neural networks, wavelet models, and state space models can also be employed in a SID context. Detailed information about these model structures are available in [18]. The key point remains the selection of an appropriate model type for the system under consideration. Among all these structures, NARMAX model class appears to be the most efficient model for this study. The dataset in this study has emerged from an environmental system and should display nonlinear behaviours. If not then also the NARMAX method should be able to reduce the representation into an ARMAX model type.

2.3 Parameter estimation

In this section, a brief description about the parameter estimation in a SID will be presented. A NARMAX model can be described as a linear-in-the-parameters representation

$$y(k) = \sum_{i=1}^{M} \theta_i \phi_i(k) + e(k) \tag{2.4}$$

where $y(k)$ is system output, Φ are the regressors formed by combining the linear and nonlinear time-lagged input-output sequence, $e(k)$ is a noise sequence. The equation 2.4 can be converted into matrix form,

$$\boldsymbol{y} = \Phi\boldsymbol{\theta} + \boldsymbol{e} \tag{2.5}$$

, the parameter vector $\boldsymbol{\theta}$ can easily be calculated from the equation 2.5.

The parameter estimation in SID can also be performed using sophisticated statistical approaches. Such as, the evaluation of maximum likelihood (ML) estimate is one of the ways of parameter estimation. An ML method tries to maximise the likelihood function, $p(y|\theta)$, in order to obtain a parameter set $\hat{\theta}_{ML}$. The $\hat{\theta}_{ML}$ can therefore be regarded as a 'true' parameter which generates the data closely

to the observed data. In practice, logarithmic likelihood functions are used to simplify the evaluation process. The logarithmic conversion is in sync with the theory as the natural log is a monotonically increasing function. The expectation maximisation is an iterative algorithm which can result into an ML estimate through the log-likelihood function. The SID under an EM framework is described in [24].

The statistical approach in parameter estimation also extends to the Bayesian framework. In the recent years an approximate version of the Bayesian inference known as Approximate Bayesian Computation (ABC) has come into limelight. The Bayesian methods particularly the ABC provides quite a few algorithms on parameter estimation. Many available literatures on these kind of algorithms have refrained from using the term 'SID' while presenting these parameter inference algorithms mainly because a SID consists of lot more steps than just parameter estimation. Nevertheless, one can easily extend these ideas and enhance the toolbox of parameter estimation in a SID context. The next chapter is dedicated to the ABC and contains some of these algorithms with necessary details.

2.4 Model structure selection

In this section various methods corresponding to the Model Structure Selection (MSS) problem will be presented. One of the forthcoming chapters in this thesis is about a novel contribution towards the MSS in a nonlinear SID. Therefore, some key literatures related to the MSS will be critically reviewed in this section.

2.4.1 Model selection via information criteria

Information theory contains a meticulous framework for model selection mainly through measurement of information loss between observed data and model simulated data. The Akaike Information Criterion (AIC) first introduced in [25] is used to estimate the relative quality of models corresponding to a given set of data. This takes into account goodness of fit across models as well as model complexity. The AIC was adapted in [26] by including Bayes' solution for selecting the best models among a set of models. This adapted version of the AIC is known as the Bayesian Information Criterion (BIC) [27]. Basic philosophy of the AIC is retained by the BIC as both of them calculate the maximum likelihood and penalise an over-fitted model. So, both the AIC and BIC give a relative estimate of information loss across several candidate models. Mathematically,

$$AIC = 2k - 2ln(\hat{L}) \tag{2.6}$$

where k is equal to the independently adjusted parameters within the model and $\hat{L}$ is equal to the maximum likelihood.

$$BIC = ln(n)k - 2ln(\hat{L}) \tag{2.7}$$

where k and $\hat{L}$ have similar meanings like the equation 2.6. An additional term n in the equation 2.7 stands for the number of data points in an observed dataset. Typically, such an information criteria method works well for about 10 or less models [28]. Dynamics of many real world systems are usually represented through a nonlinear model structure. Often the number of candidate models in such cases are so high that the AIC/BIC in its current form may not be even feasible to apply. The simulation of each candidate model and the calculation of AIC/BIC scores lead towards the computational intractability. However recently, a method came into picture, where the direct computation of AIC/BIC scores are avoided by integrating sparse regression for nonlinear system identification using SINDy [29] and information criteria based model selection [28].

In principle, a model selection method based upon information criteria can be used in any data-driven discipline. A linear model fitting should be attempted for any dataset in a first place and AIC/BIC can be very useful for obtaining a parsimonious model structure. However, the limitations of this approach in nonlinear modelling generally require other sophisticated methods.

2.4.2 Orthogonal forward regression framework

The Forward Regression Orthogonal Least Square (FROLS) is a model structure detection method, driven by the iterative addition of terms based on their Error Reduction Ratio (ERR) values. It is considered to be the most popular algorithm since its emergence [30] mainly due to its computational simplicity. The FROLS incorporates the orthogonalisation for decoupling the regressors which in turn simplifies the evaluation of ERR for each candidate term. The contribution of each term to the output variance is contained by the ERR and it is assessed by taking into consideration the decrease in Mean Squared Prediction Error (MSPE) incurred after adding the term to the existing model structure. The ERR index for all the unselected terms are calculated at each iteration and the one with the highest ERR is included in the current model structure.

In order to perform the orthogonal decomposition, firstly the equation 2.4 is converted into matrix form (equation 2.5). The orthogonal decomposition leads to

the equation 2.8 and subsequently to the the equation 2.9.

$$\boldsymbol{y} = \Phi A^{-1} A\boldsymbol{\theta} + \boldsymbol{e} \tag{2.8}$$

$$\boldsymbol{y} = W\boldsymbol{g} + \boldsymbol{e} \tag{2.9}$$

W=[$\boldsymbol{w_1}$,...,$\boldsymbol{w_M}$] is a ($N \times M$) orthogonal regression matrix, where columns are orthogonal. A is a ($M \times M$) unit upper triangular matrix, **e** is model residual error vector, **g** is the parameter vector, Φ=WA . The QR decomposition is achieved by using modified Gram-Schmidt algorithm. The orthogonalisation enables the uncoupling among the columns of W matrix. This also causes the corresponding parameters in the **g** to exhibit uncoupled behaviour. Therefore, the individual contribution of each regressor in W, while minimising the distance between one-step-ahead (OSA) prediction and the observed output can be assessed [18].

The ERR assigns some degree of importance to each regressor which is eventually used for ranking of these regressors in model. The noteworthy point here is that this assigned importance is not 'absolute' in nature and largely depends on the model under consideration. This could in fact pick up a term as a 'significant' term in the beginning, but after the detection of the complete structure, the chosen term may not be very important [31]. There is no way to prune a poor term in the original version of the FROLS. However, this issue has been addressed to a large extent by the iterative Orthogonal Forward Regression (iOFR) method, in which the FROLS is iterated with different initial regressors. This algorithm is able to prune the redundant terms and return an optimal solution. This method tries to exploit the computational simplicity of the FROLS while performing the search in regressor space [32].

2.4.3 Model selection under Bayesian framework

The concept of model selection under the ABC framework was introduced recently in [33]. This literature has adapted the standard Bayesian model selection [34] guidance, especially the Bayes' factor in its examples. The model selection algorithm is very much similar to the ABC-Sequential Monte Carlo parameter estimation. In this algorithm, an additional 'model parameter' $m \in [1,...,\psi]$ is introduced, which is discrete in nature. ψ is the total number of models. Each model has its own parameter set denoted by θ_m and unlike m, θ_m is not discrete in nature.

At each iteration, firstly a candidate model is sampled from the uniform distribution of models, $\pi(m)$. Corresponding to the sampled model, a parameter set is sampled from the prior distribution and perturbed using a perturbation kernel.

Model is simulated using the parameters obtained after perturbation. If the performance of the model meets the threshold criteria of the population level then the model is accepted as a particle and a resampling of model for the next particle takes place. If the performance of the model does not meet the threshold criteria then the model is rejected and resampling of model for the current particle takes place. The number of particles in a population is a design choice and directly relates to the computational effort of the algorithm. In an ABC-SMC parameter estimation method, final population is reached sequentially by reducing the threshold values at each step. The same approach is followed here and the algorithm stops when all the particles in the final population level is obtained.

On many occasions, the probability distribution of model parameter clearly indicates the true model among the candidate models. However this is not always guaranteed especially when the competing models are equally suitable to describe the given data. Bayes' factor is calculated from the model probability distribution to figure out the best model. The interpretation of the various Bayes' factor in a tabular form is provided in [33]. The table suggests that, when more than one model has similar probability value then even Bayes' factor fails to infer the true model.

The model selection algorithm presented in [33] opens up the ideas of model selection problems solely through an ABC methodology. The algorithm presented here can be very useful in cases where only few candidate models exist. In SID, model structure detection is a bigger problem than parameter estimation. The number of candidate models are 2^n where n denotes the number of regressors. For a system with maximum input-output lags equal to 2, the value of n reaches 34. So, the ABC-SMC model selection algorithm cannot be applied in a SID setting.

Another set of algorithms on the MSS under ABC framework was proposed by the [35]. In this literature, model selection has been divided into one-stage and two-stage categories. In the one-stage model structure detection, a quantile test is performed to gauge the significance of a parameter inferred using ABC-SMC parameter estimation algorithm. If a parameter fails this test then that gets labelled as a 'false' parameter and pruned away from the model structure. Through a numerical example this test is shown to be performing satisfactorily at least for the terms having sensitive parameters. One major criticism about this one-stage algorithm is that, it does not assess the performance of the model simulations.

In view of the above drawback, the two-stage model structure detection is also presented in [35]. This algorithm uses the BIC to take into account the model simulation performance. This algorithm has been proposed in continuation to the one-stage algorithm and is not a stand-alone method. While using this algorithm,

firstly one-stage term selection is used to prune away the 'false' parameters based upon the mentioned quantile test. Prior to quantile test, an initial sensitivity test is also performed. The Cha-Srihari distance metric is then used to order the unselected terms followed by the BIC test to order the terms based on their simulation performance. ABC-SMC is used to estimate the parameters of the final model structure obtained at the end of one-stage and two-stage term selection.

One of the criticisms about this method is that, prior to running the one-stage term selection, one needs to estimate the parameters corresponding to all the possible terms which could go substantially high for real world scenario like wetland system. The ABC-SMC in the current form does not work satisfactorily with very high dimensional parameter estimation. Practical experiences suggest that more than 10 parameters in a model would make the ABC-SMC code sluggish and may even fail. So, the pre-condition of these one-stage and two-stage term selection algorithms can be really difficult and sometimes impossible to satisfy. Another criticism is about the search mechanism in this algorithm. The terms selection algorithm in this paper [35] actually returns an ordering of the terms depending upon their contribution in the model. For many situations in SID, such kind of ordering is acceptable considering the fact that even the most popular algorithm like FROLS does the similar kind of ordering based on OSA prediction error minimisation approach but ideally an MSS algorithm should exhibit the global search for an optimal solution.

Another recent contribution in the model structure detection under the Bayesian framework was based on the Reversible Jump Markov Chain Monte Carlo (RJMCMC) methodology [36]. In this literature, both the parameter estimation and model structure detection are performed using the extension of the Metropolis-Hastings algorithm (MH). At each iteration, this method can perform birth move, death move or update move. In the birth move, a new term is randomly selected for the inclusion into the existing structure. Similarly in the death move, one of the terms from the model structure is randomly chosen for pruning. In the update move, parameter update takes place using a MH random walk. The extension of MH algorithm enables the jump between different parameter dimensions. In theory, this approach of simultaneous model structure selection and parameter estimation appears to be exciting. However, the trans-dimensional jump in the parameter space is a complex phenomena as reported in [37].

2.4.4 Model selection using randomised approach

Recently, a randomised algorithm for the model structure detection (RaMSS) was present in [37]. In this method, regressors are randomly sampled in the first it-

eration to constitute a certain number of candidate models. These models are then passed through their respective parameter estimation steps and simulation. The parameter estimation is suggested by the least square method for the computational reasons. Following the models simulation, the performance of each regressor is quantified using an index known as I_j. The idea behind this indexing is much similar to the ERR, nevertheless, the values of I_j will keep updating with iterations. The I_j is calculated by comparing the models where the regressor j is present and the models where the regressor j is not present. The value of I_j is used to update the Regressor Inclusion Probability (RIP) of the regressor j, and the regressor sampling in the next iteration will be based upon the updated RIPs of all the regressors. The algorithm is compared with the RJMCMC model structure detection presented in [36] and has a better performance in terms of computational requirements and consistency in selecting the 'true' model.

Despite exhibiting a satisfactory performance, the RaMSS cannot be generalised in other applications easily. The regressor performance index I_j depends upon the user-defined tuning parameters K and α. The RIP also depends upon a design parameter, known as γ. All these parameters induce the ad-hoc elements in the algorithm and might be difficult to adapt this method in different problems. The NARX model class is gaining popularity in wide disciplines. Hence a SID method must exhibit the robustness, so that a practitioner can use the algorithm without getting into the technical complications of tuning multiple parameters. Another limitation of the RaMSS emerges during the initial selection of regressors, which is random and without any benchmarking criteria. That means, if a 'good' regressor is left out in the 1_{st} iteration, that will never be pickup up during the entire MSS process.

2.5 Applications of SID

The SID as a dynamic system modelling methodology emerged in the context of control theory. The shift from the classical control techniques to the model based approaches necessitated innovations in the dynamic systems modelling. The inevitable complexities in modern systems such as in aerospace constrain the usage of analytical modelling approaches for their controller design. The SID being a data-driven method facilitates the blackbox modelling of dynamical systems. In the last few decades, SID particularly nonlinear SID has crossed its core domain and have been applied in a wide range of disciplines. A novel application of the SID in wetland system will be covered in the forthcoming chapter of this thesis. The rationale behind this section is to outline a few interesting applications of SID

beyond control theory. Another motivation behind this section is to highlight the practical difficulties in identifying a real system. A typical literature on a SID algorithm considers a known numerical example to illustrate the underlying methods and hence the intricacies of a real system do not get exposed from such literatures. The structure in this section has has been adapted from the [18] and a more detailed review of the SID applications can be accessed from the same source.

2.5.1 SID in space weather modelling

The relationship between relativistic electron fluxes and the solar wind parameters are studied in the [38]. Although the results reported here are interesting but the correlation approach does not guarantee the detection of all nonlinear effects. The idea was extended to the NARMAX approach and ERR based ranking of terms by [39, 40]. The ERR test enabled the selection of relevant terms signifying the relation between solar wind parameters and relativistic electron fluxes at the geostationary orbit. The energy range was kept similar to the one used by the [38]. The dataset used in this study had some missing data and therefore eight subsets of the data were extracted to ensure that missing data points do not affect the analysis. Averaging of the ERR corresponding to all the eight sets were performed.

At the energy level $1.8 - 3.5$ MeV, $n(t-1)$ has the highest ERR value and therefore, solar wind density is the most contributing term towards the electron flux. The second terms is the squared form of the solar wind density and the first two terms together accounts for about 75% in the variance of the electron fluxes. The velocity $V(t)$ factor comes into play as a third term and accounts for just 6.30% in the output. The energy level $1.8 - 3.5$ MeV is considered as a very high energy range and the wind density $n(t)$ controls the electron flux mostly in this range. As the energy range is lowered like in KeV range, $V(t)$ emerges as the main control parameter.

2.5.2 SID in detection and tracking of iceberg calving

In this study [41], dependence of Greenland iceberg calving on the variables such as surface mass balance of ice sheet and regional climate change is analysed using the NARMAX modelling approach. The I48N is an International Ice Patrol for the iceberg data which passes at 48 degree N as the name suggests. In this study, it is considered as a dependent variable and the variability of the I48N under the influence of other variables are analysed. The input variables are, Surface Mass Balance (SMB), Labrador Sea Surface Temperature (LSST), and North Atlantic Oscillations (NAO).

The nonlinear SID in this study was performed using a sliding window of thirty years for understanding the evolving trends. According to the ERR value, the SMB turns out to be the most dominant factor in explaining the variance in the I48N during the first half of the 20^{th} century. This trend was somewhat changed in the later half with increasing contributions from the NAO and LSST. The NAO and LSST are climate related indices but their increased contribution towards the I48N variation in the later half of the 20^{th} century cannot be inferred as the effects of climate change according to an ocean model, incorporated in this investigation. The strong contribution of SMB made a comeback in the recent years leading to a conclusion that I4BN variability is not much dependent upon the open ocean iceberg melting.

2.5.3 SID in modelling of synthetic bio-parts

Synthetic biology can be categorised into phases starting from the molecular and modular level and reaching up to the system level recently. Despite this area going through a continuous research growth, most of the synthetic biological systems are devised on ad-hoc methods. This study has attempted to formalise the characterisation of dynamics associated with synthetic bio-parts through the use of NARMAX modelling [42].

The input signal in this SID is 3-ox-ohexanoyl-L-homoserine lactone ($3OC_6HSL$), whereas, output is the rate of green fluorescence protein (GFP) expression. The details about these input-output and their actual significance are provided in [42]. The NARMAX model is represented in the continuous time domain using a differential equation form. There were total nine candidate terms in this case, which is a relatively simple scenario in NARMAX model and so all the possible model structures were assessed. Finally a continuous time NARMAX model structure having three parameters denoted by a_1, a_2, and a_3 were obtained. The same model structure was retained for all the experimental data and the parameters (a_1, a_2, and a_3) for all the datasets were estimated. The variations among the parameters are not so large, signifying the consistent dynamic behaviour.

2.5.4 SID in forecasting high tides in the Venice Lagoon

The Venice Lagoon is one of the most vulnerable ecosystem particularly after the flooding of 1966. Low atmospheric pressure supported by severe winds affect the tides near the northern Adriatic sea and can cause acute flooding in the region. A flood warning system can be very helpful in such situations and may tranquil the life of the local population. Such warning system based on a combination of

statistical and analytical modelling approach is presented in [43].

An SID approach involving multi-resolution wavelet models, rooted on cardinal B-spline (CBS) multi-resolution were proposed in the last one decade as a flood warning system in the Venice Lagoon [44–47]. This kind of modelling has shown a superior prediction performance as compared to the existing tools. The dataset used in this SID is on hourly basis starting from January 1990 to December 1994. These data were chopped into five sets, each set containing about 8760 observation points. The data corresponding to each set was used for model training and the next set of data was used for model evaluation purpose.

2.6 Conclusion

This chapter provides a brief description about the SID methodology. Different kinds of model structures have been presented to spotlight the features of NARMAX model class in comparison to the other competing structures. The rich features of NARMAX have transformed it into a philosophy of the nonlinear SID.

Statistical approaches in the parameter estimation have widely been used in this thesis. However, the same has not be detailed in this literature because the next chapter on the ABC will engulf most of the popular estimation methods. On the other hand, model structure detection has been critically reviewed here mainly to establish the gaps in the existing literatures on structure detection. These reviews will be more relevant in the Chapter 4, where a novel method for the model structure detection in nonlinear SID will be presented.

The preceding section contained some applications of SID. Two of them, section 2.5.2 and section 2.5.4 can be referred as the application of SID in environmental systems. The Earth's natural environment is at the receiving end in the advent of the climate change. This is linked to food security, water security, and energy security either directly or indirectly. The major portions of this thesis is themed around the sustainability issues and the modelling is at the heart of sustainable futures. Both sections (2.5.2 and 2.5.4) demonstrate the power of SID in addressing the environmental issues. This idea will be extended to the modelling of wetlands in Chapter 6.

Chapter 3

Approximate Bayesian computation

3.1 Introduction

Bayesian data analysis is a popular statistical method for drawing inferences from a given dataset using probability models. Such models also enable the quantification of uncertainties in inferences. The entire Bayesian inference consists of the following three major steps [34]:

1. Model formulation
2. Model fitting using the available data
3. Model evaluation

The first step is usually the hardest one especially in the cases where the number of candidate models are very high. The required amount of proficiency for each of these steps are quite subjective and vastly depends upon the domain of the observed data. However, irrespective of the origin of dataset, second step typically requires a lot of rigorousness. This statement will get clearer in the following sections of this chapter. In fact, the overall theme of this chapter is attributed to the second step. Model evaluation or validation is a key step in any modelling exercise because a model should exhibit a reasonable performance before any crucial analysis is done through it. Depending upon the applications and significance of a model, a goodness of fit criteria is usually adopted to assess the model performance.

The Bayesian inference problem can formally be expressed as

$$p(\theta|y) = \frac{p(y|\theta)\pi(\theta)}{p(y)} \tag{3.1}$$

In the equation 3.1, $p(y|\theta)$ is the likelihood function, $\pi(\theta)$ is the prior distribution, $p(y)$ is the marginal likelihood, and $p(\theta|y)$ is the posterior estimation. In simple words, a likelihood function can be defined as the probability of obtaining the observed data for a given parameter value. In the Bayesian inference expression, $p(y)$ is actually a normalising factor and does not get updated like the other components of the Bayes' theorem.

In principle, posterior on the left hand side of the equation 3.1 can be computed by evaluating the likelihood function but the marginal likelihood usually involves a high dimensional integral, $\int p(y|\theta)\pi(\theta)d\theta$, and hence likelihoods are intractable on many occasions. A likelihood function can also be intractable when the model has many latent states. Nevertheless, it is relatively simple to simulate the data samples from such models for a particular parameter value. This idea acquired momentum in the late nineties and a few years before it started getting referred as approximate Bayesian computation (ABC).

In the remaining sections of the chapter, ABC will be discussed thoroughly starting with meaning and significance of the ABC, followed by the current methodologies employed for implementing the ABC for inferring dataset pertaining to a wide range of domains. ABC is a statistical framework and since the last two decades lots of works have been done towards improving the efficiency and fidelity of the ABC, so that it can be trusted like a first principle method of calculating the likelihood functions. The theoretical advancements are discussed in section 3.3. Some prominent ABC applications will be covered in the section 3.4, before concluding the chapter.

3.2 ABC methods

ABC as the name suggests is an approximate process of evaluating posterior distribution in a Bayesian inference problem. However, it is quite different from the likelihood approximation [48] as here the likelihood calculation is entirely replaced by a suitable simulation type procedure [49–51]. ABC emerged firstly in the population genetics [49, 50] but in the last one decade, the methodology has evolved as an efficient statistical technique for dealing with intractable likelihood problems in many areas including systems biology, ecology, and agent based modelling [52].

3.2.1 ABC rejection algorithm

ABC rejection is the simplest form of ABC and apparently the most expensive, computation wise. This kind of rejection sampling took a formal shape in [49] and later on several improvements were made to enhance the convergence power of

this algorithm. However, the key philosophy of the ABC-rejection is still the most unbiased approach in a likelihood free method of Bayesian inference.

In this algorithm, a prior distribution of parameter, $\pi(\theta)$ is defined first of all and the point of interest is the estimation of posterior parameter denoted by $p(\theta^*|y)$. The algorithm starts by sampling θ^* from the prior distribution. Sampled parameters are also referred as particles in many literatures. A data set y^* is then simulated according to the model choice. This step actually replaces the likelihood evaluation by simulation of data through a chosen model and is the backbone of any simulation based approach in Bayesian inference. Simulated data, y^*, is compared to the observed data, y, using a distance function, d, summary statistics, S, and tolerance value, ϵ. The particles are retained, if the threshold criteria are satisfied, otherwise, the entire process repeats.

The total number of particles in an ABC-rejection algorithm is directly proportional to the computational efforts. In general, larger particle size provides a better approximation of the true posterior. The ABC-rejection algorithm can formally be stated as,

1. Sample $\theta^* \sim \pi(\theta)$
2. Simulate $y^* \sim p(y|\theta^*)$
3. If $d(S(y^*), S(y)) \leq \epsilon$, accept θ^*, otherwise reject
4. Go to step 1.

The literatures [33, 51] mention that very large number of particles were rejected in the ABC-rejection process and computationally it does not turn out to be a plausible option while dealing with a real system data. The ABC-Markov Chain Monte Carlo (ABC-MCMC) and the ABC-Sequential Monte Carlo (ABC-SMC) were developed in view of this drawback.

3.2.2 ABC-MCMC algorithm

In order to address the shortcomings of the ABC-rejection, ABC-MCMC was developed by [53]. All the notations such as θ, d, y, S, and ϵ carry the same meaning like ABC rejection algorithm, as stated in the previous subsection. The ABC-MCMC algorithm can formally be expressed as

1. Initialise θ_i, $i = 0$
2. Propose θ^* governed by a proposal distribution $q(\theta|\theta_i)$
3. Simulate $y_j^* \sim p(y|\theta_j^*)$

4. If $d(S(y_j^*), S(y)) \leq \epsilon$, go to step 5, otherwise set $\theta_{i+1} = \theta_i$ and go to step 6
5. Set $\theta_{i+1} = \theta^*$ with probability $\alpha = \min(1, \frac{\pi(\theta^*)q(\theta_i|\theta^*)}{\pi(\theta_i)q(\theta^*|\theta_i)})$ and $\theta_{i+1} = \theta_i$ with probability $1-\alpha$
6. Set $i = i$+1, go to step 2

The algorithm at its convergence results into a Markov chain with the stationary distribution $\pi(\theta \mid d(S(y_j^*), S(y)) \leq \epsilon)$ [53]. This guarantees the convergence of the ABC-MCMC algorithm to the approximate posterior distribution in principle. However, in this algorithm a very long chain is quite possible because of the correlation among samples combined with low acceptance probability. This may cause a chain to get trapped in low probability zones for very long time periods [33].

3.2.3 ABC-SMC algorithm

The ABC-SMC incorporates the Sequential Monte Carlo for sampling (SMC). The SMC was introduced in [54]. The ABC-SMC technique was formally introduced in the ABC-partial rejection control (ABC-PRC) form in [51]. The problem with a SMC sampler is that it is not possible to use an optimal backward kernel and choosing a good one is not easy. So in [33], ABC-SMC was derived from a Sequential Importance Sampling (SIS) algorithm of [55]. Arguably, this is the most reasonable version of the ABC-SMC and has been employed in other works such as [35, 56].

The ABC-SMC begins similar to the ABC-rejection where a prior distribution, $\pi(\theta)$, tolerance value, ϵ, distance function, d, summary statistics, S are chosen. In the first iteration, the value of ϵ is kept sufficiently high and this tolerance value keeps decrementing sequentially as the number of iterations increase. In the ABC-SMC intermediate distributions are generated for each iteration or population level. After the first iteration, sampling are performed from the intermediate distributions. In simple words, posterior generated at the end of an iteration becomes prior for the immediately next iteration and so on. The acceptance of a parameter depends upon the threshold criteria specific to the population level. After a parameter is sampled, it is perturbed using a defined perturbation kernel and get accepted if the threshold criteria is satisfied otherwise rejected. In this way, all the particles of a population level are generated by the algorithm. This step also facilitates the parallel sampling for all the particles, which is not possible in the ABC-MCMC. The algorithm converges at the end of final iteration, resulting into an approximate posterior distribution of the parameters corresponding to the chosen model.

The ABC-SMC will be used for the parameter estimation of wetland system in the later part of the thesis. A pseudo code of the ABC-SMC, as presented in [35], proceeds as follows.

Input number of iterations K and number of parameter samples L
prior $\pi(\theta)$ and error sequence $\epsilon_1 > ... > \epsilon_K$
At $k = 1$
  for $j = 1 : L$
    draw $\theta_j^* \sim \pi(\theta)$ and simulate $y_j^* \sim p(\mathrm{y}|\theta_j^*)$
    until $d(S(y_j^*), \mathrm{S}(y)) \leq \epsilon_1$
  end for
  set each weight $w_j^1 = \frac{1}{L}$
for $k = 2 : K$
  for $j = 1 : L$
    sample θ_j^* from $\theta^k - 1$ with probabilities w^{k-1}
    perturb θ_j^* to obtain $\theta_j^{**} \sim \zeta(\theta|\theta^*)$
    simulate $y_j^* \sim p(\mathrm{y}|\theta_j^{**})$ until $d(S(y_j^*), \mathrm{S}(y)) \leq \epsilon_k$
  end for
  Set each $\theta_j^k = \theta_j^{**}$
  Set each $w_j^k = \frac{\pi(\theta_j^k)}{\sum_{i=1}^{L} w_i^{k-1} \zeta(\theta_i^{k-1}|\theta_j^k)}$, and normalise
end for

θ_j^K obtained at the end of this loop is an estimate of the posterior distribution $\mathrm{p}(\hat{\theta}|\mathrm{y})$, where ζ is a parameter perturbation kernel, which can be a uniform or Gaussian random walk.

3.3 ABC theoretical advancements

ABC is a new framework and so lots of researches towards the theoretical advancements are underway. There are many areas in ABC where improvements are needed. The most important issue is the limitation of ABC in dealing with high dimensional parameter inference. An ABC algorithm in its standard form does not exhibit satisfactory performance with the high dimensional parameter space. On occasions like model selection using ABC, this problem can be harnessed in a positive way by selecting a low dimensional and simple model among the candidates. However, this does not eliminates the need to make ABC functional in inferring the parameters of a high dimensional problem.

Second issue in an ABC method is the choice of summary statistics. An ABC replaces the need of likelihood calculation but at the cost of computational power and an approximation in the form of summary statistics. There can be a wide

range of summary statistics applicable for a given data, not all of them can assimilate the necessary information and so a comparison of the summary statistics between simulated and observed data may not provide correct result. Thus, a protocol should exist for choosing an appropriate summary statistics.

Third problem with an ABC, particularly ABC-SMC is a choice of tolerance value at each iteration. In ABC-SMC an ϵ value is chosen at the beginning in a manner, such that the algorithm does not get stuck in low acceptance probability region of the prior distribution. This ad-hoc choice of ϵ does not guarantee an unbiased parameter inference. The choice of threshold value gets further complicated in the intermediate distributions. Ideally, the tolerance should be decreased sequentially but an equal amount of decrease in ϵ may cause the algorithm to slow down substantially towards in the last iterations. Hence, a proper theoretical guidelines must be made available for the practitioners.

The ABC framework emerged because of the likelihood complications. Generally a practitioner do not possess a high mathematical skills and so evaluating the complex integrals can be cumbersome tasks for them. ABC provides the flexibility to draw inferences solely from the data and computational facilities. All the above mentioned theoretical challenges must be addressed properly in order to make ABC acceptable in a wide range of applications. In the following paragraphs many recent theoretical developments in ABC will be covered.

3.3.1 High dimensional issue

ABC is a powerful method especially when the likelihood is intractable but it suffers from the curse of dimensionality. As the dimension of the parameter set increases, it becomes difficult to estimate the posterior. The high dimensionality problems in ABC is addressed in [57]. In this work, a machine-learning based method, for designing a functional relationship between generated summary statistics and the parameters are presented. This method seems to be a solution of many high dimensional problems of ABC in ideal scenarios. In reality the construction of such a function will only be an approximation and may not estimate the posterior in all the conditions [57].

ABC method is made to work in high dimension using Gaussian copula in [58]. In this approach, firstly bivariate posterior of all the pairs of parameters are estimated by using a two-dimensional Gaussian copula. Thereafter, these estimates are merged together to estimate the joint posterior distribution of parameters. As a by-product, this method provides an analytical expression of the joint posterior, which acts as an approximation of the likelihood. The copula structure obtained in this method will be more realistic with increase in sample size and as the true pos-

terior tends to normality. This method assumes a Gaussian dependence structure and may not give a reasonable approximation all the times.

These recent articles have provided some methods to make the ABC useful in high dimensional problem but this area needs to be researched further to come up with a robust theory for dealing with high dimension.

3.3.2 Summary statistics

A thorough review of summary statistics selection is articulated by [59]. According to this, the method of the best summary statistics selection falls into three categories: best subset selection, projection methods, and regularisation technique.

In the last few years, some interesting methods on the choice of summary statistics have appeared. A particular method of the selection of the best summary statistics among the candidate summary statistics, based upon the method of best subset selection is described in [60] . This literature uses the simulated annealing algorithm to search the best summary statistics from a set. Composite likelihood score function is used as a summary statistics to improve the accuracy of the posterior estimation in [61]. The method is exemplified using an extreme rainfall dataset. A method known as 'Maximum Mean Discrepancy (MMD)', which replaces the need of manual selection of summary statistics is discussed in [62]. The method has been named as K2-ABC by the authors and essentially it employs the MMD to build up a dissimilarity measures between the simulated and the actual observed data. A functional relationship between optimal choice of summary statistics and data is modelled using a kernel based distribution regression in [63]. Lately [64] has contributed towards optimising the weights of the distance functions in the ABC. All the summary statistics do not contain the desired level of information about the parameter of interest and so often it is not simple to weigh their significance intuitively. In this method, summary statistics are effectively combined in an automatically and adaptive manner using the optimum weights.

The accuracy of posterior distribution is very much dependent upon the choice of summary statistics. Above discussed literatures substantially contribute towards the optimum summary statistics choice but in order to cement the ABC framework, more robust techniques should be devised in due course of time.

3.3.3 Goodness of fit

Model selection is often the most discussed research topic in the ABC, whereas, goodness of fit is somewhat an ignored research area. In a situation, where all the candidate models poorly fit data, model selection using the Bayes' factor would

fail to figure out the best model. Goodness of fit belongs to the third step (model evaluation) of the Bayesian data analysis. In Bayesian framework, posterior predictive checks are very popular for the evaluation of goodness of fit. In such checks, fractions of times posterior predictive simulations differ from the observed summary statistics are calculated to obtain an index called the P-values [65].

It is quite reasonable to extend this idea to the ABC because summary statistics are calculated as part of the parameter inference and extra computations would not be required. The posterior predictive P-values are not calibrated well and this might make this index less useful on many occasions. Classical hypothesis testing framework is used to propose two types of GOF statistics in [66]. First GOF statistics is D_{prior}, calculated by taking into account the average distance between observed summary statistics and the simulated summary statistics, generated with the prior distribution. While demonstrating the first GOF statistics, summary statistics were calculated repeatedly for all the Monte Carlo samples in [66]. The P-values were uniformly distributed in this case and indicates that this first statistics is calibrated. Statistical power shows a great variations from 20 % to 100 % in the simulation example. Second goodness of fit statistics is D_{post}, which is similar to the first one methodically except one difference, that here posterior is used instead of prior. Statistical power improves in this case at the cost of increased computational power.

3.3.4 Miscellaneous topics under ABC

In this sections some miscellaneous and recent theoretical advancements under a wider realm of ABC will be discussed. Asymptotic properties and efficiency of ABC are rigorously explored in [67, 68]. The posterior mean of an ABC is asymptotically unbiased, when proposal distribution is chosen with suitable scale and location [68]. Another necessary condition is the similarity in dimension of summary statistics and parameter vectors.

The ABC-MCMC was introduced as an improvement over the ABC-rejection. In section 3.2.2, the limitations of the ABC-MCMC were discussed. The ABC-SMC appears to be more efficient and easy to implement than ABC-MCMC but in reality it is prone to some unwanted bias during the weight assignments of the particles. Theoretical statistics community is working continuously towards improving the ABC-MCMC [69, 70]. The algorithm in [70] is primarily based upon the MCMC with some modifications. In this algorithm, ideas from the subset-simulation [71], a rare-event sampler and ABC are combined together for an improved convergence. This algorithm is an improvement over the ABC-MCMC, as there is no burn-in and difficulties of initialising the chain can be avoided. Despite these

promising features the algorithm has not found many applications as compared to the standard ABC algorithms.

An adaptive SMC for ABC [72] is an improvement over the other ABC-SMC methods. The computational complexity of most of the ABC-SMC is quadratic in the number of Monte Carlo samples. In this literature, an adaptive SMC is proposed, which reduces the computational complexity from quadratic to linear in the number of Monte Carlo samples and as the name suggests, the simulation parameters are also determined adaptively as the algorithm runs. The algorithm performance is demonstrated on a toy example and the software is made available in the open source.

A regression adjustment method takes into account the frequently present linear relationship among the ABC-generated summary statistics and the model parameter in a neighbourhood of the observed summary statistics [50]. This kind of adjustment allows a higher tolerance value without affecting the posterior estimation much and hence the computational efficiency also increases. Similar idea was extended in [73] to obtain a regression adjustment using a method called the General Linear Model (GLM). The method was applied for selecting the models describing the population of western chimpanzees (Pan troglodytes verus). This method is not able to outperform regression adjustment methods but arguably it fits naturally into a standard Bayesian framework. Hence the standard methodologies pertaining to the domain of the Bayesian framework such as model averaging, model selection via Bayes' factors can be applied in this method.

Choosing a right perturbation kernel is a key step in the ABC-SMC algorithm. A locally adapted kernel is shown to enhance the overall performance of the ABC-SMC by reducing the computational requirements in [74].

3.4 ABC applications

In the late nineties, the idea of the ABC-rejection was pitched [49] and since then, ABC gained the momentum as a promising framework to deal with intractable likelihood scenarios. Initially, ABC was deemed as a technique suitable for the population genetics. Later on and particularly in the last ten years, ABC started drawing attention among the practitioners from a wide range of fields. Ecology, epidemiology, and systems biology dynamics show some resemblance at least structure wise [33]. Many key features in these areas can be represented by dynamic models either stochastic or deterministic in nature. Systems of ordinary and partial differential equations are typically used for explaining the dynamics in deterministic scenario, whereas, stochastic differential equations are employed

for stochastic models. Often a practitioner is interested in comparing various candidate models so that the one explaining the dynamics fairly are figured out. ABC plays significant roles in these application areas. The likelihood evaluation for each candidate model in these areas are difficult and sometimes impossible because of latent variables.

3.4.1 Population genetics

In population genetics, a dataset primarily comprises of haplotypes from populations and frequencies of alleles. The aim of modelling analysis is often to perceive the demographic history of the populations. The parameters of interests are generally migration rates, variation in population size, frequencies of demographic events like colonisations etc [52]. Some of the prominent literatures where ABC is employed in population genetics are [49, 50, 75]. A thorough review of ABC in population genetics can be found in [52].

3.4.2 Epidemiology

The aspects of ABC in drawing inferences from a stochastic epidemic model are described in [76]. Recently, the application of ABC for spatial SEIR(S) epidemic models is shown in [77]. The authors have developed an open-source software known as the ABSEIR during this piece of research. ABC was used for estimating the key TB transmission parameters such as, net transmission rate, doubling time and reproductive value of the pathogen in [78]. The estimation results provide the extent of the TB spread as an epidemic and are consistent with the observed dataset.

3.4.3 Systems biology

One of the earliest application of ABC in systems biology is reported in [79]. Here data on tumour mutations are used for parameter inference in a branching process model using the rejection sampling version of the ABC. The meta-hydration data from cancerous cells are used for estimating parameters linked to differentiation of cells and tissues in [80]. Recently, under the domain of systems biology, ABC is used to quantify cell-cell adhesion parameters in a cell migratory process [81]. A very useful software package in Python (ABC-SysBio) was introduced a few years ago, which can be used for calibrating models in systems biology using the ABC-SMC approach [82].

3.4.4 Ecology

Compared to other prominent application areas of ABC, ecology has not witnessed much use of ABC so far. The validation of agent based models in ecology appears to be feasible through ABC mechanism [52, 83]. The ABC-MCMC is applied in inferring species abundance data in [84]. A neutral ecological model was analysed to the infer the parameters related to regional speciation rates and local immigration of species in [85].

3.4.5 Other miscellaneous applications

ABC is used for the characterisation of mono-disperse and poly-disperse nanoparticle aggregates using the observed scattered light in [86]. ABC enables the integration of Crop Growth Model (CGM) with the Whole Genome Prediction (WGP) methods through the estimation of parameters using rejection sampling. The incorporation of CGM improves the prediction accuracy with the added biological information in WGP and thus ABC can be very useful in genomics applications [87]. ABC is applied in historical research under a new framework known as 'model based history'. Such kind of modelling approaches in historical researches can enable the historians to re-analyse the decades older hypotheses [88]. An application of ABC in cosmology is shown in [89]. An open-source software known as the astro-ABC is also described in this literature. In addition to the standard ABC implementation, this package incorporates the MPI (massive parallelisation) framework so that multiple nodes are harnessed for the simulation. The cosmological parameter inference involves non-Gaussian data, noise, multi-probe correlated datasets. The literature demonstrates that how ABC is more effective in such cases compared to the MCMC approaches. Usage of ABC in archaeology is demonstrated in [90, 91]. ABC can offer the best model selection as well as parameter estimation simultaneously. In a molecular dynamic application [92], ABC subset-simulation [70] is used and the inference results indicate the potential of ABC in many related fields such as material science.

3.4.6 Model selection

ABC has been employed in a few dynamical model selection algorithms. In general ABC is capable of figuring out the best model depending upon how efficiently a model describes the given data. This idea was formalised through an ABC-SMC model selection algorithm in [33]. This algorithm is shown to be effective in selecting the best model among candidate SIR models.

The ABC-SMC model selection is prone to falter as the number of competing models increase. Therefore, in its current form, this algorithm cannot be applied in model structure detection problem under the system identification methodology. In system identification, model structure detection is a considered as the toughest part. ABC is employed in developing two types of model structure detection algorithms, known as one-stage and two-stage model structure detection respectively in [35] .

3.5 Conclusion

This chapter provides the principles and applications of the ABC methodology. The various types of ABC algorithms starting from the basic rejection to a more practical method known as the ABC-SMC are provided with necessary details. In the forthcoming chapters, the ABC-SMC will be used for parameter inference in wetland systems as well as calibration of weathering models. Therefore, a proper pseudocode representation of the ABC-SMC is included in this chapter.

ABC method appears to be very promising as the difficulties of the likelihood evaluation are replaced. However, in the mainstream statistical communities there are apprehensions about the accuracy of this approach particularly the SMC version of the ABC. In addition, an ABC method fails to exhibit satisfactory performance in high dimensional scenarios. The choice of threshold values and summary statistics also need to be researched further. This chapter succinctly tries to review the recent theoretical advancements in ABC.

In the last part of this chapter, important applications of ABC are discussed. A wide range of applications clearly suggests that ABC is not constrained within a particular discipline. In fact as a simulation based and likelihood free approach, this is the preferred choice for many practitioners. In the forthcoming chapters, ABC will be shown to be a powerful tool in environmental system class.

Chapter 4

NARX model structure detection under ABC framework

4.1 Introduction

Nonlinear Autoregressive Exogenous (NARX) models are one of the most popular model class in the System Identification (SID) methodology. In general, an SID involves Model Structure Selection (MSS) and parameter estimation. The parameter estimation part is a simple task and can satisfactorily be performed under a deterministic framework. On the other hand, the task of MSS is not so straightforward and requires additional rigour on most of the occasions.

In a linear system, an MSS is relatively simple and commonly based upon the Akaike Information Criterion (AIC), Bayesian Information Criterion (BIC) kind of indices. Essentially these indices map the model accuracy with the model size to figure out the 'true' model. In nonlinear systems, these techniques fail to provide the accurate result as regressors can be arranged differently in a NARX model to return the same model size [37, 93]. A simpler model structure is always desired and more often the underlying science of a system can be explained through a concise model [18]. A regularisation criteria, such as, the Least Absolute Shrinkage Selection Operator (LASSO) [94] can be used to shrink the model size through penalising the model size but cannot be a precise solution for an appropriate MSS.

In a nonlinear system, the most popular method for MSS is based upon the Error Reduction Ratio (ERR) index [18, 30]. In simple words, this method works on the incremental model building principle. At each step, the importance of all the candidate regressors are evaluated and the one having the potential to improve the model performance is added in the model terms. A forward regression version of this method is known as the Forward Regression Orthogonal Least

Square (FROLS) and there are plenty of literatures on MSS using the ERR principle [32, 95, 96].

In this study, a novel algorithm, ABC-NARX-MSS, inspired from the Approximate Bayesian Computation (ABC) for the MSS in a NARX model class will be presented. In the previous chapter, ABC principle and its applications have been discussed in detail. The ABC-NARX-MSS mimics the Sequential Importance Sampling (SIS) feature from the ABC-SMC and randomly samples the model terms from a regressor set. Instead of terms-ordering based upon their contribution in the model performance, this method performs a global search in the pool of regressors to find out the optimal model structure. The number of candidate models increases tremendously as the number of regressors are increased. For many practical systems such as tropical wetlands, the maximum input-output lags can go very high, subsequently increasing the candidate terms and models. Therefore, a global search methodology in the NARX model class should be computationally efficient as well. The proposed NARX structure selection algorithm fits into the currently available computational budgets.

The chapter unrolls with basic principles of the ABC-NARX-MSS and a simple pseudocode representing the algorithm. Thereafter, the performance of this algorithm on a known example system will be presented. A comparison between the Orthogonal Forward Regression (OFR) and the ABC framework, based on the same system will also be provided. An MSS algorithm generally performs satisfactorily on a known system as the data generation takes place through the same system. The situation gets more complicated when an unknown system comes into play. Therefore, a complete SID cycle of a Canadian wetland is presented in the subsequent section. The identification of this unknown system is carried out under the ABC framework, in which the term selection part is governed by the ABC-NARX-MSS. Finally, the chapter ends with some concluding remarks.

4.2 ABC-NARX-MSS algorithm

In order to address the issues surrounding the existing MSS methods, as discussed in the Chapter 2, a novel ABC based method (Algorithm 4.1) for detecting the optimum NARX structure will be presented here. This MSS method is a global search procedure, where all the possible combinations of the regressors are within the search space. Earlier usage of ABC in an SID context performed a type of local search by ranking the regressor terms [35]. Another key feature of the ABC-NARX-MSS algorithm is its simplicity. It actually mimics the traits of the ABC-SIS by sequentially tightening the threshold criteria at each iteration and the sampling

in an iteration is based upon the information generated at the previous iteration. A global search method proposed using the Reversible Jump Markov Chain Monte Carlo (RJMCMC) [36] suffers from a wide range of complexities, as discussed in the Chapter 2. At the same time, the implementation and adaption is also not simple for [36]. The ABC-NARX-MSS algorithm also passes the generalisation test as compared to the Randomized Model Structure Selection (RaMSS) [37]. There are no tuning parameters for assessing regressors performance in the Algorithm 4.1.

The Algorithm 4.1 is a pseudo code representation of the ABC-NARX-MSS algorithm. Foremost step in this method is the normalisation of input-output data. The code presented here is for the Single Input Single Output (SISO) system, so the y and u are in vector form. In Multiple Input Multiple Output case (MIMO), these vectors will be replaced by matrices. The number of samples L is directly proportional to the computational requirements. Like any Monte Carlo sampling, higher value of L is preferred as long as that fits into the available computational budget. The threshold values $\epsilon_1 > ... > \epsilon_k$ must be chosen very carefully. The Chapter 3 highlights some of the important issues in the ABC framework and the choice of threshold values is one of the open research problem in the ABC. Practically, a very small value of ϵ_1 would make the algorithm very slow and the convergence time might tend to infinity. Too large value of ϵ_1 would return the redundant particles which could affect the further iterations. The regressor set REG should take into account the maximum plausible time lags of the system. Like any MSS algorithm, this is a crucial step here as well.

In the first iteration, number of terms (n) in a candidate model are sampled from a uniform distribution of integers, ranging from 1 to the maximum number of regressor terms possible for the assigned values of n_u (input lag), and n_y (output lag). Corresponding to the number of terms in a candidate model, regressors (reg) are sampled from their uniform priors. Regressor indices as presented in the Table 4.1 forms the basis of regressor sampling. Thereafter, parameter estimation step can be performed by either least square or ABC. A deterministic approach like the least square method is a computationally efficient way. Another way is to use a probabilistic method such as ABC rejection. In the numerical example and case study performed in this chapter, the ABC rejection was used for parameter estimation. The important point to be noted here is that, there must be a limit to the maximum number of sampling steps while using ABC rejection. Otherwise, the algorithm might get trapped in a poor model sampling and might never converge. The distance function $d(.)$ used for comparing the model performance can be something similar to L_2 norm or Mean Squared Simulation Error (MSSE).

Because of a dynamical process under study, the datasets can be compared directly without using summary statistics [33]. The histograms corresponding to the n ($prob_N$) and reg ($prob_{Reg}$) provide a distribution for these discrete variables. These distributions contain the information about regressors performance and accordingly influence the sampling in the next iteration. In the upcoming sections, the performance of this algorithm on a numerical example and an unknown real system will be discussed.

4.3 Regressor set

A NARX model structure is composed of a combination of regressors. A regressor is composed by a union of the lagged form of the system input-output variables. The amount of lags are pre-determined, depending upon the nature of the system. The total possible number of regressors in a full NARX model, is calculated by the equation 4.1 [18], where ν is the sum of maximum output lag, n_y, and maximum input lag, n_u. The l stands for the degree of polynomial, which is typically set to 3 for most of the practical purposes. The equation 4.1 suggests the amount of increase in the regressors with increase in n_y and n_u.

Generally, a NARX model does not contain the full set of regressors and a combination of these terms serve as a parsimonious model structure. For M number of regressors, there can be 2^M number of possible model structures. In this chapter, two systems will be evaluated for the ABC-NARX-MSS algorithm and both of these exhibit the same amount of input-output lag, equal to 2. The rationale behind these lag values will be elaborated in the upcoming sections. For the moment, all the regressors corresponding to n_y and n_u equal to 2 are presented in the Table 4.1. The value of l is kept 3 in this expansion.

$$M = \frac{(\nu + l)!}{\nu! l!} \tag{4.1}$$

4.4 Numerical example

The ABC-NARX-MSS algorithm was used to perform the MSS task on a known system adopted from [36]. The system (equation 4.2) is dynamic in nature and can be described as,

$$y(t) = 0.7y(t-1)u(t-1) - 0.5y(t-2) + 0.6u^2(t-2) - 0.7y(t-2)u^2(t-2) + e(t), \tag{4.2}$$

Algorithm 4.1 NARX model structure detection (ABC-NARX-MSS)

$counter_1 \leftarrow 0$
Initialise: Input data (u), output data (y), no of iterations (K), no of samples (L), full regressors set (REG), error sequence $\epsilon_1 > ... > \epsilon_k$
At $k = 1$
  while $counter_1 < L$
    Randomly sample no of terms (n) from N; where N is a uniform distribution of integers starting from 1 up till the maximum number of regressors in the set REG.
    Randomly sample the regressor indices from a uniform distribution of REG, based upon the value of n. The regressors must be unique. This leads to a regressor subset (reg), which combines to form a candidate model (M)
    Estimate the parameter of M. This can be performed by either least square or the rejection sampling (ABC rejection). In case of ABC, constrain the maximum possible parameter sampling steps.
    Simulate the candidate model M
      if $d(.) < \epsilon_1$
        $counter_1 \leftarrow counter_1 + 1$
      else
        reject the model.
  end while loop
Generate the histogram ($prob_N$) for the 'n' of all the 'L' models
Generate the histogram ($prob_{Reg}$) for the 'reg' of all the 'L' models
for $k = 2 : K$
  $counter_k \leftarrow 0$
    while $counter_k < L$
      Randomly sample n from $prob_N$
      Randomly sample the regressor indices from $prob_{Reg}$, depending upon the n. The regressors must be unique. This leads to a regressor subset (reg), which combines to form a candidate model (M)
      Estimate the parameter of M
      Simulate the candidate model M
        if $d(.) < \epsilon_k$
          $counter_k \leftarrow counter_k + 1$
        else
          reject the model.
    end while loop
Generate the histogram ($prob_N$) for the the 'n' of all the 'L' models
Generate the histogram ($prob_{Reg}$) for the 'reg' of all the 'L' models
end for loop

Index	1^{st} linear element	2^{nd} linear element	3^{rd} linear element
1	$y(t-2)$		
2	$u(t-2)$	$u(t-2)$	
3	$y(t-1)$	$u(t-1)$	
4	$y(t-2)$	$u(t-2)$	$u(t-2)$
5	$y(t-2)$	$y(t-2)$	$u(t-2)$
6	$y(t-1)$	$y(t-1)$	$u(t-1)$
7	$y(t-2)$	$y(t-2)$	
8	$u(t-2)$		
9	$u(t-1)$	$u(t-1)$	$u(t-1)$
10	$y(t-1)$	$y(t-2)$	$y(t-2)$
11	$y(t-2)$	$u(t-2)$	
12	$y(t-1)$	$u(t-1)$	$u(t-1)$
13	$u(t-1)$	$u(t-2)$	$u(t-2)$
14	$y(t-2)$	$y(t-2)$	$y(t-2)$
15	$y(t-1)$	$u(t-1)$	$u(t-2)$
16	$y(t-1)$	$y(t-2)$	
17	$y(t-2)$	$u(t-1)$	$u(t-1)$
18	$y(t-1)$	$y(t-1)$	
19	$y(t-1)$	$u(t-2)$	$u(t-2)$
20	$y(t-1)$		
21	$u(t-1)$	$u(t-1)$	$u(t-1)$
22	$y(t-2)$	$u(t-1)$	
23	$y(t-1)$	$y(t-1)$	$u(t-2)$
24	$u(t-1)$	$u(t-1)$	
25	$u(t-1)$	$u(t-2)$	
26	$y(t-1)$	$y(t-2)$	$u(t-1)$
27	$y(t-1)$	$y(t-1)$	$y(t-2)$
28	$y(t-1)$	$y(t-1)$	$y(t-1)$
29	$y(t-1)$	$y(t-2)$	$u(t-2)$
30	$u(t-1)$		
31	$y(t-2)$	$y(t-2)$	$u(t-1)$
32	$y(t-1)$	$u(t-2)$	
33	$u(t-1)$	$u(t-1)$	$u(t-2)$
34	$y(t-2)$	$u(t-1)$	$u(t-2)$

Table 4.1: Candidate regressor terms. Each term has a maximum polynomial order of 3, which means at the most 3 linear terms in product form can constitute a regressor term.

the input signal $u(t)$ is assumed to be white noise, uniformly distributed in the interval [-1, 1]. The $e(t)$ is assumed to be white noise with a Gaussian distribution. The mean and standard deviation for this Gaussian distribution are set to 0 and 0.01 respectively. The standard deviation for $e(t)$ in [36] was kept at 0.004, which has been purposely increased to 0.01 here to test the performance of the algorithm

in an increased level of noise.

A brief description of the RJMCMC based MSS steps followed in [36] to recover the model structure of this system has been presented in the Chapter 2. The same system (equation 4.2) was also used in [37] to test the RaMSS algorithm. Here, the Algorithm 4.1 is used to detect the model structure of the same system in a more noisy situation.

The remotely sensed environmental data used in this thesis consists of 156 data points. Therefore, the performance of this algorithm in MSS was assessed by constraining the total data points to 200. The rationale is very simple, that if the algorithm works satisfactorily on a known system under the limited number of data points then it should also work correctly for an unknown system having similar number of observations.

The ABC-NARX-MSS is fundamentally a sampling method of inference hence it should be run multiple times to gauge the uncertainty about the the sampling process [97]. Hence this algorithm was executed 10 times on the same input-output data. Out of 10 sequences, every time the algorithm converged to return 'true' model in the seven sequential steps. The L_2 norm was introduced as a distance measure $d(.)$ to compare a model performance with the specified threshold value, ϵ_k. The threshold values were set to, $\epsilon_1 = 3.5$, $\epsilon_2 = 3.0$, $\epsilon_3 = 2.5$, $\epsilon_4 = 2.0$, $\epsilon_5 = 1.5$, $\epsilon_6 = 1.0$, and $\epsilon_7 = 0.5$.

The MSS steps for a trial are shown here step wise step. The iteration number 1 to 4 are shown in the figure 4.1, whereas, the iteration number 5 to 7 are shown in the figure 4.2. The histograms corresponding to each iteration represent the regressors distribution ($prob_{Reg}$) and number-of-terms distribution ($prob_N$) respectively. Notations *reg* and *n* are exactly the same as used in the Algorithm 4.1. The indices of regressors in these histograms refer to the regressor set presented in the Table 4.1. The histograms corresponding to the iteration number 7 shows that all the four terms have been recovered accurately by the algorithm. The application of ABC-NARX-MSS on an unknown system will be discussed in the section 4.6.

4.5 Comparison between ABC-NARX-MSS and FROLS

This chapter presents a novel ABC-NARX-MSS algorithm, which is shown to be working accurately on a numerical example. In this section the ABC-NARX-MSS will be compared with the standard FROLS algorithm under the OFR framework [18]. There are some criticisms about the OFR framework in an SID, as discussed in the previous chapter, and the ABC-NARX-MSS or other similar works such as [36, 37] have tried to address those issues. Despite some issues with the OFR

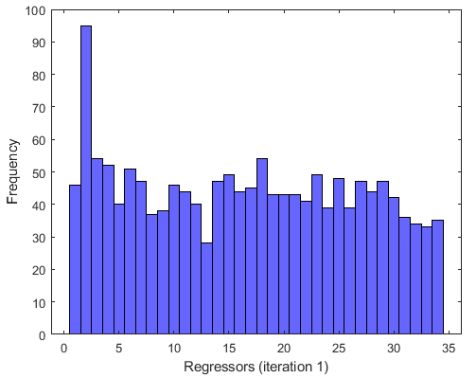

(a) Iteration 1 (*reg*)

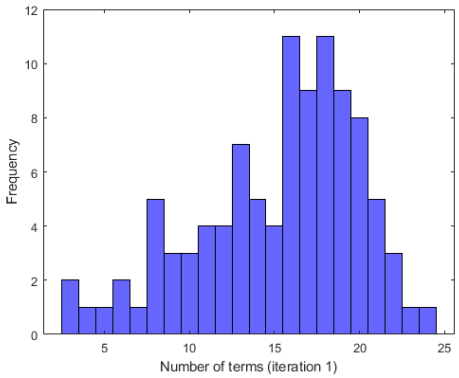

(b) Iteration 1 (*n*)

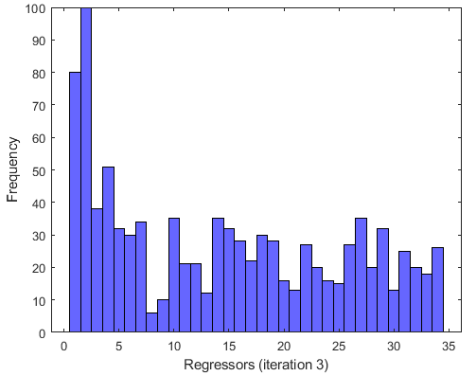

(c) Iteration 3 (*reg*)

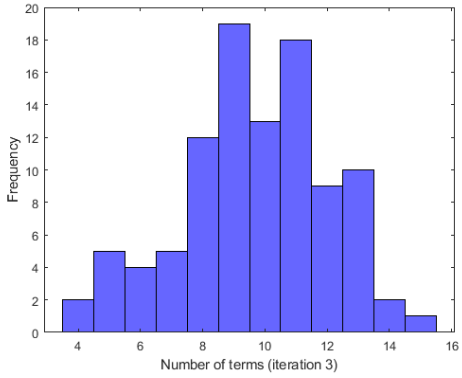

(d) Iteration 3 (*n*)

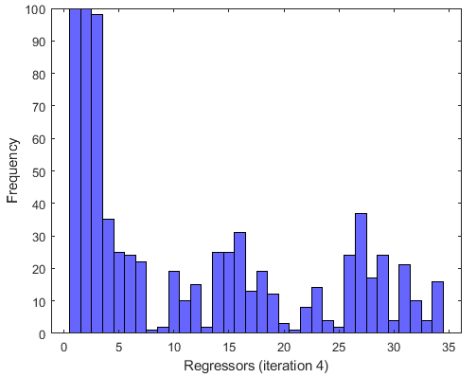

(e) Iteration 4 (*reg*)

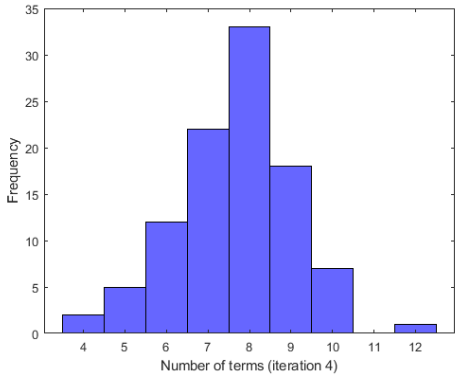

(f) Iteration 4 (*n*)

Figure 4.1: MSS steps for a known system (Iteration $1-4$).The histograms corresponding to regressors on the left hand side are essentially $prob_{Reg}$ mentioned in the Algorithm 4.1 , whereas, the histograms corresponding to number of terms on the right hand side represent $prob_N$.

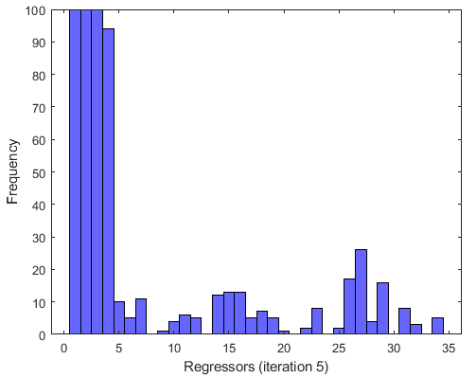

(a) Iteration 5 (*reg*)

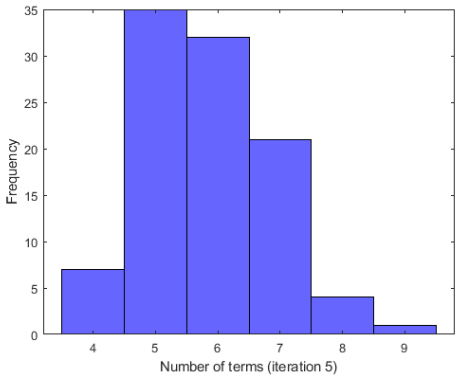

(b) Iteration 5 (n)

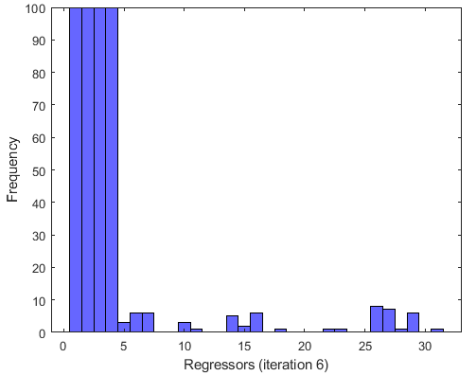

(c) Iteration 6 (*reg*)

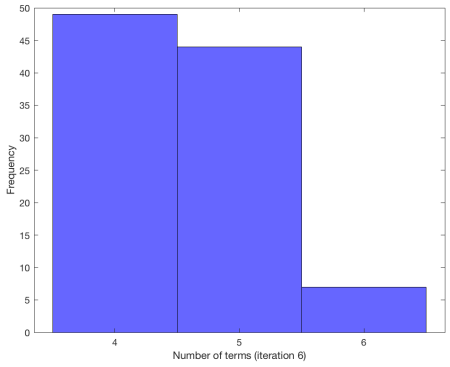

(d) Iteration 6 (n)

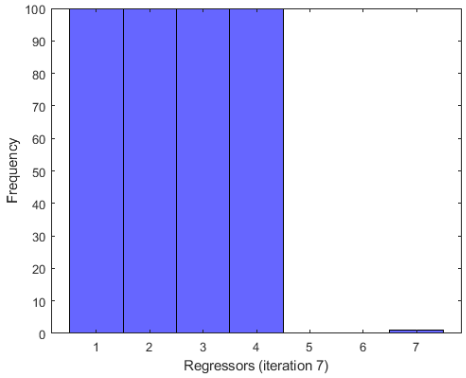

(e) Iteration 7 (*reg*)

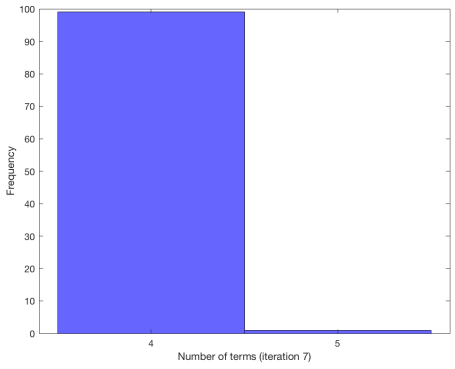

(f) Iteration 7 (n)

Figure 4.2: MSS steps for a known system (Iteration $5-7$). The histograms corresponding to regressors on the left hand side are essentially $prob_{Reg}$ mentioned in the Algorithm 4.1 , whereas, the histograms corresponding to number of terms on the right hand side represent $prob_N$.

framework, it is still the most popular approach especially in the control theory. The prime reason behind this popularity is its computational efficiency. On most of the occasions, the FROLS is able to identify the model correctly. Therefore, the FROLS was applied on the example system (equation 4.2) to highlight the benefits of the ABC-NARX-MSS algorithm.

The numerical example (equation 4.2) used in this chapter has previously been chosen in the [36, 37] to demonstrate the performance of the respective MSS algorithms. The data generation and the noise level were kept similar to the section 4.4. The FROLS algorithm was applied thrice on the equation 4.2. Firstly, the n_y and n_u were set to 2, then to 3 and finally to 4. With increase in the maximum lag values, the number of candidate regressors also increases. The total number of terms for the Case 1 ($n_y = n_u = 4$) is 164, for the Case 2 ($n_y = n_u = 3$), the value reduces to 83 and for the Case 3 ($n_y = n_u = 2$), the number of regressors in the superset reaches to 34. The results of the FROLS algorithm for the Case 1 are summarised in the Table 4.2, where, the linear components of each term are separated by columns. The 'ERR' denotes the error reduction ratio, and the 'Parameter' is the estimated parameter. Similarly, the results for the Case 2 are summarised in

Term	1^{st} lin. element	2^{nd} lin. element	3^{rd} lin. element	ERR	Parameter
1	$y(t-4)$	$u(t-2)$	$u(t-2)$	0.4525	0.0171
2	$y(t-2)$			0.2458	-0.2040
3	$y(t-1)$	$u(t-1)$		0.1822	0.7754
4	$u(t-2)$	$u(t-2)$		0.0931	0.6007
5	$y(t-2)$	$u(t-2)$	$u(t-2)$	0.0258	-0.8104

Table 4.2: Summary of FROLS results corresponding to the Case 1.

the Table 4.3. The results of the most simplistic scenario, Case 3 are summarised

Term	1^{st} lin. element	2^{nd} lin. element	3^{rd} lin. element	ERR	Parameter
1	$u(t-2)$	$u(t-2)$		0.4635	0.6047
2	$y(t-2)$	$u(t-2)$	$u(t-2)$	0.3274	-0.6960
3	$y(t-2)$			0.1041	-0.5075
4	$y(t-1)$	$u(t-1)$		0.1036	0.7620

Table 4.3: Summary of FROLS results corresponding to the Case 2.

in the Table 4.4.

The ERR criteria based ranking corresponding to the existing structure can lead to the inclusion of a redundant term in the beginning phase of the FROLS algorithm. This clearly reflects in the Case 1 results as shown in the Table 4.2. The first term picked by the FROLS is not a 'true' term and there is no way to prune away that term in the original version of the algorithm. However the later

Term	1^{st} lin. element	2^{nd} lin. element	3^{rd} lin. element	ERR	Parameter
1	$y(t-2)$			0.4747	-0.4870
2	$u(t-2)$	$u(t-2)$		0.3353	0.5998
3	$y(t-1)$	$u(t-1)$		0.1460	0.6942
4	$y(t-2)$	$u(t-2)$	$u(t-2)$	0.0433	-0.7118

Table 4.4: Summary of FROLS results corresponding to the Case 3.

modified versions of the FROLS such as [32] can sort out this issue with an iterative mechanism. As the number of candidate regerssors decrease due to reduced model order in the Case 2 and Case 3, the FROLS managed to pick up the correct terms as shown in the Table 4.3 and 4.4 respectively.

The ABC-NARX-MSS algorithm in principle does not pick up a term unless the model constituted from the term satisfies the threshold criteria of a particular iteration. As the iteration level of the ABC-NARX-MSS increases, the threshold criteria gets further narrowed and any redundant regressor will not be picked up. Eventually, the exclusion of a poor regressor will get reflected into the regressor inclusion probability at the next iteration. However, the ABC-NARX-MSS will get slower if the maximum lag values are increased, but the underlying principle of the algorithm suggests that at the convergence 'true' model will definitely be chosen. One might have to increase the sequential step k, if a 'spurious' term is masking a 'true' term from getting selected. In any sequential sampling procedure under the ABC framework, ideally the final threshold value ϵ_K should be tending to zero.

4.6 SID of a real system using ABC-NARX-MSS

In this section, a full cycle of SID will be demonstrated for an unknown Canadian wetland under the ABC framework. A wetland is an inundated land surface, where the fraction of inundation exhibits variations throughout a year. The wetlands, their characteristics and modelling will be discussed in details in the forthcoming chapters of the thesis. In the present context, the Canadian wetland is simply an unknown dynamical system, which was identified using the ABC-NARX-MSS. Following the structure detection, ABC-SMC was employed for the parameter estimation of the Canadian wetland. The obtained model was simulated using a fresh dataset, obtained from the same source.

4.6.1 Model structure selection

The input and output of the wetland system are average temperature (Avg Tmp) and wetland fraction (fw) respectively, and shown in the figure 4.3. The criteria for input selection in a wetland will be discussed in the later chapters. Here, the emphasis is on testing the method (Algorithm 4.1) rather than characterising the Canadian wetland. The input-output data were transformed using the z-score standardisation to cast them into similar range.

The values of n_y and n_u were set to 2, similar to the numerical example (equation 4.2) and hence the regressors indices of the Table 4.1 are applicable here as well. The ABC-NARX-MSS steps are shown in the figure 4.4 and 4.5. All the notations such as, n and reg have the same meaning as mentioned in the Algorithm 4.1. The MSS algorithm nearly converged at the end of 19 iterations, which is comparatively higher than the numerical example demonstrated in the above section. This clearly indicates that detecting an unknown system is not simple and the number of iterations could go substantially high. For the sake of simplicity, n_y and n_u were constrained to 2. Incidentally, the choice of input-output lag matched with the model structure in this case and the Algorithm 4.1 converged. In cases, where the system can only be represented with higher lag values, the MSS algorithm might never converge and the initial choice of n_y and n_u would have to be tuned accordingly.

The model structure of the Canadian wetland can be formed by combining the regressor indices, 1, 21, 26 and 30, in any order. This results into a NARX representation of the system

$$y(t) = \theta_1 u(t-1) + \theta_2 y(t-2) + \theta_3 u^3(t-1) + \theta_4 y(t-1)y(t-2)u(t-1) + e(t) \quad (4.3)$$

4.6.2 Parameter estimation

The estimation of parameters corresponding to the obtained model structure is the next main step after the structure detection in an SID. Keeping in view the ABC framework, ABC-SMC was used for estimating the Canadian wetland parameters. The detailed features of the ABC-SMC have been presented in the previous chapter. The selection choice of the SMC version over the other variants of the ABC can also be deduced from the discussions of the previous chapter.

ABC-SMC generates the intermediate distributions, however, here only the posterior distribution corresponding to the final population level are presented in the figure 4.6. Instead of maximum a posteriori (MAP), mean value of these

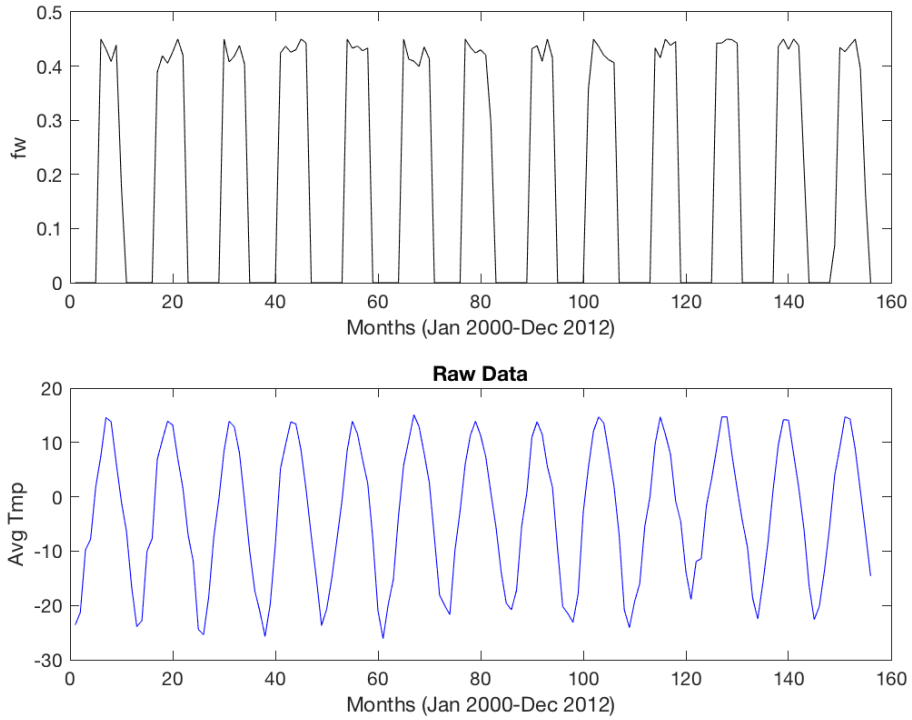

(a) Raw data (Canadian wetland)

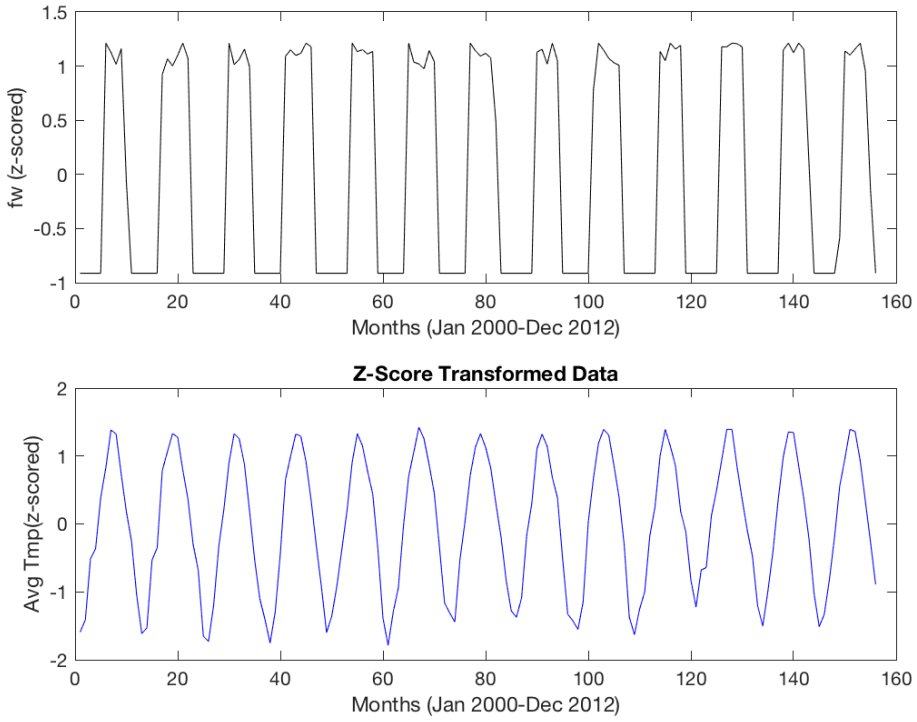

(b) Z-Scored data (Canadian wetland)

Figure 4.3: Input (average temperature) and output (wetland fraction) time series data from January 2000 until December 2012 − Canadian wetland.

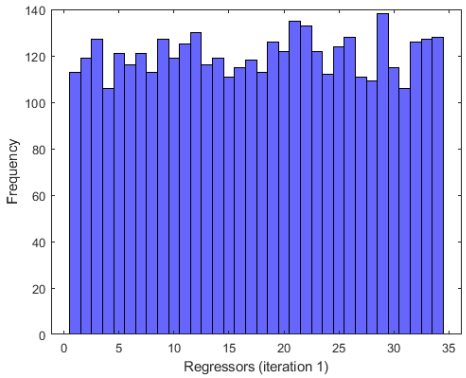

(a) Iteration 1 (*reg*)

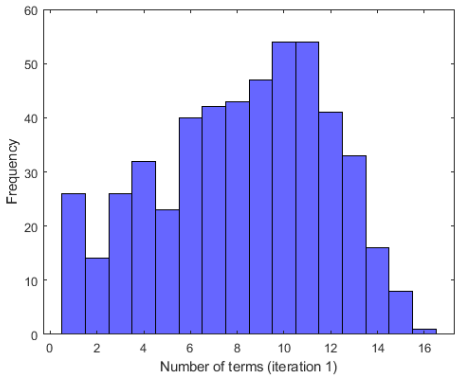

(b) Iteration 1 (*n*)

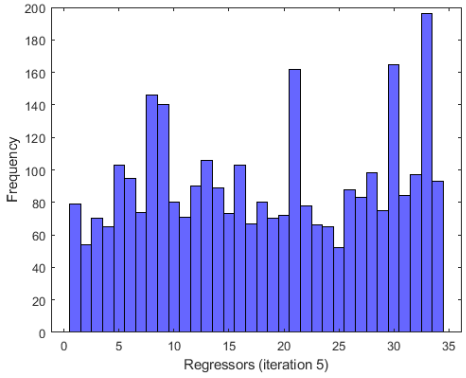

(c) Iteration 5 (*reg*)

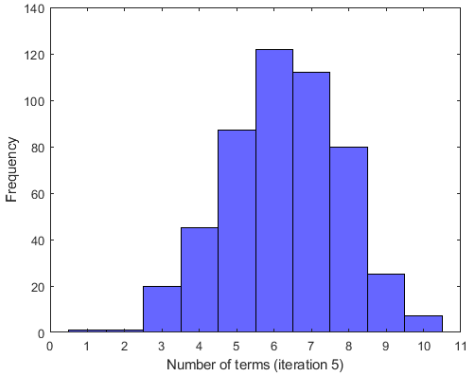

(d) Iteration 5 (*n*)

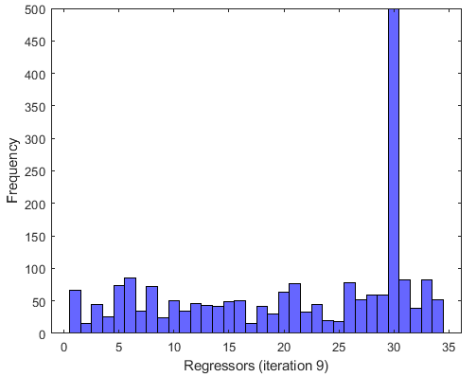

(e) Iteration 9 (*reg*)

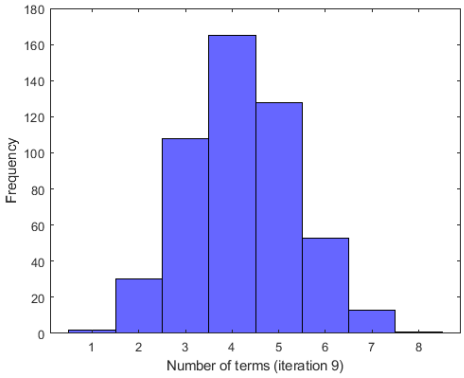

(f) Iteration 9 (*n*)

Figure 4.4: MSS steps for an unknown wetland system (Iteration $1-9$). The histograms corresponding to regressors on the left hand side are essentially $prob_{Reg}$ mentioned in the Algorithm 4.1 , whereas, the histograms corresponding to number of terms on the right hand side represent $prob_N$.

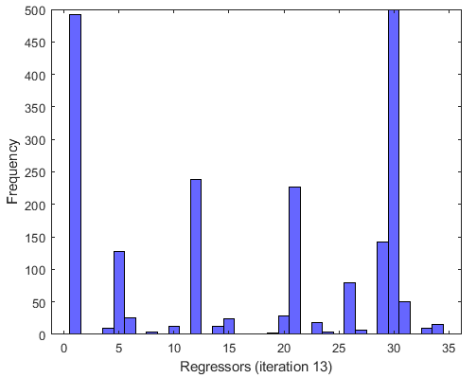

(a) Iteration 13 (*reg*)

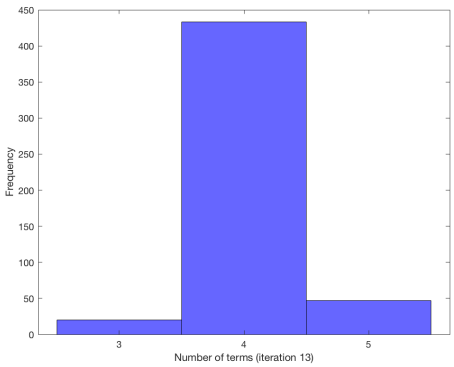

(b) Iteration 13 (*n*)

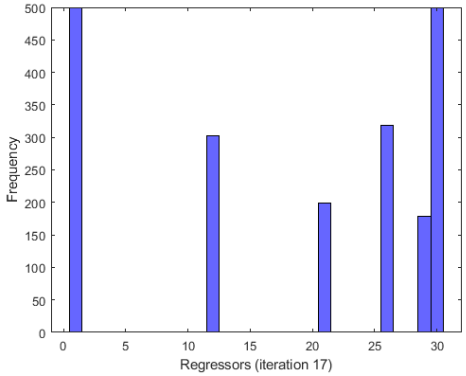

(c) Iteration 17 (*reg*)

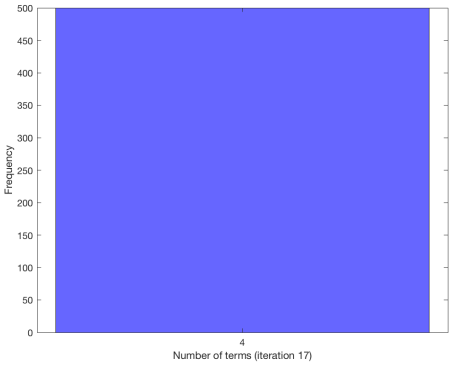

(d) Iteration 17 (*n*)

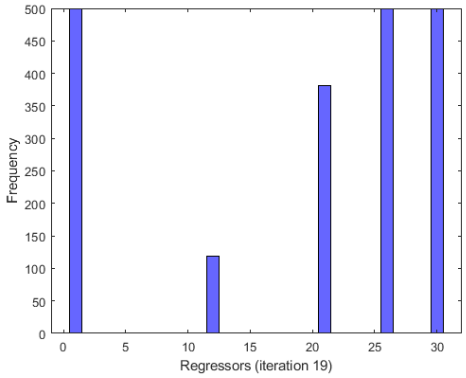

(e) Iteration 19 (*reg*)

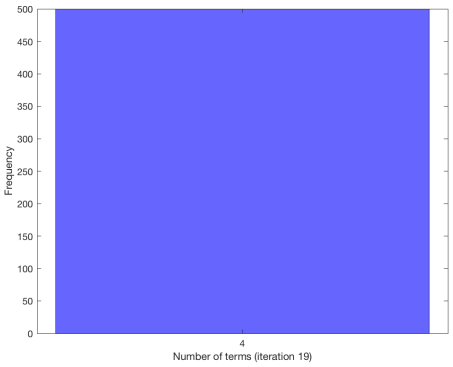

(f) Iteration 19 (*n*)

Figure 4.5: MSS steps for an unknown wetland system (Iteration 13 – 19). The histograms corresponding to regressors on the left hand side are essentially $prob_{Reg}$ mentioned in the Algorithm 4.1 , whereas, the histograms corresponding to number of terms on the right hand side represent $prob_N$.

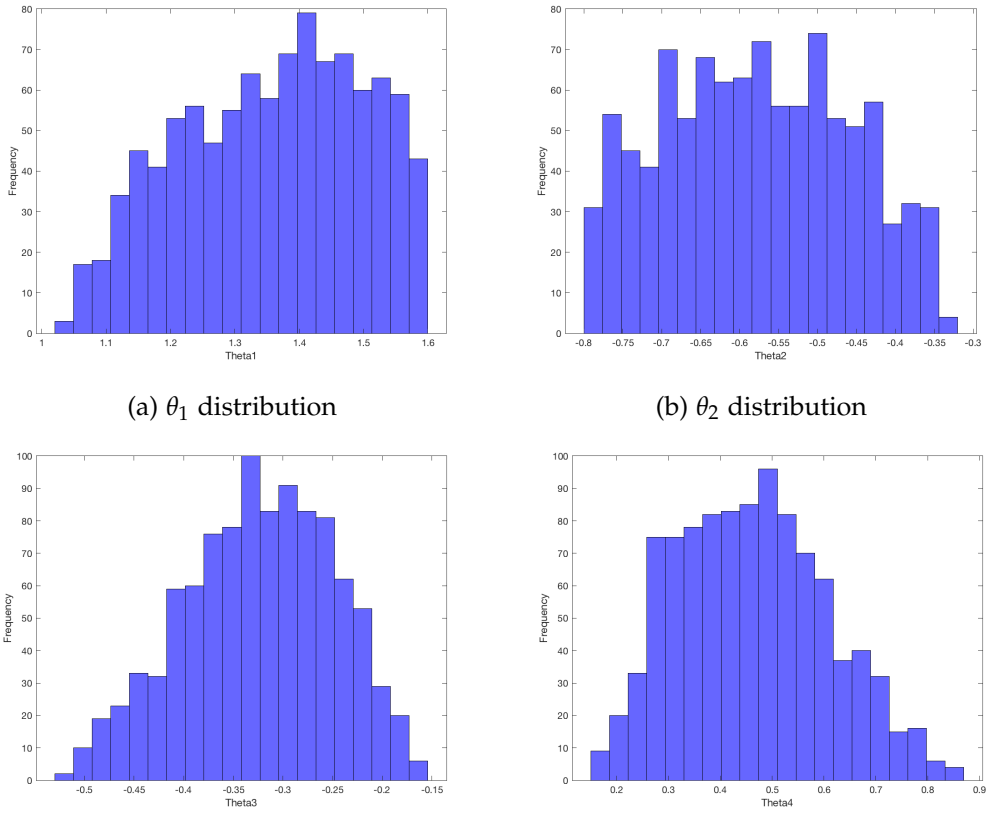

(a) θ_1 distribution

(b) θ_2 distribution

(c) θ_3 distribution

(d) θ_4 distribution

Figure 4.6: Posterior parameter distribution of Canadian wetland.

parameter distributions were plugged into the model simulation process.

4.6.3 Simulation results

In the beginning of this section, a NARX structure of the Canadian wetland was determined. The same model was then passed through the parameter estimation process and finally the averaging of parameter distributions provided a robust set of Canadian wetland parameters. These values were plugged into the model to obtain model predicted output. The full simulation result is shown in the figure 4.7. Approximately 50 % of the data (until 80^{th}) month was used for training the model, whereas, the remaining data from 81^{st} month onwards is a fresh testing data from the same source.

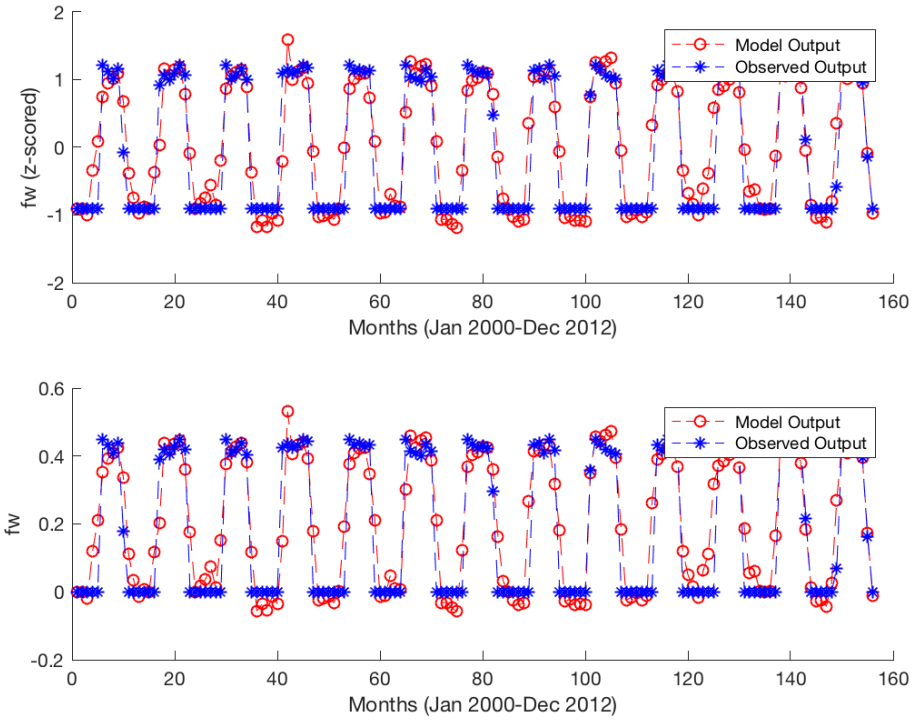

Figure 4.7: Model predicted output (MPO) simulation results for Canadian site. The simulation results are shown for the standardised data (top) and the data in its actual range (bottom), obtained after inverse transformation.

4.7 Conclusion

This chapter presents a novel algorithm for the terms selection in a NARX model class, based upon the ABC framework. The previous chapters on the reviews of SID have highlighted the possible issues associated with the MSS tasks in a local search method such as the FROLS. A local search typically involves the ranking of the regressors in order of their significance and ignores all the possible combination of those regressors. The criticism associated with a local search mechanism has mostly been addressed under probabilistic frameworks.

The ABC-NARX-MSS is another addition in a series of algorithms performing the global search in the regressors space. The algorithm mimics the SIS sampler and reduces code complexity by a straightforward sampling procedure. The sequential decrease in the threshold value ϵ ensures that the initial iterations do not get sluggish because of a poor prior choice. The significance of a regressor at each iteration is updated depending upon the number of times the regressor was picked up in the performing models. The algorithm was implemented using

a MATLAB script in this study but the provided pseudocode can be utilised easily for extension to any other platforms such as Python. The algorithm can also be adapted to include the models apart from NARX, nevertheless, the sampling procedure would remain the same and in accordance to the ABC.

The performance of the ABC-NARX-MSS was tested upon a known example system as well as an unknown Canadian wetland system. The sequential steps demonstrated through the histograms exhibit the convergence power of the algorithm in a limited computational budget. This MSS algorithm picked up the correct terms for both the systems. A thorough SID cycle for a Canadian wetland, solely under the ABC framework and the associated simulation results, embolden the acceptability of a probabilistic approach in an identification process. The example system was also passed through the FROLS algorithm with varying lag values. As the maximum lag of input-output increases to 4, the FROLS picks up a 'false' term in the beginning. The advantages with the ABC-NARX-MSS in such situations, towards selecting only the 'true' terms have been discussed in this chapter.

Within probabilistic framework also, the ABC-NARX-MSS has en edge over the other competing methods. For instance, in the RaMSS algorithm [37], one has to tune some parameters depending upon the dataset and the system. The ABC-NARX-MSS is free from any such ad-hoc tuning of algorithm's parameters. The presented algorithm is also a much simpler method as compared to the [36]. In principle, the RJMCMC approach performs the MSS and parameter estimation simultaneously but that comes at the cost of heavy computational requirement. The method no doubt offers a sound theoretical basis for the MSS in a stochastic framework but that also makes it less adaptable and difficult to implement.

The ABC-NARX-MSS algorithm has mainly been motivated by the critical issues corresponding to OFR framework. Despite some criticism, OFR framework is considered to be an efficient algorithm mainly due to its low computational requirements. The Chapter 2 has already demonstrated the usage of SID in a wide range of fields and most of these application areas have relied upon the OFR technique. The SID has its origin in the control theory and practitioners in this field still regard the forward regression method as the best way of term selection. Therefore, this chapter does not negate the importance of the OFR framework in SID. However, a parallel probabilistic approach is an attempt to expand the SID as a complete package for the identification in a data driven scenario.

Part II

Data driven modelling of wetlands

Chapter 5

Wetlands and their modelling challenges

5.1 Introduction

A wetland is a land area that is inundated with water (figure 5.1) and displays seasonal variations because of soil properties, climatic condition and orography of the site. Wetlands are considered to be a major source of methane emission. Besides positive emissions of greenhouse gases like methane, wetlands proffer various types of vegetations allowing the sequestration of organic carbon and regulating the carbon cycle. Evapotranspiration resulting due to wetlands have substantial effects on the energy exchange between atmosphere and land surface. This complex phenomena links the climatic variables with the wetland extent of a region [98, 99].

The exhaustive mapping of the global wetlands are recorded by the Ramsar Convention, an intergovernmental treaty providing the framework for wetland conservation. According to the Ramsar Convention's formal definition, wetlands include a wide variety of habitats such as marshes, peatlands, floodplains, rivers and lakes, and coastal areas such as saltmarshes, mangroves, and seagrass beds, but also coral reefs and other marine areas no deeper than six metres at low tide, as well as human-made wetlands such as waste-water treatment ponds and reservoirs [100].

The wetlands being a significant player in the greenhouse gas exchange should be included in the climate models for analysing the different scenarios of the Intergovernmental Panel on Climate Change (IPCC). The influence of wetlands in the environmental processes and local climate encouraged the collation of global wetland datasets in eighties [101]. These datasets are static in nature and cannot

explain the seasonal variations of wetlands. In the last decade, remote sensing techniques came into action for capturing the dynamics of wetlands. The wetland fraction of a site cannot be measured directly and there are some well structured methodologies for deriving the extent of wetland from the remotely sensed primary-variables. Essentially a remote sensing method provides the wetland distribution in a time series, typically on the monthly basis. Recently, these time series datasets are being used to develop the models representing the inundation of a site as well as calibrating some process based existing wetland models [102, 103].

In this chapter, some popular wetland models will be critically reviewed. These models are mostly analytical in nature and have been embedded by the approximations of several complex processes governing the wetland extent of a site. The next chapter is a novel contribution towards wetland modelling based on a data-driven framework. This chapter will be utilised in pointing out the requirements of a data-driven approach in wetland models and the limitations of the existing process based modelling methodologies.

Figure 5.1: A typical wetland picture (courtesy of pexels.com).

5.2 State-of-the-art of wetland models

5.2.1 Wetland extent and peatland accumulation using TOPMODEL approach

Peatlands constitute a significant portion of wetlands on the earth surface and have substantial roles in the global carbon cycle. Typically a peatland can sequester a large amount of carbon and a recent study [104] tries to analyse the effects of peat accumulation on carbon cycle through a dynamic modelling approach. In this modelling analysis, a dynamic global vegetation model known as the LPJ (Lund-Postdam-Jana) was linked with a wetland model and a module representing the accumulation and decay of peat. The point of interest in this review study is the wetland model part which is based on the TOPMODEL framework. The TOPMODEL is a topography based hydrological model, which is in relevance since the last forty years and has been applied in a broad range of catchments [105]. The wetland model in [104] is dynamic in nature and determine the water table and inundation fraction.

The TOPMODEL, being a topography based model requires the topographic parameters. It works on the Compound Topographic Index (CTI), which is equal to $ln(\alpha_i/tan(\beta_i))$, where α_i is a dimensionless index representing the area draining at the point i and $tan(\beta_i)$ signifies the slope at the point i. The governing equation 5.1 in the TOPMODEL evaluates the local water table (z_i) at the point i using the mean water table ($\bar{z}$), the CTI denoted by χ_i, grid cell mean CTI index ($\bar{\chi}$), and a parameter f explaining the exponential decline of transmissivity with depth. The equation 5.1 is used to determine the inundation fraction corresponding to a grid cell in the model. The TOPMODEL approach is quite appealing in principle but it consists of several pitfalls mainly arising due to the approximations associated with the CTI parameters. The approach has also been criticised by the developers of this approach [105]. Wetland extents are underestimated in flat terrains because of the limitations of the TOPMODEL approach in [104]. High resolution CTI parameters are provided in [106], which can be used to determine the inundation at a much finer scale.

$$z_i = \bar{z} + \frac{1}{f}(\chi_i - \bar{\chi}) \tag{5.1}$$

5.2.2 LPJ-wsl model using TOPMODEL approach

The TOPMODEL approach has been implemented to assess the wetland distributions at the global level but has overestimated the wetland distributions and

the duration of inundation on many occasions. The availability of time series data [102, 103] and surveys on inundation fraction have helped in assessing the anomalies associated with a typical TOPMODEL based model. Some improvements in wetland modelling under the TOPMODEL framework were presented in [107]. In this study, constraints were proposed to bridge the difference between model predicted wetland extent and the satellite datasets. The CTI parameters were also revised to take into account the seasonal cycles of wetlands using updated topographic data. In order to formalise these updates a new form of the Dynamic Global Vegetation Model , known as the LPJ-wsl (Lund-Postdam-Jana $WaldSchneeundLandschaft$) has been proposed. Technically speaking, the LPJ-wsl also includes the TOPMODEL approach but soil thermal dynamics are included as well. A soil water freeze and thaw (FT) cycle and snow ageing factors have also been included in this updated model in the view of boreal regions. In a nutshell, this scheme is an improvement over the previously discussed TOPMODEL methods and currently in practice for the large scale modelling.

5.2.3 Wetland Extent Dynamics (WEED) model

The WEED model [108] is based on the hydrology model of the Max Planck Institute for Metrology (MPI-M) and describes the wetland extent dynamics. The model displays a good performance for the high northern latitudes when compared to the observed data. The seasonal variation of the wetland extent associated with the snow-melt process in the northern region is fairly represented by this model. In addition, the precipitation cycles of the tropical regions are also satisfactorily explained by the WEED. Potential evapotranspiration (PET) plays very important roles in such kind of analytical modelling approaches. In MPI-M the PET part is in very simplified form and the calculation is not sufficiently rigorous. This is a plausible reason behind the overestimation of wetland extents in the tropical zones under the WEED scheme. Further details about this methodology is not available at the moment but like any process based approach, this model is also prone to the uncertainties resulting from the topographical variations.

5.3 Wetland models inter-comparison

The significance of wetlands in methane emission and regulation of biogeochemical cycle entails the quantification of variations in wetland distribution. The US Climate Change Science Program (CCSP, 2008) also suggests the similar approach including the assessments of climate change effects on wetlands. Recently, a

project known as the WETCHIMP [109, 110] involved in total ten models for simulating the wetland extents across the globe. At least eight models in this project are global models. The modelling results were compared with the observed data. The observational datasets can be divided into two categories: satellite based observation [102, 103] and wetland mapping product [111]. A satellite based observed wetland dataset is also referred as Global Inundation Extent from Multi-Satellites (GIEMS), whereas, Kaplan 2007/K07 is a static mapping product from [111]. A GIEMS set is a more updated form as compared to a static mapping product. Nevertheless, in the WETCHIMP project both categories of data are used for the comparison purpose.

Among all the models in this project, SDGVM and UVic-ESCM were not been fed with any observed data in the course of parameterisation and their simulation (from 1993 to 2004) are directly compared with the K07 and GIEMS. The model outputs are very much different from the observed data, particularly the SDGVM is overestimating the inundation across all the sites on the shown choropleth map. The inter-comparison of models also demonstrates a high level of uncertainties. They are in somewhat agreement near the northern latitudes but fail to show any similarities near the equatorial regions.The cyclic patterns of the inundation also show a high degree of mismatch among the models. There is a scope of improvement in the observed dataset as well, mainly the data resolutions should be in sync with the model outputs [110].

5.4 Data-driven modelling in hydrology

All the existing literatures on wetlands modelling rely upon some sorts of analytical approaches. Some of the important studies on wetlands modelling and the WETCHIMP project, as discussed in the previous sections support this fact. A data-driven modelling method often serves as an alternative to an analytical method, like in a hydrological process, where are the dynamics are too complex. Physically, a wetland system encompasses at least some aspects of hydrological processes. Therefore in this section, a very popular data-driven modelling framework in hydrology, known as, Data Based Mechanistic (DBM) modelling will be discussed.

In a DBM modelling approach, firstly the model structure is identified through objective statistical inference of the available data based on a linear transfer function (TF) model. The parameters of the TF model can vary over time and are estimated using a recursive estimation method. Any nonlinear and non-stationary system behaviour are reflected through the time or state dependent variation in

the parameters. Sometimes a simple input-output transfer function model can possess a reasonable predictive power but may not pass a mechanistic interpretation related to the underlying science of the system. The DBM approach of modelling ensures that the model terms are able to relate with the physical, biological, ecological or chemical terms [112, 113].

The relationship between rainfall and river flow is of great interest among the hydrology community. A DBM has been employed in [112] for the model structure detection and parameter estimation for explaining the nonlinear relationship between rainfall and flow. Essentially, this paper involved the estimation of transfer function model representing a rainfall-flow dynamical process by employing recursive estimation approach. The DBM approach as used herein [112] can turn out to be a useful tool for modelling other interesting environmental processes. Recursive estimation also allows the usage of the DBM in designing real-time, self-adaptive management system.

A stochastic DBM approach to modelling of rainfall-flow at the catchment scale is compared with a deterministic alternative top-down modelling approach [114] in [115]. The data in this comparative study is collected from the River Hodder in the UK and hourly-sampled for a total period of 20 days. This study [115] demonstrates that a DBM can identify the nonlinear models corresponding to the dynamics exhibited by rainfall-flow processes even under a limited length of observation dataset.

A toolbox compatible with the MATLAB software, known as, CAPTAIN emerged in parallel to the DBM modelling research [116]. This toolbox is developed around a transfer function and state space framework and extends the functionality of MATLAB for the identification and estimation of a broad range of models. Both state dependent and time variable parameters are considered in the CAPTAIN toolbox. This MATLAB extension tool contains various model structures particularly useful for data-driven modelling of the processes in an environmental system.

5.5 Conclusion

This chapter begins with the definition and significance of wetlands in the ecosystem. As an important component of the Earth's Critical Zone, wetland modelling is a crucial contribution in the next chapter of this thesis. The reason of interests in the wetland patterns is mainly linked to the associated carbon cycle and the spectrum of biodiversity supported by wetlands.

This chapter succinctly presents a survey of the existing state-of-the-art models

related to the inundation of a land surface. The mathematical details of the analytical approaches have been avoided. The broader theoretical basis of such models are more relevant in this thesis as at no point an analytical modelling of wetlands will be attempted herein. A recent project on the comparison of various models, called the WETCHIMP, has been discussed in the end to emphasis the limitations of the existing wetland models. The WETCHIMP project has a clear message that neither the existing models are capable to explain the wetland extents fairly nor the available observed datasets are detailed enough to perform the modelling at the multiple scale. This thesis will try to address the accuracy problems in wetland dynamics using a data-driven framework in the next chapter. However, the observed data will still be similar to the GIEMS employed in the WETCHIMP.

Chapter 6

Tropical wetlands modelling

6.1 Introduction

A wetland is a land area that is saturated with water. Most of the wetlands exhibit seasonal variations because of soil characteristics, vegetations, climate variables and orography of a site. Wetlands play major roles in the greenhouse gas exchange especially methane, support certain kinds of vegetations such as paddy, control the climate of a region through energy exchange and support a wide range of biodiversity on earth. The wetland extent of a region is usually quantified by the wetland fraction, which is the fraction of inundated land area at a time.

In the environmental modelling community, wetlands have remained a noteworthy issue because of the dependence of many environmental variables on wetland extents. The relationship among these variables are too complex to be simplified using mathematical expressions. All the major climate models at the moment have not been able to incorporate the wetland dynamics convincingly [108, 117]. In the last chapter, state-of-the-art of wetland models available so far had been discussed. All those models essentially follow a process based approach and are derived upon several assumptions. The last chapter critically analysed the pros and cons of all such models.

In a nutshell, there is a consensus on at least two points regarding wetlands - (a) wetland distribution can only be described correctly through a dynamic modelling approach (b) wetland fraction exhibits high amount of nonlinearity with environmental variables. In this study, the System Identification (SID) methodology is used for the identification of a nonlinear dynamic model structure of tropical wetlands across the globe, using the remotely sensed data. The chosen nonlinear model is Nonlinear Autoregressive Exogenous (NARX), a widely popular model class in control theory and other application area such as, biomedical engineering,

econometrics, mechanical systems, synthetic biology, space weather modelling etc [18].

The wetland fraction data using a remote sensing technique are available for multiple tropical sites [118]. In this study, a single model structure has been developed using the Forward Regression Orthogonal Least Square (FROLS) algorithm of the SID, representing the common underlying processes, governing the wetland extents of all the tropical regions across the globe. This is the first novelty of this chapter. Following the model structure detection, the Approximate Bayesian Computation (ABC) is used for estimating the parameters of sites from Amazon, Africa and Asia regions. This resulted into a parameter mapping corresponding to the developed wetland distribution model and can be used to simulate the model for a specific site pertaining to the tropics of the globe. This is the second novel contribution of the chapter. Forecasting of wetland distribution for a site could be key in the future land management practices. The model is validated against a fresh data set, derived using the similar remote sensing technique.

This chapter begins with a simplistic case, where just three tropical sites have been chosen to obtain an integrated wetland model. In this stage, the model structure detection and parameter estimation have been carried out using the FROLS approach. In the next stage, the Bayesian inference in the form of ABC has come into action for mapping the parameters of all the available tropical sites. The model performance corresponding to all the sites are shown using the choropleth maps. The contributions of this chapter along with some proposed future works towards the wetland distribution modelling are discussed in the concluding remarks.

6.2 Wetland modelling: a system identification problem

The wetland modelling in this study follows a data-driven approach, using a dataset obtained through remote sensing technique [118]. The available data contains the environmental and vegetation variables such as average temperature, soil water content, leaf area index, evapotranspiration, transpiration, and wetland fraction. All the data points form a monthly time series and are available from January 2000 to December 2012. The wetland fraction (fw), which is also the system output can be defined as a fraction of site that is an inundated-wetland. In total, the input-output data are available from 94 tropical sites, separated by 0.5×0.5 degree geographically (figure 6.1).

A wetland model could be used for the forecasting purpose only if all the future inputs are available. This constrains the choice of input and the average

temperature becomes a natural choice mainly because of its availability from the CMIP5 models [117]. The output of interest is wetland fraction, and hence the whole modelling can be perceived as a Single Input Single Output (SISO) system identification.

In this SISO system, we have a blackbox having a function of lagged inputs and outputs and the aim is to determine this blackbox fairly. This function essentially describes the dynamics of the system, which in this case is the wetland system. As mentioned in the introduction, this function is expected to be a nonlinear dynamic function of input-output. In SID terminology, the underlying function in the blackbox can be referred as the model structure. In this study, a parametric form of the SID is considered hence the underlying function will be parameterised appropriately. The actual significance of these parameters will be apparent in the coming sections.

In summary, the posing of wetland modelling as an SID problem provides an opportunity to exploit many robust and popular methodologies of SID and extend those techniques in an environmental system. These methods have the potential to overcome the challenges being faced in a typical process based modelling of such class of environmental systems.

Figure 6.1: Tropical sites having spatial resolution of 0.5×0.5 degree. Remotely sensed data of all the dotted sites are available.

Site	Region	Latitude (in deg.)	Longitude (in deg.)
1	Amazon	-2.75	-57.25
2	Africa	13.75	19.25
3	Africa	10.25	23.25

Table 6.1: Geographical coordinates of tropical wetlands sites used for modelling in Stage 1.

6.3 Stage 1: Least square method

In this study, modelling of wetland distribution commenced with the standard least square methodology for both the model structure detection and parameter estimation. The FROLS algorithm, described in the last chapter was employed in this stage of identification. Here the number of sites were limited to just three. The modelling was performed for individual sites firstly and thereafter an integration was carried out to obtain a tropical wetland model. The results of this stage have been reported in [119]. The following subsections describe the detailed steps followed in this stage.

6.3.1 Input-output characteristics

As mentioned earlier, the SISO system approach was chosen in order to make the model capable of predicting the future scenarios. In addition to this feature, single input system also helps in avoiding the modelling complications incurred because of multiple variables. In this stage, three wetland sites across the tropics formed the part of Orthogonal Least Square (OLS) type modelling.The geographical coordinates of all these sites are presented in the Table 6.1. The figure 6.2, 6.3 and 6.4 represent the input-output data of the site1, site2 and site3 respectively. The raw data of each site is transformed using z-score standardisation, in order to constrain the input-output into similar range.

All the sites falls into the tropical zones of the globe and therefore, the range of average temperature exhibited by these sites are nearly same. The wetland fraction corresponding to the site 1 (Amazon) is on higher side as compared to the other two African sites. The wetland distribution depends upon many factors including the local topography. So, even the sites belonging to a similar climate might show large variations in their inundation fraction.

6.3.2 Model structure detection - Individual wetland sites

In this study, NARX modelling approach was used for identifying the dynamics of a wetland system. The regressors matrix ϕ is built up by including all the possible

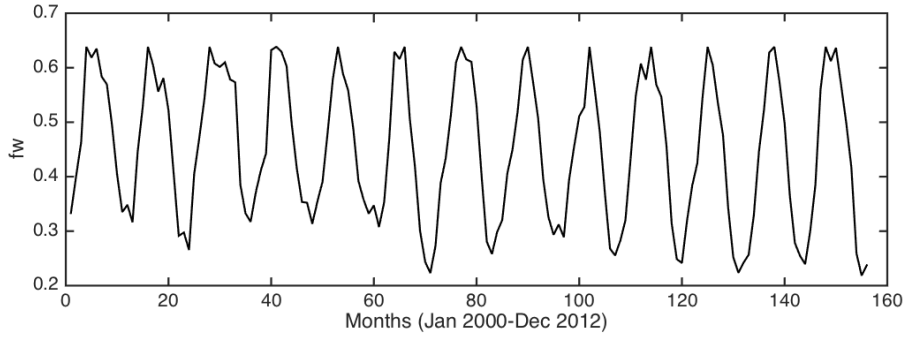

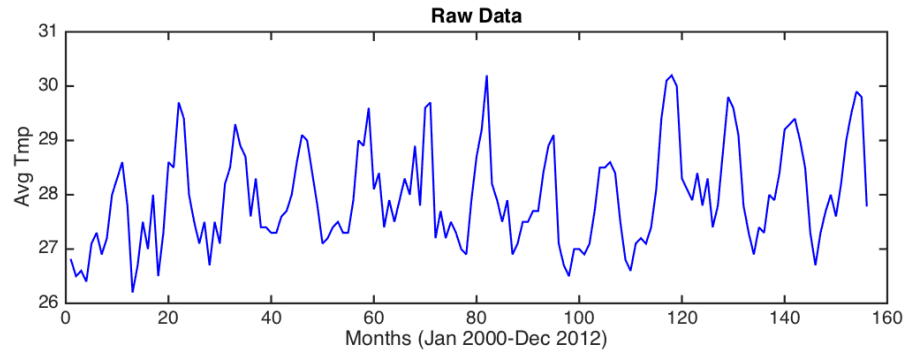

(a) Raw data (site 1)

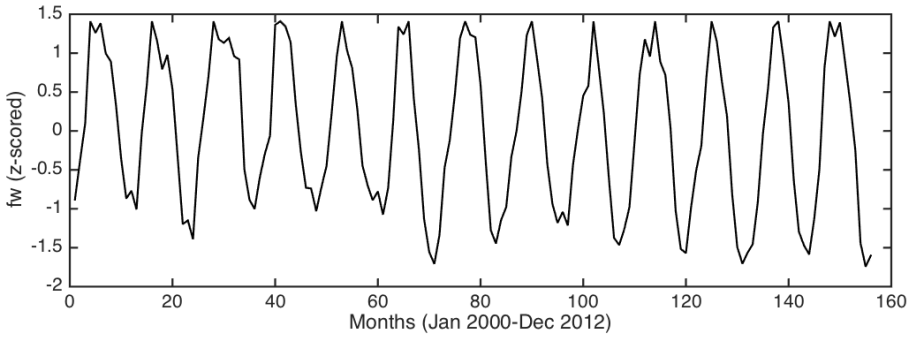

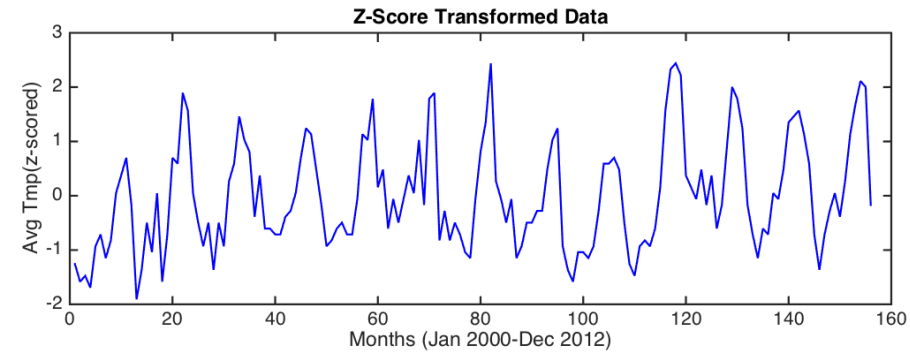

(b) Z-Scored data (site 1)

Figure 6.2: Input (average temperature) and output (wetland fraction) time series data from January 2000 until December 2012 − site 1

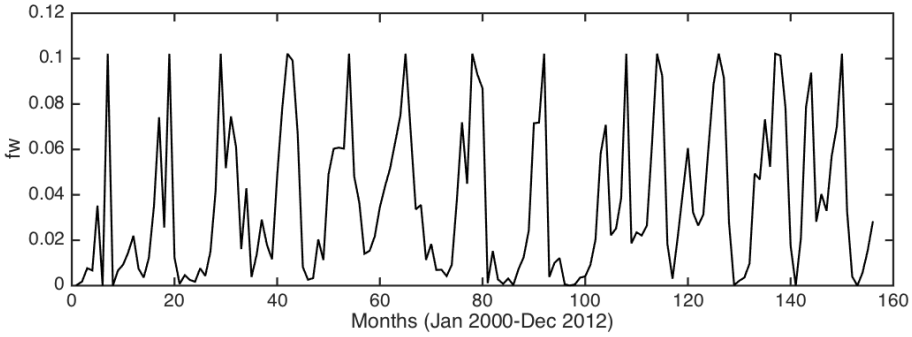

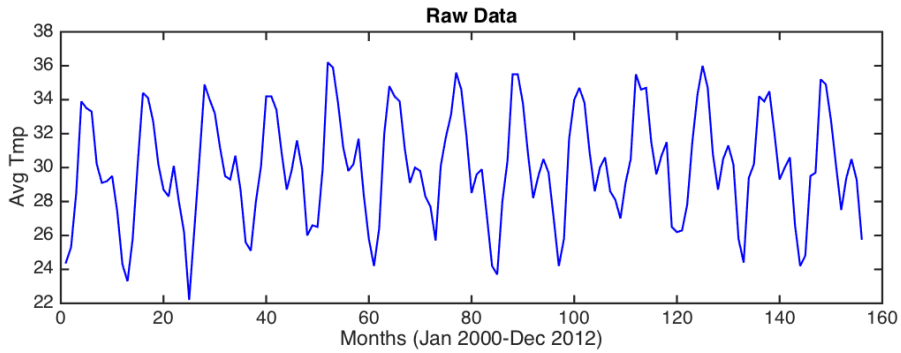

(a) Raw data (site 2)

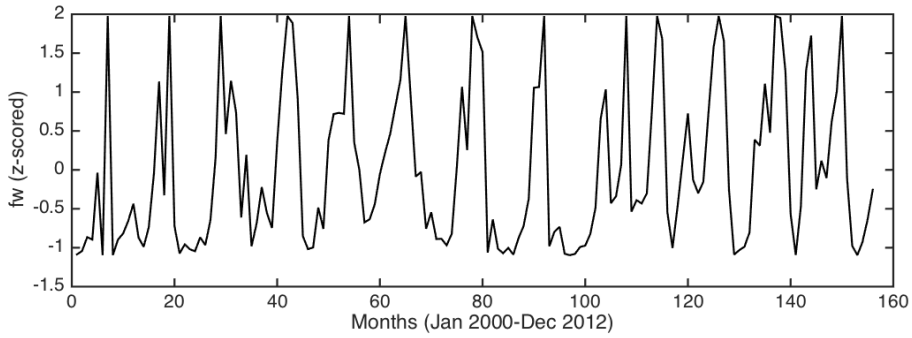

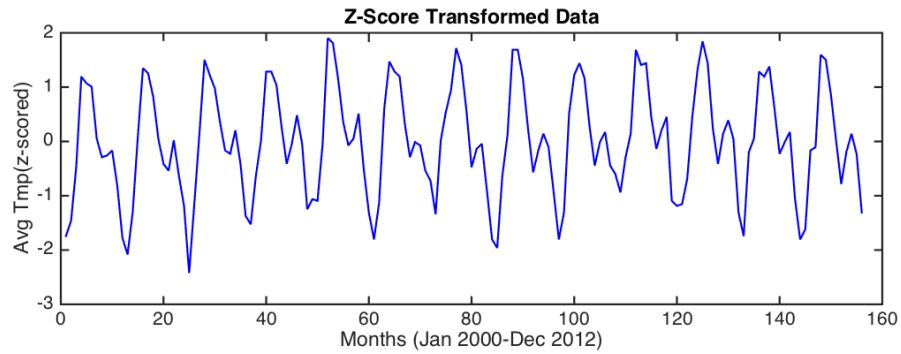

(b) Z-Scored data (site 2)

Figure 6.3: Input (average temperature) and output (wetland fraction) time series data from January 2000 until December 2012 − site 2

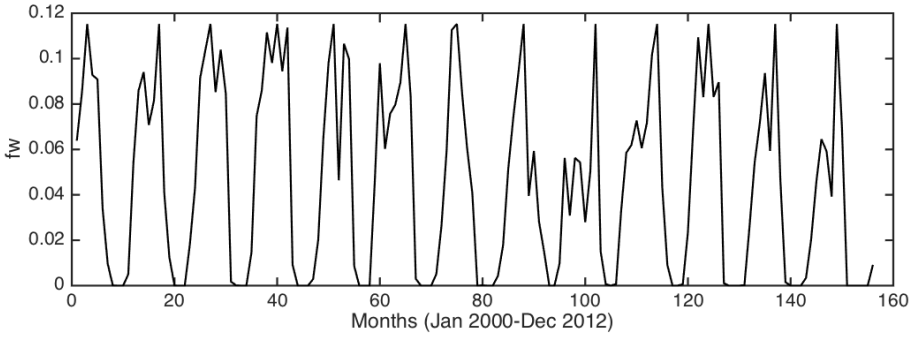

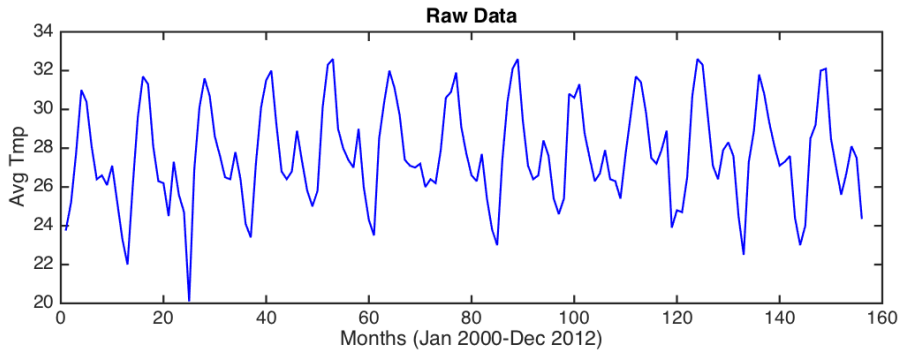

(a) Raw data (site 3)

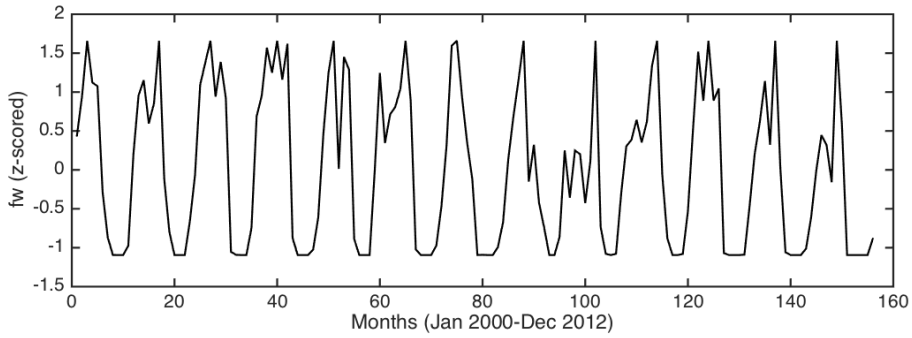

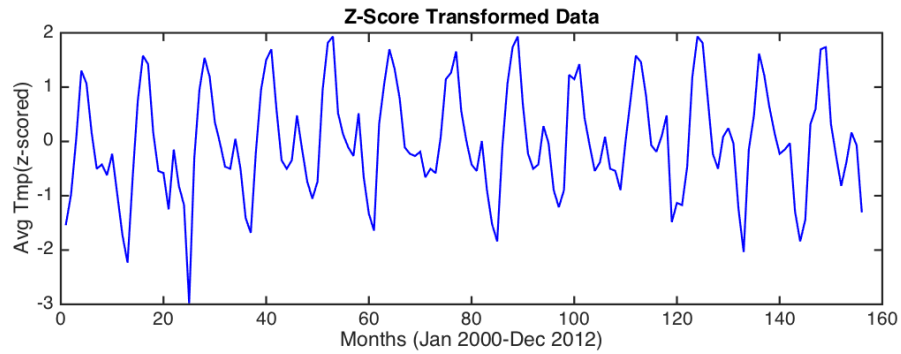

(b) Z-Scored data (site 3)

Figure 6.4: Input (average temperature) and output (wetland fraction) time series data from January 2000 until December 2012 − site 3

Term no.	Parameter	ERR
1	-0.2172	0.7636
2	0.8230	0.0715
3	-0.4045	0.0648
4	-0.1616	0.0104
5	0.1236	0.0085
6	0.1080	0.0044

Table 6.2: NARX model parameters and Error Reduction Ratio (ERR) corresponding to the site 1. Model terms are ranked according to their ERR values.

terms corresponding to the maximum input lags (n_u), maximum output lags(n_y) and polynomial order(n_p).

The ϕ_j matrix corresponding to each tropical site j,

$$j \in [1, 3]$$

was formulated by assigning $n_u = 6$, $n_y = 6$ and $n_p = 3$. The seasonal cycle of input-output data was used as a rough guideline to choose the maximum lag values in this stage. To obtain a model structure explaining the dynamics of $Site_j$, the ϕ_j regression matrix was arranged using the lagged input-output variables, as explained in the Chapter 2. Following this step, the FROLS was applied on the ϕ_j to obtain a parsimonious model structure for each site. The model derived for the site 1 is shown in the equation 6.1.

$$\begin{aligned} \hat{y}(t) = \theta_1 \cdot \hat{y}(t-6) + \theta_2 \cdot \hat{y}(t-1) + \theta_3 \cdot \hat{y}(t-3) \\ +\theta_4 \cdot u(t-1) + \theta_5 \cdot \hat{y}(t-1) \cdot \hat{y}(t-2) \cdot \hat{y}(t-3) \\ +\theta_6 \cdot \hat{y}(t-1) \cdot \hat{y}(t-1) \cdot \hat{y}(t-6) \end{aligned} \tag{6.1}$$

Similarly, model structures for the site 2 and site 3 are shown in equation 6.2 and 6.3 respectively.

$$\begin{aligned} \hat{y}(t) = \theta_1 \cdot u(t-6) + \theta_2 \cdot \hat{y}(t-1) + \theta_3 \cdot u(t-5) \\ +\theta_4 \cdot \hat{y}(t-1) \cdot u(t-3) \\ +\theta_5 \cdot \hat{y}(t-5) \cdot u(t-2) \cdot u(t-3) \\ +\theta_6 \cdot \hat{y}(t-1) \cdot \hat{y}(t-1) \cdot \hat{y}(t-6) \end{aligned} \tag{6.2}$$

Term no.	Parameter	ERR
1	0.2926	0.3171
2	0.4650	0.1063
3	-0.2160	0.0734
4	-0.3652	0.0569
5	-0.3423	0.0352
6	0.2271	0.0282

Table 6.3: NARX model parameters and Error Reduction Ratio (ERR) corresponding to the site 2. Model terms are ranked according to their ERR values.

Term no.	Parameter	ERR
1	-0.0171	0.5023
2	-0.7727	0.1263
3	-0.2100	0.0641
4	0.5359	0.0346
5	0.3345	0.0280
6	0.1421	0.0264

Table 6.4: NARX model parameters and Error Reduction Ratio (ERR) corresponding to the site 3. Model terms are ranked according to their ERR values.

$$\begin{aligned} \hat{y}(t) = \theta_1 \cdot \hat{y}(t-6) + \theta_2 \cdot u(t-5) \\ +\theta_3 \cdot \hat{y}(t-5) \cdot u(t-2) \cdot u(t-3) + \theta_4 \cdot \hat{y}(t-1) \\ +\theta_5 \cdot \hat{y}(t-1) \cdot \hat{y}(t-1) \cdot u(t-5) \\ +\theta_6 \cdot u(t-3) \cdot u(t-3) \cdot u(t-6) \end{aligned} \tag{6.3}$$

The obtained model structure for each site is parameterised by the six parameters namely, θ_1, θ_2, θ_3, θ_4, θ_5 and θ_6. Models corresponding to the site 1 (equation 6.1) and site 3 (equation 6.3) are mainly driven by output, whereas the model representing the site 2 (equation 6.2) is a input driven model. The parameter values and the Error Reduction Ratio (ERR) corresponding to the site 1, site 2 and site 3 are presented in the Table 6.2, 6.3, and 6.4 respectively.

The prediction of wetland extent for a site can be made using such site specific models. Nevertheless, most often the purpose of a modelling exercise is to understand the science behind the process. The wetland dynamics of all these sites should be characterised using a simple and common model structure because all of them lie between the Tropic of Cancer and Tropic of Capricorn. In order to validate this hypothesis, an integrated model structure for all three sites were obtained and is explained in the next subsection.

θ_1	θ_2	θ_3	θ_4	θ_5	θ_6
1.1981	-0.0326	0.2509	-0.1961	-0.0262	-0.0265

Table 6.5: Estimated parameters of the NARX model corresponding to the integrated tropical wetland model developed in Stage 1.

6.3.3 Integrated tropical wetland model

For deriving a single model structure, explaining the dynamics of the tropics, the ϕ matrix of the three tropical sites (ϕ_1, ϕ_2, and ϕ_3) were arranged in vertical order to form a combined Φ matrix of the tropics. Following this merging step, the FROLS was applied on the Φ in similar ways, as explained in the previous subsection. This resulted into a parsimonious model structure containing six terms, shown in the equation 6.4.

$$\begin{aligned} \hat{y}(t) &= \theta_1 \cdot \hat{y}(t-1) + \theta_2 \cdot \hat{y}(t-2) \cdot \hat{y}(t-3) \cdot \hat{y}(t-4) \\ &+\theta_3 \cdot \hat{y}(t-1) \cdot \hat{y}(t-6) + \theta_4 \cdot \hat{y}(t-1) \cdot \hat{y}(t-3) \cdot \hat{y}(t-6) \\ &+\theta_5 \cdot u(t-3) \cdot u(t-3) + \theta_6 \cdot \hat{y}(t-1) \cdot \hat{y}(t-1) \cdot \hat{y}(t-1) \end{aligned} \tag{6.4}$$

The obtained model structure (equation 6.4) has six parameters namely, θ_1, θ_2, θ_3, θ_4, θ_5 and θ_6. The parameter vector $\boldsymbol{\theta} = [\theta_1, \theta_2, ..., \theta_6]$ was calculated using the steps described in the section 2.3 and 2.4 of the Chapter 2. The parameters values are listed in the Table 6.5. This integrated version of wetland model exhibits substantial difference from the site specific models obtained earlier. The terms in the equation 6.4 follow the ERR ranking, which means the first term is contributing the most towards output variance. The most significant term in this model contains the output like site 1 and site 3 models but unlike those models, here the lag value is 1 for the first term.

6.3.4 Simulation results

The tropical wetland model structure shown in the equation 6.4 shows the relationship among the current output y, past inputs $u(t-n_u)$, and past outputs $y(t-n_y)$. The model terms are ranked according to their ERR values. Clearly, the term $y(t-1)$ is having the highest ERR, which means the wetland fraction in a month depends mostly on the wetland fraction of the previous month. All the terms except the fifth one contains the lagged outputs, which means the model is mainly driven by its previous outputs. The fifth term accounts for the average temperature but interestingly the $u(t-3) \cdot u(t-3)$ term signifies that a temperature

Site	Region	Std. deviation (fw)	Mean (fw)
1	Amazon	0.1332	0.4507
2	Africa	0.0332	0.0364
3	Africa	0.0419	0.0458

Table 6.6: Basic statistical information of the wetland fraction data (output) corresponding to all three sites used for modelling in Stage1.

value influences the wetland distributions after 3 months.

The performance evaluation of obtained wetland model was done using a new dataset of all the sites. The raw data were processed through z-scored standardisation during the model structure detection and parameter estimation. Therefore, the model output (fw) was passed through inverse transformation process for scrutinising the wetland fraction in its actual range. The mean and the standard deviation values of the raw data corresponding to all the three sites are given in Table 6.6. The simulation results of the site 1, site 2, and site 3 are shown in the figure 6.5, 6.6, and 6.7 respectively. The data until August 2006 (80^{th} month) was employed for the estimation, whereas, the data from September 2006 (81^{st} month) onward is the new data, used entirely for the model evaluation task. The One Step Ahead (OSA) prediction results match very closely with the observed values for all the sites. This indicates that, the derived model shown in the equation 6.4 satisfactorily represents the wetland dynamics of all the three tropical wetland sites. The same idea could be extended for obtaining a global tropical wetland model.

The purpose of such kind of environmental modelling is also to predict the future scenarios. For instance climate change is expected to increase the average global temperature substantially by the end of this century. The Intergovernmental Panel on Climate Change (IPCC) scenario RCP 8.5 [6] describes the change in climate variables under the 'business-as-usual' scenario. One of the main motivations behind modelling the tropical wetlands distribution is to analyse the effects of climate change under the RCP 8.5 on wetlands. Therefore, Model Predicted Output (MPO) of the model must explain the wetland fraction fairly. The OSA prediction results generated from the obtained model are showing satisfactory performance (figure 6.5, 6.6, and 6.7). However, the model is prone to fail in producing a reasonable MPO, mainly because it ignores the intricacies of topographies corresponding to various sites. A single parameter set is insufficient to explain the topographical variations exhibited by these sites despite following a similar dynamic. In reality, all the sites differ a lot in topographic details such as orography. The detailed explanation of the factors affecting wetlands and their incorporation into the process based models are explained in the previous chapter.

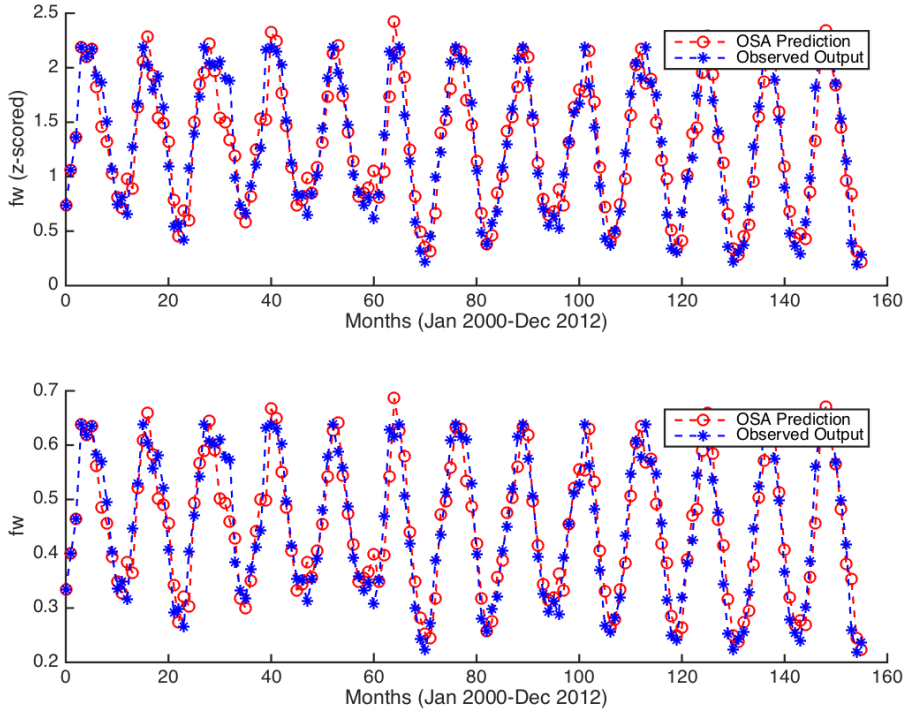

Figure 6.5: One Step Ahead (OSA) simulation results for site 1. The simulation results are shown for the standardised data (top) and the data in its actual range (bottom), obtained after inverse transformation.

The model obtained in this stage considers just three sites. Once all the tropical sites are taken into account, the topographical complexities will further increase. To address these issues the modelling was switched to the next level known as stage 2. In the next stage, Bayesian framework will be used for estimating the parameters of all the sites separately.

6.4 Stage 2: ABC method

In this stage of modelling, all the available data corresponding to the tropics were used for obtaining a common global tropical model. The model structure detection steps are similar to the stage 1, but here the topographical variations of the sites are addressed by estimating their parameters separately using an ABC method. ABC is considered to be a likelihood free method, where the intricacies of likelihood functions are replaced by exploiting the enhanced computational power. The theoretical details surrounding the Bayesian inference and particularly the ABC are discussed in the Chapter 3. In this section emphasis would be to demonstrate the

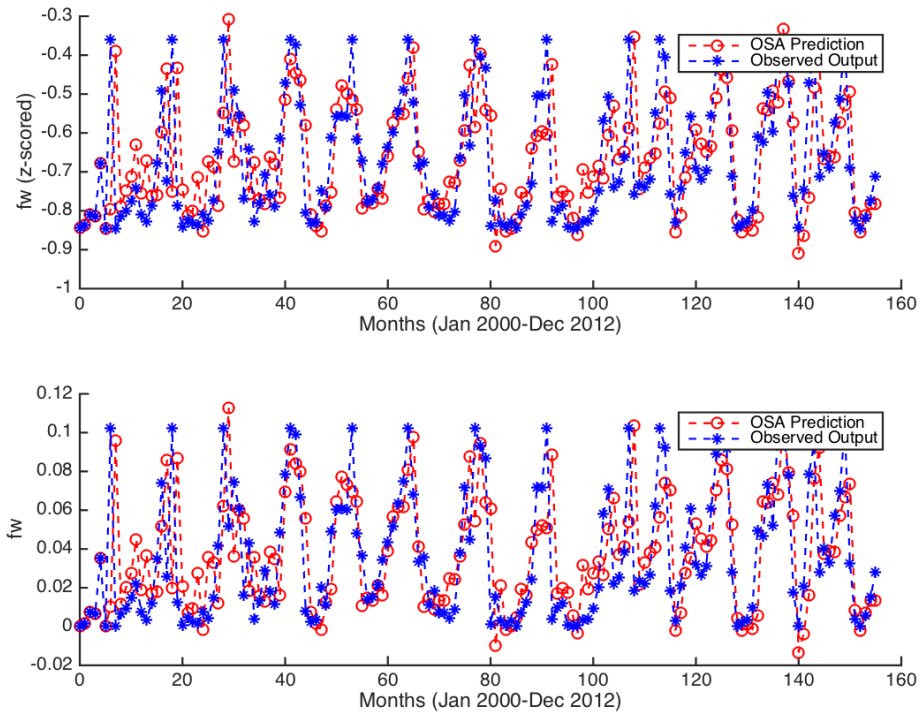

Figure 6.6: One Step Ahead (OSA) simulation results for site 2. The simulation results are shown for the standardised data (top) and the data in its actual range (bottom), obtained after inverse transformation.

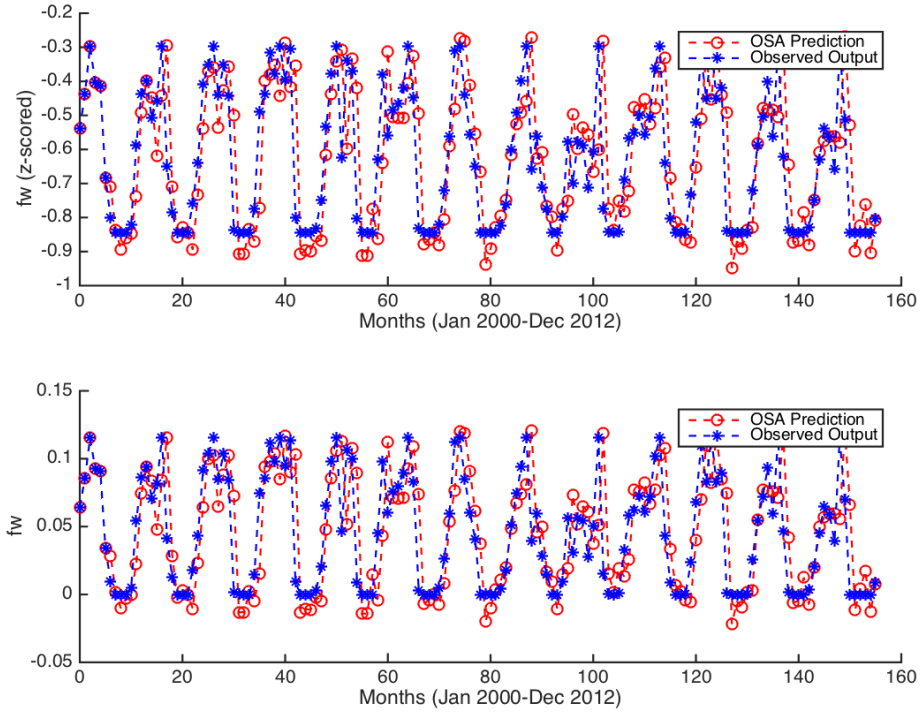

Figure 6.7: One Step Ahead (OSA) simulation results for site 3. The simulation results are shown for the standardised data (top) and the data in its actual range (bottom), obtained after inverse transformation.

practical application of the framework for developing a robust tropical model.

6.4.1 Data analysis

The data characteristics of all the tropical sites are not shown in this chapter, as that would make the whole document clumsy. This is why, one sample site from each region - Amazon, Africa, and Asia will be discussed throughout this chapter. The sites within a particular region do exhibit some topographical variations, as described earlier, but are still driven by similar climates. Hence, the input-output characteristics of a sample site from each region will be assumed to be the characteristics of the entire region. The geographical coordinates of these sample sites are contained in the Table 6.7. Like the stage 1, z-score standardisation was performed on raw data for all the sites (figure 6.8, 6.9, and 6.10).

Prior to the actual modelling steps, some basic analyses such as correlation of output (fw) with input ($AvgTmp$) (figure 6.11a, 6.12a, and 6.13a) and autocorrelation of output (fw) (figure 6.11b, 6.12b, and 6.13b) were performed. The seasonal behaviour of wetland distributions for all three regions, as shown in the figure 6.8, 6.9, and 6.10 also reflect from their autocorrelation plots. The values of autocorrelation decreases up till 6^{th} or 7^{th} lag terms, then increases again, but finally at the 18^{th} or 19^{th} lag terms, the autocorrelation measures reach to their minimum. The autocorrelation plots in these figures are shown until 20^{th} lag terms. The correlation measures as shown on the vertical axes will keep shrinking as the number of lags increases further.

Correlation between $AvgTmp$ and fw for all the three regions reveal that except Amazon no region exhibits a good amount correlation between these variables. The average magnitude of fw in Amazon is very high compared to Asia and Africa. This could be a possible explanation for a better correlation of fw with $AvgTmp$ compared to other regions. The lower values of fw might have been inducing a lesser dependence on climate inputs. In such cases, where the fw is not correlated nicely with temperature, other input variables, depending mostly upon the land characteristic such as soil water content could be used as input. The correlation analysis between fw and other variables were not performed because the prime aim of this modelling exercise is to obtain a robust model capable of making reliable predictions to understand the effects of increasing global temperature and climate change on wetlands. In order to predict the future scenarios, the future inputs must be available while simulating the model. This requirement acts like a major constraint and there is no other option except using a weather variable like average temperature as the input. SID is a data-driven method so undoubtedly, inclusion of sites such as Africa and Asia, where the inputs and outputs are not

Site	Region	Latitude (in deg.)	Longitude (in deg.)
1	Amazon	-3.75	-63.75
2	Africa	10.75	18.25
3	Asia	18.75	82.25

Table 6.7: Geographical coordinates of sample sites from each tropical region - Amazon, Africa, and Asia.

correlated well, posed some modelling challenges.

Selection of maximum time lags for input (n_u) and output (n_y) is a key step in a NARX modelling method. The maximum lag values is directly proportional to the computational time required for the model development. In this modelling step, first of all time series plots for all the three regions were inspected. It is interesting to note the seasonality in the data. The values of fw starts increasing from January up till June/July and then starts decreasing until December/Januray. In this study, the values of maximum time lags for both inputs and outputs were set in an iterative manner, starting from n_u, n_y equals to 1 until n_u, n_y equals to 12. The model performance in terms of data fitting started improving consistently up till n_u, n_y equals to 6, whereas, the performance declined for the higher lag values. After careful consideration, both the n_u and n_y were set to 6.

6.4.2 Model structure detection: Global tropical wetland model

A simple NARX model, capable of describing the dynamics of the global tropical wetlands was obtained in this study. The model structure detection was carried out similar to the stage 1. The ϕ_j matrix corresponding to each tropical site j,

$$j \in [1, 94]$$

was constructed by setting $n_u = 6$, $n_y = 6$ and $n_p = 3$. Eventually, the ϕ_j regression matrix was arranged using the lagged input-output variables, as explained in the Chapter 2. For deriving a single model structure, explaining the dynamics of the tropics, the ϕ matrix of all the tropical sites (ϕ_1,..., ϕ_{94}) were arranged in vertical order to form a combined Φ matrix of the global tropics. After this merging process, the FROLS was applied on the Φ, as explained in the previous section. This resulted into ranking of terms based on their ERR values. Finally a parsimonious model structure representing the global tropical wetland dynamics was obtained (equation 6.5). The model contains total six terms and is quite compact

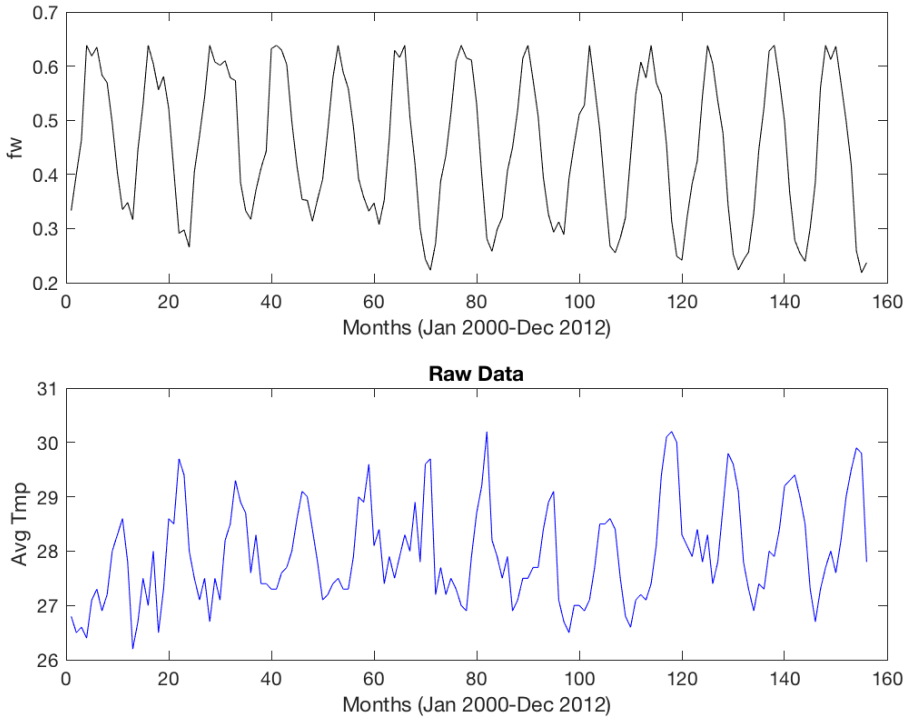

(a) Raw data (Amazon)

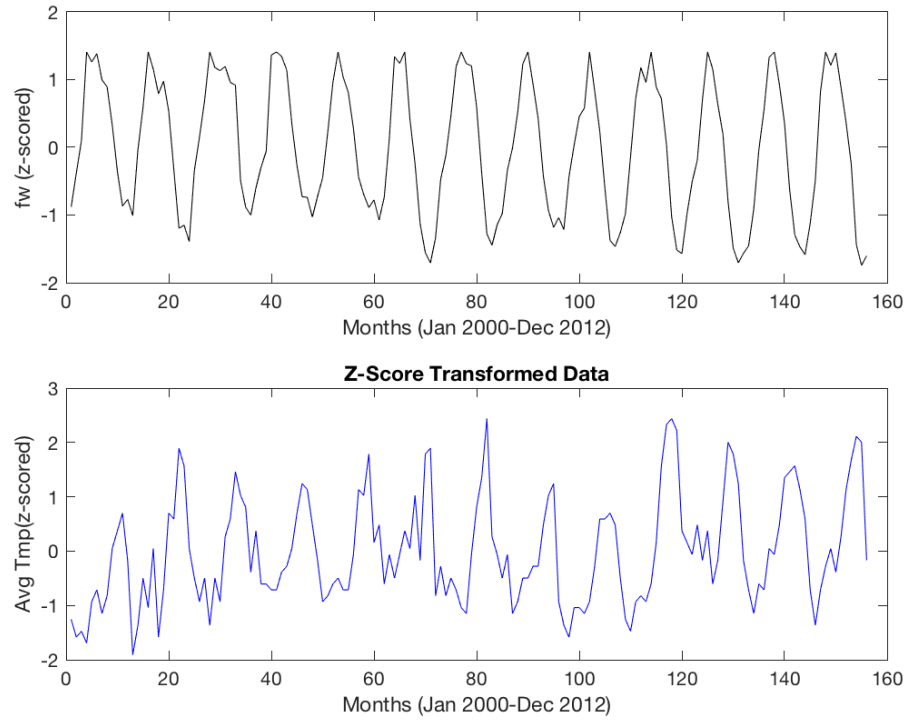

(b) Z-Scored data (Amazon)

Figure 6.8: Input (average temperature) and output (wetland fraction) time series data from January 2000 until December 2012 − Amazon region.

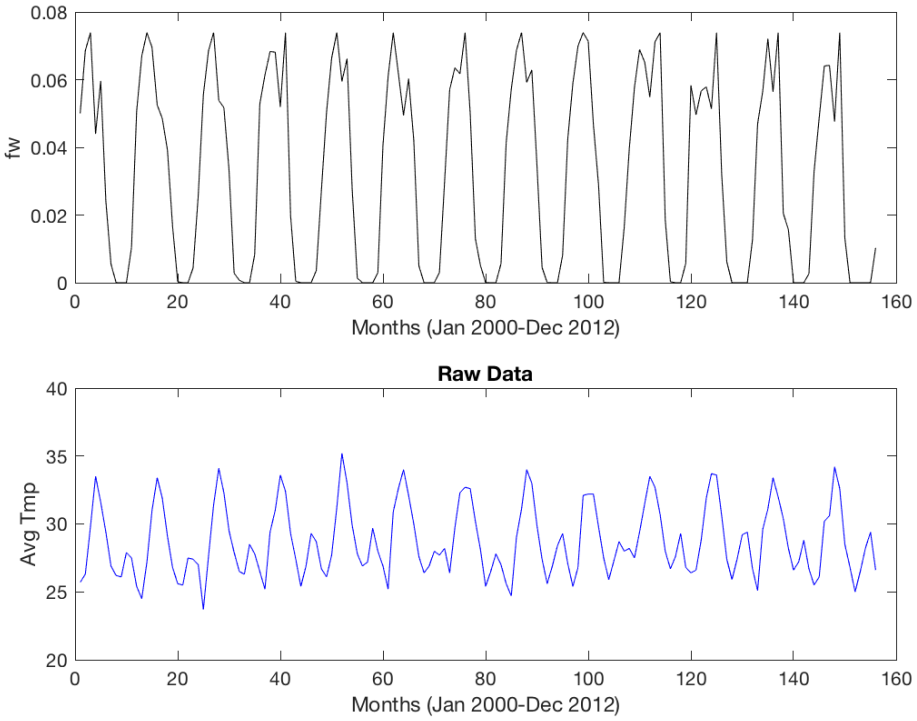

(a) Raw data (Africa)

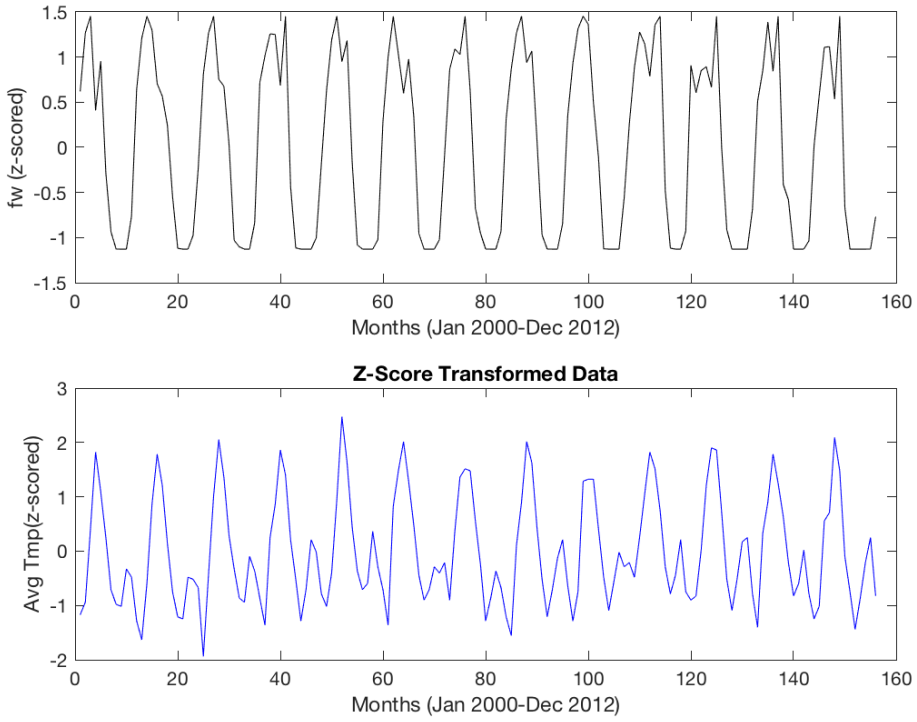

(b) Z-Scored data (Africa)

Figure 6.9: Input (average temperature) and output (wetland fraction) time series data from January 2000 until December 2012 − African region.

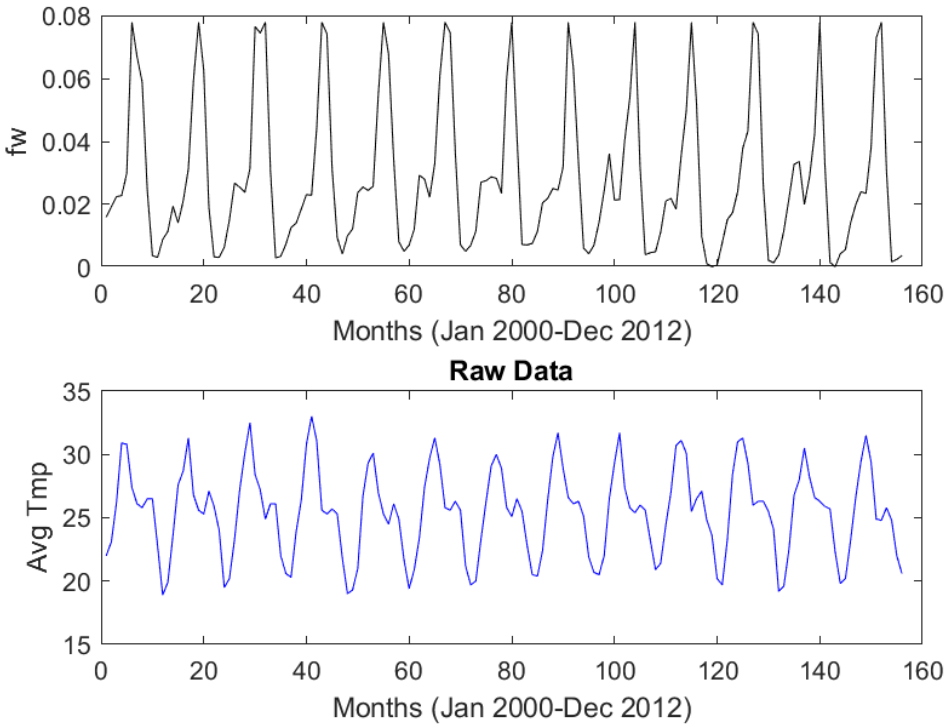

(a) Raw data (Asia)

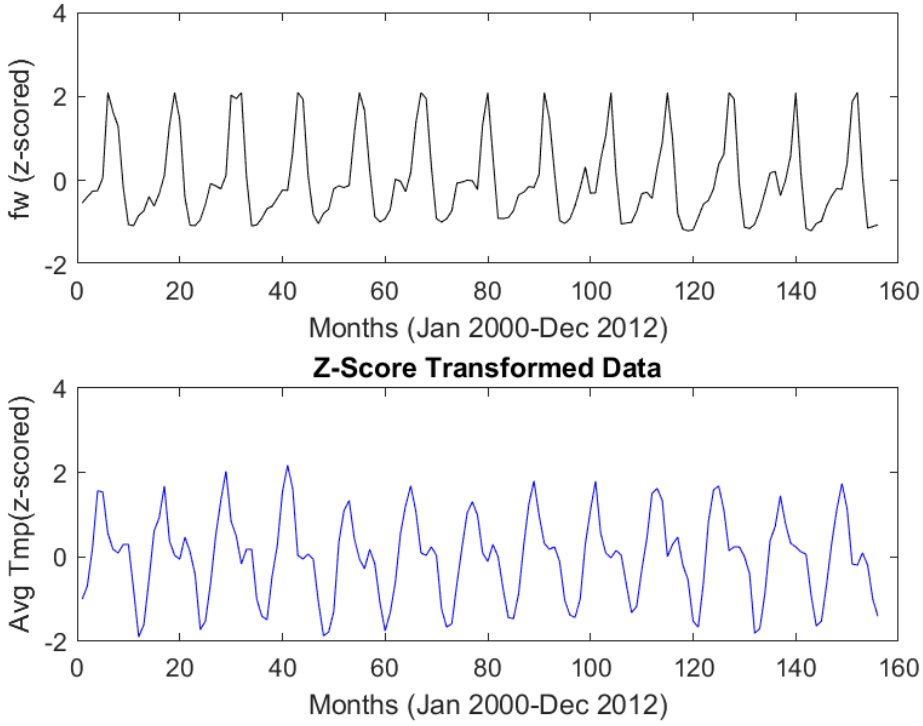

(b) Z-Scored data (Asia)

Figure 6.10: Input (average temperature) and output (wetland fraction) time series data from January 2000 until December 2012 − Asian region.

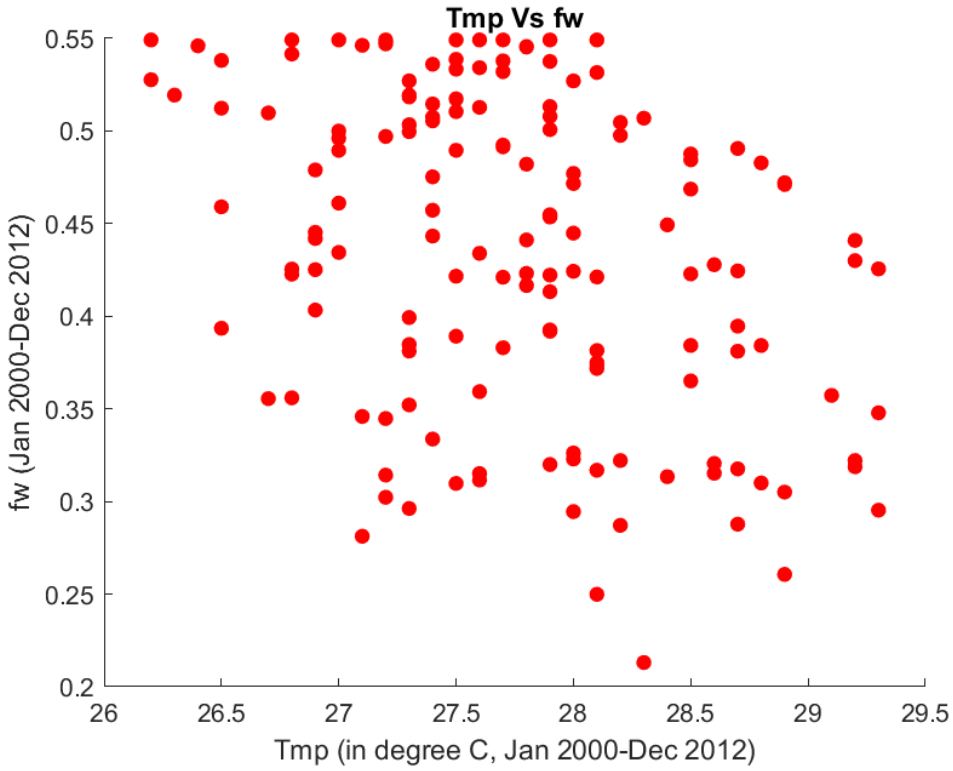

(a) Correlation analysis

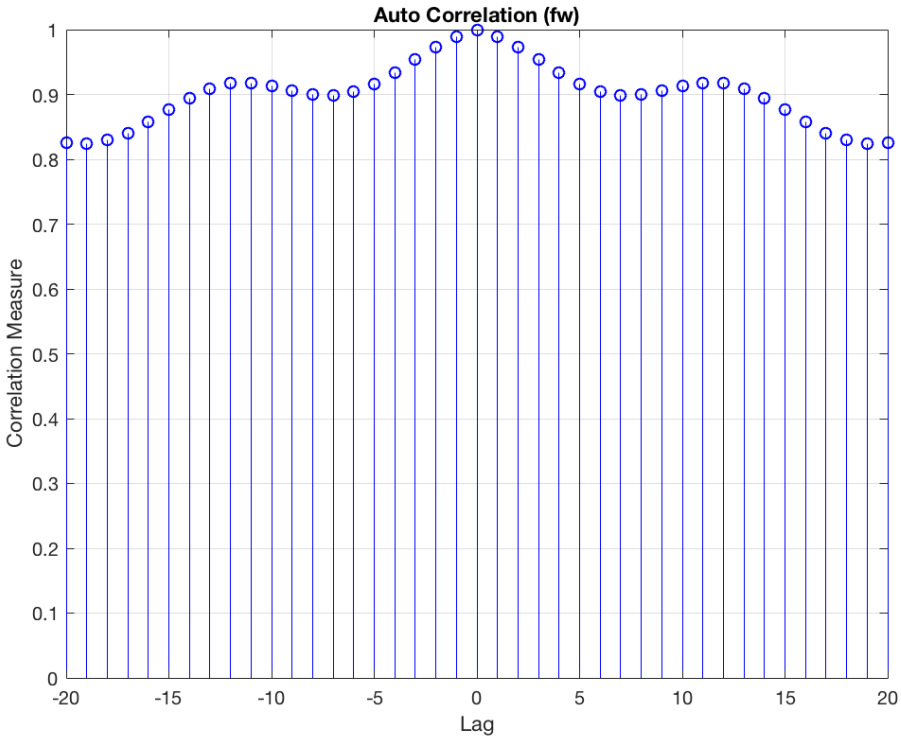

(b) Autocorrelation analysis

Figure 6.11: Data analysis of Amazon region. (a) Correlation between average temperature and wetland fraction, (b) Autocorrelation of wetland fraction.

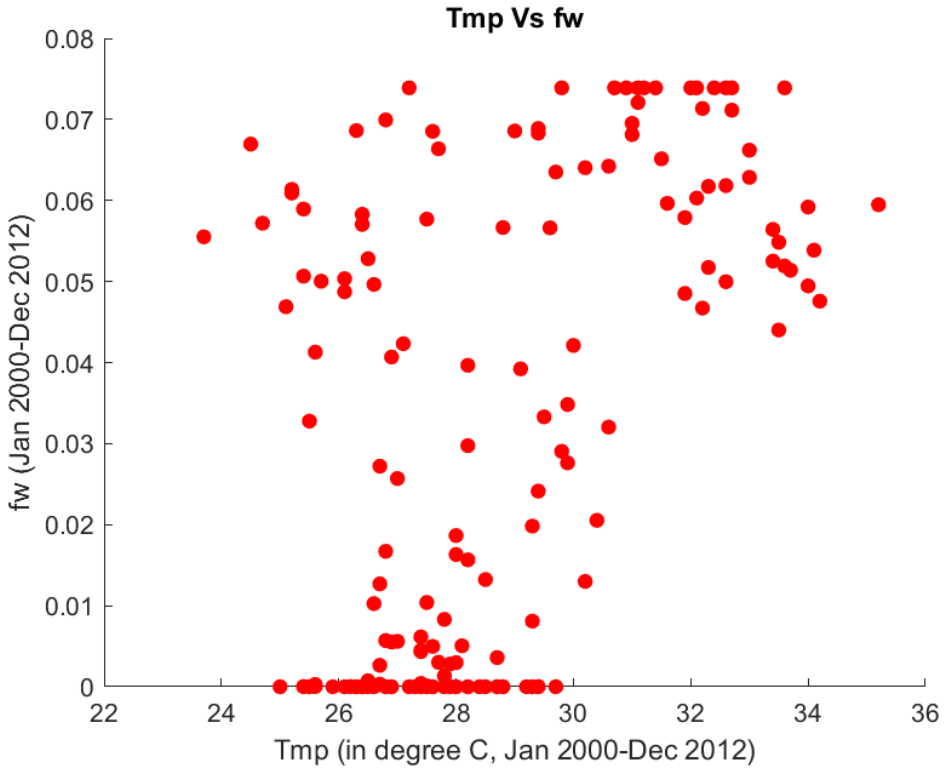

(a) Correlation analysis

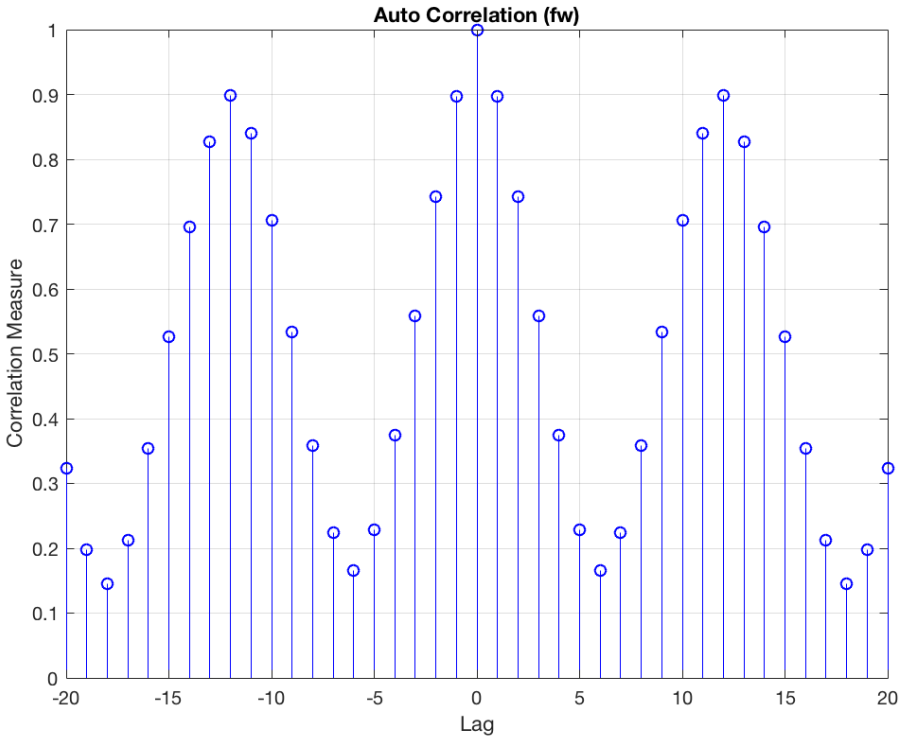

(b) Autocorrelation analysis

Figure 6.12: Data analysis of African region. (a) Correlation between average temperature and wetland fraction, (b) Autocorrelation of wetland fraction.

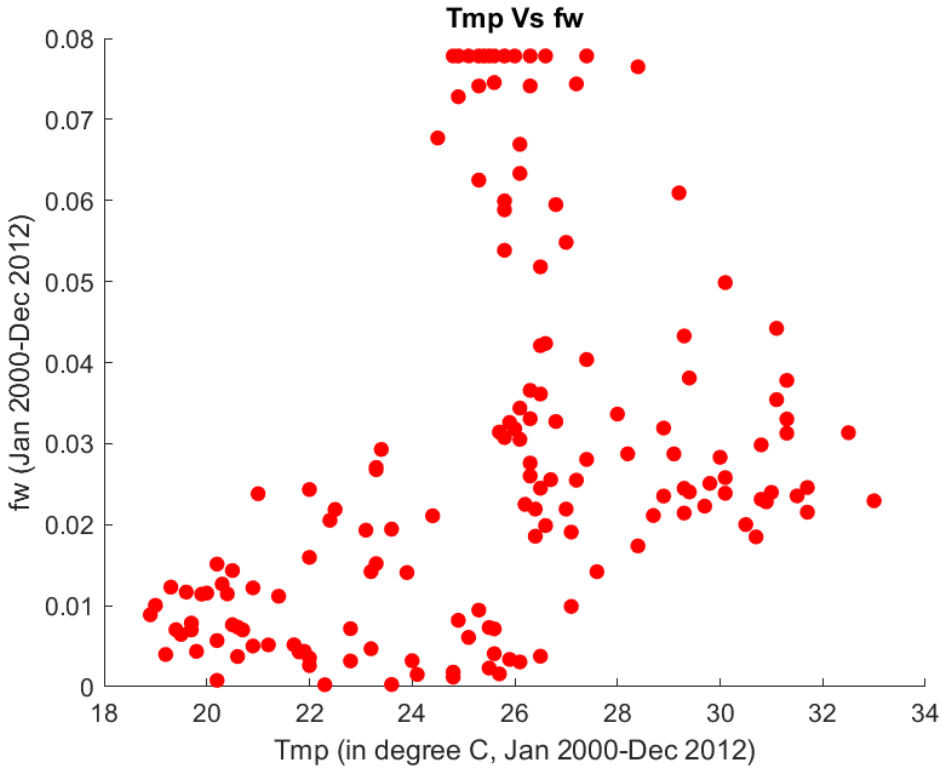

(a) Correlation analysis

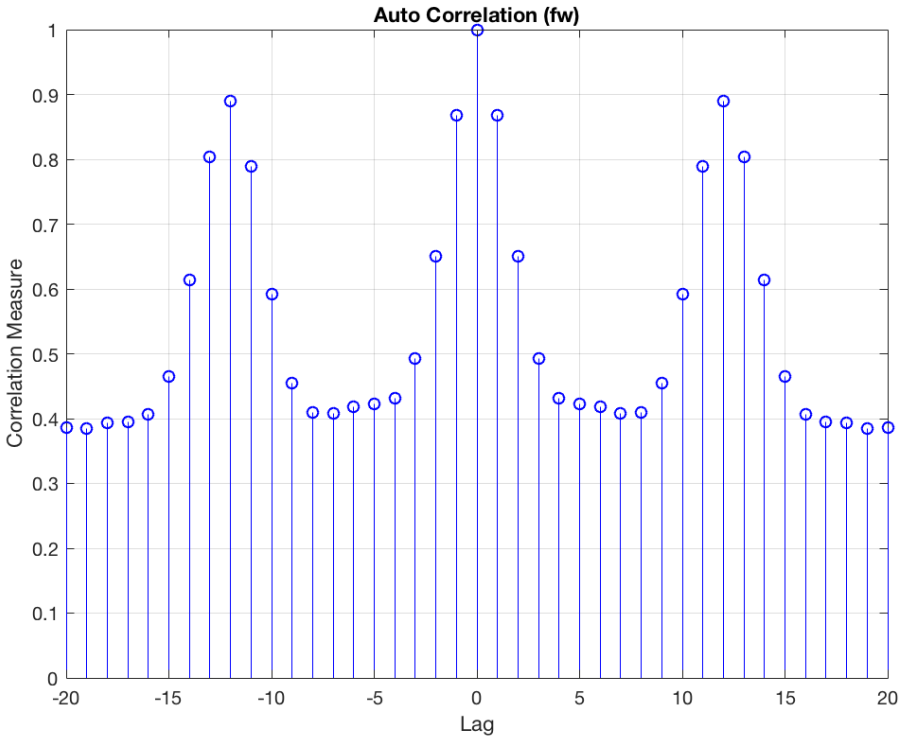

(b) Autocorrelation analysis

Figure 6.13: Data analysis of Asian region. (a) Correlation between average temperature and wetland fraction, (b) Autocorrelation of wetland fraction.

as compared to some analytical models discussed in the last chapter.

$$\begin{aligned} \hat{y}(t) = \theta_1 \cdot \hat{y}(t-1) + \theta_2 \cdot \hat{y}(t-2) \cdot \hat{y}(t-2) \cdot \hat{y}(t-6) \\ +\theta_3 \cdot u(t-1) \cdot u(t-6) + \theta_4 \cdot \hat{y}(t-1) \cdot u(t-1) \cdot u(t-6) \\ +\theta_5 \cdot u(t-5) \cdot u(t-6) + \theta_6 \cdot \hat{y}(t-5) \end{aligned} \tag{6.5}$$

6.4.3 ABC based parameter estimation

The ABC-SMC was used for the parameter estimation of all the available tropical sites across the globe. In the Chapter 3, the ABC-SMC algorithm had been presented in a purely theoretical sense. In this section, the algorithm steps will be presented again but with the exact values of threshold, population steps, particle size etc. This is the ABC-SMC algorithm as presented in [35] and the same was implemented in this study. Tropical wetland model parameter estimation steps according to the ABC-SMC are as follows,

- Number of iterations was set to $K = 11$ and number of parameter samples $L = 1000$.
- Prior distribution of parameters is denoted by $\pi(\theta)$ and error sequence as, $\epsilon_1 > ... > \epsilon_K$.
- ϵ_1 was set to $2d_{min}$ and ϵ_K was kept at d_{min}, where the d_{min} was determined by running the basic version of ABC for L samples. d_{min} is actually the least value among all the L distance measure.
- L_2 norm was used for the distance function $d(.)$ in the following steps.
- Parameter perturbation kernel ζ was chosen to be uniform random walk.

These listed information were used to parameterise the ABC-SMC algorithm, stated below.
Input number of iterations K and number of parameter samples L
prior $\pi(\theta)$ and error sequence $\epsilon_1 > ... > \epsilon_K$
At $k = 1$
  for $j = 1 : L$
    draw $\theta_j^* \sim \pi(\theta)$ and simulate $y_j^* \sim p(\mathrm{y}|\theta_j^*)$
    until $d(S(y_j^*), \mathrm{S}(y)) \leq \epsilon_1$
  end for
  set each weight $w_j^1 = \frac{1}{L}$
for $k = 2 : K$
  for $j = 1 : L$

sample θ_j^* from $\theta^k - 1$ with probabilities w^{k-1}
perturb θ_j^* to obtain $\theta_j^{**} \sim \zeta(\theta|\theta^*)$
simulate $y_j^* \sim p(\mathrm{y}|\theta_j^{**})$ until $d(S(y_j^*), \mathrm{S}(y)) \leq \epsilon_k$
end for
Set each $\theta_j^k = \theta_j^{**}$
Set each $w_j^k = \frac{\pi(\theta_j^k)}{\sum_{i=1}^{L} w_i^{k-1} \zeta(\theta_i^{k-1}|\theta_j^k)}$, and normalise
end for

θ_j^K obtained at the end of this loop is an estimate of the posterior distribution $\mathrm{p}(\hat{\theta}|\mathrm{y})$, where ζ is a parameter perturbation kernel, which can be a uniform or Gaussian random walk.

6.4.4 Parameter distribution

Bayesian statistical inference provides a probability distribution of parameters instead of point estimates of parameter values. An optimisation method such as least square in the stage 1 returned an optimal set of parameters. That does not provide any information about the sensitivity of model to the different parameters. In real world situation, the data is often noisy and hence an unbiased parameter can not be estimated easily. The NARMAX model structure however tries to address this issue with 'moving average' part, which is essentially a noise modelling. In practice, obtaining a NARMAX model structure is very difficult and hence this study was based on NARX model class.

As mentioned in the beginning of this section, parameter estimation for all the sites became imperative after the first stage of modelling. In addition to the current method (ABC), there are also some other potential deterministic approaches for estimating the parameters of all the sites. The Bayesian inference, particularly the ABC appears to be a better choice mainly because the ABC returns the shape of all the intermediate distributions without any additional computational effort. These distributions could be employed for analysing the sensitivity of model to different parameters. A model exhibits higher sensitivity towards the parameters, which got inferred in earlier population and have a very small interval in the subsequent distributions. If there is not much changes in a parameter distribution, as the iteration progresses and the distribution remains nearly same like the first population then the particular parameter may not be inferred through the current data [33].

In this study the ABC comprised of 11 iterations, which generated 11 populations of parameter distributions. At the beginning of the algorithm, parameters were sampled from the uniform distribution. In a Bayesian inference, we can in-

duce our knowledge about the system. In this case, informed prior distribution in the beginning was based on the least square estimates. Nevertheless, the prior was uniformly distributed with a reasonable range as shown in the figure 6.14, 6.16, and 6.18. These scatter plots incorporate the intermediate distributions of all the parameters for all the regions under study and can be regarded as a summary of all the steps followed by the ABC-SMC algorithm. First iteration, which is essentially an ABC rejection step generated the first set of posterior distribution (population 1). For the second iteration, parameters were sampled from the population 1. Which means posterior at the population 1 serves as a prior for the population 2. The posterior distributions for all the iterations till the K^{th} iteration were estimated in a similar fashion.

The posterior parameter distribution is shown using the histograms in the figure 6.15, 6.17, and 6.19 for the Amazon, African and Asian regions. According to these distributions the tropical wetland model appears to have higher sensitivity towards the parameters θ_1, θ_5, and θ_6. All these parameters exhibit very narrow interval in the their posterior distribution. Joint probability shown using the scatter plots of the intermediate distributions (figure 6.14, 6.16, and 6.18) indicate that θ_1 and θ_6 are cancelling out each other. The exact interpretation of this phenomena especially in the context of their effects on the wetland fraction will be discussed in later part of this section.

6.4.5 Model characteristics

A NARX model representing the dynamics of the tropics was developed in this study. In the previous subsections, modelling steps have been discussed. Unlike an optimisation approach, the Bayesian inference generated a distribution of parameters instead of a unique set of parameter values. The model characteristics can not be teased apart thoroughly unless a set of parameter values are extracted from the available distribution. Averaging of parameter values in a distribution provides a robust set of parameter. The remote sensing data used for the parameter estimation in this study is susceptible to be affected by noise present in the satellite measurement setup. Therefore, averaging seems to be a better choice than a more popular choice known as maximum a posterior (MAP) estimate. In simple words, MAP is the mode of a parameter distribution. The averaged parameter sets of all the sample sites, calculated as 'true parameters' are presented in the Table 6.8.

The model structure gives a general impression that, it is an output driven model as the first term contains a lagged output term. First term and its positive parameter values for all the regions signify that, the wetland distribution in

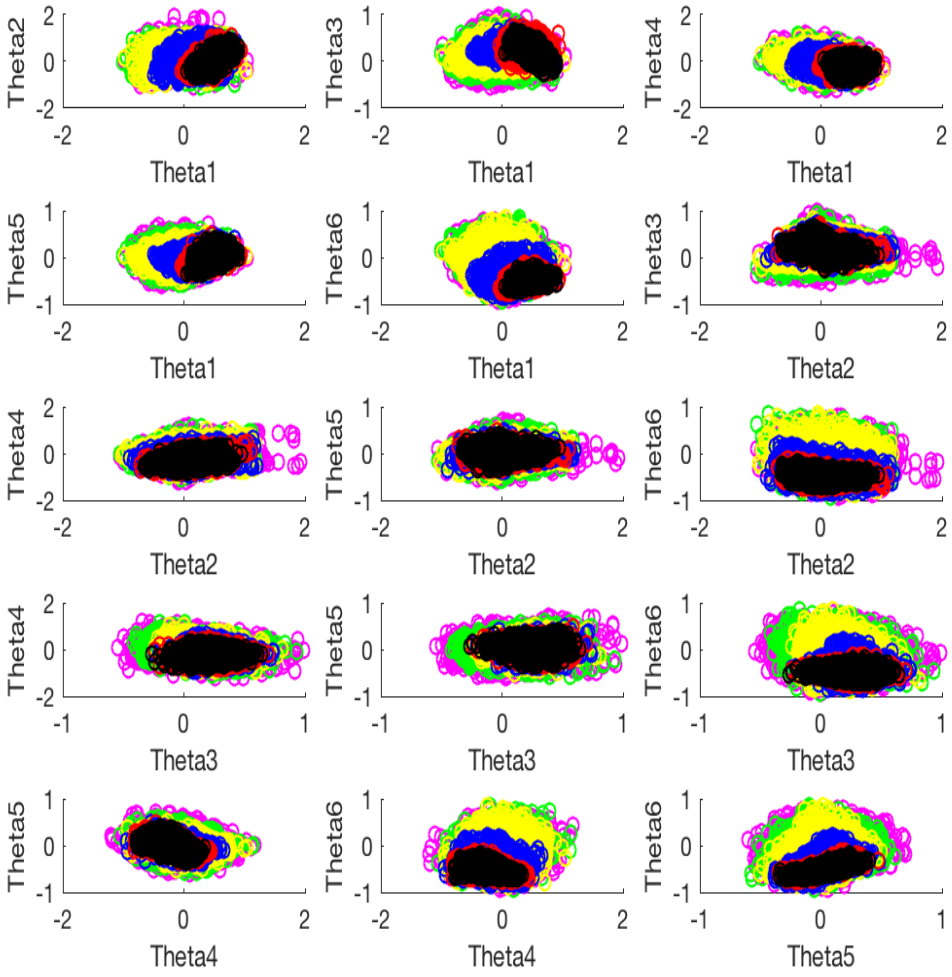

Figure 6.14: ABC-SMC intermediate steps – Amazon. (Magenta – Population 1, Green – Population 2, Yellow – Population 5, Blue – Population 7, Red – Population 9, Black – Population 11). All the scattered plots among parameters demonstrate the sequential steps of the ABC, which shrink the parameter space after every iteration. These plots also show the joint probability of any two parameters.

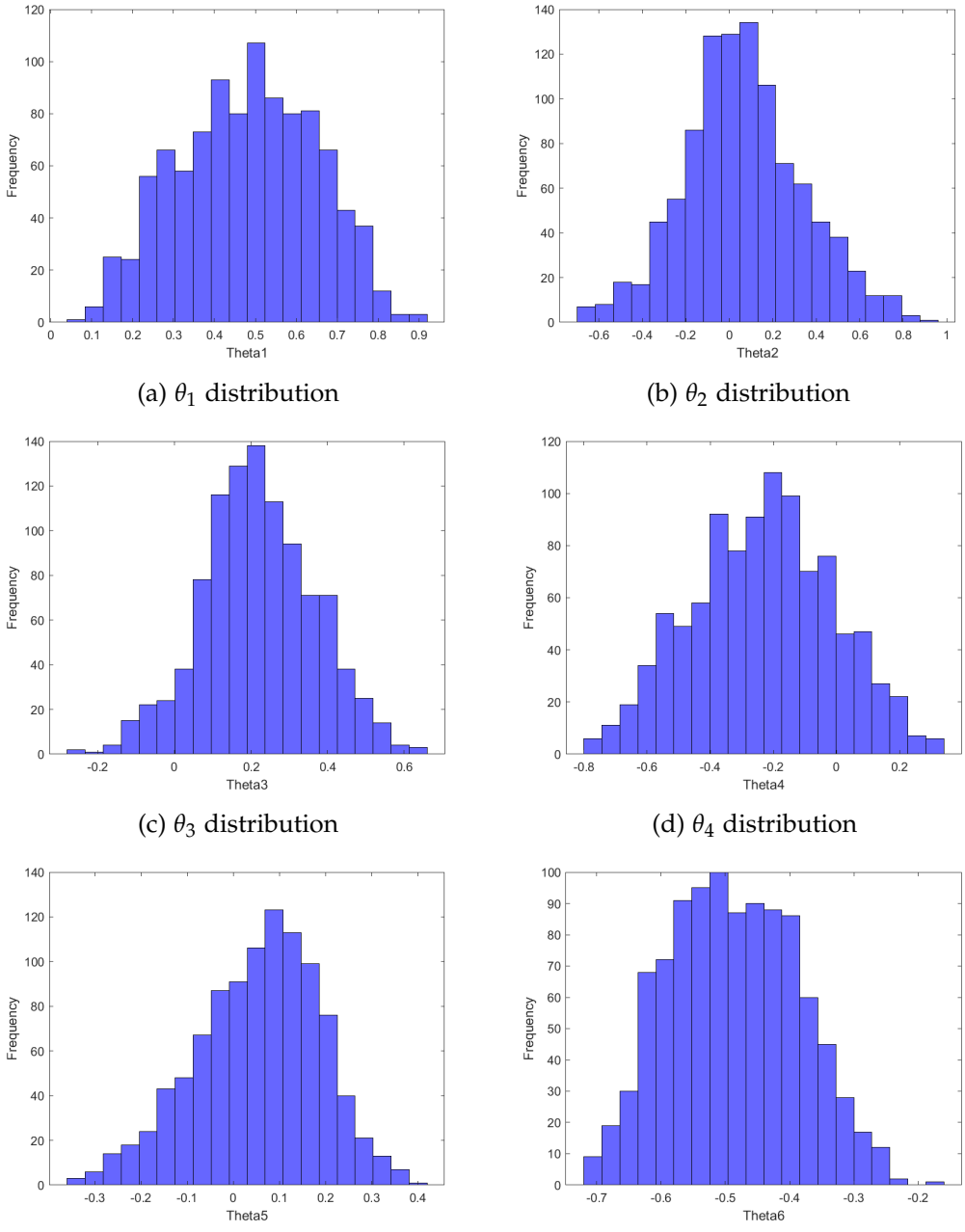

(a) θ_1 distribution

(b) θ_2 distribution

(c) θ_3 distribution

(d) θ_4 distribution

(e) θ_5 distribution

(f) θ_6 distribution

Figure 6.15: Parameter distribution at the final step (posterior) − Amazon.

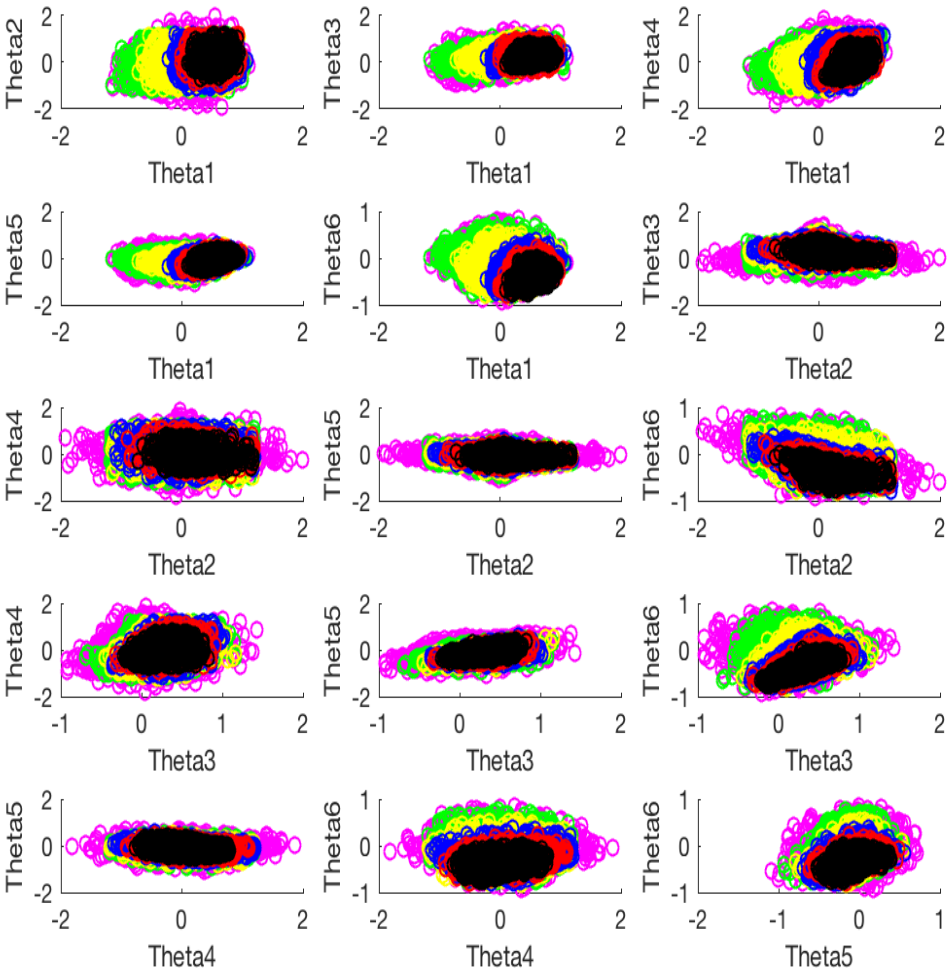

Figure 6.16: ABC-SMC intermediate steps – Africa. (Magenta – Population 1, Green – Population 2, Yellow – Population 5, Blue – Population 7, Red – Population 9, Black – Population 11). All the scattered plots among parameters demonstrate the sequential steps of the ABC, which shrink the parameter space after every iteration. These plots also show the joint probability of any two parameters.

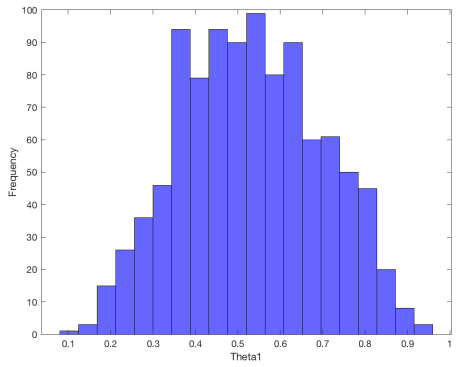

(a) θ_1 distribution

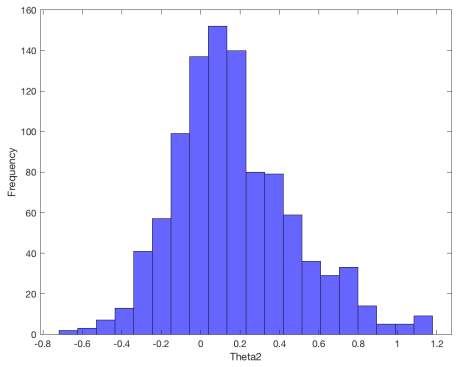

(b) θ_2 distribution

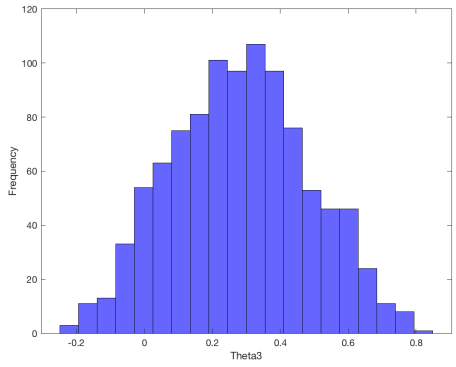

(c) θ_3 distribution

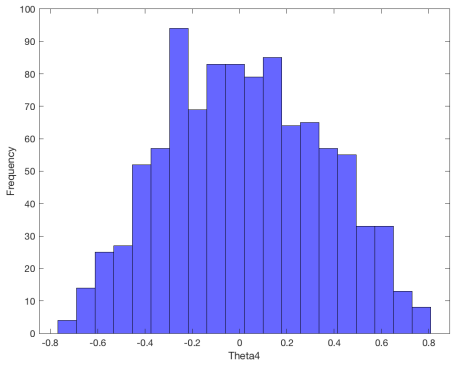

(d) θ_4 distribution

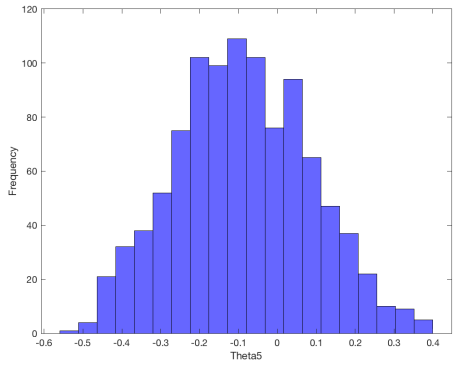

(e) θ_5 distribution

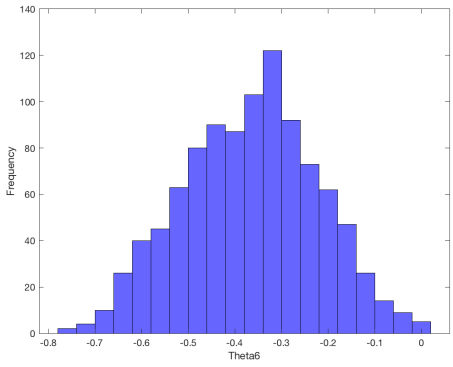

(f) θ_6 distribution

Figure 6.17: Parameter distribution at the final step (posterior) − Africa.

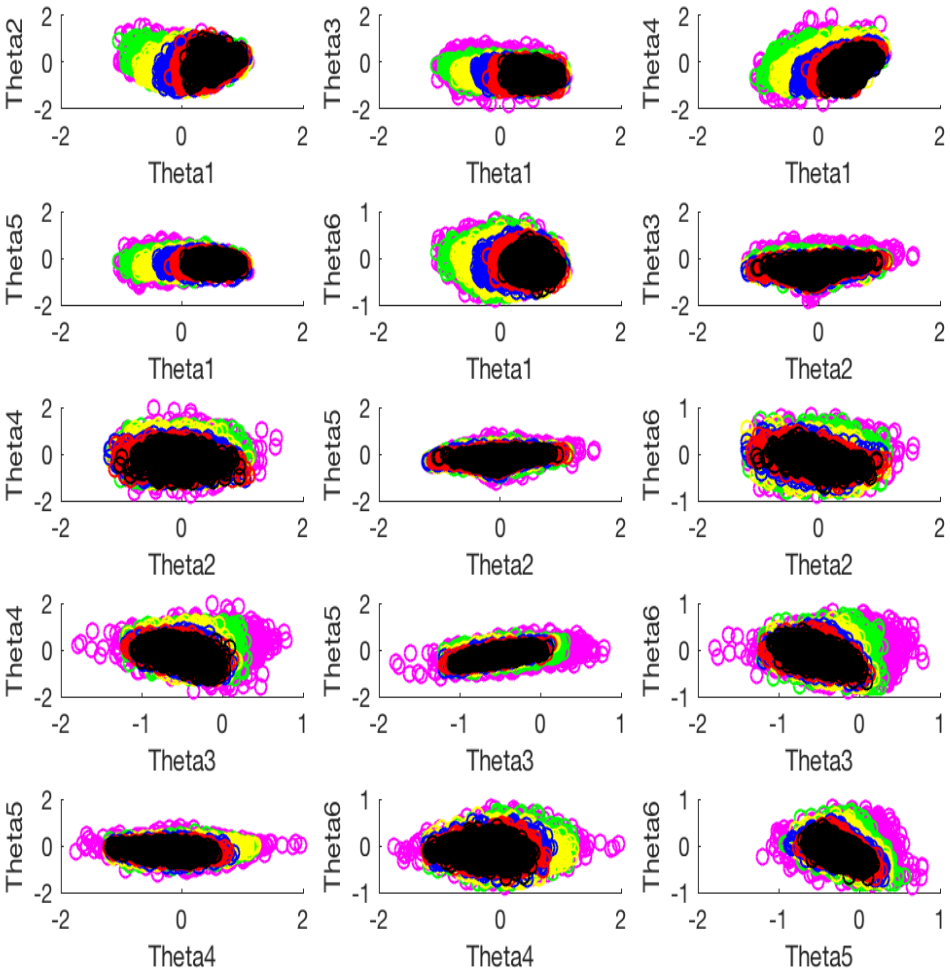

Figure 6.18: ABC-SMC intermediate steps - Asia. (Magenta – Population 1, Green – Population 2, Yellow – Population 5, Blue – Population 7, Red – Population 9, Black – Population 11). All the scattered plots among parameters demonstrate the sequential steps of the ABC, which shrink the parameter space after every iteration. These plots also show the joint probability of any two parameters.

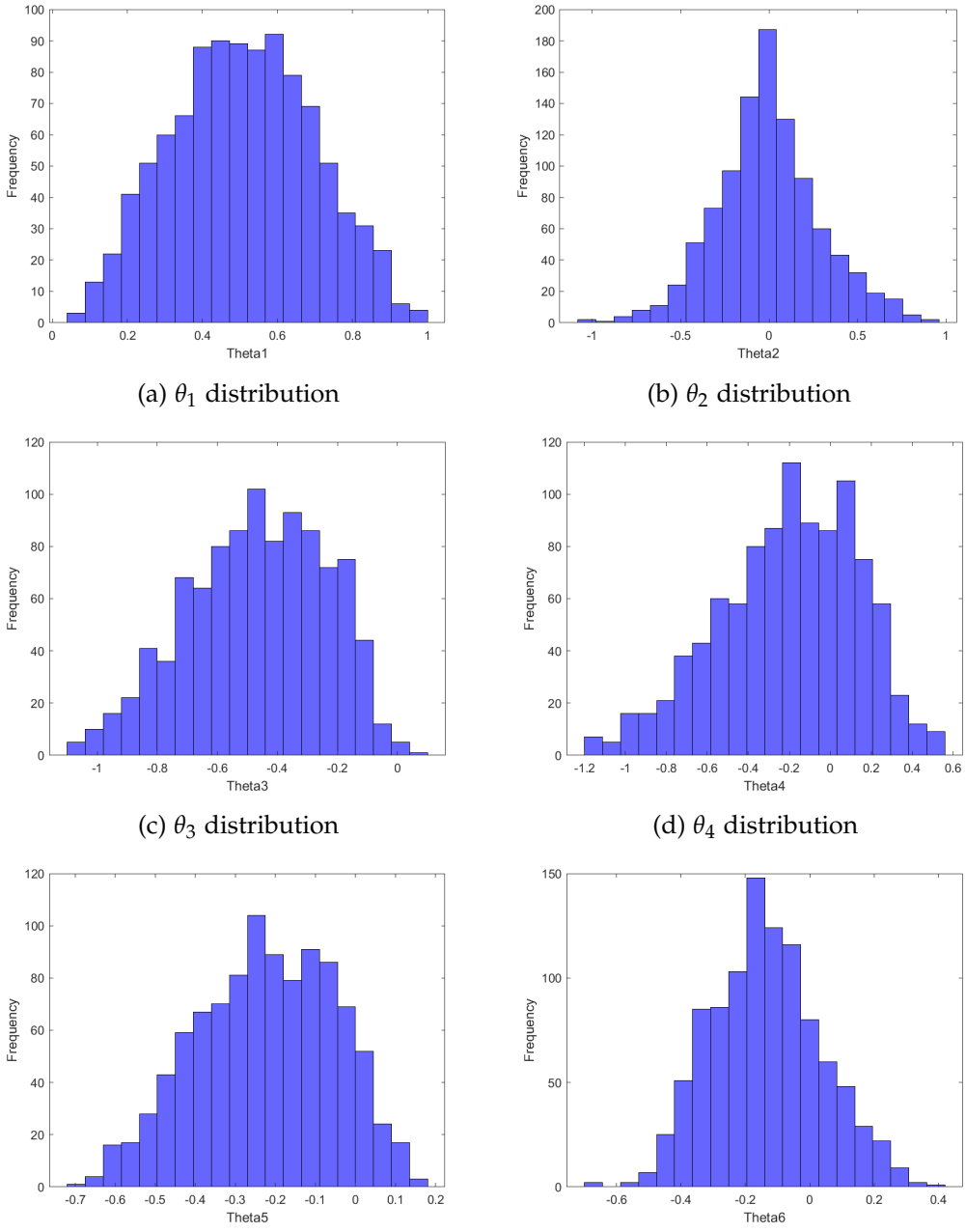

(a) θ_1 distribution

(b) θ_2 distribution

(c) θ_3 distribution

(d) θ_4 distribution

(e) θ_5 distribution

(f) θ_6 distribution

Figure 6.19: Parameter distribution at the final step (posterior) − Asia.

Region	θ_1	θ_2	θ_3	θ_4	θ_5	θ_6
Amazon	0.592	0.022	0.036	-0.265	0.102	-0.511
Africa	0.577	-0.022	0.048	-0.001	0.026	-0.546
Asia	0.628	-0.020	-0.511	0.063	-0.232	-0.311

Table 6.8: Parameter Sets (calculated by averaging the corresponding posterior distribution).

the previous month contributes mostly towards the fraction of wetland in the current month. This also fits perfectly with the physical characteristics of wetlands. Change in wetland distribution is not a very fast process, so the current extent of inundation should not vary much from the last month. Second most contributing term also contains the time lagged wetland fractions but up to lag 6. This means, the chosen output lag value at the beginning of the modelling was a right decision. Third and fifth term contain only the time lagged input variable. This means, even though model is mostly output driven, temperature plays some roles towards the inundation of a land area in tropics. The last term is entirely based on output like the first term, but the parameter values are approximately equal and opposite to the first term. At first, it gives an impression that both these terms are sort of canceling each other but that is not the case here. The wetland fraction is following a cycle, where crests and troughs are separated at around 6 months interval. So, the wetland fraction values do not repeat in 6 months time, in fact an approximate repetition can be noticed after an interval of 12 months. To ensure that the last term is not redundant, the term was eliminated on a trial basis to obtain a model containing just the first five terms. In that case, model performance deteriorated dramatically.

6.4.6 Simulation results

The global tropical wetland model developed in this section is supposed to be an improved version of the model developed solely using the least square technique in the last section. Firstly, the present model incorporates all the available tropical sites in the modelling steps. Secondly, the parameter of all the sites are estimated separately so that the topographical details are captured in the form of parameter. Nevertheless, a single model structure of the tropics manifests the common dynamics of all the tropical sites.

In the last section, model simulation was evaluated using their OSA. Obviously, the OSA prediction does not guarantee a robust predictive capability of the model. Here, MPO will be used for demonstrating the performance of the model across three regions of the tropics - Amazon, Africa, and Asia. In this case also, model

Site	Region	Std. deviation (fw)	Mean (fw)
1	Amazon	0.0862	0.4394
2	Africa	0.0286	0.0323
3	Asia	0.0236	0.0285

Table 6.9: Basic statistical information of the wetland fraction data (output), corresponding to all three sample sites from Amazon, Africa, and Asia regions.

structure detection and parameter estimation was performed using the z-scored data. Therefore, the wetland fraction (fw) was passed through inverse transformation process to demonstrate the fw in its actual range, which lies between 0 and 1. The mean and the standard deviation of the raw data corresponding to all three regions are presented in the Table 6.9.

The simulation results of the Amazon, African, and Asian regions are shown in the figure 6.20, 6.21, and 6.22 respectively. The data until August 2006 (80^{th} month) was used for the estimation, whereas, the data from September 2006 (81^{st} month) onward is the fresh data, used solely for the model evaluation purpose. The MPO prediction results are in sync with the observed data for all the regions. Thus the NARX wetlands model (equation 6.5) fairly represents the wetland dynamics of the tropical regions across the globe. A satisfactory performance of the MPO also emboldens the predictive power of this model.

6.5 Parameter mapping

The parameter mapping all the three regions - Amazon, Africa, and Asia are shown in the figure 6.23, 6.24, and 6.25.

This modelling approach is considering a climatic variable (average temperature) as the key driver for calculating the inundation of a land area. In reality, wetland distribution depends upon a wide range of topographical factors such as, vegetation type, soil porosity, orography etc. For instance, a site having more paddy fields will naturally have more inundation than the sites having other kind of crops. Similarly, a site having high amount of soil organic matter would result into an enhanced level of soil porosity and a highly porous condition might limit the inundation. All the sites falling between the Tropics of Cancer and Tropics of Capricorn are exhibiting similar types of climates, especially the temperature range do not vary much. This feature was utilised in the current modelling process for obtaining a common model structure of all the tropical wetlands.

Topographical variations of the wetland sites are incorporated using the CTIs in the TOPMODEL approach of wetland modelling [105–107]. In the last chap-

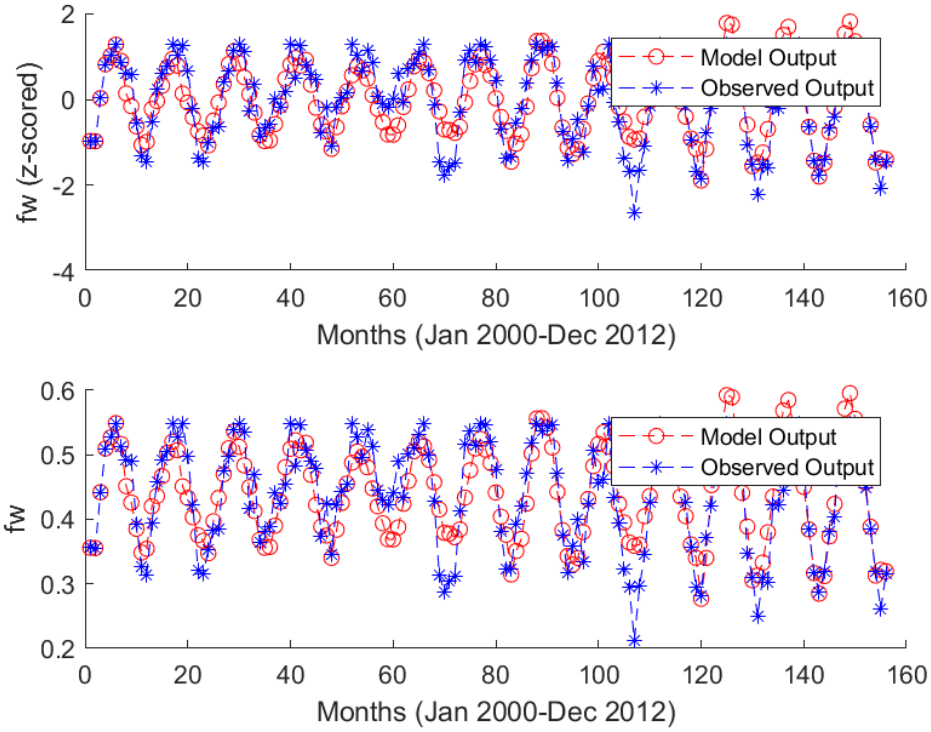

Figure 6.20: Model predicted output (MPO) simulation results for Amazon site. The simulation results are shown for the standardised data (top) and the data in its actual range (bottom), obtained after inverse transformation.

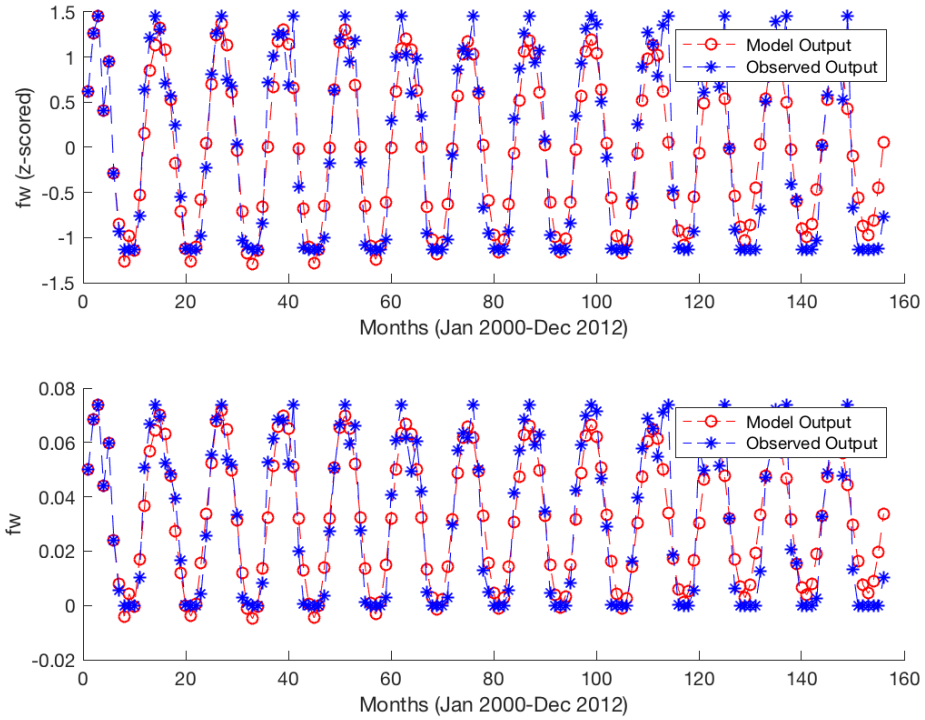

Figure 6.21: Model predicted output (MPO) simulation results for African site. The simulation results are shown for the standardised data (top) and the data in its actual range (bottom), obtained after inverse transformation.

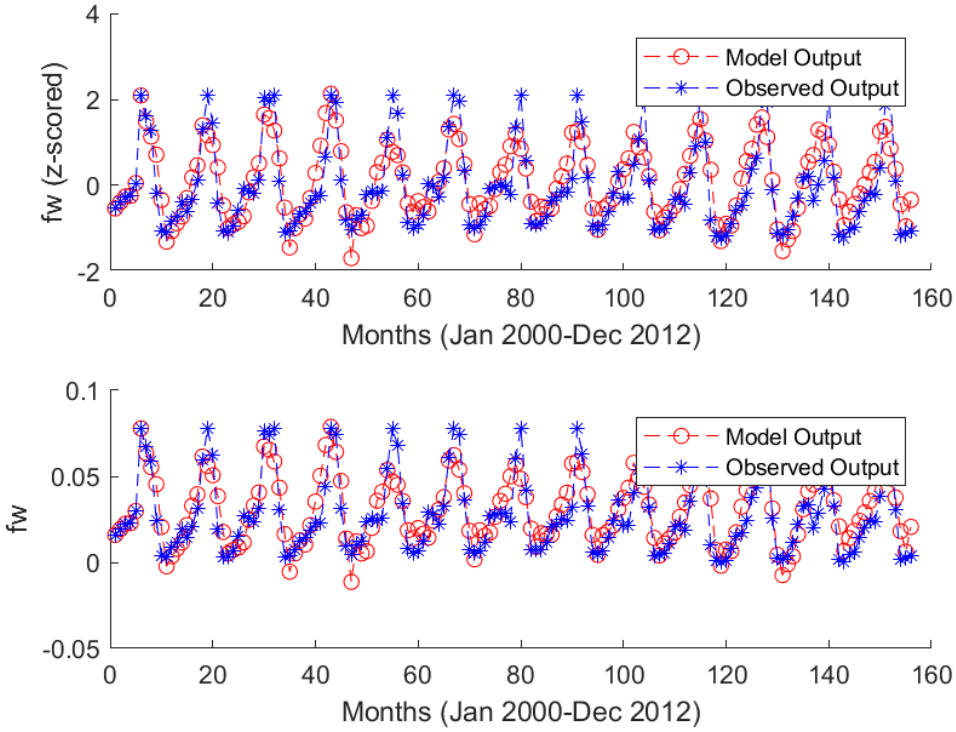

Figure 6.22: Model predicted output (MPO) simulation results for Asian site. The simulation results are shown for the standardised data (top) and the data in its actual range (bottom), obtained after inverse transformation.

ter, this methodology was discussed in detail. In this study, separate parameter sets for each site takes into account such kind of topographical variations. The third and fifth terms in this model contain only the input variables, which is temperature. All the regions - Amazon, Africa, and Asia show very little variations among the two parameters θ_3 and θ_5 corresponding to these two terms. This goes perfectly with the underlying logic that climate inputs do not vary much among the tropical sites. First and the last term contain only the output variable, which is wetland fraction. The parameters corresponding to these two terms θ_1 and θ_6 exhibit a large variations. Again this fits perfectly with the above argument that, wetland distribution can vary significantly as the topography varies. The current NARX model does not incorporate the topographical factors directly but the lagged versions of wetland fraction (output) in the model do compensate for several complex topographical processes affecting the inundation.

6.6 Model performance

The developed wetland model was simulated for all the available sites. The mean fw (figure 6.26), mean annual maximum fw (figure 6.27) and mean annual minimum fw (figure 6.28) of both the simulation results and the actual observed data were compared. A similar kind of comparison has been made in the WETCHIMP project [109, 110]. In the previous chapter, results reported in the WETCHIMP project were critically analysed. In summary, the NARX model developed in this study is a much simpler description than the process based models used in the WETCHIMP. The comparison of basic statistics between the simulated results and the observed values place this NARX model in a higher fidelity zone, especially in terms of the prediction power exhibited by this model.

Only the tropical sites were available in this study compared to a truly global range of sites in the WETCHIMP. So one might argue that the NARX model is still not a true global model. However, the structured methodologies and a rigorous parameter inference based upon the Bayesian framework could certainly be employed to extend the current model to a global wetlands model. Obviously, the dynamics shown by a temperate region or other regions like Siberia would differ from the dynamics shown by the tropical region. In that case, maybe more than one model structure could be developed representing each climate region of the globe.

Another criticism which might come into play is that, the WETCHIMP project do not use any observed data in their model and try to predict the inundation based on the processes governing the water table and water flow in a site. On the

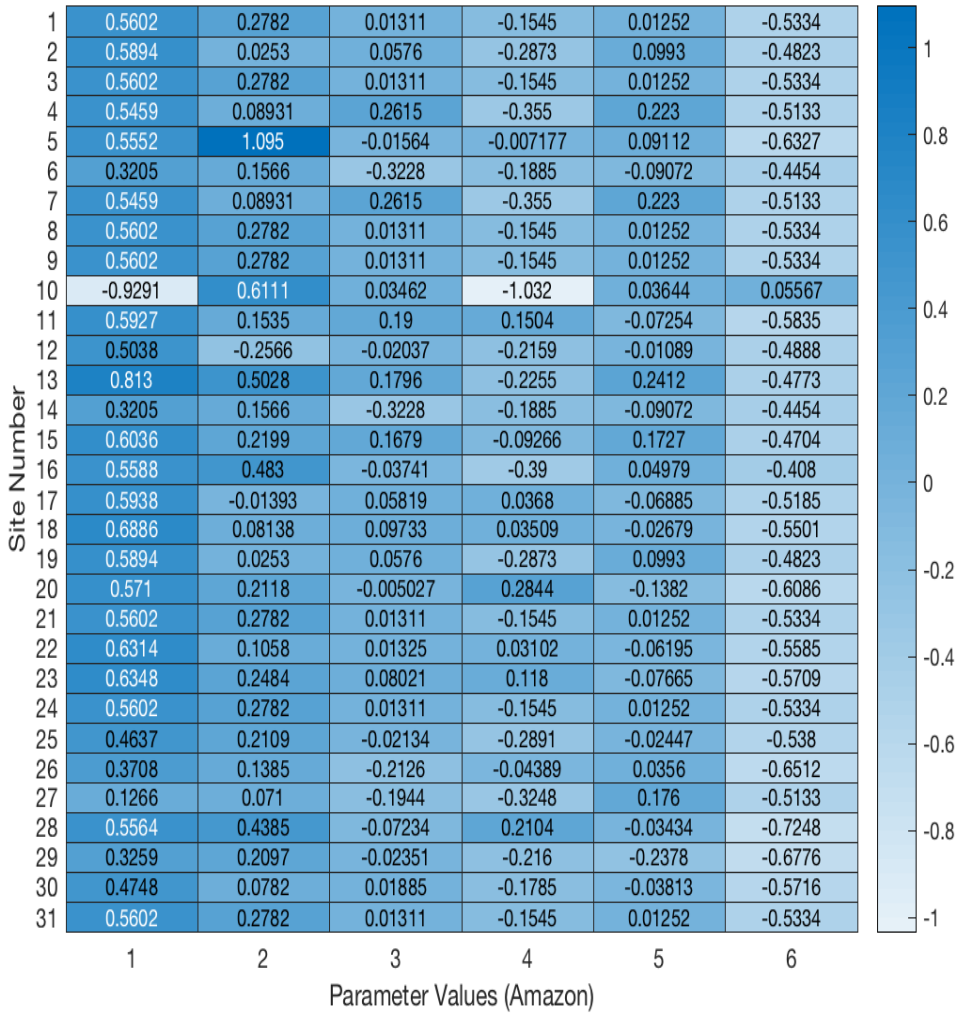

Figure 6.23: Mapping of tropical wetland model parameters corresponding to the Amazon region of the globe.

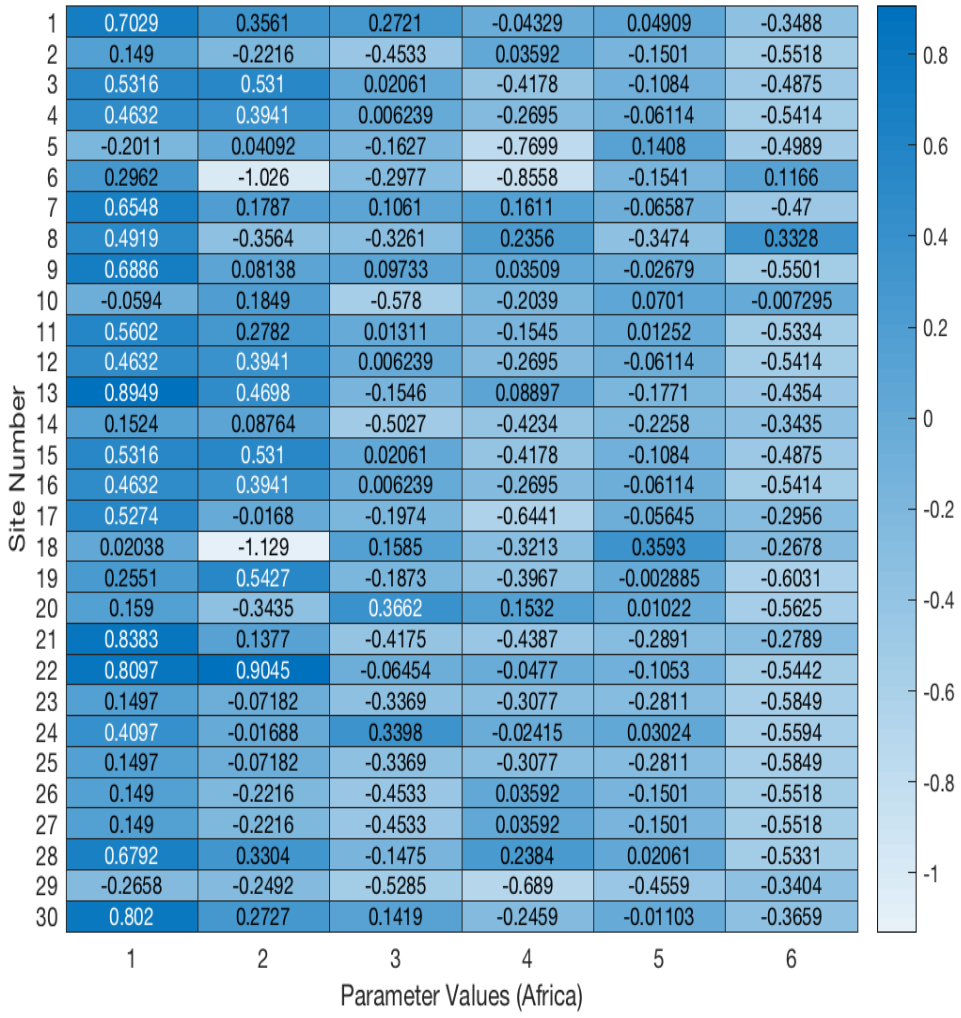

Figure 6.24: Mapping of tropical wetland model parameters corresponding to the African region of the globe.

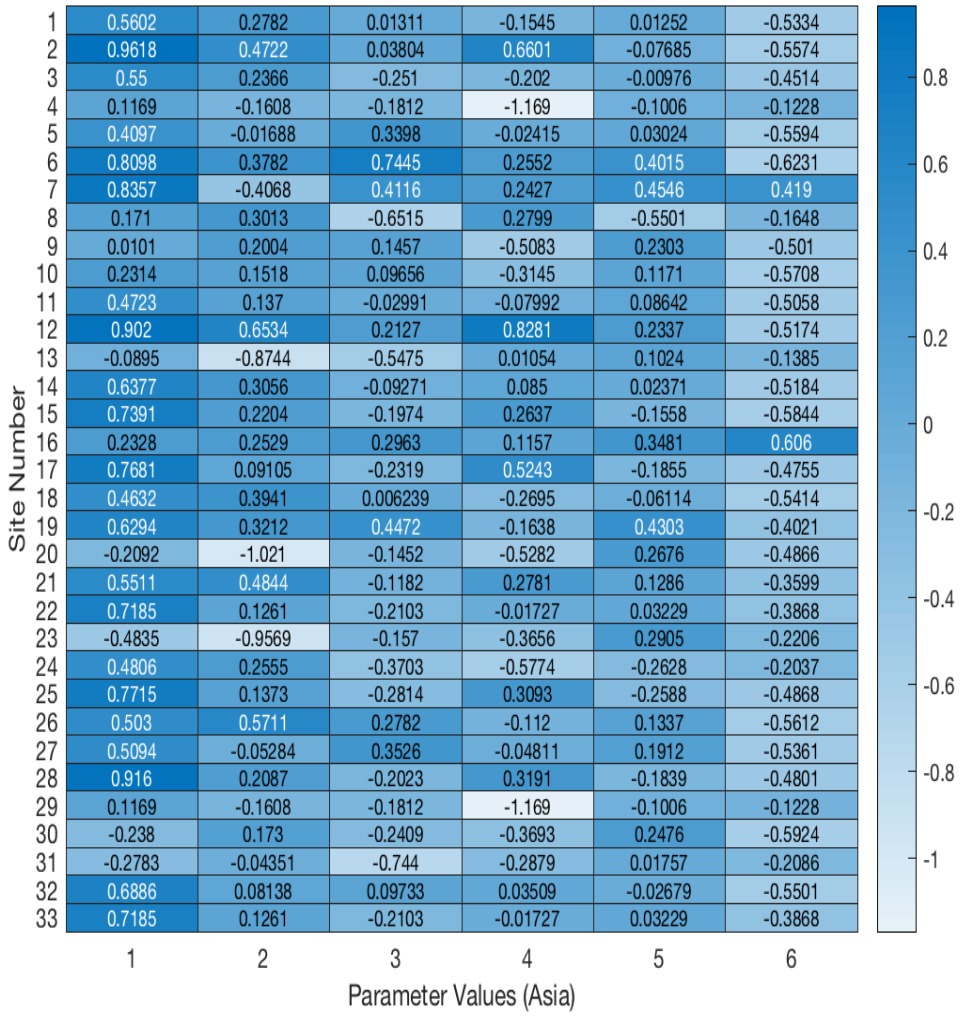

Figure 6.25: Mapping of tropical wetland model parameters corresponding to the Asian region of the globe.

other hand, prior information about a site in form of data is fed into the NARX modelling approach. But that can strongly be countered with the very fact that, process based modelling and data-driven modelling are distinctly two different frameworks. Each of these frameworks has its own advantages and disadvantages. If the prime purpose is to predict the extent of wetland distribution at the century end under the effects of climate change, then a NARX model exhibiting a good prediction efficiency would serve the purpose. However, if the purpose is to analyse the various actual factors governing the inundation in a month then obviously one would prefer a process based model, which is not yet available.

6.7 Conclusion

This chapter describes the modelling of tropical wetlands using the system identification methodology. The dataset used in the modelling exercise was generated and processed using the remote sensing technology. Wetland distribution is quantified here as wetland fraction, which is actually the fraction of land area showing the characteristics of wetlands. The characteristics of wetlands and the official benchmark for classifying them are based upon the criteria of the Ramsar Convention. The available dataset contains the environmental variables such as, evapotranspiration, soil water content, average temperature, and wetland fractions as monthly time series. Among these variables, wetland fraction naturally becomes the output of interest for the modelling purpose whereas the average temperature is considered as the input of the system. So, from systems perspective the whole problem of wetland modelling was posed as a SISO system identification. Input and outputs have a very different range so the data were standardised using the z-score normalisation, prior to any modelling steps. The entire study was categorised into two stages.

In the first stage, only three tropical sites were used for obtaining a parsimonious NARX wetland model. The model structure detection and the parameter estimation were carried out solely under a deterministic framework. This enabled a simple model demonstrating satisfactory OSA performance but that was not enough, as the prime purpose was to obtain a model useful for making robust predictions of wetland distribution under the future climate change scenarios.Therefore, the entire modelling was shifted to the next stage where the parameter estimation was carried out under a probabilistic framework known as the ABC. This enabled a mapping of model parameters corresponding to the sites scattered through the tropics of the globe. The MPO in this stage showed satisfactory performance. In addition to a satisfactory prediction power, this approach also generated

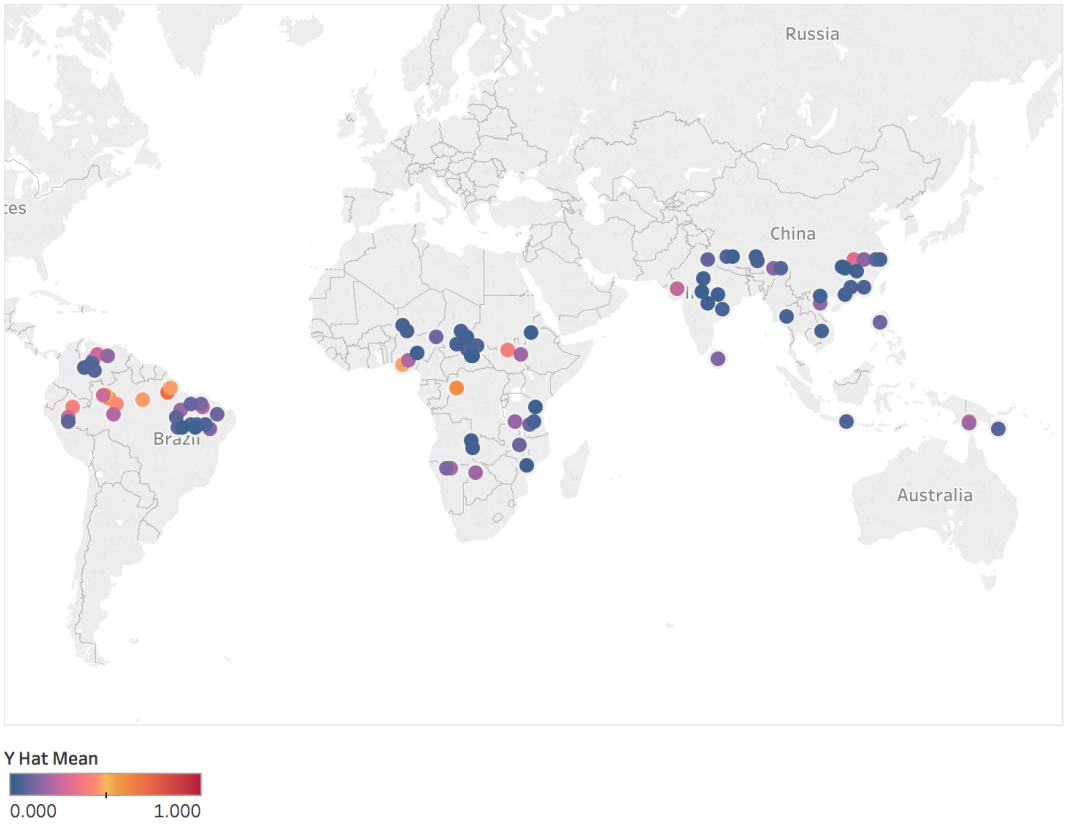

(a) yhat mean (model output)

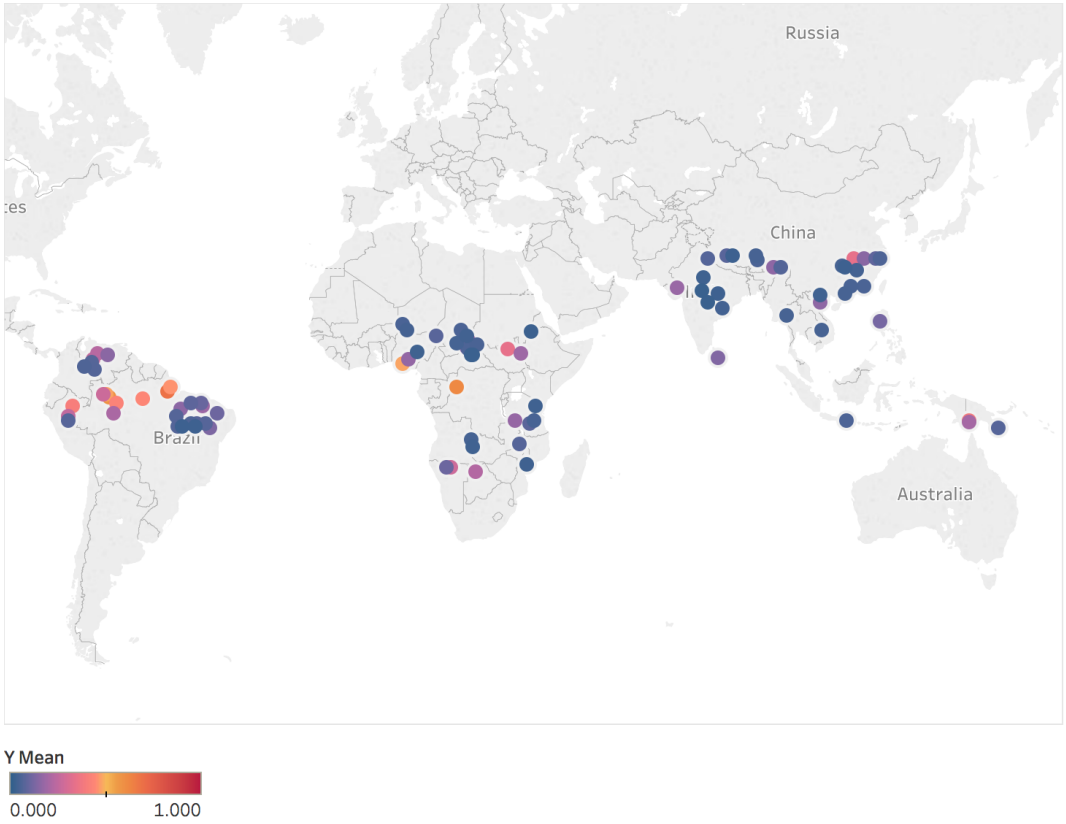

(b) y mean (observed output)

Figure 6.26: Mean wetland fraction (from 2008 to 2012) comparison between the model output and observed output.

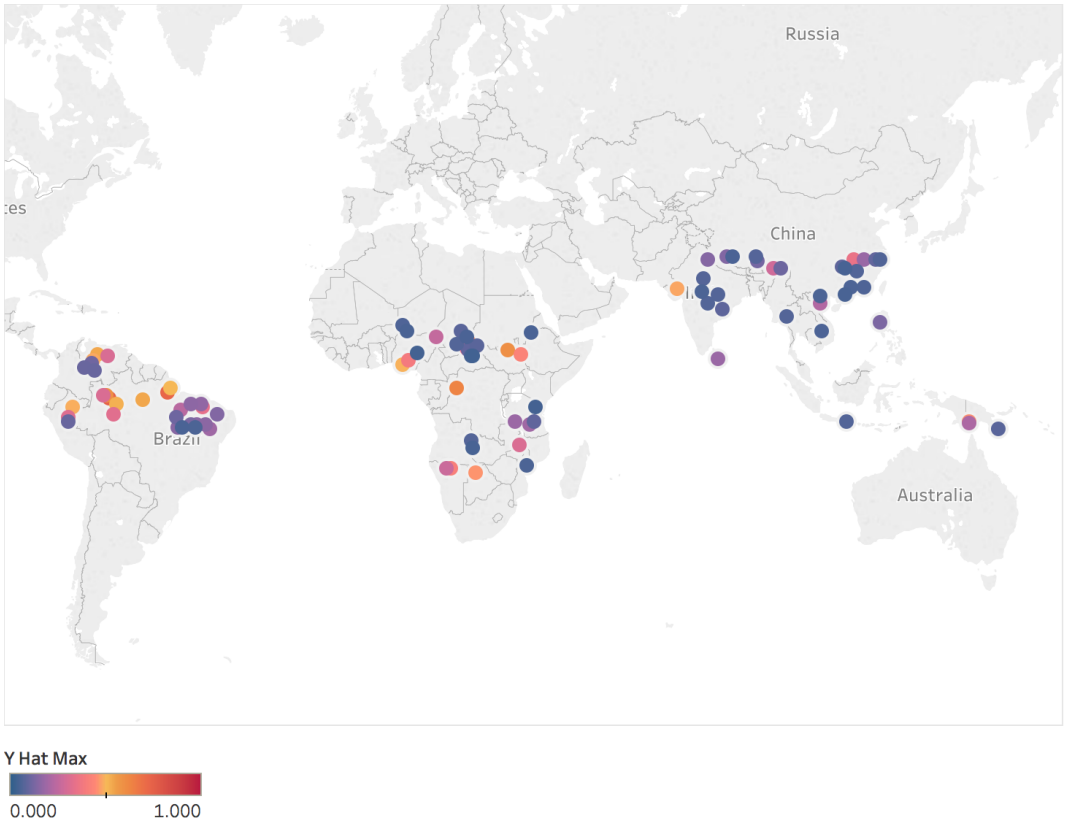

(a) yhat maximum (model output)

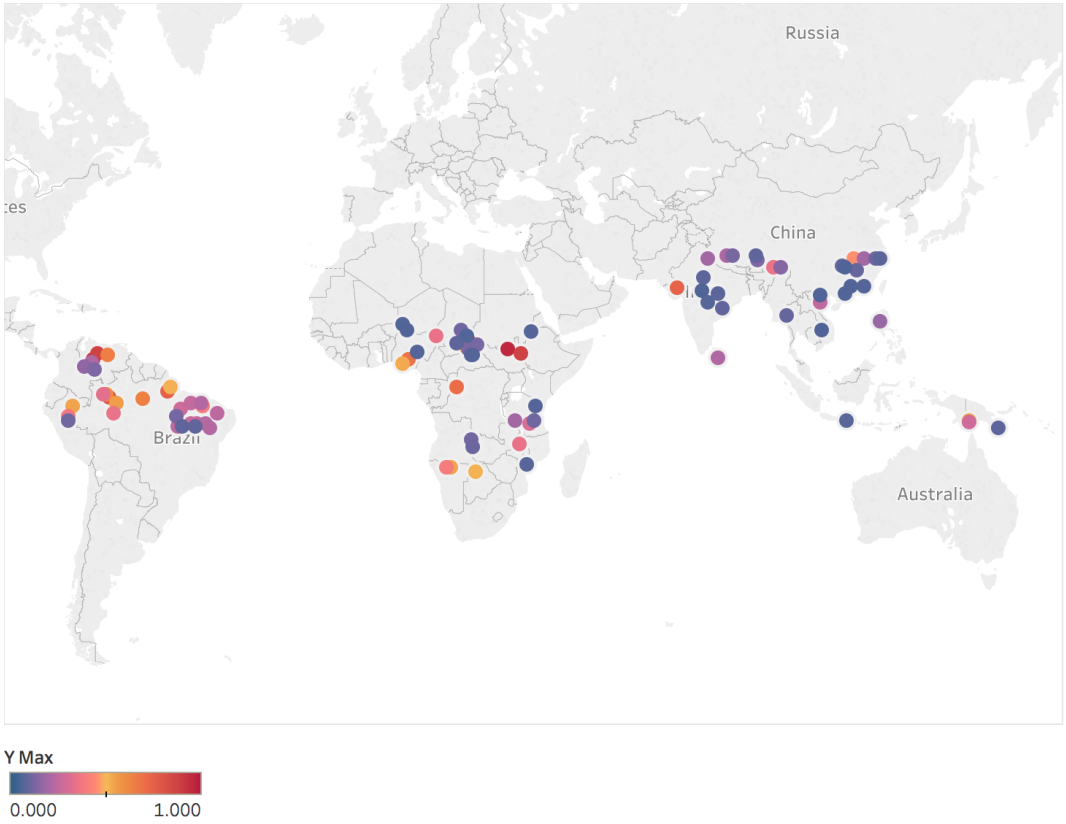

(b) y maximum (observed output)

Figure 6.27: Mean annual maximum wetland fraction (from 2008 to 2012) comparison between the model output and observed output.

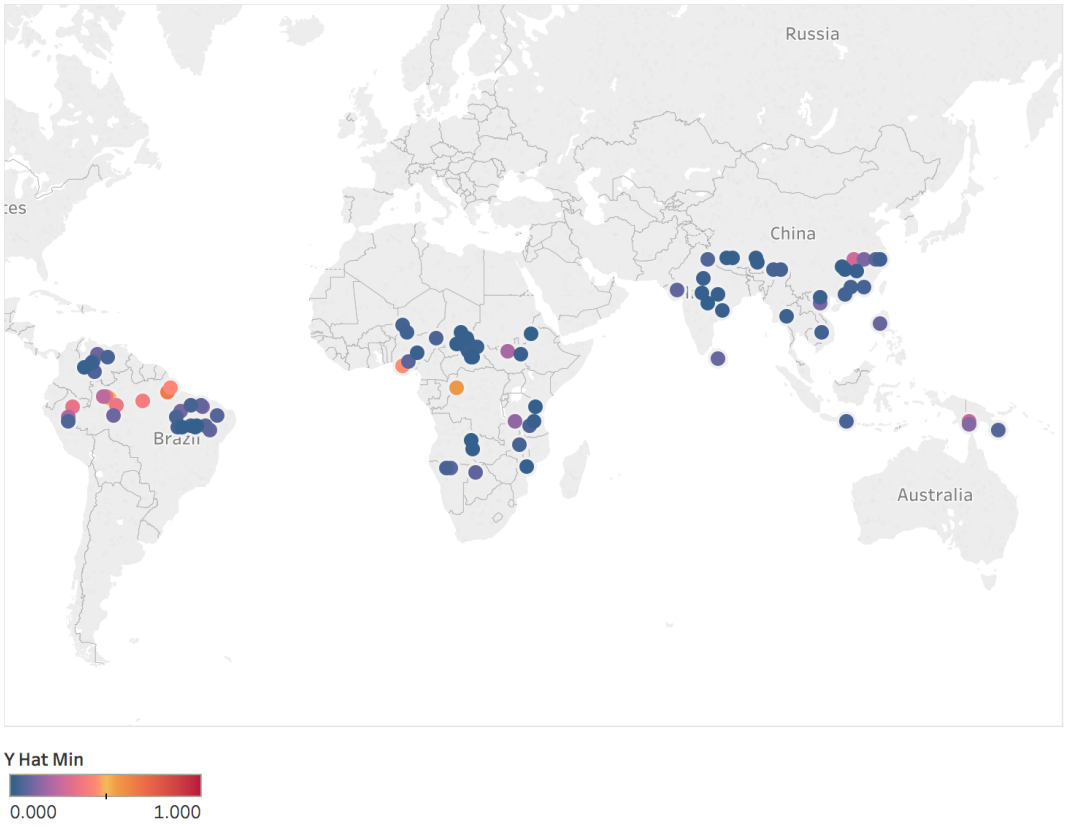

(a) yhat minimum (model output)

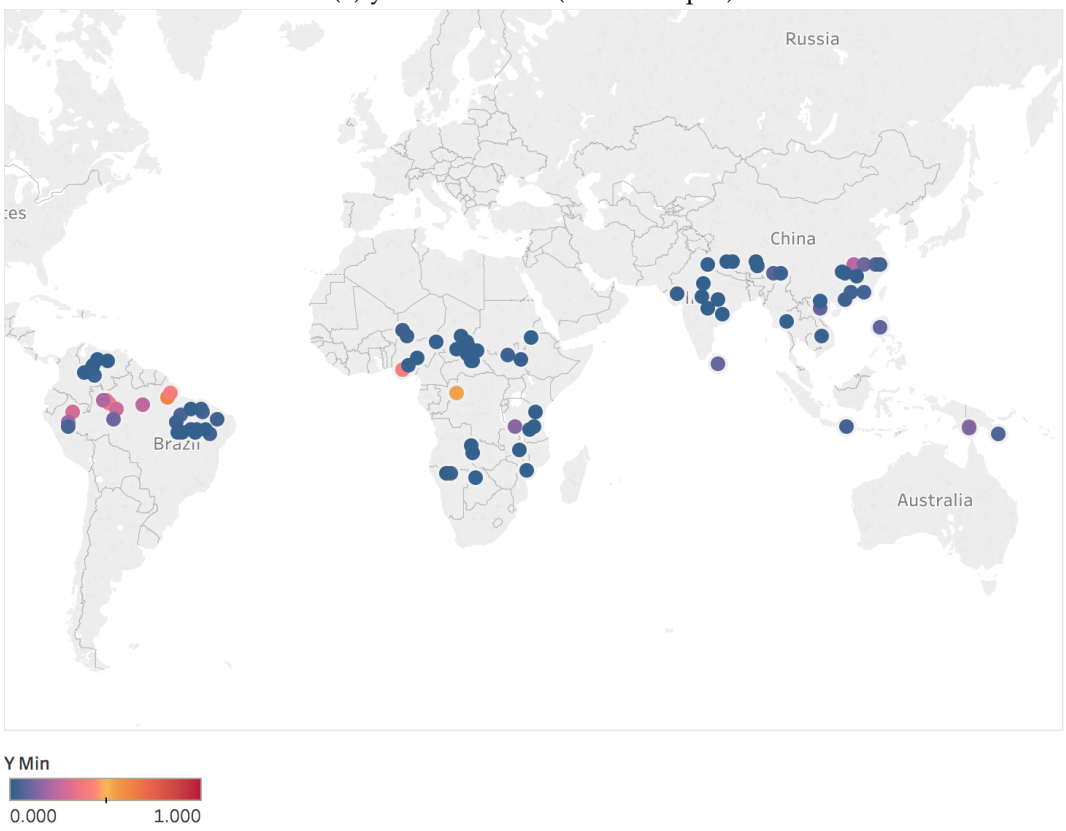

(b) y minimum (observed output)

Figure 6.28: Mean annual minimum wetland fraction (from 2008 to 2012) comparison between the model output and observed output.

the probability distribution of estimated parameters. Through these distributions, sensitivity of model to the various parameters could also be analysed.

Climate change is expected to change many environment variables especially the average global temperatures. IPCC scenarios RCP 8.5 (business as usual) suggests that under the current level of green house gas emission the average temperature is set to increase substantially by the century-end. The wetland model developed in this study can be used to evaluate the distribution of tropical wetlands in the advent of climate change. A similar approach could be used to model the wetlands of the entire globe. Wetland dynamics do show variations among different climate regions. So, a global wetland model might include a suite of models corresponding to each climatic zone.

The currently available sites show a spatial resolution of 0.5×0.5 degree. In some situations, one might want to analyse the wetlands situated between two different sites. So in future, a methodology for approximating the parameter sets of a zoomed-in site could be developed. Some of these modifications could enable a proper global wetland model, which could be integrated with existing climate modelling suites for a more accurate representation of greenhouse gas and energy exchange with atmosphere.

Part III

Analytical modelling of enhanced weathering

Chapter 7

Enhanced weathering: potentials and challenges

7.1 Introduction

Natural chemical weathering of rocks is a geological process through which the atmospheric carbon dioxide on the earth is sequestered. Approximately 0.25 Pg of carbon per year is absorbed naturally [120] and this is an important factor by which the temperature of this planet is maintained in a range suitable for the existence of life. Enhanced weathering (EW) is an accelerated form of such kind of rock weathering, which is expected to escalate the carbon absorption process while rendering some other essential ecosystem services in parallel.

A tremendous increase in the greenhouse gas emission, particularly after the industrial revolution has affected the climate negatively. The climate change has already perturbed the food cycle in the last few decades and is expected to get further aggravated in the coming years [121]. An increasing global population which is expected to cross 11 billion by the year 2100 [2], greenhouse gas emission because of the intense agricultural practices, depletion of fertile top soil [122], and finite resources of inorganic fertilisers add further complications in dealing with the food security and climate change simultaneously. Enhanced weathering appears to be a plausible option to tackle the challenges of food security and climate change while restoring the soil essential functions [123–125].

In the UNFCCC COP 21 (Paris agreement), all the parties agreed to make efforts for keeping the average global temperature to below 2 degree Celsius above the pre-industrial levels. In addition, they also agreed to bring measures for limiting the temperature increase to 1.5 degree Celsius. However, the global mean temperature has already crossed the 1 degree Celsius mark and with the current

warming rate it is set to cross the 1.5 degree Celsius in the next thirty years of time [126]. The Intended Nationally Determined Contribution (INDC) is a new international agreement resulting from the COP21, which outlines the proposed action steps by each party towards meeting the targets of the Paris agreement. The developing economies as per their INDC cannot phase out the fossil fuels rapidly as that would hamper the pace of their economic development. These factors suggest that the ambitious targets of the COP 21 is not possible unless the CO_2 mitigation policy incorporates a combination of Negative Emission Technologies (NETs) actively by the mid of this century [127, 128]. An NET is supposed to capture the atmospheric carbon to cause the reverse of positive emission, as suggested by its name.

Enhanced weathering is a type of NET, which involves the application of crushed form of calcium and magnesium containing rocks. This chapter will provide the basic mechanism of enhanced weathering and its potential in tackling the climate change issues, food security, ocean acidity etc. In addition, several logistics issues, policy issues and other implementation challenges will also be discussed. Currently, enhanced weathering is in a concept phase and computer modelling of the process is the most effective way to analyse its effects on climate and soil-vegetation systems. Therefore a comprehensive survey of the state-of-the-art models representing the weathering processes will also be presented in this chapter. Finally the feasibility of this NET based upon several pros and cons will be discussed in the concluding section.

7.2 Basic mechanism of enhanced weathering

The basic weathering reactions of a carbonate and silicate minerals will be discussed in this section. A mineral usually exists in the rock form where typically other minerals are also present. The enhanced weathering of a rock thus involves the weathering of more than one mineral simultaneously. Irrespective of a mineral, the weathering reaction involves the reaction of mineral with the atmospheric carbon dioxide in presence of weathering agent such as water and carbonic acid. This step leads to the formation of bicarbonate anions and metallic cations. Eventually, the bicarbonates combine with metallic cations to form the carbonates. The bicarbonates, as the intermediate phase of the weathering reaction, sequester the carbon in the aqueous form or get locked in the form of carbonates [129].

Calcium carbonate is a commonly found carbonate mineral. As explained above, it reacts with the carbonic acid to release Ca^{2+} cations and HCO_3^- anions. Interestingly, the $CaCO_3$ weathering do not act as a net sink of the atmospheric

CO_2 as the same amount of CO_2 is released bak to the atmosphere upon the formation of carbonate on the product side. So obviously the use of $CaCO_3$ in enhanced weathering is ruled out. At the same time, its usage as a liming agent in the intense farming scenarios should also be evaluated carefully because although the soil acidity can be reduced by the application of crushed calcium carbonate in the farmland, it will also emit CO_2 on the other hand [130]. The weathering reaction of calcium carbonate can be expressed as [125]
$CaCO_3 + CO_2 + H_2O \rightarrow Ca^{2+} + 2HCO_3^- \rightarrow CaCO_3 \downarrow + CO_2 \uparrow + H_2O$

Olivine (Mg_2SiO_4), a silicate mineral is considered to be suitable for enhanced weathering. One of the prime reasons for its suitability is its easy availability in the form of basalt rock. Precisely saying, olivine contains iron in addition to magnesium. The magnesium rich form of olivine as discussed in this section is actually known as forsterite. In many literatures the term olivine and forsterite are overlapped, in fact the iron rich version of olivine known as fayalite is expressed explicitly in order to avoid any confusion. Like the $CaCO_3$ weathering, Mg_2SiO_4 also reacts with carbonic acid to release Mg^{2+} and bicarbonate anion as intermediate products but here only 50% of the absorbed CO_2 is released back to the atmosphere. Therefore, the weathering of olivine acts as a net sink for the sequestered carbon dioxide. Olivine weathering also produces silicon, which is mostly positive for the local soil system. The alkalinity of the soil is enhanced in both the weathering reactions but the net absorption of CO_2 makes the olivine a good replacement for the calcium carbonate as a liming agent. The weathering reaction of olivine can be described as [125]
$Mg_2SiO_4 + 4CO_2 + 4H_2O \rightarrow 2Mg^{2+} + 4HCO_3^- + H_4SiO_4 \rightarrow 2MgCO_3 \downarrow + SiO_2 \downarrow$
$+2CO_2 \uparrow + 4H_2O$

7.3 Basalt as an optimum silicate weathering rock

The choice of rock for enhanced weathering depends upon many factors but the availability of rocks is the prime constraint. All the silicate rocks are finite resources on the earth surface and hence a rigorous mineralogical survey is a prerequisite to select the optimum rock. A simulation study of enhanced weathering was performed using three kinds of rocks namely, basalt, dunite, and harzburgite in [131]. This literature provides the total available resources of all three rocks and compared to other two rocks dunite is the most scarce rock. However, a dunite rock contains about 80% forsterite by weight and exhibits the most efficient weathering.

Mineral	Weight frac.
Augite	0.208
Fayalite	0.05
Forsterite	0.115
K-feldspar	0.061
Labradorite	0.43
Ilmenite	0.05

Table 7.1: Weight fractions of available minerals in a basalt rock sample.

The harzburgite and basalt are available in abundance and even with century long application, these resources will not deplete [131]. Despite containing higher fraction of forsterite, harzburgite does not result into a good choice because of lower fraction of augite. The augite releases a a wide range of cations such as Na^+, Ca^{2+}, Mg^{2+}, and Al^{3+}. So the basalt emerges as the optimum choice, considering its availability and minerals ratios. The weight fractions of minerals in basalt are provided in the Table 7.1. The augite is present in a large amount compared to other minerals, whereas, forsterite with 0.115 weight fraction put the basalt into a reasonable choice for enhanced weathering applications. A snapshot of basalt with some weathering patches is shown in the figure 7.1.

7.4 Potentials of enhanced weathering

7.4.1 Atmospheric carbon sequestration

The carbonate and silicate weathering reactions in the above sections suggest the amount of CO_2 sequestration in principle. Nevertheless, the actual absorption of the atmospheric carbon by enhanced weathering can follow broadly two pathways. The first way is the passage of bicarbonate anions and cations to the ocean through runoff. This route of carbon absorption also helps in reducing the ocean acidification and in turn protecting the coral reefs. An ocean is a natural sink of the carbon and store a lot more quantity of carbon than total atmospheric carbon dioxide [124]. Another way is the sequestration of carbon in the form of carbonate formation, as a result of the secondary products in a silicate/carbonate rock weathering reaction. The reactions of $CaCO_3$ and Mg_2SiO_4 weathering, shown in the above section validate this mechanism appropriately.

7.4.2 Negative emission technologies review

An NET removes the greenhouse gas from the atmosphere. The necessity of NET towards meeting the ambitious objectives have been discussed in the introduction

Figure 7.1: A snapshot of basalt rock, showing the fraction of weathered part on the surface (courtesy of pixabay.com).

of this chapter. In this section, all the popular NETs will be reviewed briefly. A more detailed review on the NETs covering all the facets of these technologies is presented in [10].

Some of the popular NETs are − Bioenergy with Carbon Capture and Storage (BECCS), Direct Air Capture of CO_2 (DAC), Enhanced Weathering (EW), Afforestation and Reforestation (AR). The BECCS technique though promising requires high amount of infrastructure and the land usage can also conflict with the food security criteria. The DAC is also constrained by the energy requirements and the associated costs. The AR techniques require lower investments as compared to the BECCS and DAC but the quantification of CO_2 capture is not simple here. On the other hand, the EW may offer many impetus in addition to carbon capture, such as improved crop yield, rejuvenation of soil etc. However, the EW faces challenges in terms of other logistic issues such as mining and transportation of silicate rocks, policy level challenges etc.

7.4.3 Enhanced weathering on cropland

Currently, EW is mostly in a concept phase and the practical implementation is very limited. In this section some examples of the catchments scale deployment of mineral rich rocks and theoretical assessments of the silicate dissolution will be provided. Many of these studies have been carried out to quantify the effects of silicate rock dissolution. About $10-15$ Mkm^2 of the croplands can be used for the deployment of basalt weathering resulting into the sequestration of about $200-800$ kg of CO_2 per tonne of basalt applied [132]. The usage of inorganic fertilisers for a prolonged period fills up the farmland with excessive amount of protons during the cation exchange processes. This causes the acidification of soil in an intense farming practice leading to the reduced nutrient uptake by plants and subsequently lower yield. Liming of the farmland with $CaCO_3$ is the most common technique to maintain the soil pH. However, this method actually emits substantial amount of carbon, back into the atmosphere. The weathering of silicate rock can maintain the soil pH without contributing towards the greenhouse gas emission.

The weathering of silicate rocks in a farmland can also benefit the crop growth through the release of essential nutrients. An increased level of soil pH can enhance the nutrients uptake [133]. Basalt weathering do release a wide range of macronutrients and micronutrients and these can positively contribute towards the crop yield [134]. An increased level of biomass production also raises the level of soil organic carbon. The rate of mineral weathering depends a lot upon soil water, a weathering agent. An increased level of soil organic carbon can actually

improve the soil water retention and thus the weathering rate of basalt will also increase [135]. So in summary, amendment of farmland with basalt powder has many positive impacts on the soil-vegetation system and these processes actually complement each other. The release of trace element like nickel in large quantities is definitely undesired in a food chain. The enhanced weathering of silicate rocks come up with this drawback and therefore, a rigorous research in this direction must be made.

A theoretical assessment [133] suggests that the application rate of $10-50$ $t{\cdot}ha^{-1}yr^{-1}$ of basalt in the North American arable land, having soya or corn as the major crop, could sequester $0.2-1.1$ Pg of CO_2 in the long run. The total area considered in this calculation is 70×10^6, and the diameters of particle lie in the $10-30$ μm range. Such kind of theoretical calculations embolden the idea behind enhanced weathering but few catchment level assessments are required to understand the practical efficiency and limitations of accelerated weathering. One of the earliest experiment was performed by [136], where woallastonite, a silicate rock powder was deployed only once at the rate of 3.5 $t \cdot ha^{-1}$ on the 11.8 ha land area for about 24 months. This experiment resulted into the decrease of acidity as well as an increase in Ca^{2+} cation. Similarly, a field trial in Mauritius was carried on sugarcane, in which basalt at the rate of 20 $t \cdot ha^{-1}$ was added in addition to the standard dosage of NPK fertilisers. The results of the basalt treatments showed about 30% increase in total yield over the five growing cycles of sugarcane [124, 137].

7.5 Survey of existing weathering models

Enhanced weathering as an NET is considered to be an emerging technology. From the above sections, the uncertainties surrounding the implementations and effects of enhanced weathering can easily be understood. The associated costs and policy complications add up to these uncertainties. In view of all these factors, presently a rigorous computational simulation analysis of enhanced weathering occupies the driving seat. In this section, some existing models, representing the weathering processes will be discussed. Many of these models can be adapted to incorporate the enhanced weathering of minerals. This review will also help to figure out the optimum model for the simulation analysis of enhanced weathering in the coming chapters of the thesis.

7.5.1 Sheffield Weathering Model

The Sheffield Weathering Model (SWM) [131] is a recent addition to the the suit of weathering models. This is a global dynamic model driven by a Dynamic Global Vegetation Model (DGVM). In this model, soil hydrology is represented by a water balance equation and it calculates the necessary soil chemistry as well. However, soil dynamics are not calculated in the SWM. It includes the CO_2 consumption and being recently developed, it also contains the enhanced weathering features. On the down side, it does not include the Green House Gas (GHG) production and crop growth processes.

7.5.2 WITCH

The WITCH numerical model [138] represents the weathering processes at the catchment scale. Like SWM, this is also a dynamic model driven by the DGVM outputs. Soil hydrology in this case is inputted for each layer, whereas, soil chemistry is calculated similar to the SWM. CO_2 consumption is explained in this model but enhanced weathering cannot be simulated by the WITCH. Like the SWM, GHG production and crop growth processes are not incorporated in this model.

7.5.3 PROFILE

The PROFILE [139, 140] is a non-dynamic catchment scale model. Instead of DGVM output, this model is driven by site specific data. Soil hydrology and soil chemistry calculation is similar to the WITCH in this case. Apart from these features, the PROFILE does not represent anything about the GHG production, crop growth processes and the enhanced weathering.

7.5.4 SAFE and MAGIC

The SAFE [141] model is a dynamic catchment scale model. Like the WITCH, it is mainly driven by the site specific data. Soil hydrology and soil chemistry calculations are also described in a similar fashion within this model. GHG production, crop growth cycles and the artificial weathering cannot be simulated using the SAFE. Another model known as the MAGIC [142] represents the same level of processes but with limited number of soil layers as compared to the SAFE.

7.5.5 APSIM and DayCent-Chem

The APSIM [143] is a dynamic site level model. In this case, soil hydrology is represented by the Richard's equation. Unlike the above discussed models, it

incorporates the emission of N_2O and CO_2 gases. Crop growth processes are also represented by this model. Despite all the key features, it lacks a module for describing the enhanced weathering and hence it can only be used to assess the linkage between natural weathering with the vegetation processes. The DayCent-Chem is another model, representing the processes similar to the APSIM but on contrary this model can be extend to a catchment scale.

From the above survey, APSIM and DayCent-Chem appears to be the reasonable choices for the inclusion of enhanced weathering module. The integration of an additional model would also require the easy availability of source codes as well as the fidelity of model in representing the specific processes. The deployment of enhanced weathering in a farmland might necessitate the consideration of several processes within the ECZ. Therefore, it is not so straightforward to pick up the best model for the simulation of enhanced weathering at this stage. In the forthcoming chapters a further analysis about the model choice will be presented along with some additional details.

7.6 Sustainable sources for enhanced weathering

The amount of silicate powders required for enhanced weathering at a large catchment scale can be very high. The quantity of rock powder also depends upon the application rate and the local field and climatic conditions. Technically, mining of basalt can meet the requirements but there are some costs associated with the mining, including the effects of mining on local climates. Therefore, enhanced weathering as an answer for sustainable futures must be driven by sustainable mineral sources, at least partly. In this section some possible sustainable sources of silicate minerals will be discussed. Like the very idea of enhanced weathering, most of these methods are also in concept phase and requires a thorough research.

The industrial and silicate mining waste contains about $7 - 17\ PgYr^{-1}$ of reusable silicates and these can be used to supplement the requirements of silicate powder in weathering. A cement production plant also generates some waste materials, which could be employed for enhanced weathering needs. A substantial amount of demolition and civil construction wastes are typically used for the landfill purposes. These can also be routed for the enhanced weathering application. A steel manufacturing plant produces a huge amount of slag containing rich amount of calcium silicate. Some of these recycled slags have already been used for the liming of acidic soil for enhancing the crop productivity. Steel making is a continuous process as it is linked with several infrastructure developments. Therefore, a proper recycling framework in steel industries could drive the sustainable

enhanced weathering. Mill ash and silicon containing residue in sugarcane industries could also be used in weathering [124, 132, 144].

7.7 Challenges of enhanced weathering

Weathering of basalt releases some amount of trace elements such as nickel and chromium. In an accelerated weathering settings, these elements can increase tremendously in the soil system. The presence of these metals in large quantities could harm the food chain. A research framework in this direction must be developed soon, as the proposed implementation of enhanced weathering in farmland will not be allowed by policy makers unless the idea of 'food security' is supported by a a secured 'food chain'.

The mining of rocks, grinding and distributing over the farmlands/forestlands require a tremendous amount of energy. The presently employed technologies in mining and grinding could reduce the efficiency of carbon capture by about $10 - 30$ % [145]. Clearly, the usage of renewable energy in producing the rock powder could revamp the entire preparatory phase of enhanced weathering. A cost analysis of enhanced weathering is prone to lots of uncertainties but a very crucial step to bring all the stakeholders on board. Initial estimates suggest that, per tonne of CO_2 absorption might cost USD $52 - 480$, in which the grinding and transportation of rock powder contribute the most [132].

The intense mining and grinding of rocks for the weathering would also affect the environment, local flora and fauna negatively. The grinding of mineral particles would involve the dust particles in micro-metre range and can easily be inhaled by the workers at the site. The presence of high amount of silica could cause silicosis in the nearby population. Deposition of unweathered basalt particles in the ocean bed could induce sedimentation in the long run. Other effects of unweathered basalt in the soil pores and ocean bed are yet to be explored [146].

7.8 Conclusion

This chapter presents the basic theories associated with the silicate and carbonate weathering reactions. From the stoichiometric analysis, silicate rocks are the best bet for enhanced weathering purposes. The COP 21 (Paris agreement) presents a very ambitious target of reducing the green house gas emission for limiting the average global temperature to 1.5 degree Celsius from the pre-industrial time. The recent Intergovernmental Panel on Climate Change (IPCC) reports have acknowledged the need of an effective NET in the CO_2 mitigation framework. The choice

of an NET is a debatable issue currently. This chapter has reviewed some existing NETs and the cost associated with them. Among all the competing NETs, enhanced weathering appears to be a reasonable choice. The enhanced weathering technique provides other incentives in the form of improved crop productivity, soil rejuvenation, maintaining soil pH etc.

This chapter also explores the candidate silicate rocks. The availability of basalt and minerals ratio makes it as a reasonable choice for the enhanced weathering purposes. Nevertheless, the mining, grinding, and transportation of basalt requires lots of energy. In order to justify the usage of enhanced weathering for sustainable futures, the energy requirements should also come from some sustainable sources. In addition, the mining of fresh basalt should be replaced by the recycling of silica containing industrial wastes. The side effects of enhanced weathering on environment, if any, should also be explored. So far, some negative impacts of enhanced weathering on food chain, in the form of deposition of excess nickel and chromium are reported. Undoubtedly, these facets must be researched rigorously before the implementation of enhanced weathering at the catchment scale.

Geo-engineering processes as the name suggests 'engineer' the Earth's surface. In the short terms, these amendments might not be a matter of concern as long as some economical, environmental and social values are garnered but a 'sustainable' policy decisions are not short-sighted. This applies to the enhanced weathering as well. Actual implementation of such accelerated weathering, particularly in the farmlands would have to pass through the policy makers of a state. The global impact of enhanced weathering will also require a consensus among all the parties, something similar to the UNFCCC COPs.

Overall, enhanced weathering as an NET appears to be a plausible choice for curtailing the global temperature while improving the soil health and crop yield. This fits in sync with some of the goals outlined in the United Nations Sustainable Development Goals (UN SDGs).

Chapter 8

Integrated enhanced weathering critical zone model

8.1 Introduction

Enhanced weathering is a geo-engineering process under which, the weathering of naturally occurring silicate and carbonate rocks are accelerated through crushing them into fine particles by artificial means and subsequently distributing the powdered rocks on the land surfaces. In the previous chapter, motivation behind enhanced weathering, basic theories associated with the weathering processes, practical limitations and challenges surrounding such kind of accelerated weathering were discussed. The last chapter also contained some recent trends in modelling of enhanced weathering and the gaps in the existing modelling literatures.

In this chapter, a novel calibrated version of enhanced weathering process model will be presented. Here, the modelling approach is mainly analytical, governed by a shrinking sphere methodology. Enhanced weathering belongs to a wider domain of the Earth's Critical Zone (ECZ) processes, and hence in reality, it is dynamically linked with the complex soil-vegetation processes of the land surface. As elaborated in the last chapter, majority of the weathering literatures oversimplify such complex interactions, especially the vegetation and bioturbation processes are mostly ignored, while analysing the rock weathering. In this study, the enhanced weathering model is thus integrated with all the key soil-vegetation processes. This is the second novel contribution of this chapter. The naturally occurring minerals weather continuously and very slowly in all the conditions. Hence, the natural weathering processes had been kept intact, while integrating the enhanced weathering features in the soil system.

The theoretical weathering rate parameters (k), prescribed for modelling pur-

poses are often higher than the actual weathering. All the enhanced weathering modelling literatures prior to this study have considered the theoretical rate constants in their models resulting into a higher rate of weathering. In scenarios, where the effects of enhanced weathering on CO_2 sequestration is of prime interest, even a slightly high weathering rate would result into an erroneous prediction. Unfortunately, very few literatures on the quantification of field level weathering exist presently. In this study, the calibration of enhanced weathering model is based on [15]. The same literature was also referred for validating and comparing the key solutes concentrations under the effects of olivine weathering. Post model validation, a case study was performed on a Greek Critical Zone Observatory (CZO), known as Koiliaris. This particular site was chosen for the case study mainly due to the availability of input parameters corresponding to this site.

The chapter unfurls with a brief description of soil-vegetation processes and the associated models used in this study. Thereafter, a mathematical derivation of a shrinking sphere process will be presented followed by an algorithm using that process for representing the enhanced weathering of a mineral. As discussed earlier, the integration of all the key processes pertaining to the ECZ is essential for analysing the weathering thoroughly. So, an integration mechanism of enhanced weathering with other process models will be described schematically. The model calibration, validation and case study will precede the concluding remark of this chapter.

8.2 Earth's Critical Zone process models

An European Commission funded research project, Soil Transformation in European Catchments (SoilTrEC), involving many universities and researchers across the European Union, provided an integration framework of a set of soil-vegetation process models. The overarching aim of this project was to quantify the processes relevant to the soil ecosystem services in the ECZ [7].

A majority of these process models, except the one explaining the soil structure and $C/N/P$ dynamics were adapted from their respective sources in the SoilTrEC project. These models have gone through rigorous calibration and validation across a wide range of CZOs in Europe and thus satisfy most of the benchmarking criteria. The collaboration of this PhD project with the SoilTrEC project group enabled an easy access of the source codes and default input parameters. These ECZ models were subsequently integrated with the developed enhanced weathering model hence the underlying processes corresponding to each model are outlined in the following subsections for a clearer understanding.

8.2.1 Water-flow, heat-flow and solute-transport model

The flow of water, heat and transport of solutes are among the key dynamic processes taking place within the soil layers. The Hydrus-1D [12], an open source software, incorporates all these processes categorically [14]. In this model, water flow within the soil layers is described by the Richard's equation,

$$\frac{\partial \theta}{\partial t} = \frac{\partial (k \frac{\partial h}{\partial z})}{\partial z} + S \tag{8.1}$$

where θ represents the volumetric water content, t stands for time, z is the vertical coordinate in a soil profile, k stands for the unsaturated hydraulic conductivity, h is the pressure head and S is the source/sink of water. k and h are proportional to θ in the Richard's equation.

The heat transfer within the soil layers is represented by the convection-diffusion equation in the Hydrus-1D,

$$\frac{\partial C_p(\theta) T}{\partial t} = \frac{\partial (\lambda(\theta) \frac{\partial T}{\partial z})}{\partial z} - C_w \frac{\partial qT}{\partial z} - C_w ST \tag{8.2}$$

where $C_p(\theta)$ denotes the volumetric heat capacity of the porous medium, T stands for the temperature, $\lambda(\theta)$ is a measure of the thermal conductivity of the soil, C_w represents the volumetric heat capacity of water, q stands for the water flux derived by the Darcy's Law.

In this model, solute transport for each solute k is explained by the advection-dispersion equation,

$$\frac{\partial \theta c_k}{\partial t} = \frac{\partial (\theta D_k^w \frac{\partial c_k}{\partial z})}{\partial z} - \frac{\partial q c_k}{\partial z} + S c_k^S - r_k + p_k \tag{8.3}$$

where c_k denotes the concentration of component k, D^w stands for the diffusion/dispersion coefficient corresponding to the liquid phase, c_k^S denotes the concentration at the source/sink, r represents the nutrient uptake by plants, and p is the solute production rate.

8.2.2 Soil C/N/P dynamics and structure model

This model is known as the Carbon, Aggregation, and Structure Turnover (CAST). The CAST was developed recently [13], as an improvement over the ROTH-C [147]. In this model, four kinds of carbon pools are assigned for the Soil Organic Matter (SOM), known as, Decomposable Material Fractions of Plant Litter (DPM), Resistant Material Fractions of Plant Litter (RPM), microorganisms pool (BIO) and

Humus (HUM). The model is mainly driven by the plant litter as input, which accounts for the Plant Organic Matter (POM). The formation of macro-aggregates around the POM and subsequent disintegration into micro-aggregates are simulated by the model. The CAST also simulates the depolymerisation of the available HUM into Low Molecular Weight Nitrogen (LMWN) and Low Molecular Weight Phosphorus (LMWP). Following the depolymerisation, mineralisation of LMWN and LMWP into inorganic N and P take place. C/N and C/P ratio of each pool is used for calculating the amount of organic N and P.

Soil aggregates are divided into three categories − AC1, AC2, and AC3. The AC1 represents the silt-clay sized aggregates, AC2 is referred as micro-aggregates, and AC3 is regarded as macro-aggregates. A healthy soil condition is directly proportional to the amount of AC3 available in a soil profile. The soil macro-aggregates have a better water retention capacity and provides the right condition for plant growth. Water Stable Aggregate (WSA) is commonly used for the categorisation of aggregates based on their stability factors .

In summary, the CAST incorporates most of the steps of the N and P cycles. For N, the model simulation includes mineralisation, nitrification, denitrification, ammonium adsorption and ammonium volatilisation. The reactions for the P are also carried out in the similar fashion. These processes are very significant for a plant growth as N and P are among the major macronutrients. A plant can uptake LMWN and LMWP in addition to the inorganic N and P available in the system. The process of organic matter transformation in the CAST model results into the release of base cations such as Ca^{2+}, Mg^{2+}, and K^{+}. Soil pH is also varied because of organic mater transformation.

8.2.3 Vegetation process model

The carbon and nutrients dynamics in a plant-soil system need to be analysed for understanding the ECZ processes thoroughly. The PROSUM model was devised recently [14], where the plant-growth, nutrient uptake, water uptake and litter productions can be simulated simultaneously. The model explains the key vegetation processes for the available amount of light, nutrients, water, CO_2 and temperature. A wide range of vegetation types including herbaceous and woody plants can be described through this model.

Essential plant nutrients are categorised as macronutrients and micronutrients. Nitrogen, phosphorus , potassium, calcium, sulphur, magnesium, carbon, oxygen, and hydrogen fall under the category of plant macronutrients. Among these nutrients, hydrogen, oxygen, and nitrogen contribute towards 95% of biomass or yield value. The micronutrients catalyse the photosynthesis process and some other es-

sential functions in the plant systems. Often, micronutrients are required in very limited quantity. All the plant nutrients need to be present in appropriate quantity and ratio for a proper growth of plant. Cation exchange is the main process through which cations like Mg^{2+} are taken up by a plant. Such kinds of exchange is triggered by pumping H^+ in the root system, which then displace the cations attached to the negatively charged soil particle for plant uptake. Therefore, prolonged farming cycles often witness an increased level of H^+ or acidity in the soil system [148].

All the above mentioned processes including many other complex interactions between plant system and environment are satisfactorily captured in the PROSUM model. The prime purpose of this model development was to link the effects of plant litter on soil structure changes, as explained in the above subsection. The model does not incorporate the precise information such as long term effects of pH change on nutrient uptakes. Nevertheless, the calculation of maximum C/nutrient ratio, maximum nutrient uptake, actual nutrient uptake, derivation of the underground and aboveground biomass are fairly represented by this model.

8.2.4 Bioturbation process model

In geology, bioturbation is defined as the perturbation of sedimentary deposits by fauna. In a soil system, bioturbation plays many important roles and hence methodology in [149] was adapted by [14] to come up with a bioturbation model. In this model, essentially a fraction of water, specified by the modeller and solid chemical components are mixed and passed over all the soil layers. The mixing process is representative of the real bioturbation process, in the presence of soil fauna.

8.2.5 Chemical equilibrium and natural weathering model

A chemical equilibrium in the context of soil system refers to the water saturation and solid exchange with the gas phases. The method reported in [150] was used to develop this chemical equilibrium model by [14].

A model called SAFE [14] was formulated for describing the natural weathering of major minerals, mainly adapted from [151]. The SAFE model assumes that naturally occuring minerals are available in abundance and will never deplete. This is why, an artificial weathering, where the surface area of rock changes eventually, cannot be represented by the SAFE.

8.3 Enhanced weathering model development

8.3.1 Weathering rate expression

In this modelling study, the weathering rate of a mineral is governed by the equation 8.4 adopted from [152]. This rate expression has previously been applied in several modelling exercises, as reported by [152]. The formulation of this expression has a vivid experimental foundation, which is out of scope to discuss in this thesis. In the equation 8.4, $Rate_m$ on the left hand side refers to the weathering rate (mol/s). The surface area normalised unit of the weathering rate is given by $mol\ s^{-1}\ m^{-2}$. SA denotes the mineral surface area (m^2). i refers to the individual weathering agent, which in this study can be either H^+, OH^-, or H_2O. m refers to the individual mineral corresponding to the silicate rock. In this study basalt rock is considered, so m can be a mineral corresponding to the basalt composition. $k_{i,m}$ ($m^{-2}\ s^{-1}$) refers to the weathering rate constant corresponding to the i^{th} weathering agent and m^{th} mineral. Similarly, $E_{i,m}$ ($kJ\ mol^{-1}$) refers to the apparent activation energy, R ($kJ\ mol^{-1}\ K^{-1}$) is the universal gas constant. T (K) is the temperature. a_i ($mol\ l^{-1}$) is the molar activity of the i^{th} weathering agent. $n_{i,m}$ refers to the reaction order corresponding to the m^{th} mineral for the i^{th} weathering agent. Q_m=$\prod_j a_j^{s_j}$ refers to the ion activity product of the soil pore water, where a_j denotes the activity of j^{th} solute, s_j relates to the stoichiometry on the product side of the m^{th} mineral weathering equation. Ksp_m accounts for the solubility of the m^{th} mineral.

$$Rate_m = SA_m \sum_i [k_{i,m} exp[\frac{-E_{i,m}}{R}(\frac{1}{T} - \frac{1}{298.5})] a_i^{n_{i,m}} (1 - [\frac{Q_m}{Ksp_m}])] \tag{8.4}$$

8.3.2 Enhanced weathering algorithm formulation

The weathering rate expression discussed in the above subsection was adopted in this study for developing a shrinking sphere type analytical model, describing the weathering of a mineral. In the equation 8.4, mineral surface area denoted by SA will decrease as the weathering reaction progresses. The SAFE model explaining the natural weathering does not consider this factor mainly because the natural weathering is very slow in general and the abundant minerals will not deplete substantially during the simulation time period. However, in enhanced weathering, mineral surface area will have tremendous effects on the weathering rate. Therefore in this study, a mineral particle is assumed to be perfectly sphere in shape, which will shrink with the rock dissolution.

The area of a single mineral particle, a, is given by $4\pi r^2$, where r denotes the

radius of the particle. The mass of this particle, m, can be expressed as $\frac{4\rho\pi r^3}{3}$, where ρ denotes the density of mineral. The ratio $\frac{m}{a}$ therefore simplifies to $\frac{\rho r}{3}$, which means at any time step, t, in the model $\frac{m_t}{a_t}$ can be expressed as $\frac{\rho r_t}{3}$. By substituting a_t with $4\pi r_t^2$, r_t relates to m_t through the expression

$$r_t = (\frac{3m_t}{4\rho\pi})^{1/3} \tag{8.5}$$

Some more assumptions were made to simplify the modelling task without compromising with the desired level of precision in the output of interest. The assumptions are similar to [131], which is a recent literature on the analysis of enhanced weathering for stabilising the global temperature. According to the first assumption, rock particles are considered as perfect mono-mineralogical spheres. In reality, a rock particle contains several minerals and their spatial configuration within the rock particle is not certain. The diameter of a particle was kept in the micrometer range. The total mineral surface area would increase sharply as the diameter is further reduced but considering the current grinding facilities, 10 μm as the initial diameter is an optimum choice [124]. According to the second assumption, all the distributed rock particles are supposed to weather, without any loss due to runoff or flooding. In reality, rocks in the powdered form are set to be eroded away in the event of heavy rainfall or wind. The mineral particles in reality can also get aggregated with the passage of time under several external factors, but in this modelling procedure they are assumed to maintain their original structure.

A basic version of the enhanced weathering pseudocode, based on the above mentioned shrinking sphere approach is provided in the Algorithm 8.1. This pseudocode represents the weathering of a single mineral and can easily be customised to include more than one mineral as per the first assumption. The weathering rate expression given in the equation 8.4 is valid for one mineral, and hence for multiple minerals, the weathering rate corresponding to each mineral will be evaluated separately. These mineral specific rates will be taken into account for calculating the consumptions or productions of ions. In situations where a silicate rock is supposed to be added repeatedly instead of one-off addition, the Algorithm 8.1 will have to be run for each periodic addition of rock. The rate expression in the equation 8.4 is driven by mineral surface area, which in turn is driven by the mass of mineral in a time step. So, the freshly added rock will have higher surface area than those added in the preceding intervals. In that case, at a time step, the Algorithm 8.1 will run for all the 'periods' of rocks-addition separately and in parallel. At the end of the time step, the production or consumption of ions will

Algorithm 8.1 Enhanced weathering

$counter \leftarrow 1$
Initialise: Total mass (M), radius (r), reaction order (n), density (ρ), molar mass, apparent activation energy (E), solubility constant (K_{sp}), universal gas constant (R), weathering rate constant (k), total tweathering period ($tweathering$)
Import: molar activity (a_i) and T corresponding to this time step.
Evaluate: total number (N) of olivine particles using the M and ρ, total mineral surface area (SA) using N and r, weathering rate ($Rate$) using the equation 8.4.{Q_m=0 at this stage}
while $counter<tweathering$
  Update: number of moles of olivine (c) {$Rate$ at the previous time step is used to update the current c}, total mass of olivine (M), mass of single particle (m), radius (r), surface area (SA).
  Import: molar activity (a_i) and T corresponding to this time step.
  Evaluate: ion activity product (Q) of the soil solution and weathering rate ($Rate$). {this step results into release/absorption of ions on the soil surface. In reality, this change in ionic concentration are passed into soil layers through the soil pore water. This must be taken into account while integrating this code with ECZ model}
  $counter \leftarrow counter+1$
end while loop

be calculated by the algebraic summation of released or consumed ions due to the weathering of rock particles, exhibiting variation in their masses and surface area in accordance to the timing of their addition.

8.4 Integration of enhanced weathering model

In this study, an enhanced weathering (EW) process model using the Algorithm 8.1 was implemented using the Fortran 90 programming language. The ECZ process models explained in the section 8.2 were also coded in the Fortran language and the source codes of all the models were made available through the SoilTrEC project.

The standalone version of the enhanced weathering do not demonstrate the effects of weathering on soil-vegetation process and vice-versa. In addition, the Algorithm 8.1 also requires the temperature and pH values at each time step, which can be made available easily once the model is linked with a dynamic process model like the Hydrus. The overarching aim of this modelling exercise was to analyse the effects of enhanced weathering on the critical zone processes under the various climatic condition, so a code level integration was performed to link the developed EW model with the existing ECZ models.

8.4.1 Integration mechanism

During the SoilTrEC project, a program known as the Integrated Critical Zone Model (ICZM) was developed which essentially linked all the key ECZ models. As explained in the section 8.2, natural weathering was also conceptualised using the SAFE model. In the ICZM, the released cations from the natural weathering module are passed into the Hydrus, where they are combined with cations from all other sources in the soil system. The concentration of a solute in the ICZM is interpreted through pore water concentration in the model outputs. As a first step towards the integration of the EW with the ICZM, the ionic concentration change resulting due to the EW at a time step was clubbed with the ionic concentration change because of natural weathering. So essentially, the ions-concentration-change effects passed on to the Hydrus is an amalgam of all sorts of weathering in the soil system. As a prerequisite, the time step of both the natural and enhanced weathering models were kept same. This step ensured the correct linking of outputs emerging from the EW. In the next step, input requirements of the EW, such as temperature and pH were taken care off through passing these inputs dynamically from the ICZM at each time step. All the intermediate complexities such as maintaining the charge balance, calculating the biomass production from the plant nutrient uptake was automatically sorted out by the well calibrated ICZM structure.

The integrated version of the EW will be referred as the Integrated-Enhanced Weathering-Critical Zone Model (IEWCZM) throughout the remaining portions of the thesis. The novelty of this model comes from the incorporation of phenomena like bioturbation and the linkage of vegetation processes with the EW. As discussed in the previous chapter, none of the weathering process model takes into account all these factors simultaneously.

8.4.2 Coupling of IEWCZM modules

The IEWCZM's main program steers the Hydrus, weathering, chemical equilibrium, CAST, PROSUM, and bioturbation modules. The modules are processed sequentially using a time step algorithm, once the inputs are made available. The CAST, weathering, PROSUM and bioturbation models have a time step of one month, on the other hand Hydrus is governed by smaller time steps.

The figure 8.1, describes the integration of all the modules within the IEWCZM and the time steps associated with these sub-models. The coupling of sub-models in the original ICZM has been explained in [14] and the idea is very similar in this case, except for an additional component in the weathering module. The starting

point in the main program is Hydrus, where the amount of solutes and water corresponding to each soil layer are calculated. These nutrients are ideally available for plant uptake but there are many masking effects on the uptake process and the actual uptake will be corrected by the PROSUM model subsequently. The PROSUM is supposed to be the consumer of major nutrients whereas, CAST and weathering modules are responsible for the production of solutes. The IEWCZM therefore calculates the consumption and production rate corresponding to these modules. The nutrients released by the CAST and weathering are flagged as 'available' nutrients for the plant uptake in PROSUM module. The PROSUM then performs its own calculation to calculate the actual uptake depending upon the maximum possible uptake and many other parameters. Nevertheless, the CAST is mainly driven by the plant litters generated by the PROSUM, so that factor is carefully considered, while linking the modules with the IEWCZM. In the next step, several calculations in the Hydrus are repeated until the time steps add up to 1 month. In order to update the solute concentration and water content emerging out of the Hydrus module, production and consumption rates related to the CAST, PROSUM and weathering are multiplied by the variable time steps of the Hydrus. As explained in the description of chemical equilibrium model, the prime purpose of this module is to ensure that mobile and immobile phases are equilibrated. Hence, the chemical equilibrium sub-model is run after each time step of the Hydrus. The bioturbation module comes into action at the end of month for redistributing water and solute concentrations. In the last, chemical equilibrium module is processed again and in this way the calculations within the IEWCZM continues till the end of simulation.

The key input parameters of the IEWCZM are shown in the [153]. Detailed parameter types can also be accessed through the respective models websites and the cited sources.

8.5 IEWCZM calibration

The rate of weathering, as stated in the equation 8.4 is governed by the weathering rate constant, $k_{i,m}$, where i denotes the weathering agent and m stands for the mineral type. The rate of weathering is very sensitive to this parameter as evident from the rate expression. A comprehensive compilation of the theoretical rate constants are available in the [152] and this source has been referred for the weathering rate constants in many available literatures. A theoretically derived rate constant in laboratory is usually several order of magnitude higher than the catchment scale investigation [15]. Therefore, the weathering rate calculated using

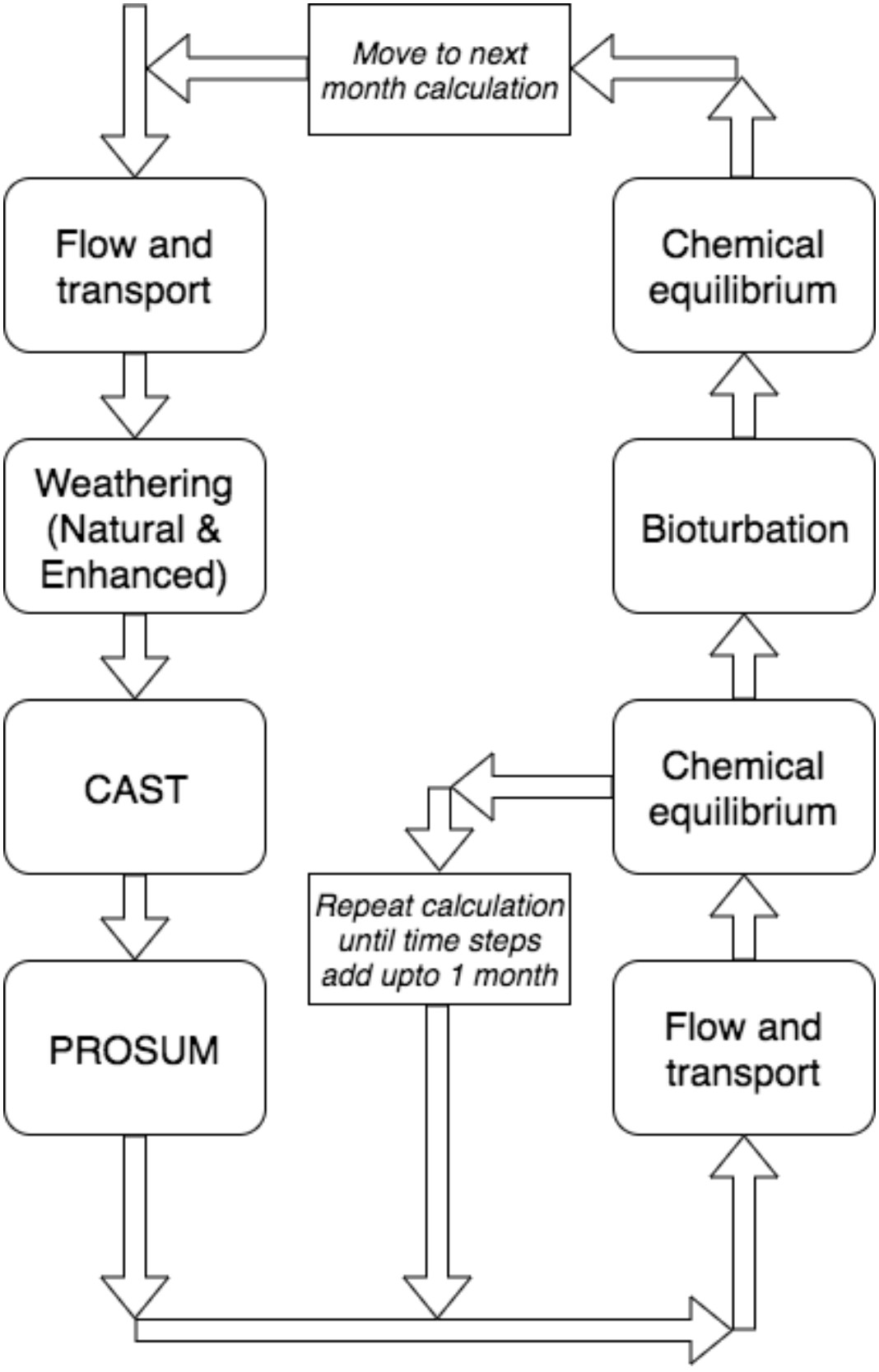

Figure 8.1: IEWCZM integration mechanism. The blocks represent the sub-models linked together to form the IEWCZM.

the parameters from [152] is not accurate on most occasions.

A column of soil containing the samples from the Oxfordshire region was returned to the laboratory for calculating the dissolution rate of olivine in [15]. In this study, the material surface area normalised dissolution rate was between $10^{-16.4}$ to $10^{-15.5}$ $molcm^{-2}s^{-1}$. This is the first literature, which takes into account the field level conditions while calculating the weathering rate of olivine. The purpose of the IEWCZM is to analyse the EW in the actual field type conditions, so a calibration process of the weathering rate constant, $k_{i,m}$ was performed by keeping the [15] as reference.

The calibration was executed using the rejection algorithm under the Bayesian framework. Ideally, the $k_{i,m}$ for both the weathering agents, H^+ and H_2O, should have been considered but in the [15], just H^+ is taken as the weathering agent. This factor constrained the rate expression to just k_{H^+}, which will be simply denoted as k in this section. The k was converted into logarithmic scale and the prior for k varied from $-log15$ to $-log5$. The total number of particles in the rejection algorithm was kept at 5000, which is a reasonably high value in the Monte Carlo sampling. Since the total number of observed data point was limited to just one, so computationally, the whole calibration was a simple job. The calibration result with the posterior distribution of k is shown in the figure 8.2. The simulated data were compared directly with the observed data and the number of data point was also limited to just one. This resulted into a very narrow range for posterior. The near-uniform distribution of the posterior can also be justified using the same argument. The logarithmic scale also limits the posterior range to a narrow band compared to the values in their actual scale. The mean of this posterior will be accepted as the 'true' parameter while plugging in the value of k in the IEWCZM.

8.6 IEWCZM sensitivity analysis

According to the rate expression (equation 8.4), the rate of weathering depends upon the three external variables , pH, temperature (T), and mineral surface area (SA). The Q_m term in the rate expression, known as the ion activity product, is an internal variable and cannot be controlled during the weathering process. During an artificially induced weathering, the rate of weathering is of prime importance. An optimum rage of weathering rate can be achieved by providing the appropriate combination of pH, T, and SA. The T and pH depend upon the local climate and soil characteristics, which suggest that the enhanced weathering rate will vary spatially and the site of application should be chosen carefully. However, SA

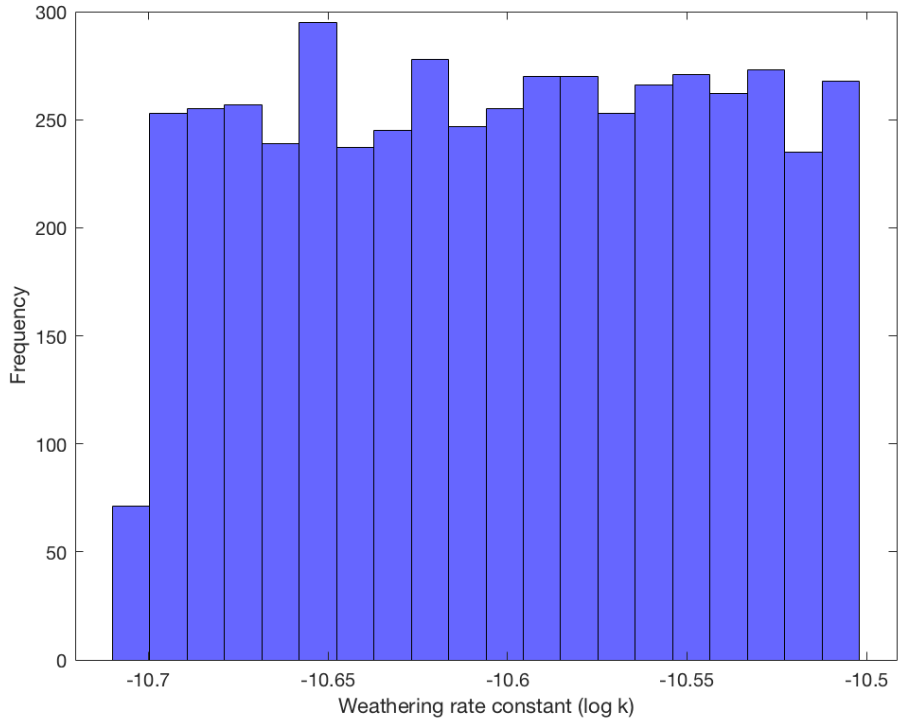

Figure 8.2: Weathering rate constant (k) estimation using the rejection sampling under the Bayesian framework.

depends largely on the mass of olivine and can be tuned as per the availability of olivine and the desired rate of weathering. In view of these factors, sensitivity of weathering rate on all three key variables are discussed in this section.

8.6.1 Sensitivity on mineral mass

The SA acts as a rate deciding parameter in the rate expression. The shrinking sphere methodology explained in this chapter came into picture precisely for incorporating the SA variation in the rate calculation. The derivation performed in the section 8.3 clearly reflects the dependence of SA on mass of mineral (M). The figure 8.3 shows the sensitivity of the weathering rate on mineral mass while keeping the other parameters constant. Clearly, the rate increases very sharply by increasing the mass of olivine. Nevertheless, there would be a fixed budget for the mineral mass during the actual implementation of the enhanced weathering and hence the M may not be increased beyond a certain limit. The conversion of M into SA is also noteworthy at this stage, as this largely depends upon the radius of mineral particle. Currently, the minimum feasible radius of a mineral particle

is in μm range.

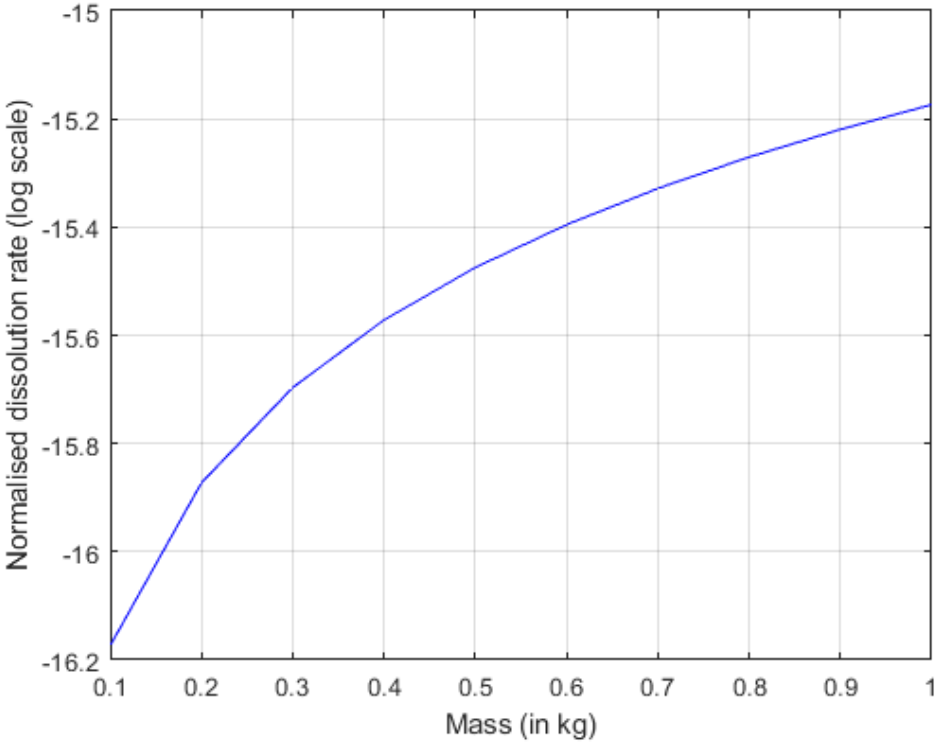

Figure 8.3: Sensitivity of weathering rate on mineral mass (M). All the other parameters such as T, pH etc. are kept fixed.

8.6.2 Sensitivity on pH and temperature

The fixed budget of silicate rocks definitely makes choice of weathering site an important factor during the implementation of enhanced weathering. The pH of soil and temperature depend largely upon the climatic conditions of a region. The pH also depends greatly upon the land management practice of a site. Hence in this study, the sensitivity of weathering on temperature and pH was simultaneously analysed (figure 8.4). For a clearer description the same result was teased apart in two dimensional views (figure 8.5). According to these analyses, the weathering rate increases with increase in temperature while a decrease in the rate is noticeable with increasing pH values. The entire sensitivity analyses is based upon the parameterisation of the IEWCZM as per the experimental set up in the literature [15]. However, the chosen range of both the pH and temperature provides a glimpse of the weathering, even outside of a typical temperate climatic regions. Based upon these analyses, the enhanced weathering appears to be more

effective in a tropical region. The sensitivity with respect to the pH suggests that, this kind of accelerated weathering would be positively catalysed in the acidic soil conditions.

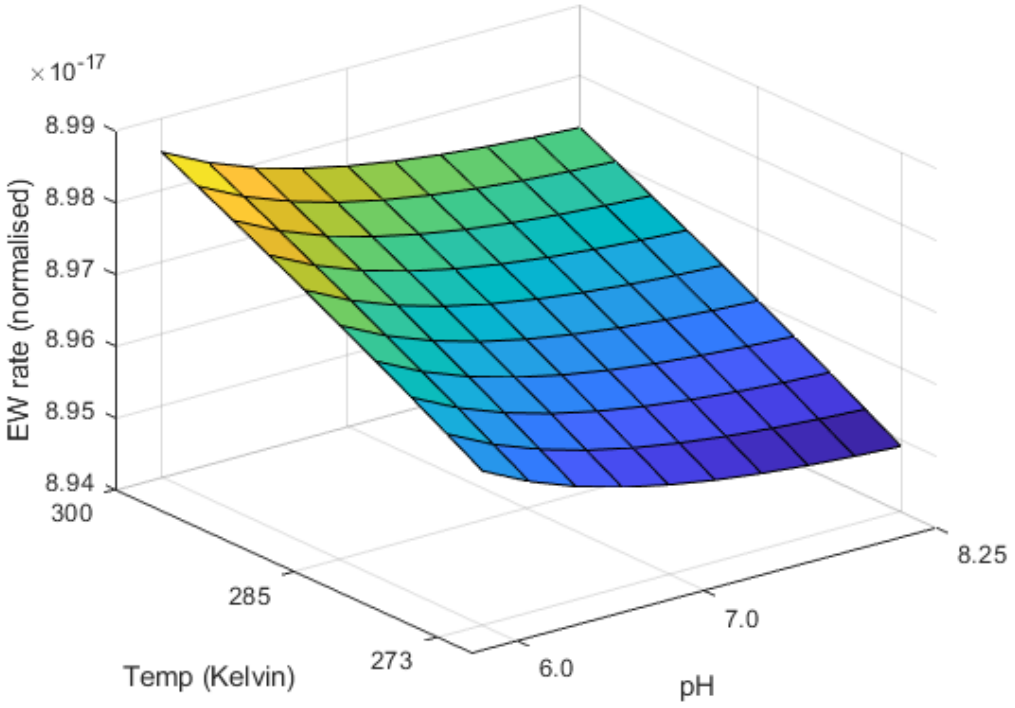

Figure 8.4: Sensitivity of weathering rate on temperature (T), and soil pore water pH.

8.7 IEWCZM validation

The integration of the EW model with the ECZ models resulted into the IEWCZM, which was calibrated according to a recently published experimental results [15]. In principle, the IEWCZM should be able to represent the EW and its linked processes. The simulation of the IEWCZM for analysing the future scenarios needed some more fidelity test and hence the results from the same literature [15] were used for the model validation purpose. The initial concentration of the solutes were maintained similar to the reference literature and the simulation was performed for the 133 days. The simulated concentration of Mg^{2+} and Si are shown in the figure 8.6. The experimental data are not shared by the [15], so its exact comparison with the results reproduced by the IEWCZM could not be made. In

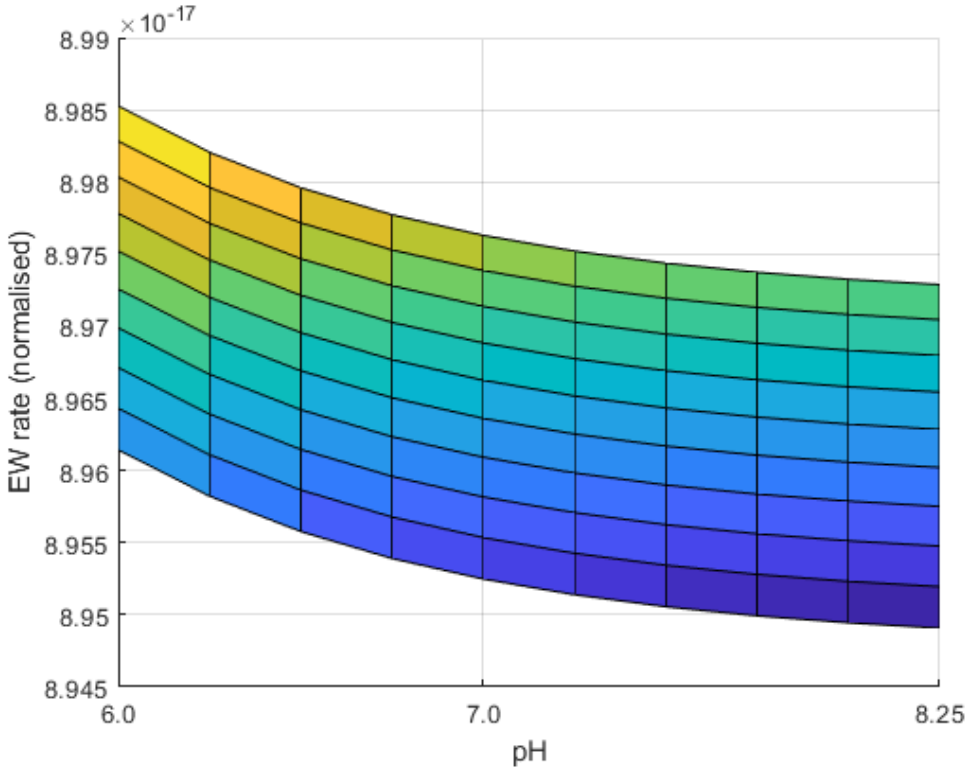

(a) Sensitivity of weathering rate on soil pore water pH.

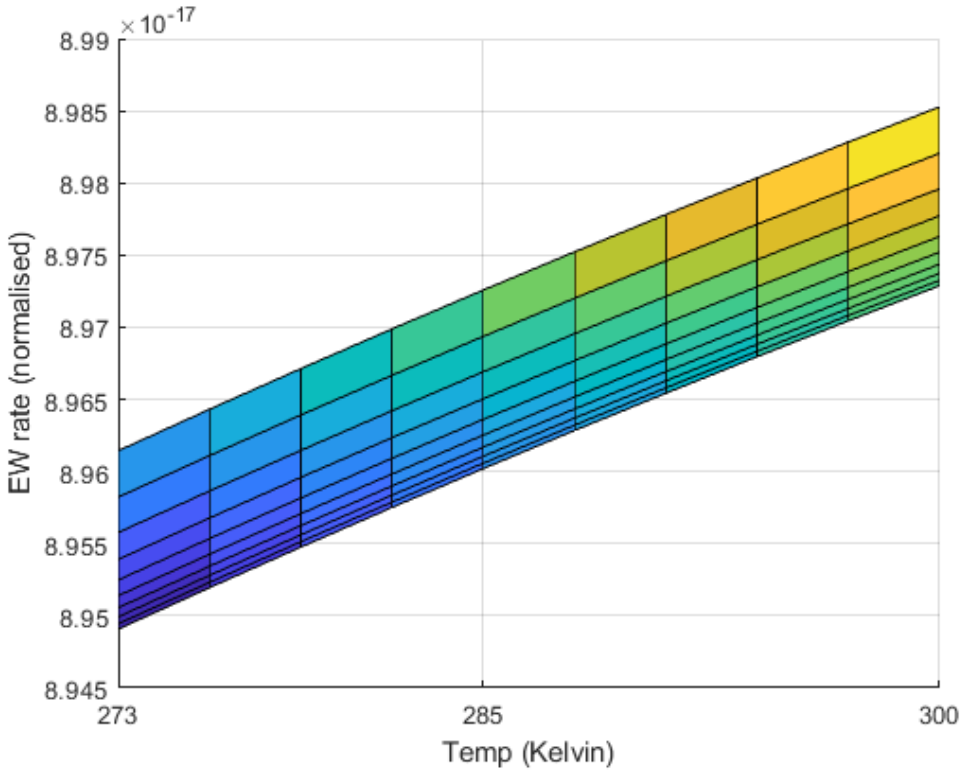

(b) Sensitivity of weathering rate on temperature (T).

Figure 8.5: Two dimensional view of weathering rate sensitivity with respect to pH and temperature.

addition to solutes initial concentration, the IEWCZM needed to be parameterised with several other kind of inputs. These parameters are specific to the soil profile and the experimental conditions. In absence of these details, default values were used for the IEWCZM parameterisation. Therefore, in the simulation results, solute concentrations show some deviations from [15]. Nevertheless, the overall trend and the effects of olivine treatment on a solute concentration are nearly same. In reality, an increase in Mg^{2+} and Si concentration due to weathering will reflect in the soil and vegetation system.

8.8 IEWCZM case study

Enhanced weathering of silicate rocks have multiple benefits in a vegetation process. In the previous chapter, the potential of enhanced weathering for increasing the crop yield while reducing the soil acidity have been discussed. The process of weathering is not something new but the effects of artificially accelerated weathering in the farmland are not very clear at the moment. The modelling analysis is the only way to assess the effects of enhanced weathering on a crop cycle. This method will have to exhibit at least some of the hypothesised effects on plant growth, before a thorough simulation analysis or the actual implementation is made. The reference literature [15] used for the calibration and validation of the IEWCZM does not consider any vegetation in its experimental setup. Therefore, a case study was performed on a published results [154] of the ICZM simulation. In this literature, tomato and weeds are considered as plants and their growth is simulated using the ICZM for the various treatments. The ICZM does not contain the enhanced weathering module so these results will be labelled as 'control' scenarios. The parameter values and the initial conditions used during the simulation of the ICZM in [154] was made available for this research.

In this case study, two treatments of the [154], namely, Inorganic Fertilisation (IF) and Municipal Solid Waste Compost (MSWC) were considered. The EW part of the IEWCZM was parameterised for the olivine treatment, at the rate of $10 kgm^{-2}$, whereas all the other parameters relevant to the soil-vegetation processes were inherited from the [154]. This enabled a precise comparison between the olivine treatment and control scenarios for both the treatments. The IF treatment is shown in the figure 8.7a. The accumulated carbon refers to the above ground biomass and is directly linked to the total yield. The higher peaks refer to the tomato growth whereas, lower peaks are representing the weeds between the harvesting and sowing of tomato. The literature [154] compares the field experiment results of tomato growth with the ICZM simulation and hence in a way it

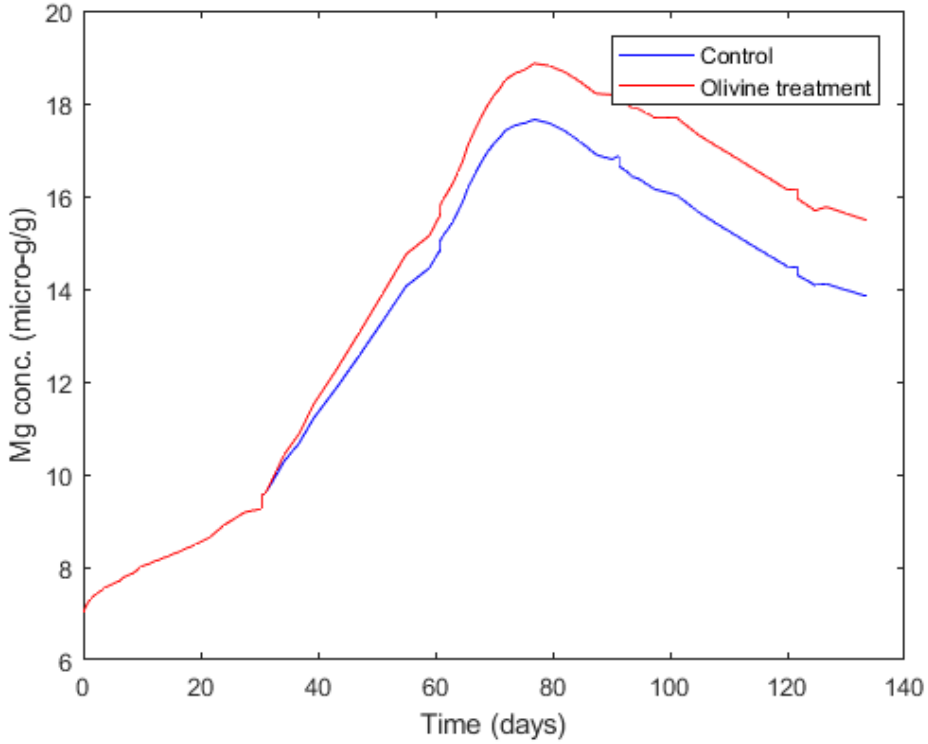

(a) Mg^{2+} concentration in the soil pore water.

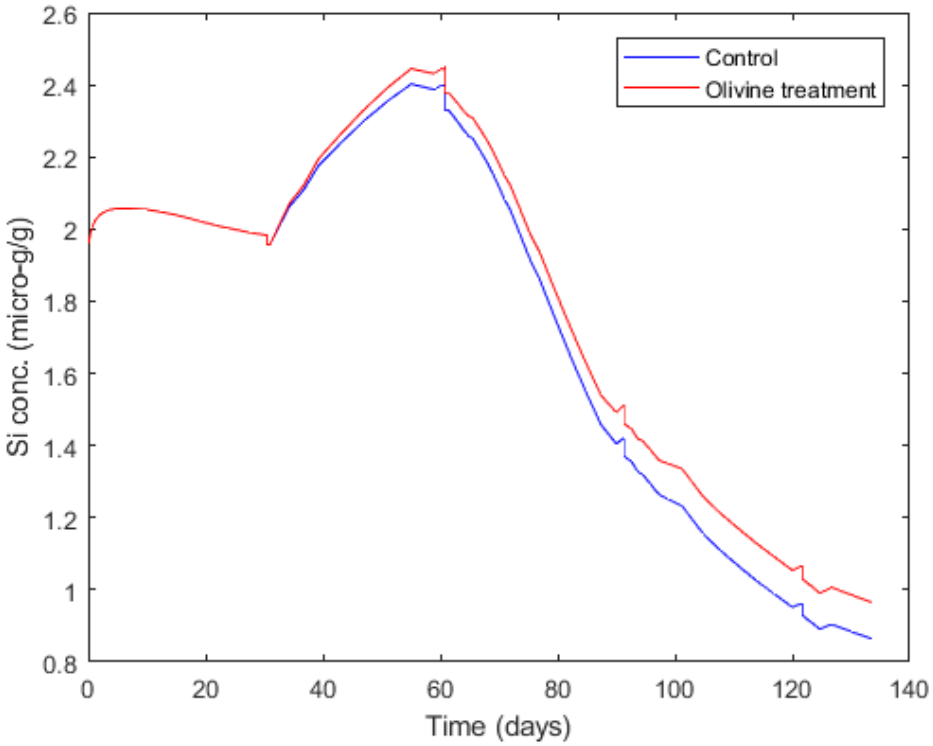

(b) *Si* concentration in the soil pore water.

Figure 8.6: IEWCZM validation results. Solutes concentration in a times series are shown for 133 days.

also emboldens the predictive power of the vegetation processes in the IEWCZM. Clearly, the olivine treatment has caused an increase in the net tomato production and suggests the applicability of the enhanced weathering in food security. Nevertheless, a more rigorous simulation analysis will be required before making this argument stronger. The figure 8.7b provides a similar comparison for the MSWC treatment. However, for analysing the cereal crops, MSWC might not be very useful as compared to the IF treatment.

8.9 Conclusion

Enhanced weathering being a geo-engineering technique would have profound effects across the ECZ. A rigorous analysis of those effects is a prerequisite for the actual implementation of such kind of artificial weathering. Like any negative emission technology, enhanced weathering comes up with its own pros and cons. The advocates of this method are trying to collate the evidences in support of enhanced weathering but the official regulations and logistic issues pose some constraints for the evaluation of this method in an actual field settings. The simulation analysis thus become imperative in the purview of these challenges.

In this study, an analytical framework for the development of enhanced weathering process model is presented. The algorithm is applicable for a single mineral but an extension scheme to incorporate multiple minerals is also provided subsequently. The algorithm was implemented in the Fortran in order to make it compatible with the similar kind of process models coded in the same language. The ECZ processes are interlinked, so the developed weathering model was integrated with some existing models representing the critical zone processes. The integrated model is known as the IEWCZM.

The enhanced weathering as a methodology is in its early stage, so not many results are available to benchmark the model performance. The calibration and validation of the IEWCZM was performed using a near-field type experimental results from the Oxfordshire region of England. The IEWCZM is supposed to be used as a tool for analysing the effects of enhanced weathering on the atmospheric carbon sequestration as well as for predicting the change in soil-vegetation variables. A published result corresponding to the Koiliaris region in Greece was used as a case study to demonstrate the potential of enhanced weathering in increasing the crop yield. The sensitivity of the weathering rate on the key variables such as temperature, soil acidity and mineral was also performed and the results are systematically presented in this chapter.

The enhanced weathering model algorithm presented in this chapter can be

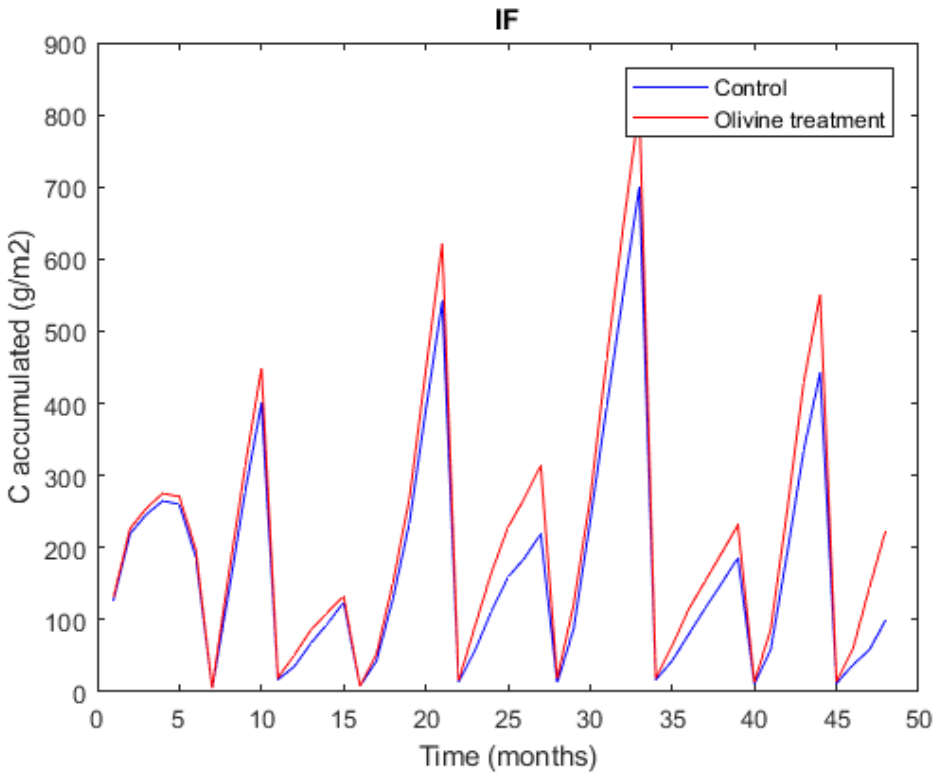

(a) Aboveground biomass under the IF treatment.

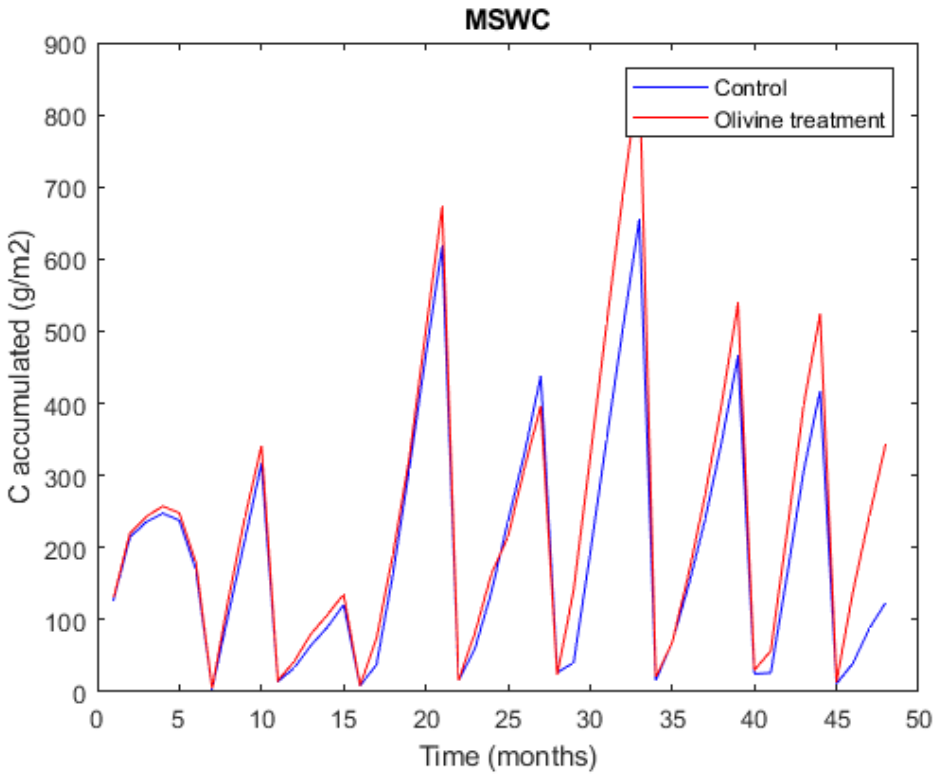

(b) Aboveground biomass under the MSWC treatment.

Figure 8.7: A case study performed on the the Koiliaris CZO. The 'control' results for both the treatments (IF and MSWC) refer to the tomato plant biomass simulation using the ICZM. 'Olivine treatment' refers to the addition of olivine at the rate of $10 kgm^{-2}$.

used to develop a customised weathering model and the same can be integrated with any standard soil-vegetation process models. In simple words, the model proposed here is not tied up with a particular software platform or the choice of particular ECZ models. The model verification tests results in this chapter are quite encouraging and the IEWCZM can be used for performing the scenario evaluations of any site as long as minimum level of model parameterisation is ensured.

Chapter 9

Enhanced weathering in the UK conditions

9.1 Introduction

The global population is expected to cross 9 billion by the year 2050 [1]. This will substantially have repercussions upon the food security, clean water, and energy needs of the future and current generations. All these issues are set to get further aggravated because of climate change and its effects on almost all the natural resources of the earth.

According to the World Bank (WB) report climate change is one of the greatest societal challenge and has a potential to push additional 100 million people into poverty by the year 2030 [9]. All the international organisations such as, the United Nations (UN), the WB and their sister wings have carried out tremendous amount of researches in the last two decades for figuring out the sustainable ways to counter the problems of growing population, food security, water security, energy security, climate change, extreme poverty etc. Most of their surveys and researches have concluded that these issues cannot be solved through de-coupled approaches, as they are interlinked, and can only be tackled through an integrated viewpoint.

In the year 2015, the UN repackaged their flagship programme known as the Millennium Development Goals (MDG) into the Sustainable Development Goals (SDG). Altogether, seventeen SDGs have been proposed to transform the world towards a better and sustainable future. The research outcomes of this chapter are centred around two prime SDGs namely – 'Climate Action' and 'Zero Hunger'.

Enhanced weathering of silicate rocks is a geo-engineering tool for the sequestration of atmospheric carbon dioxide. A shrinking-sphere type analytical model,

representing the enhanced weathering process was developed in this project. The previous chapter contains the details about the enhanced weathering model development, integration with existing soil-vegetation process models, calibration and validation. This integrated version of enhanced weathering model is known as the IEWCZM.

In this chapter, the IEWCZM is employed to evaluate the scenarios relevant to the accelerated weathering of a silicate rock, in the UK climatic conditions. This is the first novel contribution of the chapter. The simulation analysis is firstly performed for the West Yorkshire region and then extended to the entire UK, under some reasonable assumptions. The CO_2 absorption due to enhanced weathering is calculated for all the UK arable lands, until the end of the century. This is the second novel contribution of the chapter.

The remaining portions of the chapter unfold by presenting the soil and climate characteristics of the base site (Leeds farm) situated in the West Yorkshire region of England. Subsequently, experimental design, scenarios categorisation, simulation results of each scenario and the net CO_2 sequestration steps are presented. In the concluding remark, potential of such kind of accelerated weathering, as observed through this study and the limitations of this simulation analysis are discussed.

9.2 Leeds farm

The Leeds farm refers to the University of Leeds facility at Bramham, located in the West Yorkshire region. The University of Leeds has three farms with automatic weather monitoring systems, dedicated for the research and innovation purposes. The experimental designs for analysing the effects of enhanced weathering require the parameterisation of the IEWCZM. The next section will elaborate on the parameters required for the IEWCZM simulation and hence those details are avoided herein.

In this study, the analysis is constrained to the UK climatic condition. The entire UK land area were divided into 104 grid cells separated by the 0.5 degree $\times$ 0.5 degree geographically. Ideally, the simulation of the IEWCZM for the whole UK should incorporate the details of all the grid cells in the form of parameters. Practically, it was impossible to collect the input data for all the grids. Therefore, the Leeds farm was used for collecting the soil profile input data. The collected data was used for parameterising the soil inputs such as ionic concentration, fertilisers rate etc. In the following subsections, the data types and their characteristics will be discussed.

Serial no.	Solute	Conc. (mol/l)
1	Mg^{2+}	7.7×10^{-4}
2	Ca^{2+}	1.0×10^{-3}
3	Na^{+}	1.1×10^{-4}
4	H_4SiO_4	2.4×10^{-4}
5	HCO_3^{-}	1.9×10^{-3}
6	H^{+}	2.18×10^{-8}

Table 9.1: Solutes initial concentration in the soil pore water.

9.2.1 Soil characteristics

The Leeds farm supports a variety of crops including wheat and barley for the university research studies. So in a general sense, the soil at the site can be regarded in good health or at least continuously monitored for better conditions. The pore water concentration of the major solutes, as recorded in 2016 are presented in Table 9.1.

9.2.2 Leeds climate

Climate inputs play important roles in soil reactive transport models such as the Hydrus [12] and all the linked models like the IEWCZM, where the transport of solutes and water in the soil profile are thoroughly represented. A solute's concentration at a time instant is primarily dependent upon the amount of precipitation at the previous few time steps. The climate characteristics of the Leeds farm can be observed from the past precipitation (figure 9.1a) and temperature data (figure 9.1b). These data are available in the open source from the archive of the UK Met Office. Because of some unknown reasons, this dataset does not contain the measured temperature values from January 1929 to September 1929. This has caused a gap in the time series plot (figure 9.1b) of temperature. Both, average rainfall and temperature have not changed much in the last 100 years but this trend is expected to show some deviations in the next 100 years because of climate change effects. In this study, the future projections of weather inputs (precipitation and temperature) using a CMIP5 model [117] are used for parameterising the IEWCZM. These projected data will be shown in the following sections.

9.3 IEWCZM setup and experimental design

The full parameterisation of the IEWCZM may require hundreds of parameters and variables. The full list of these parameters are available in the ICZM user manual [153], available on request at the http://www.herslab.tuc.gr/downloads/1d-

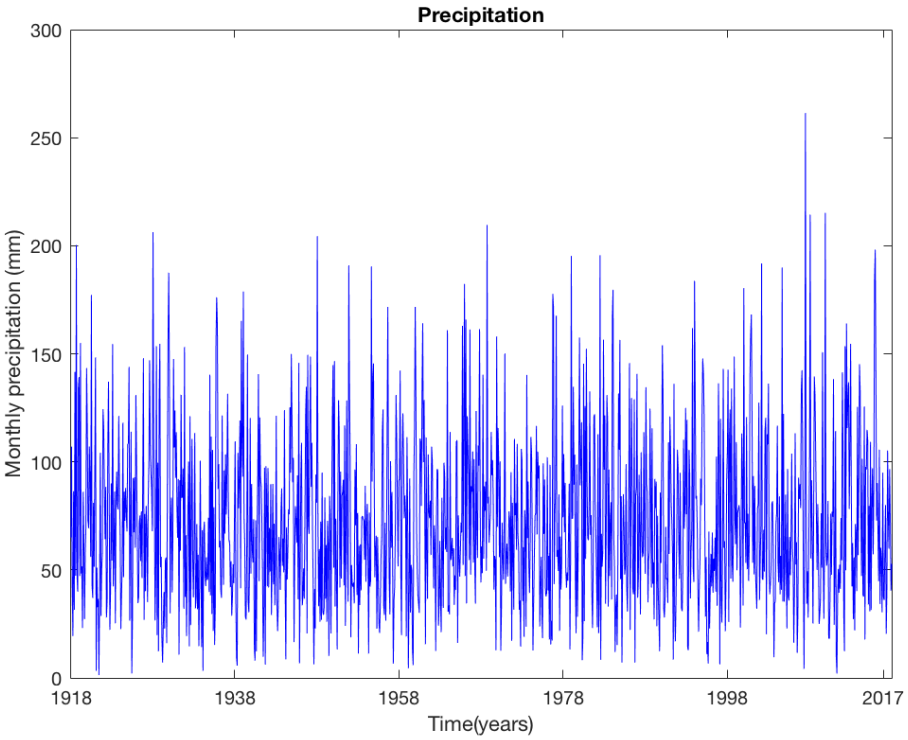

(a) Precipitation

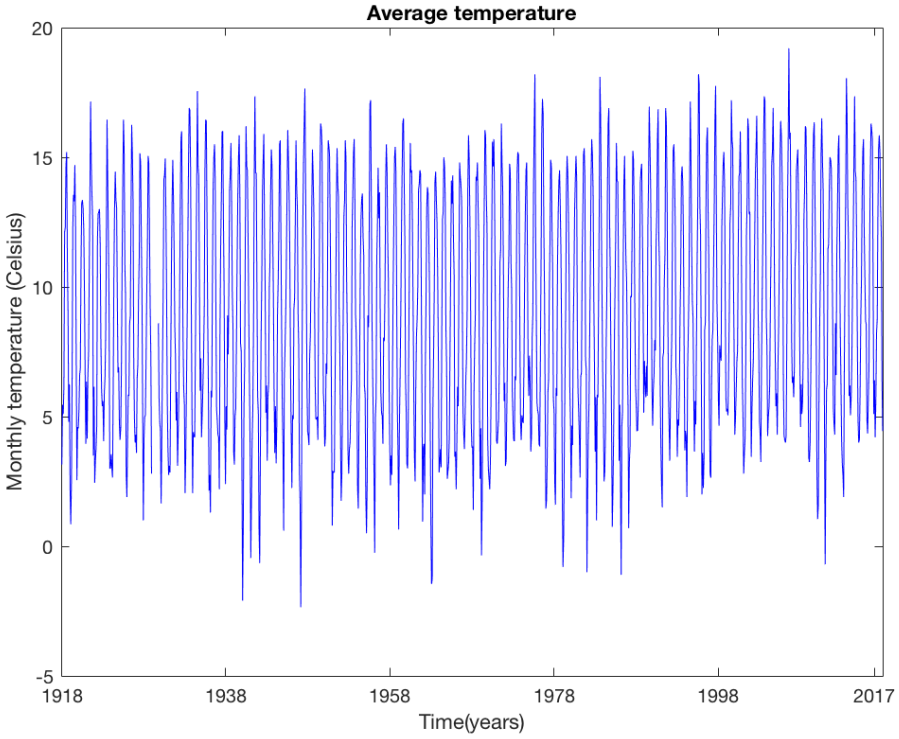

(b) Temperature

Figure 9.1: Historical climate data (Leeds farm).

icz-model. The default values of many such parameters are also available in the manual. A parameter needs to be tuned according to the modelling requirements. For the present study, major inputs are – time series weather data, evapotranspiration (calculated within Hydrus), solutes initial concentration, fertiliser input rates, tillage rate, and harvest rate. The details about these inputs are explained using graphs/tables in the appropriate sections.

The effects of enhanced weathering in the UK climatic condition were categorised into two phases. In the first phase, simulation was performed for Leeds farm. In the second phase, simulation was extended to the 104 sites across the UK. The first phase considers just one site and hence the effects of enhanced weathering on ionic concentrations, plant-nutrient uptake and crop yield are analysed rigorously in this phase. This phase was further divided into two scenarios. In the first scenario, basalt was added only once at the beginning of the model simulation and the total period of simulation was limited to three years. The second scenario takes into account the yearly addition of basalt and the simulation was carried till this century end. Both the scenarios were compared to the baseline scenario, where no basalt was added at all. The baseline scenario will also be referred as 'control' throughout this chapter.

9.4 Baseline condtion

The baseline parameterisation of the IEWCZM was performed using the available field data from Leeds farm. The initial concentration of the major solutes are presented in the Table 9.1. Winter wheat was considered as the crop type, mainly because the UK climate offers the suitable conditions for wheat production. One of the motivations of analysing the enhanced weathering as an NET is due to the added benefits it provides in improving soil fertility by increasing the plant nutrients availability. Therefore, wheat as a crop can be used to gauge the efficiency of the enhanced weathering in addressing the CO_2 sequestration as well as food security.

An inorganic fertiliser such as NPK mixture is a standard practice for the wheat farming across the UK. In this study, $10-20-20$ mixture of the NPK was used as a fertiliser. The NPK fertiliser mixtures are denoted by the ratio of N, P, and K in the mixture. So, $10-20-20$ NPK means, 10% nitrogen, 20% phosphorus and 20% potassium are present in the mixture. The nitrogen application rate was limited to $200 kg/ha$. Ideally, the fertilisers are applied using the irrigation water. However, in this simulation study water input is limited only to precipitation. The sowing, tillage, harvesting, and fertiliser dosage are represented in the Table 9.2.

Month	Jan	Feb	Mar	Apr	May	Jun	Jul	Aug	Sep	Oct	Nov	Dec
Plant type	Wt[1]	Wt	Wt	Wt	Wt	Wt	Wt	Wt	Wd[2]	Wd	Wt	Wt
Water input	R[3]	R	R	R	R	R	R	R	R	R	R	R
Tillage	No	No	No	No	No	No	No	No	No	Yes	No	No
Fertlisation	No	No	No	No	No	No	No	No	No	No	Yes	No
Harvest	No	No	No	No	No	No	No	Yes	No	Yes	No	No

[1] wheat; [2] weed; [3] rain

Table 9.2: EWICZM baseline set-up.

9.5 Scenario 1: One-off basalt addition

In this scenario, basalt was added only once at the rate of $5kg/m^2$ in the beginning of the simulation. The simulation period lasts from January 2017 to December 2019. The weather input projections such as precipitation (figure 9.2a) and temperature (figure 9.2b) were simulated through a CMIP5, corresponding to the RCP 8.5 (business-as-usual) scenarios of the Intergovernmental Panel on Climate Change (IPCC).

The basalt dissolution reaction from the previous chapter clearly suggests that the addition of powdered basalt in a soil profile will release cations (Mg^{2+}, Ca^{2+}, Na^{+}, K^{+} etc.), while absorbing the H^{+} ions. The theory also suggests that increase in availability of these nutrients should also increase the biomass or grain yield. In the following subsections, the simulation results pertaining to this scenario and its comparison with the baseline conditions are shown.

9.5.1 Mg cation concentration

The forsterite (Mg_2SiO_4) forms about 11.5% of basalt by mass. The dissolution of basalt raised the level of Mg^{2+} concentration in the soil pore water. The figure 9.3a shows the change in Mg^{2+} concentration with respect to the baseline. Three years simulation period is converted into days (1095 days) to clearly interpret the concentration change. The basalt application rate of $5kg/m^2$ is not sufficient enough to induce enormous change in soil pore water concentration. The same result is zoomed in (figure 9.3b) to support the hypothesis that such kind of artificial weathering could actually result an increase in cations.

9.5.2 Na cation concentration

Similar to forsterite, basalt also contains other minerals including labradorite and augite. The labradorite and augite forms about 43% and 20.8% of basalt by mass respectively. These are complex minerals containing Na, Ca, Al, Si, Mg, Fe, Ti,

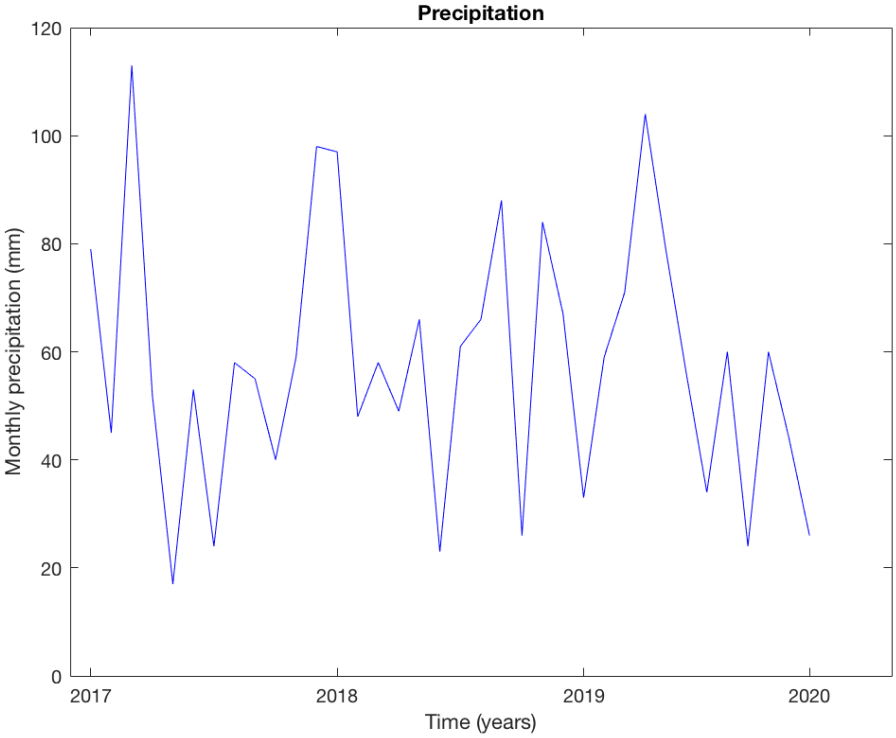

(a) Precipitation

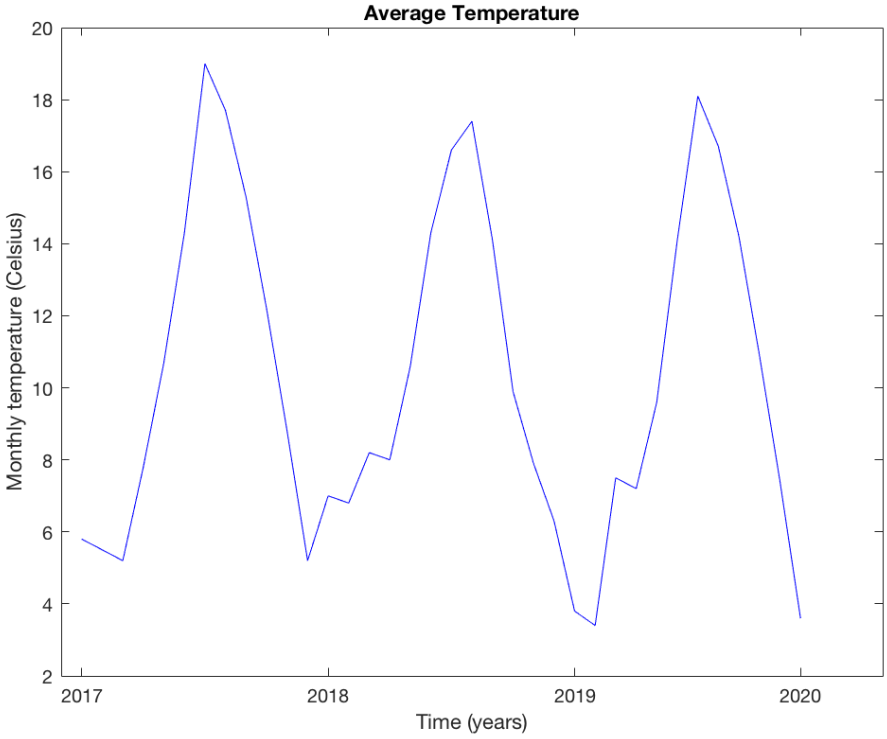

(b) Temperature

Figure 9.2: Weather projection data from the CMIP5 (Leeds farm).

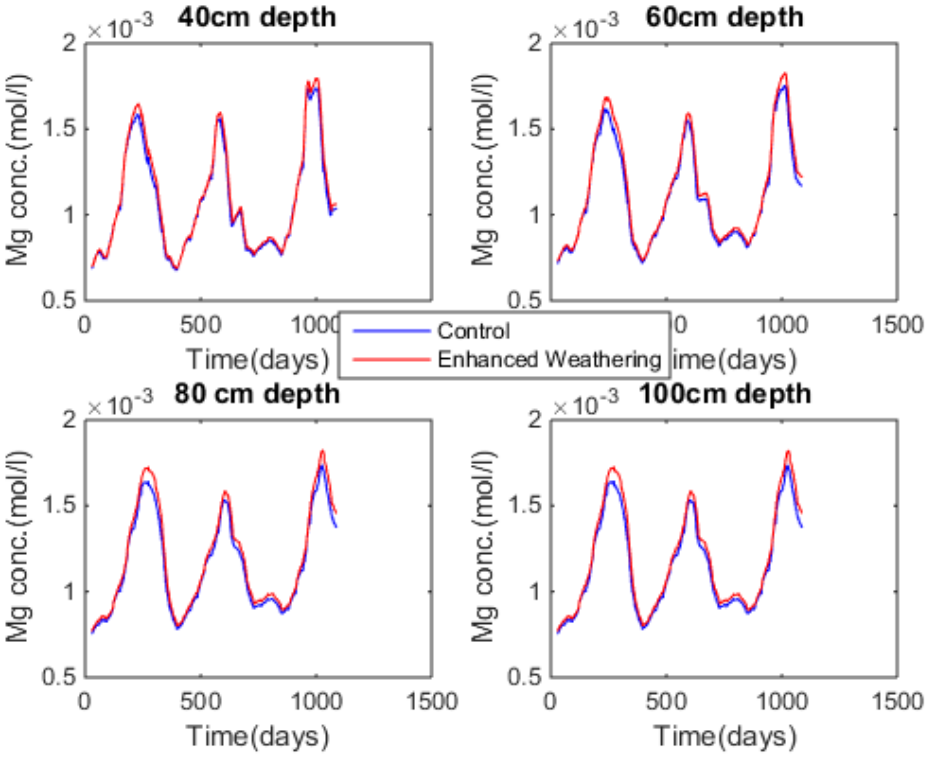

(a) Mg^{2+} concentration

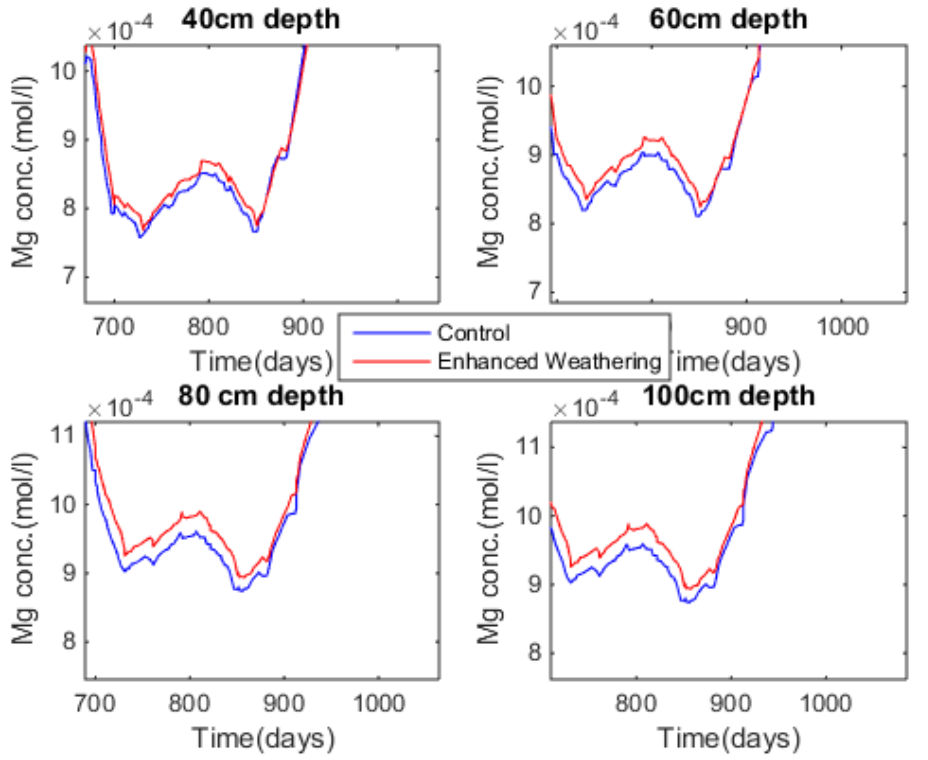

(b) Mg^{2+} concentration (zoomed-in)

Figure 9.3: Magnesium cation concentration in four different layers of the soil profile.

and O. The effects of basalt addition on Na^+ concentration is essentially caused because of these two minerals (figure 9.4a). A zoomed in (figure 9.4b) version like Mg^{2+} emboldens the idea behind enhanced weathering.

9.5.3 Si concentration

Silicon in the form of H_4SiO_4 is a major product of all the silicate minerals present in the basalt. Silicon in general is considered to have positive implications upon the soil fertility [124]. The weathering mechanism of basalt generates substantial amount of silicon and hence the concentration of Si in pore water is increased (figure 9.5a, 9.5b).

9.5.4 Ca cation concentration

Labradorite and augite in a basalt also contribute to the addition of Ca cations as the weathering progresses. The pattern is similar to the other ions concentrations (figure 9.6a, 9.6b). The Ca^{2+} concentration may not show an increase in concentration, if the precipitate formation in the form of carbonates are taken into account. In reality, HCO_3^- tends to combine with available cations for the carbonate formation. However, the carbonate precipitates are not considered in this model simulation mainly due to the limitation of the IEWCZM.

9.5.5 pH

pH is a logarithmic representation of the hydrogen ion concentration. It plays several important roles in the plant-soil system. pH and its significance especially in the context of plant nutrient uptake have been discussed in the previous two chapters. In summary, pH of a neutral solution is 7, pH lower than 7 means the solution is acidic and the pH more than 7 means the solution is basic. The reaction mechanism of basalt involves the reduction of H^+ ion concentration and hence the pH of soil pore water becomes higher than the baseline (figure 9.7a, 9.7b).

9.5.6 Plant nutrients uptake

Plant nutrients are categorised into macronutrients and micronutrients. Major macronutrients include, nitrogen, phosphorus, potassium, magnesium, calcium, sulphur, carbon, oxygen, and hydrogen. The roles played by these macronutrients and micronutrients have been discussed in the previous chapters. Among the macronutrients, plant uptake of nitrogen, phosphorus, and potassium are analysed in this subsection.

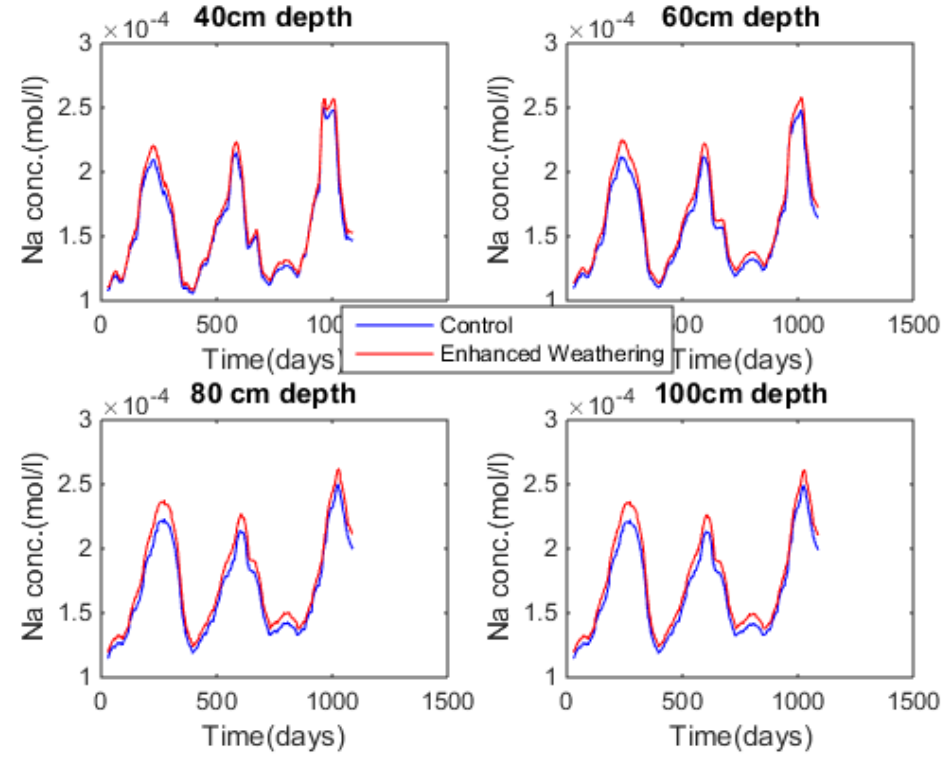

(a) Na^+ concentration

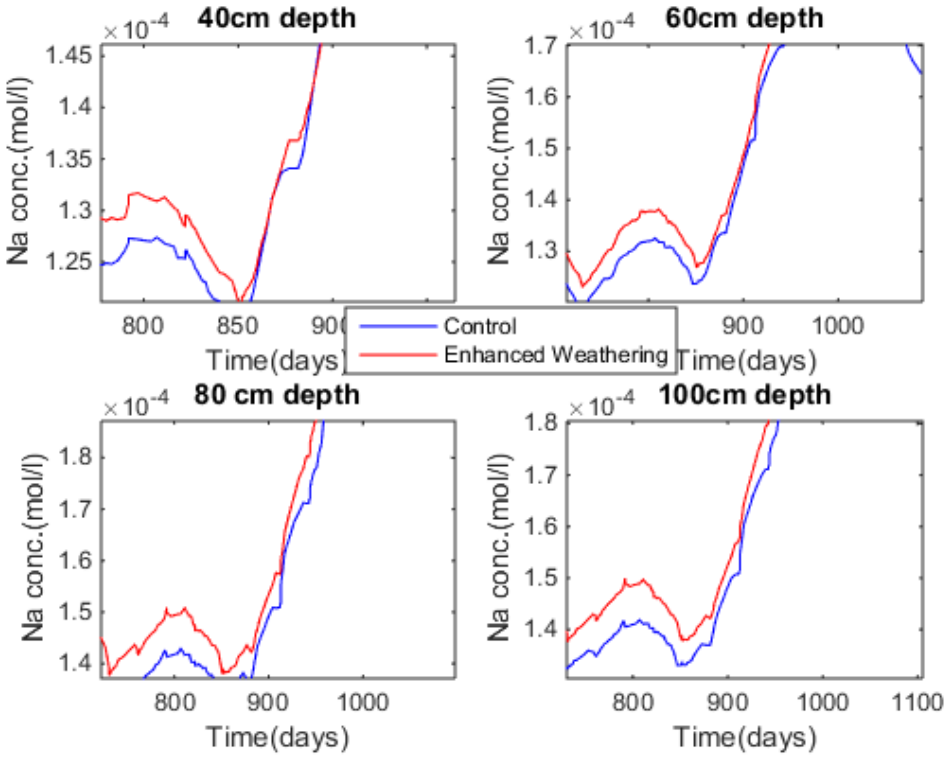

(b) Na^+ concentration (zoomed-in)

Figure 9.4: Sodium cation concentration in four different layers of the soil profile.

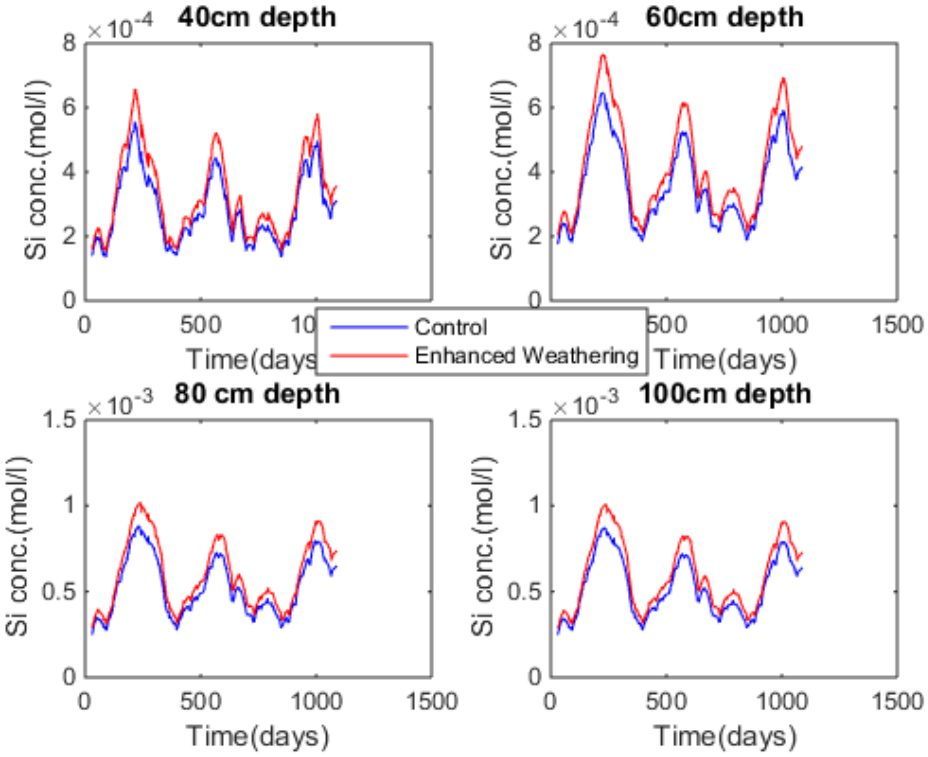

(a) *Si* concentration

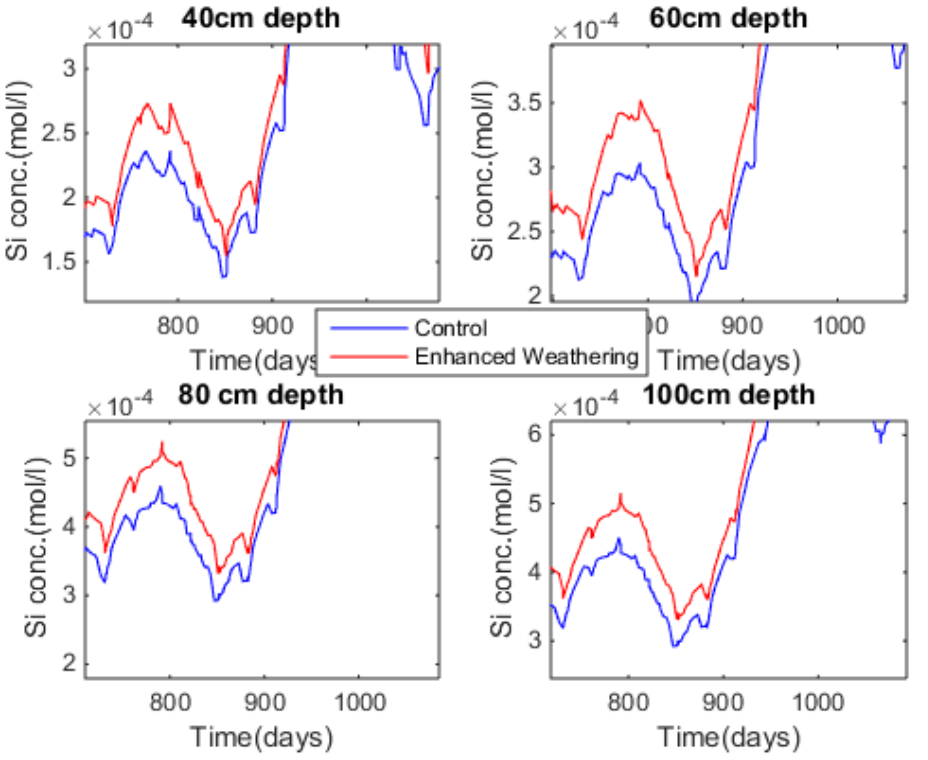

(b) *Si* concentration (zoomed-in)

Figure 9.5: Silicon concentration in four different layers of the soil profile.

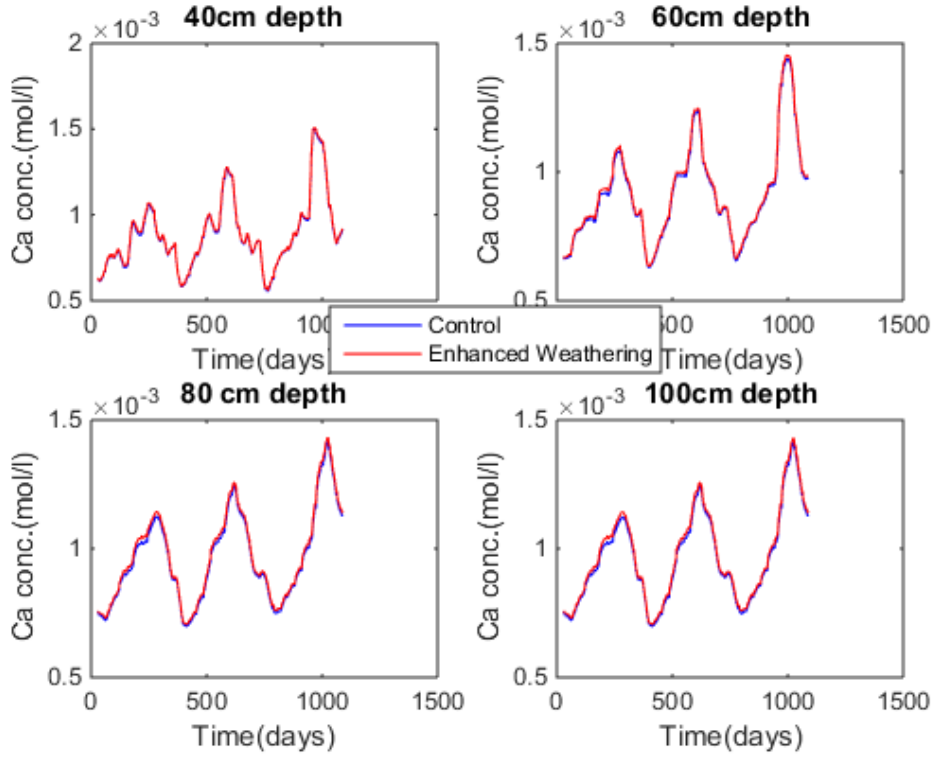

(a) Ca^{2+} concentration

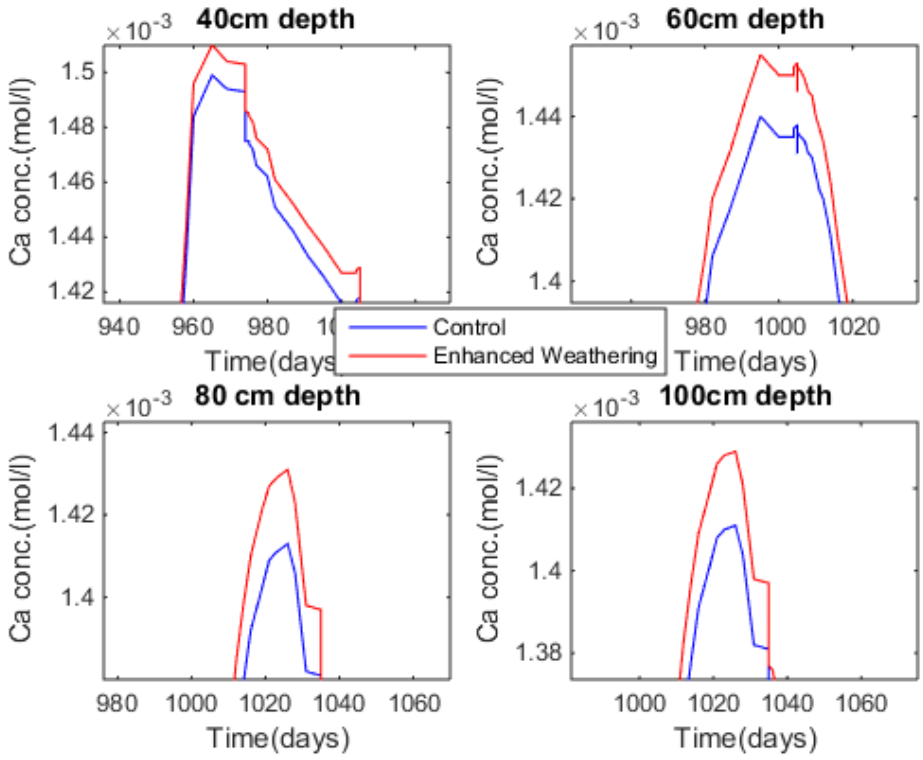

(b) Ca^{2+} concentration (zoomed-in)

Figure 9.6: Calcium cation concentration in four different layers of the soil profile.

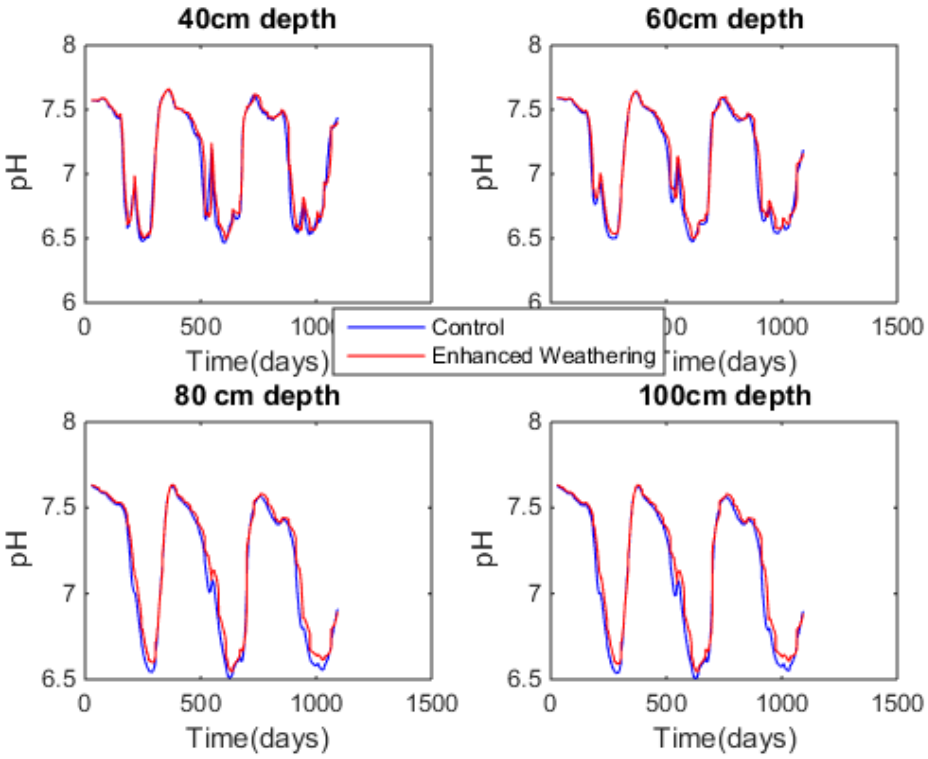

(a) pH

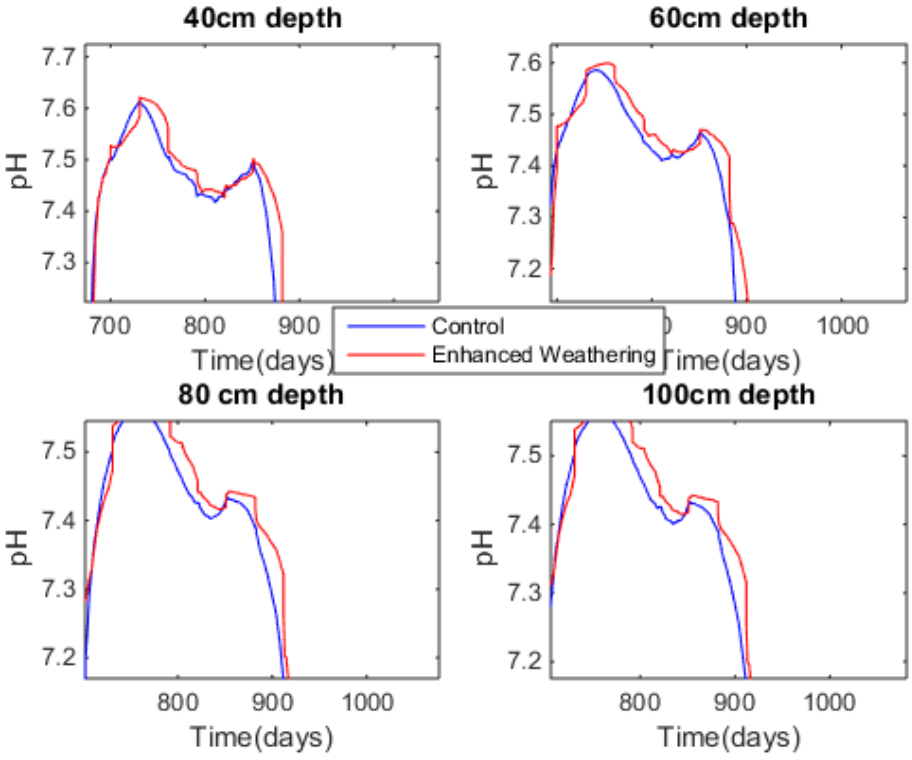

(b) pH (zoomed-in)

Figure 9.7: Soil pore water pH in four different layers of the soil profile.

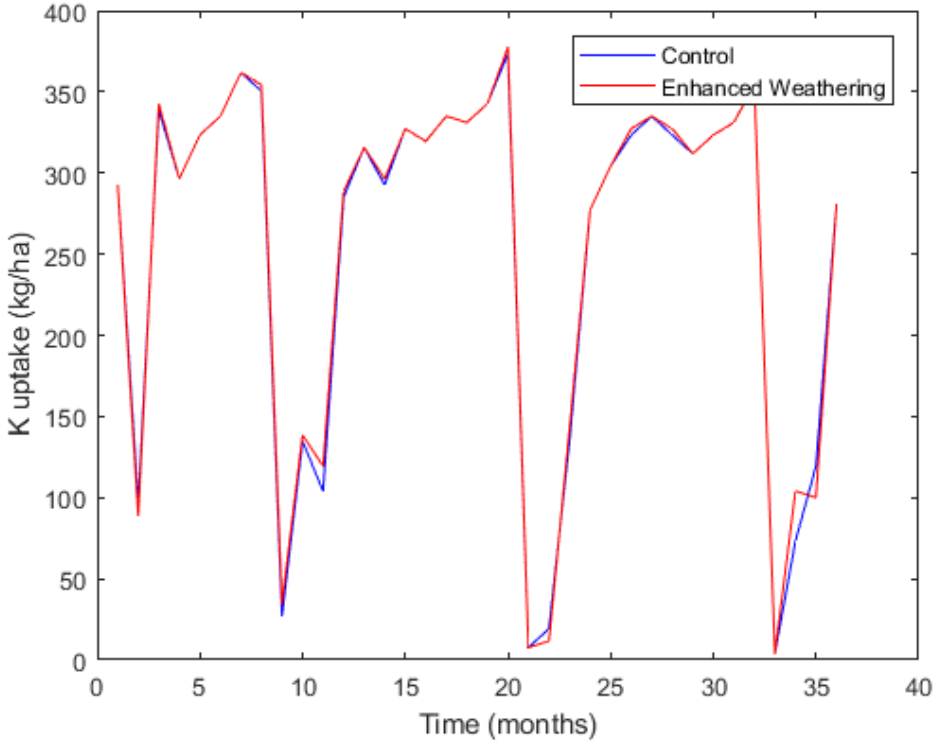

Figure 9.8: Potassium uptake by plant.

Nitrogen and phosphorus do not constitute the part of basalt whereas, potassium is present in mineral K-feldspar. The mass contribution of K-feldspar is only 6.1% of basalt and the weathering rate constant corresponding to this mineral is lower than other major minerals present in basalt. Hence, weathering of basalt does not release potassium in large quantity. In reality, change in pH should also have some effects on plant macronutrients uptake, including nitrogen and phosphorus, but the IEWCZM is not able to incorporate those effects. Therefore in this simulation study, only potassium uptake will be highlighted (figure 9.8). Potassium uptake comparison between baseline and enhanced weathering indicates that an increased application rate of basalt should increase potassium uptake as well.

9.5.7 Biomass and grain yield

Biomass is directly linked with the total yield. Approximately 95% of the total biomass is related to the macronutrients carbon, hydrogen, oxygen, and nitrogen [148]. In this scenario, among these nutrients, potassium, magnesium, and calcium exhibit an increased concentration level. The simulation result shows a slight enhancement (0.5%) in the biomass with the current application rate of basalt.The

total biomass was converted into grain yield by using the harvest index [155] equal to 0.47.

9.5.8 Remark: Scenario 1

The simulation results under this scenario clearly suggests that enhanced weathering of silicate rock like basalt causes some increase in the major ionic concentration including pH. The raised level of few essential plant nutrients also results into slight increase in crop yield. The idea behind enhanced weathering is to absorb atmospheric CO_2 while increasing the crop yield. However, at the current application rate ($5kg/m^2$, one-off), the technique can not be leveraged fully. Therefore, the simulation analysis was shifted to the next scenario, where the basalt application rate was tuned to match the desired objectives.

9.6 Scenario 2: Yearly basalt addition

In this scenario, the IEWCZM was parameterised for the same site (Leeds farm) like the scenario 1. The simulation period starts from year 2017 and lasts until the century end. Basalt was applied at the rate $5kg/m^2$, on yearly basis. The model incorporates the shrinking sphere approach for modelling the change in basalt particle as weathering progresses. This means that mineral particle size would decrease as the weathering progresses. Nevertheless, the addition of fresh basalt every year increases the net particles almost exponentially. The particle was considered as 10 μm, based on the recommendations from [131].

The IEWCZM requires the precipitation and temperature inputs in time series. Similar to the scenario 1, a CMIP5 model was used to obtain the weather inputs projection till the century end (figure 9.9a, 9.9b). All the projected data are based on the RCP 8.5 scenario of the IPCC.

9.6.1 Mg cation concentration

Mg^{2+}cation shows an increase of 114.9% in the pore water concentration (figure 9.10) at the century-end. Unlike scenario 1, the concentration level pertaining to the enhanced weathering shows an exponential kind of change, especially towards the century-end. This is mainly attributed to the yearly addition of basalt at the constant rate. Sudden spikes in the Mg^{2+} concentration are triggered by the sudden changes in precipitation, few time steps prior to the spikes. Solute transport in the IEWCZM is governed by the Hydrus module, as discussed in the previous chapter. Whenever, there is a sudden change in the precipitation, the solutes

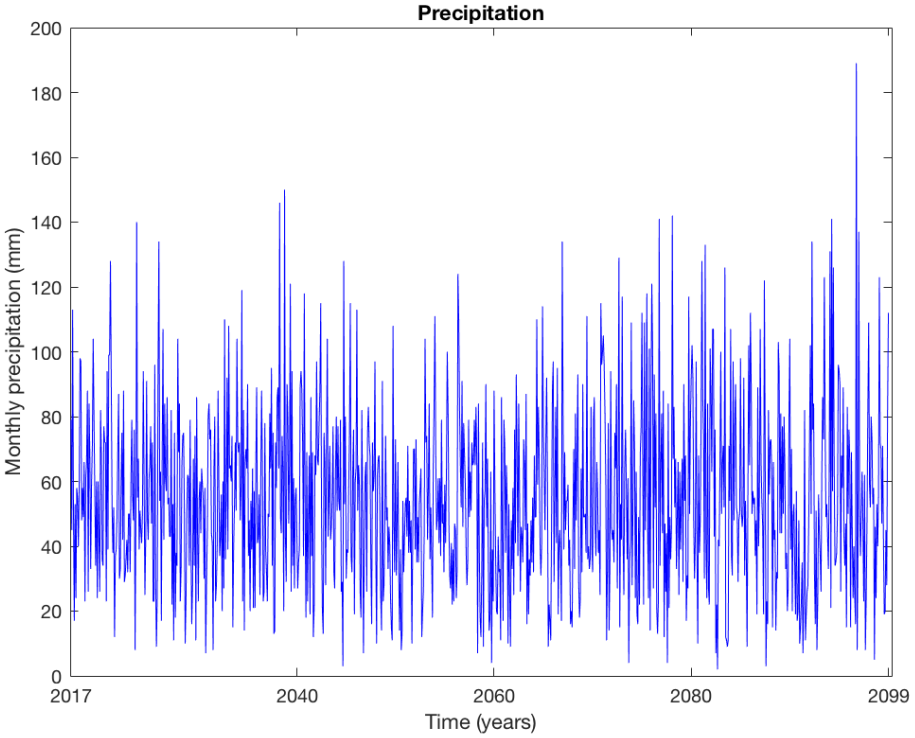

(a) Precipitation

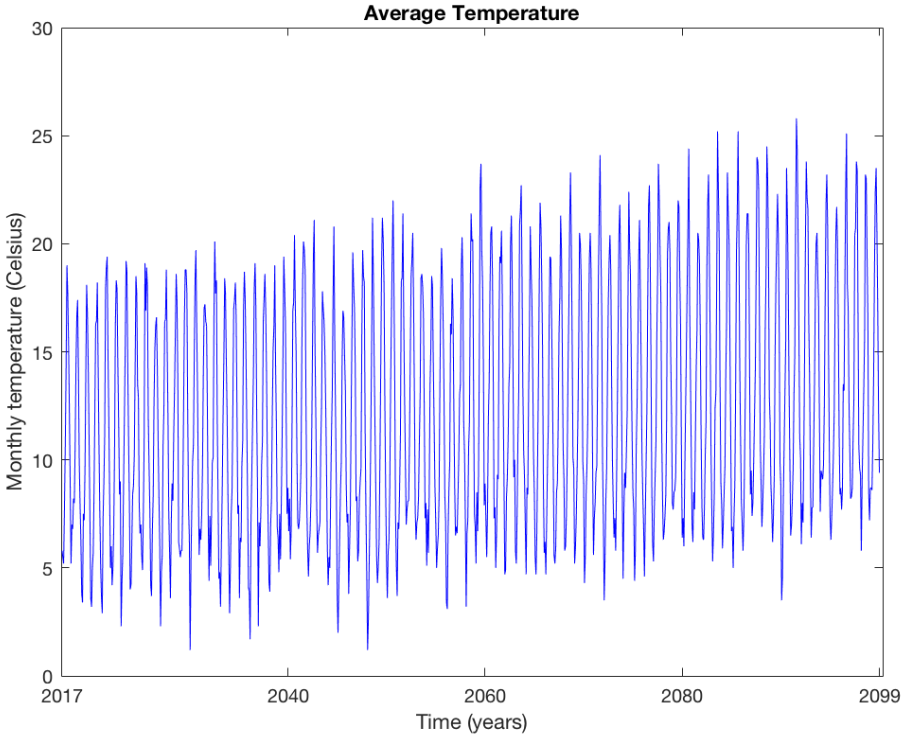

(b) Temperature

Figure 9.9: Weather projection data from the CMIP5 (Leeds farm)

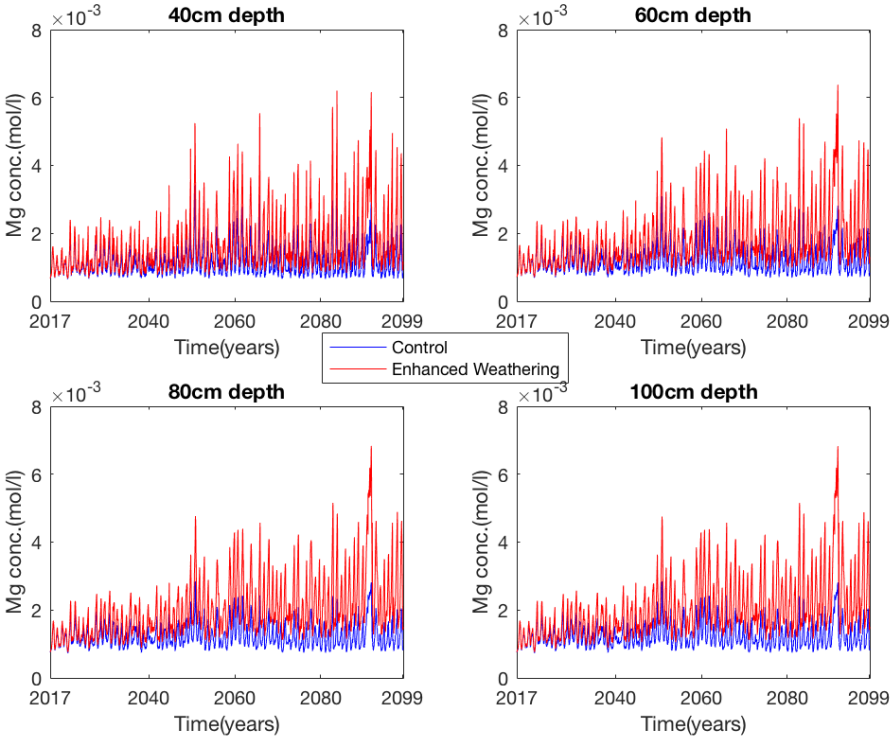

Figure 9.10: Mg^{2+} concentration in four different layers of the soil profile.

presents in the top layers of the soil are flushed towards the bottom of the soil profile through the soil pore water. The concentration of solutes are observed through the soil pore water in the IEWCZM. Therefore, a sudden change in precipitation results into a sudden increase in solute concentration, visible in the form of spikes.

9.6.2 Na cation concentration

The mineral sources of Na^{+}cations in a basalt rock are discussed in the previous scenario. In this scenario, concentration of Na^{+} increases by about 266.4% in 2099 (figure 9.11) . Na is also a plant macronutrient and therefore such an increased level emboldens the motivations behind enhanced weathering. All the major characteristics of the Na^{+}, such as exponential feature and spikes are similar to Mg^{2+} and can be interpreted in similar ways.

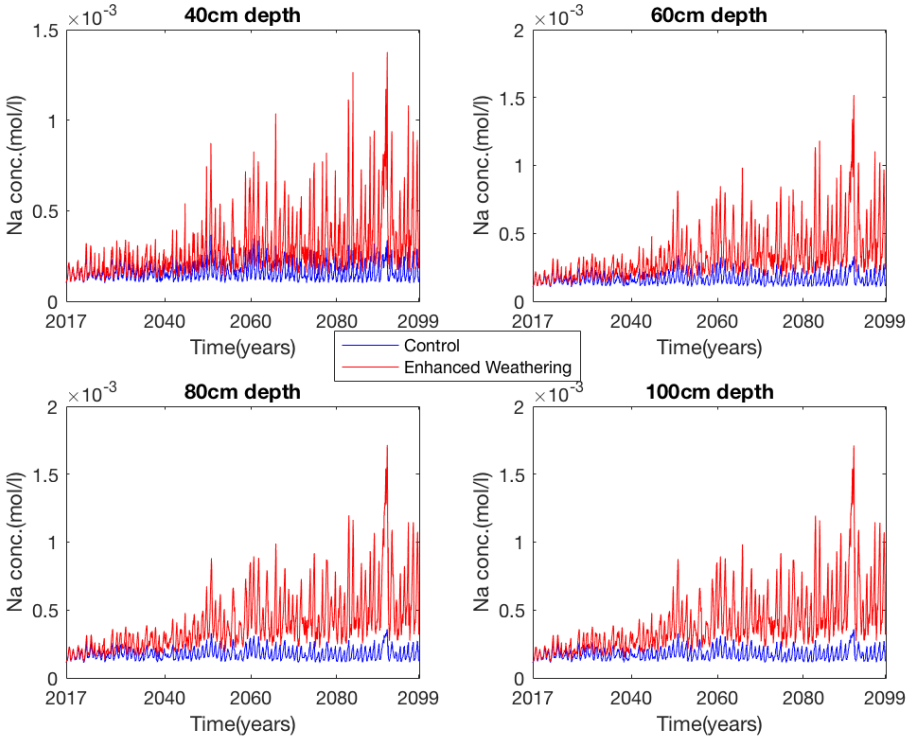

Figure 9.11: Na^+ concentration in four different layers of the soil profile.

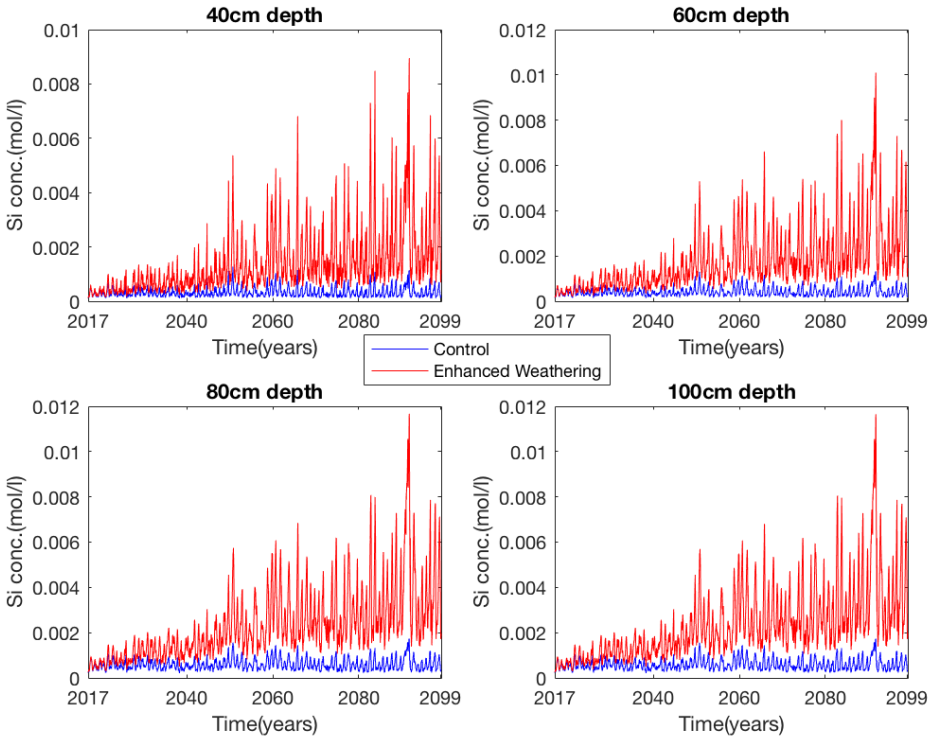

Figure 9.12: *Si* concentration in four different layers of the soil profile.

9.6.3 Si concentration

The concentration of silicon increases with enhanced weathering. According to this simulation study, the concentration of silicon is expected to increase by 585% by the century-end (figure 9.12). The potential benefits of such an enhanced level of silicon in the soil system are not analysed in this study. However, the available literatures [156, 157] strongly indicate the advantages associated with increased amount of silicon in the soil system.

9.6.4 Ca cation concentration

Ca^{2+}concentration increases by about 118.7% towards the end of year 2099 (figure 9.13). The carbonate formation was not assumed in the model, because of the model limitation as well as for demonstrating the effects of enhanced weathering in terms of increased level of major cations. In reality, bicarbonates will combine with calcium to form calcium carbonates. Similarly, the formation of carbonates is also applicable for other cations.

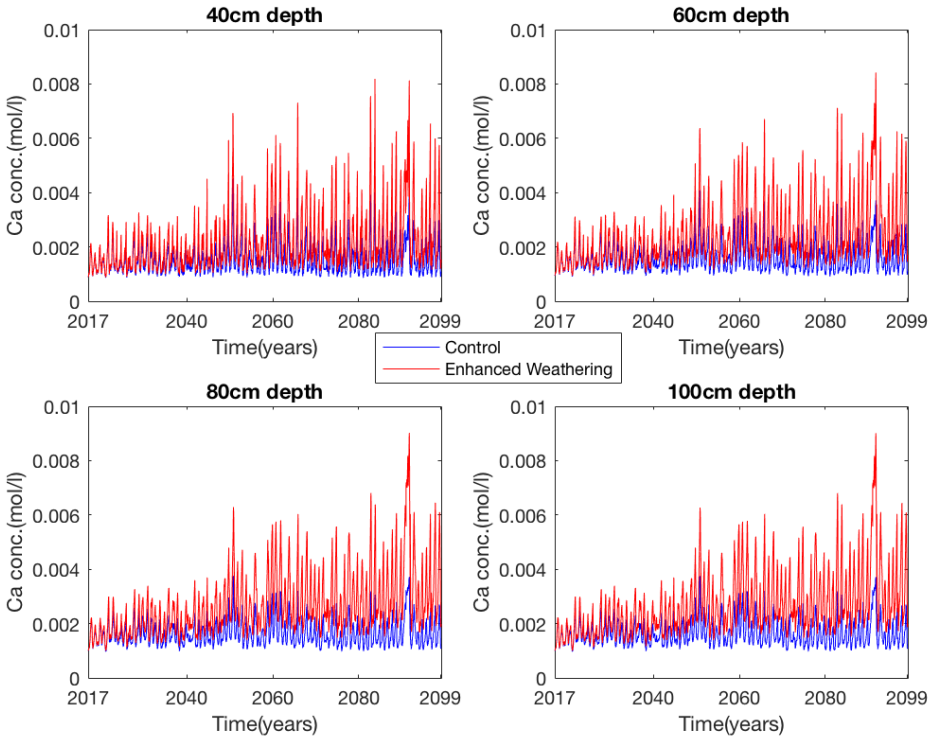

Figure 9.13: Ca^{2+} concentration in four different layers of the soil profile.

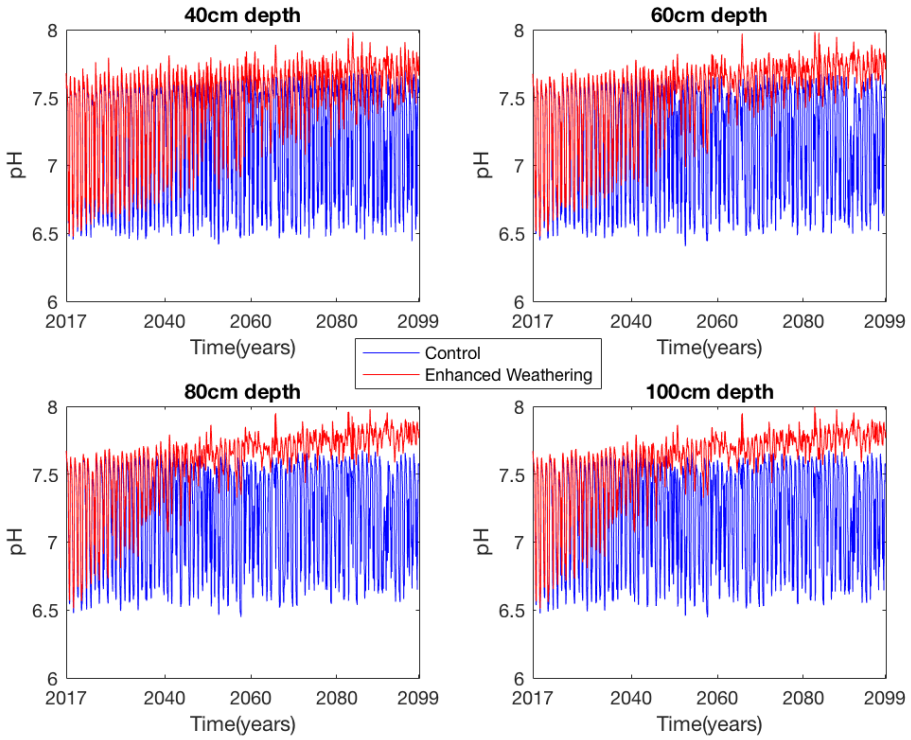

Figure 9.14: Soil pore water pH in four different layers of the soil profile.

9.6.5 pH

The weathering reaction of basalt consumes the H^+ ions and this increases almost exponentially, when the basalt is entered into the soil system on yearly basis (figure 9.14). pH is a standard way to represent the H^+ concentration and the simulation results show an increase of about 9% in the pH by the end of this century, under the current scenario of enhanced weathering. One of the shortcomings of the IEWCZM is that, the effects of pH is not transferred into plant nutrient uptake. Improving this shortcoming was not within the scope of this research. Due to intense farming, ion exchange on the soil sites increases rapidly. A nutrient is typically passed into plant system by replacing cations with H^+. This exchange mechanism increases the soil acidity after some farming cycles. An increased level of acidity in soil reduces the fertility of the soil. Traditionally, liming is being used to increase the pH of agricultural soil. Enhanced weathering has a potential to replace the liming process through powdered basalt. The underlying theory and simulation results suggests that silicate rocks provide many other benefits than a mere liming process.

9.6.6 Summary of soil pore water concentrations

All the key solute concentrations including pH in the soil pore water under the Scenario 2 (yearly basalt addition) have been presented above. In this subsection, those results will be summarised in a tabular form (Table 9.3) for the ease of understanding the effects of yearly basalt addition on the solutes – Mg^{2+}, Na^{+}, Si, Ca^{2+}, and H^{+}.

Sr. No.	Solute	Conc. ↑(in %)
1	Mg^{2+}	114.9
2	Na^{+}	266.4
3	Si	585.0
4	Ca^{2+}	118.7
5	H^{+} (as pH)	9.0

Table 9.3: Percentage increase in concentration of key solutes until the century end (2099). Increase in concentration of these solutes are attributed to the effects of enhanced weathering of basalt causing the release of cations and the absorption of hydrogen ions.

9.6.7 Plant nutrients uptake

Types of plant nutrients and their significance have already been discussed in the previous section and previous chapters. In this subsection, the simulation results corresponding to the N, P, and K uptake, quantitative figures and their implications will be discussed.

Nitrogen is available in the soil system through natural weathering processes and NPK fertiliser mixture. Enhanced weathering of basalt in principle does not provide additional nitrogen containing ions. Change in pH due to weathering should have affected the nitrogen uptake but the IEWCZM is not able to convert those changes into nutrient uptake. Similar to nitrogen, phosphorus is also available in the soil system mainly due to natural weathering of rocks and NPK fertiliser, added in each growing season. Basalt weathering does not contribute towards phosphorus addition in the soil systems and its uptake remains unchanged from the baseline.

Unlike nitrogen and phosphorus, potassium has an extra source in the form of K-feldspar present in basalt. However, an excess amount of potassium in the soil system causes the 'luxury' uptake eventually leading to reduction in magnesium uptake. This situation is not desired as magnesium too plays important roles in a plant growth. Hence, the vegetation module in the IEWCZM takes this factor into consideration and a continuous increase in the potassium level because of

basalt weathering does not reflect at all the times during simulation. Therefore despite an overall increase in potassium uptake due to weathering, at various instants, a drop in the uptake is also noticed. In year 2060, the simulation shows an increase of 4.1% in the potassium uptake, whereas, by the century-end this figure increases to about 15.7%. The weathering rate constants of K-feldspar is not high like forsterite, therefore effects on the plant uptake is also not very high. Nevertheless, an enhanced level of potassium, magnesium, and calcium should play some positive roles in the net crop yield.

9.6.8 Biomass and grain yield

Total biomass production is directly linked with the crop yield, provided the harvest index is correctly figured out. The calculation steps for converting the biomass into grain yield is same as described in the Scenario 1. In this scenario, the availability of Mg, Ca, and K increase rapidly, as the weathering of basalt proceeds. These effects are transferred into an increased amount of total biomass.The wheat yield is obtained from the total biomass using the harvest index equal to 0.47. The simulation results corresponding to yield shows exactly the same trend like biomass.

In year 2060, this simulation predicts an increase of 2.9 % in wheat yield, which will further increase to about 9.4 % by the end of this century. The difference between yield corresponding to enhanced weathering and natural weathering is shown in the figure 9.15. The yield difference plot shows some negative values too. These are attributed to the weeds. In control scenario, after each harvest period, weeds grow naturally on the land. In enhanced weathering scenario, the excessive amount of basalt rock powder on the top surface hinders the growth of weeds. Hence, there is a reduced growth in weeds and that reflects on the difference plot.

9.6.9 Remark: Scenario 2

The Scenario 2 was designed on the basis of the observations of the previous scenario. One-off addition of basalt was not able to provide the desired functionalities of enhanced weathering process. Under the current scenario, basalt in the powdered form was applied every year starting from 2017 until 2099. The dose of basalt was kept fixed at the rate $5kg/m^2$. The simulation results show an exponential increase in the concentration of all the major ions except hydrogen. The weathering process consumes hydrogen ion and hence there is a decrease in its concentration resulting into an increased level of pH in the soil pore water.

The nitrogen and phosphorus uptake by plants do not show much change

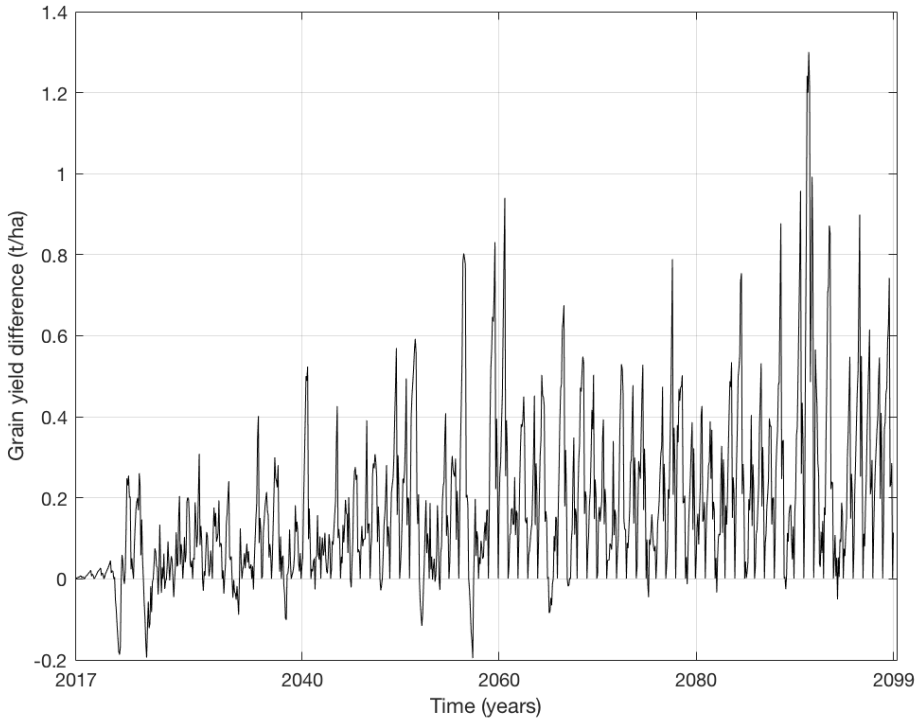

Figure 9.15: Difference between grain yield in enhanced weathering and control scenario.

under the enhanced weathering conditions but in general, the potassium uptake increases as the weathering progresses. Overall, these changes were transferred into the total biomass and subsequently into the grain yield. About 9.4 % increase in the wheat production, while reducing the soil acidity and absorbing the anthropogenic carbon appears to be a good proposition.

The motivation garnered from this scenario led to the extension of the IEWCZM throughout the UK regions. In the next section, UK wide simulation analysis are discussed.

9.7 UK wide simulation

The parameterisation of the IEWCZM requires data from the soil profile, vegetation, and local climate. The entire UK land area can be divided into approximately 104 grid cells, separated by 0.5 degree $\times$ 0.5 degree geographically. Ideally, one should parameterise the IEWCZM with data from all these sites, which was not possible in this project. Therefore, the soil condition and vegetation types for all

the sites were assumed to be the same like the Leeds farm. However, climate data like precipitation and average temperature are relatively easy to obtain for all these sites. Hence, the UK wide simulation was carried out by keeping the soil conditions similar but varying the weather data according to the CMIP5 projections. Like the Leeds farm, RCP 8.5 was considered for all these sites as well.

The plant nutrient uptake, ions concentration, pH, and biomass changes have been analysed in the previous sections under both the scenarios. Since the soil and vegetation conditions are kept constant for all the sites, so these variables do not show any substantial variations.

The prime objective of the enhanced weathering is to absorb the anthropogenic carbons from the atmosphere. The CO_2 absorption is directly linked with the Dissolved Inorganic Carbons (DIC) absorbed during the weathering process. The correct calculation of CO_2 sequestration, throughout the UK can only be achieved by taking into account the net DIC absorbed by all the grid cells. In the following subsections, the detailed steps for calculating the absorptions of atmospheric carbon, occurred because of accelerated weathering will be discussed.

9.7.1 CO_2 calculation steps

CO_2 absorbed for a particular site is calculated through the DIC content in the pore water. In this study, only HCO_3^- was considered as DIC. The CO_2 calculation was carried using the following algorithm:

1. Concentration of HCO_3^- at the end of a time-step is given in mol/litre. Using the water content (in litre), the concentration was converted into number of moles of HCO_3^-.

2. The above steps were performed for both the baseline condition as well as enhanced weathering scenario.

3. At the end of the model simulation, total number of moles of HCO_3^- collected in baseline as well as enhanced weathering scenarios were calculated.

4. Number of moles of HCO_3^- collected in baseline was subtracted from the number of moles of HCO_3^- collected in enhanced weathering scenario. This took into account the carbon absorbed naturally such as due to rainfall. The interest was in calculating the CO_2 absorbed due to enhanced weathering only.

5. Number of moles of absorbed CO_2 was calculated from the number of moles of HCO_3^-, using the stoichiometry from [125] .

6. Number of moles of CO_2 was converted into mass unit such as gram or kilogram.

7. Arable land area in each grid cell was calculated using the crop fractions.

8. CO_2 absorbed per metre square was multiplied by the arable land area for each grid. This gave the total amount of CO_2 sequestrated in each cell.

9. Finally the amount of CO_2 absorbed in each grid was added to obtain the net CO_2 absorbed across the UK.

The results obtained by following the above steps are shown in the Table 9.4. The amount of CO_2 sequestrated by the Leeds region (Site 66) by 2060 is 6.92 kg per metre square, which increases to 26.28 kg per metre square by the century end. The CO_2 absorption shows an exponential nature (figure 9.16). The above calculation is based entirely on the stoichiometric properties shown by the weathering reactions and the available amount of soil pore water. A more detailed analysis by considering the carbon emitted during the mining and crushing of basalt and transportation to the site of application will decrease the net carbon sequestrated. In future works, such studies involving all the logistics can be coupled with the IEWCZM simulation results to get a more accurate picture of the carbon absorption under enhanced weathering.

Site no.	Lat.	Lon.	Crop frac.	$CO_2 m^{-2}$(kg)	Tot. CO_2 (g)
1	54.75	-7.75	0.006	26.54	4.51×10^{11}
2	54.25	-7.75	0.001	26.57	1.21×10^{11}
3	54.75	-7.25	0.005	25.24	3.55×10^{11}
4	54.25	-7.25	0.014	25.27	8.97×10^{11}
5	54.75	-6.75	0.037	26.51	2.45×10^{12}
6	54.25	-6.75	0.017	25.28	1.13×10^{12}
7	55.75	-6.25	0.003	26.55	2.46×10^{11}
8	54.75	-6.25	0.014	25.31	9.22×10^{11}
9	54.25	-6.25	0.028	25.31	1.77×10^{12}
10	50.25	-5.25	0.052	24.78	3.27×10^{12}
11	55.75	-4.75	0.048	26.52	3.20×10^{12}
12	55.25	-4.75	0.056	26.58	3.77×10^{12}
13	51.75	-4.75	0.013	24.27	8.26×10^{11}
14	57.75	-4.25	0.056	24.16	3.44×10^{12}
15	56.25	-4.25	0.046	25.27	2.93×10^{12}
16	55.75	-4.25	0.060	25.28	3.82×10^{12}
17	55.25	-4.25	0.016	24.77	1.04×10^{12}

18	53.25	-4.25	0.013	24.10	7.88×10^{11}
19	51.75	-4.25	0.022	24.27	1.33×10^{12}
20	50.75	-4.25	0.043	24.14	2.60×10^{12}
21	55.75	-3.75	0.082	24.78	5.10×10^{12}
22	55.25	-3.75	0.069	26.58	4.60×10^{12}
23	53.25	-3.75	0.0002	24.03	1.67×10^{10}
24	52.75	-3.75	0.012	25.27	8.17×10^{11}
25	52.25	-3.75	0.002	24.75	1.82×10^{11}
26	51.75	-3.75	0.005	24.79	3.37×10^{11}
27	50.75	-3.75	0.056	24.15	3.42×10^{12}
28	56.75	-3.25	0.034	25.28	2.19×10^{12}
29	56.25	-3.25	0.076	24.12	4.62×10^{12}
30	55.75	-3.25	0.037	24.26	2.24×10^{12}
31	55.25	-3.25	0.020	24.77	1.29×10^{12}
32	54.75	-3.25	0.027	24.16	1.64×10^{12}
33	53.25	-3.25	0.006	24.05	3.86×10^{11}
34	52.75	-3.25	0.021	24.80	1.36×10^{12}
35	52.25	-3.25	0.011	24.74	7.17×10^{11}
36	51.75	-3.25	0.035	24.77	2.19×10^{12}
37	50.75	-3.25	0.039	24.14	2.39×10^{12}
38	57.25	-2.75	0.054	24.07	3.29×10^{12}
39	56.75	-2.75	0.166	24.07	1.00×10^{13}
40	55.75	-2.75	0.088	24.16	5.35×10^{12}
41	55.25	-2.75	0.010	24.77	6.36×10^{11}
42	54.75	-2.75	0.036	24.81	2.27×10^{12}
43	54.25	-2.75	0.031	24.09	1.87×10^{12}
44	53.75	-2.75	0.037	24.09	2.28×10^{12}
45	53.25	-2.75	0.037	24.06	2.26×10^{12}
46	52.75	-2.75	0.079	24.06	4.76×10^{12}
47	52.25	-2.75	0.098	24.06	5.89×10^{12}
48	51.75	-2.75	0.018	24.14	1.14×10^{12}
49	51.25	-2.75	0.045	24.10	2.71×10^{12}
50	50.75	-2.75	0.045	24.15	2.76×10^{12}
51	57.25	-2.25	0.020	24.04	1.21×10^{12}
52	55.75	-2.25	0.181	24.09	1.09×10^{13}
53	55.25	-2.25	0.017	24.05	1.03×10^{11}
54	54.75	-2.25	0.004	24.10	2.88×10^{11}
55	54.25	-2.25	0.002	24.26	1.75×10^{11}

56	53.75	-2.25	0.037	24.14	2.26×10^{12}
57	53.25	-2.25	0.020	24.30	1.25×10^{12}
58	52.75	-2.25	0.121	24.04	7.29×10^{12}
59	52.25	-2.25	0.062	24.05	3.73×10^{12}
60	51.75	-2.25	0.081	24.09	4.91×10^{12}
61	51.25	-2.25	0.086	24.17	5.25×10^{12}
62	50.75	-2.25	0.059	24.16	3.59×10^{12}
63	55.25	-1.75	0.122	24.05	7.38×10^{12}
64	54.75	-1.75	0.069	24.02	4.19×10^{12}
65	54.25	-1.75	0.052	24.76	3.27×10^{12}
66	53.75	-1.75	0.073	26.28	4.79×10^{12}
67	53.25	-1.75	0.058	24.15	3.55×10^{12}
68	52.75	-1.75	0.165	24.05	9.96×10^{12}
69	52.25	-1.75	0.149	24.04	8.98×10^{12}
70	51.75	-1.75	0.150	24.09	9.06×10^{12}
71	51.25	-1.75	0.090	24.13	5.44×10^{12}
72	60.25	-1.25	0.007	24.14	4.42×10^{11}
73	54.25	-1.25	0.145	24.05	8.72×10^{12}
74	53.75	-1.25	0.136	25.27	8.62×10^{12}
75	53.25	-1.25	0.083	24.03	5.03×10^{12}
76	52.75	-1.25	0.111	24.05	6.73×10^{12}
77	52.25	-1.25	0.159	24.03	9.60×10^{12}
78	51.75	-1.25	0.122	24.13	7.39×10^{12}
79	51.25	-1.25	0.140	24.12	8.47×10^{12}
80	50.75	-1.25	0.062	24.08	3.75×10^{12}
81	54.25	-0.75	0.170	24.06	1.02×10^{13}
82	53.75	-0.75	0.121	24.05	7.29×10^{12}
83	53.25	-0.75	0.188	24.08	1.13×10^{13}
84	52.75	-0.75	0.145	24.02	8.71×10^{12}
85	52.25	-0.75	0.167	24.05	1.00×10^{13}
86	51.75	-0.75	0.031	24.02	1.88×10^{12}
87	51.25	-0.75	0.015	24.16	9.36×10^{11}
88	53.75	-0.25	0.093	24.06	5.60×10^{12}
89	53.25	-0.25	0.176	24.04	1.06×10^{13}
90	52.75	-0.25	0.185	24.05	1.11×10^{13}
91	52.25	-0.25	0.167	24.04	1.00×10^{13}
92	51.75	-0.25	0.008	24.05	5.12×10^{11}
93	51.25	-0.25	0.009	24.04	5.62×10^{11}

94	53.25	0.25	0.139	24.05	8.39×10^{12}
95	52.75	0.25	0.215	24.05	1.29×10^{13}
96	52.25	0.25	0.194	24.07	1.71×10^{13}
97	51.75	0.25	0.022	24.04	1.37×10^{12}
98	51.25	0.25	0.016	24.10	1.01×10^{12}
99	52.75	0.75	0.239	24.04	1.44×10^{13}
100	52.25	0.75	0.230	24.09	1.38×10^{13}
101	51.25	0.75	0.041	24.08	2.49×10^{12}
102	52.75	1.25	0.187	24.08	1.12×10^{13}
103	52.25	1.25	0.230	24.06	1.38×10^{13}
104	51.25	1.25	0.052	24.06	3.18×10^{12}

Table 9.4: CO_2 absorbed across the UK sites. Crop fraction denotes the fraction of arable land in a grid cell. CO_2 per metre square is calculated by the IEWCZM for each grid cell. Total CO_2 for each grid cell is calculated using the total land area in a cell, crop fraction and CO_2 per metre square.

The above calculation is performed under the Scenario 2, where basalt is added at the rate of $5kg/m^2$ on yearly basis. Using the information from the Table 9.4, the net sequestrated CO_2 across the entire UK by the century end is 4.55×10^{14} gram. The CO_2 absorption data from the Table 9.4 is shown in a choropleth map (figure 9.17) for a clearer visualisation. In future work, the figure 9.17 can be compared with the climate inputs of all the points on the choropleth map. A correlation between the weathering rate and variables like temperature and precipitation can guide the selection of sites for an efficient enhanced weathering process.

9.8 Conclusion

Enhanced weathering, a geo-engineering technique for the sequestration of anthropogenic carbon dioxide from the atmosphere was analysed in this study. The IPCC report suggests that the objectives of the COP 21 (Paris Agreement) cannot be achieved merely by cutting down the emission. There is a strong need to implement an NET in parallel. Among few other options, enhanced weathering as an NET offers some extra advantages like reducing the soil acidity and increasing the soil fertility in addition to capturing the atmospheric carbon. Until now, these theoretical possibilities surrounding the enhanced weathering have not been verified thoroughly. This study performs the simulation analysis of the enhanced weathering in the UK climatic condition.

The entire simulation study was performed in two phases. In the first phase,

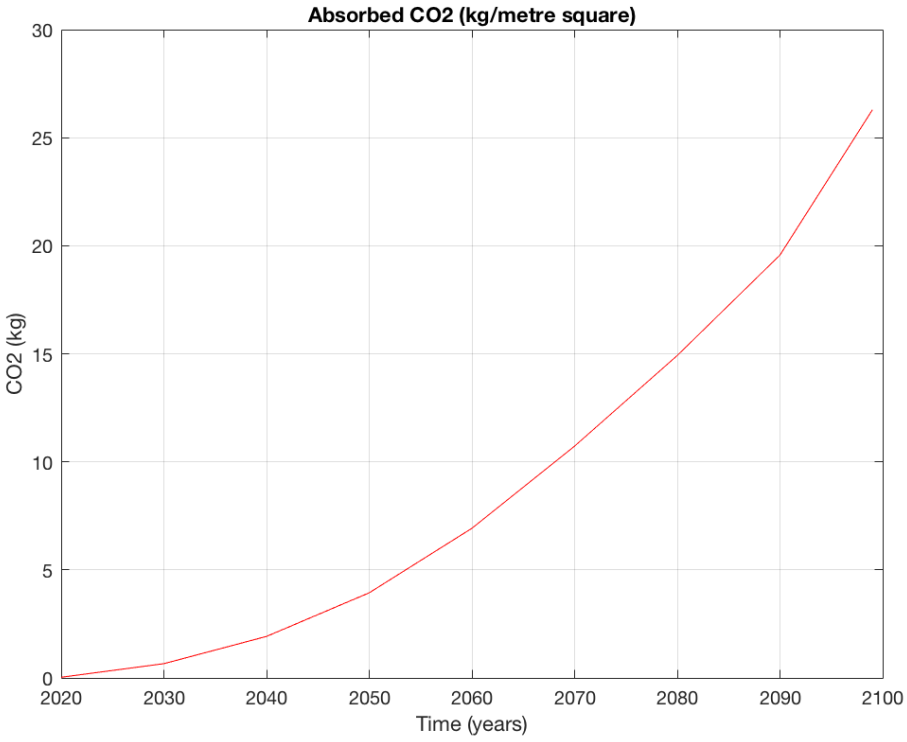

Figure 9.16: CO_2 absorbed (Leeds region).

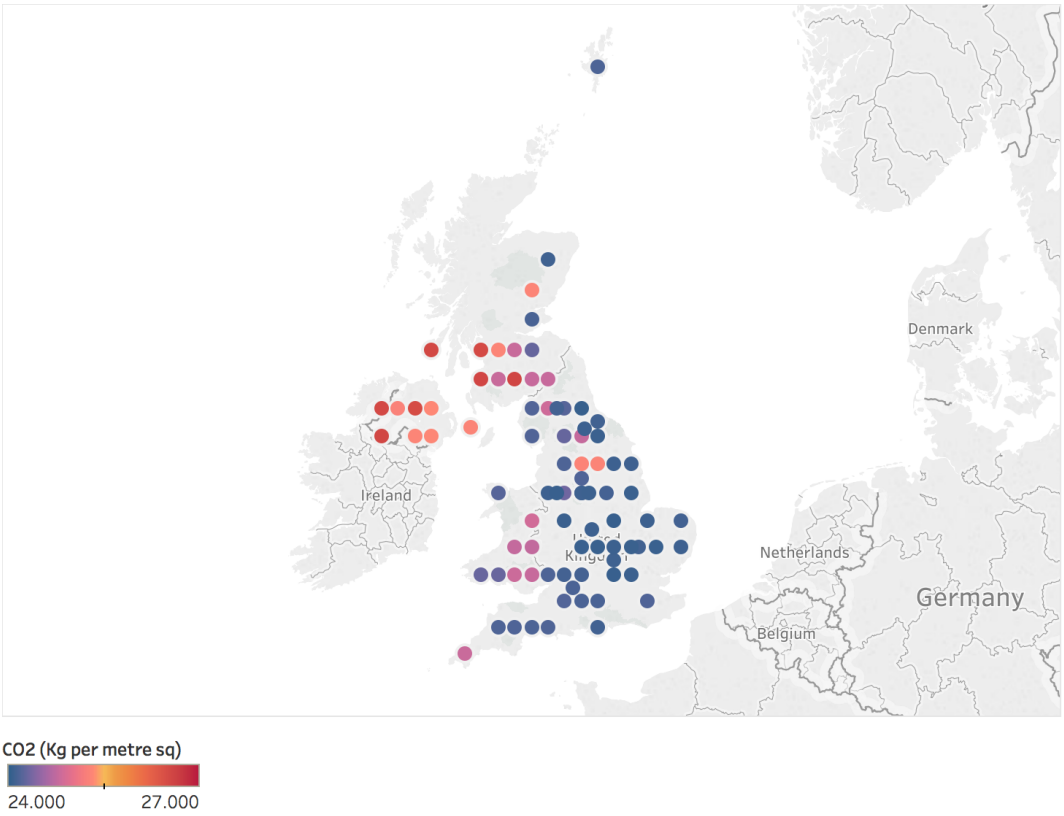

Figure 9.17: CO_2 absorbed across the UK.

Leeds farm conditions were employed for evaluating the two scenarios of the enhanced weathering and comparing them with the baseline conditions. First scenario incorporated the addition of basalt only once at the rate of $5kg/m^2$ whereas, in the second scenario basalt application was carried out on yearly basis at the same rate. In the second phase, the Scenario 2 was extended to the entire UK regions for calculating the net CO_2 absorbed till the century-end.

The weathering of silicate rock is heavily influenced by the weather inputs especially precipitation. Most of the UK regions receive a good amount of precipitation. Therefore, this country appears to be a plausible option for the implementation of enhanced weathering. High temperature is another key factor for the fast weathering. The UK cannot match with the temperature range of the tropical regions but the RCP 8.5 projection shows that the climate change would push the average temperature of this country on a bit higher side. This could escalate the weathering process at least till the mid of century. So, it turns out to be an interesting area for further research.

The simulation results strongly suggests that, the enhanced weathering as an NET, has a potential to curb the atmospheric carbon and bring down the global

temperature substantially. In parallel, it can also enhance the soil-fertility and wheat production to some extent. The inorganic fertilisers are currently employed during the production of all major crops. The simulation in this chapter shows that, silicate rock addition do not interfere with the positive effects of fertilisers. In fact, a slight increase in crop yield suggests that basalt powder can be applied in parallel to fertilisers. So the question is, can we eliminate the use of NPK fertilisers completely by replacing with basalt powder? The answer is 'No', because basalt does not contain the minerals rich in nitrogen and phosphorus. Among NPK only potassium is available in basalt and that too in very small quantity.

The soil acidity reduces substantially due to weathering and in principle it should improve the overall nutrient uptake. However, this effect was not apparent in this simulation study, mainly because of some limitations of the model. The effects of trace elements like deposition of nickel as a byproduct of prolonged weathering was also not covered under this research.

This study is a simulation analysis of the theoretical hypotheses surrounding the enhanced weathering and is based on some reasonable assumptions. The actual implementation of the enhanced weathering at the farm level would require a lot more rigorous simulations and field experiments. In addition to the scientific and technological challenges, engaging with other stake holders such as farmers and policy makers would also be essential for the implementation of this NET.

Chapter 10

Conclusion

10.1 Concluding remarks

This thesis demonstrates the potential of interdisciplinary research methods in analysing the systems related to environmental and food sustainability. In addition to the contributions in form of weathering and wetland systems modelling, an investigation towards the theoretical advancement in System Identification (SID) method also forms the part of this thesis.

The concluding remarks of this project are summarised here:

1. A novel algorithm (ABC-NARX-MSS) for the model structure selection in nonlinear system identification was developed. The ABC-NARX-MSS is placed under the probabilistic framework and Approximate Bayesian Computation (ABC) is at the heart of this method. It carries out the global search in the regressor space and returns an optimal solution. The ABC-NARX-MSS is tested on an example system and correctly recovers all the 'true' terms in a fairly noisy condition.

2. The identification of an unknown system has always been a challenging job and any new method in SID should ideally pass through this challenge. Therefore, a full cycle of the SID was performed on a Canadian wetland using the ABC-NARX-MSS for model selection and the Sequential Monte Carlo (SMC) version of the ABC for parameter estimation. The simulation results suggest that all the relevant terms were correctly picked up by the newly developed algorithm. The ABC-NARX-MSS is computationally more efficient than the other competing methods under probabilistic framework. It is easy to extend for incorporating more model classes, at the same time it is also very simple to implement on any platform.

3. A compact nonlinear model of the tropical wetlands containing just the six terms was devised in this project. The application of nonlinear SID in wetland modelling as well as obtaining a parsimonious model structure explaining the wetland dynamics of the tropics are novel additions in the wider domain of environmental systems. The parameter set of all the available sites were estimated using the ABC-SMC technique and the estimation process is relatively straightforward and transparent as compared to the Compound Topographic Index (CTI) parameters of the TOPMODEL based models.

4. In reality, the dynamics of a wetland depends upon lot many environmental variables as well as topography of the site. The obtained tropical wetland model is based upon a Single Input Single Output (SISO) system, where the input is average temperature. The temperature of all the tropical sites are nearly in similar range and this feature also reflects from the parameter mapping, where the parameters of input based terms do not exhibit much variations. On the other hand, parameters corresponding to the lagged outputs terms diverge the most, signifying the topographical variations.

5. A calibrated Enhanced Weathering (EW) model using an analytical method was obtained. The weathering rate constants in most of the theoretical evaluations are based on laboratory results. Recently, it has been shown that weathering is relatively slower in field conditions hence the rate constants following the laboratory experiments are not accurate. The calibration part in this modelling takes this factor into account. Another novelty comes from the integration of the weathering model with the other process models of the Earth's Critical Zone (ECZ) leading to the development of the IEWCZM. The integrated model shows the positive effects of EW on the biomass production in Koiliaris, a Critical Zone Observatory (CZO) in Greece.

6. The potential of EW in sequestering the anthropogenic carbon and increasing the wheat yield across the entire UK is simulated using the IEWCZM. The EW process, when the crushed basalt powder is applied at the rate of 5 $kgm^{-2}yr^{-1}$, can absorb approximately 0.455 Pg of carbon until the century end with some reasonable improvement in the wheat yield as well. The EW as a Negative Emission Technology (NET) clearly demonstrates the potential of addressing the climate change mitigation and food security in parallel. However, the actual implementation of the EW depends upon a more rigorous research where all the facets of this NET on the ecosystem could be analysed.

10.2 Future works

1. The ABC-NARX-MSS in thesis searches the regressor space where the maximum lags for input-output were constrained to two. The algorithm demonstrates a good computational efficiency with the limited lag values. However, for generalising the ABC-NARX-MSS and establishing this algorithm over the other competing methods under probabilistic framework, it needs to be tested on larger lag values. The algorithm is expected to converge even with high amount of maximum lags but the computational requirements will be the key factor to observe.

2. The dynamics of wetlands vary with climatic zones. That means, wetlands in boreal and temperate climate zones exhibit different dynamics than a tropical wetland. The wetland model developed in this thesis accounts for tropical regions. The similar approach can be extended to devise the models explaining the dynamics of other climate zones. In this way, a global wetland model could come into existence and the same could be coupled with the existing climate models for a more accurate calculations of the biogeochemical cycles and the effects of climate change.

3. The current sites in the available dataset are separated by 0.5 degree $\times$ 0.5 degree geographically. The climate models often operate at a finer resolution, so a mechanism for interpolating the parameters between the sites could be formulated. A Global Inundation Extent from Multi-Satellites (GIEMS) dataset provides the dynamic variations in the wetland fraction but at the cost of precision. A precise parameterisation of the model can overcome this shortcoming of remote sensing technique in studying wetland dynamics.

4. The climate change effects are categorised into different scenarios, Representative Concentration Pathways (RCP), by the Intergovernmental Panel on Climate Change (IPCC), such as RCP 8.5, RCP 6.0, RCP 4.5, and RCP 2.6. The developed wetland model can be simulated for all the scenarios to assess the impact of climate change on wetland extents.

5. The enhanced weathering (EW) model developed in this thesis considers all the minerals in a rock to be a uniform sphere for the sake of simplicity. In reality, mineral do exhibit variations in their shape and that could have significant effects on weathering rate as well. Hence, the same algorithm can be extended to incorporate the detailed mineralogical information. The IEWCZM model works at the soil profile scale because the original ICZM is basically a profile scale model. Therefore, the simulations performed using

the IEWCZM assumes the uniform soil profile. In reality a catchment can have numerous types of soil profile and thus a catchment scale model will be more accurate in simulating the effects of EW on a farmland.

6. In this thesis, EW simulation in the UK condition has been presented. The method appears to be a promising way for addressing the climate change mitigation and food security simultaneously. However, only single crop in the form of winter wheat is considered in this simulation analysis. Other major crops of the UK such as sugar beet and barley can be simulated to present a more realistic picture. This simulation study assumes that the soil characteristics of the entire UK are same and only the climatic inputs are varied. For a more accurate analysis, the IEWCZM can be parameterised with the site specific soil details.

7. The entire modelling studies of this thesis, which include the wetland dynamics and EW can be glued together at some level of abstraction under the systems engineering framework. A code level integration of different models often constrain the addition/removal of modules. Being parts of the Earth's Critical Zone, both the wetland and weathering dynamics depend upon many common variables such as evapotranspiration and temperature. So a unification mechanism of these dynamics at some acceptable level of abstraction could be very useful for the domain experts.

The innovations in the field of data inference particularly devising methods where the modern computational facilities are fully utilised will serve many goals of the UN SDGs. This also requires the ease of data availability by international organisations for the research and innovation purposes.

Bibliography

[1] G. Pison. The population of the world (2013). *Population & Societies*, (503):1, 2013.

[2] H.C.J. Godfray, J.R. Beddington, I.R. Crute, L. Haddad, D. Lawrence, J.F. Muir, J. Pretty, S. Robinson, S.M. Thomas, and C. Toulmin. Food security: the challenge of feeding 9 billion people. *Science*, page 1185383, 2010.

[3] X. Leflaive. Water Outlook to 2050: The OECD calls for early and strategic action. In *Global Water Forum*, 2012.

[4] V. Marchal, R. Dellink, D. van Vuuren, C. Clapp, J. Château, E. Lanzi, B. Magné, and J. van Vliet. OECD environmental outlook to 2050: The consequences of inaction. 2012.

[5] S. Bringezu, H. Schütz, W. Pengue, M. O'Brien, F. Garcia, R. Sims, R.W. Howarth, L. Kauppi, M. Swilling, and J. Herrick. Assessing global land use: balancing consumption with sustainable supply. 2014.

[6] R.K. Pachauri, M.R. Allen, V.R. Barros, J. Broome, W. Cramer, R. Christ, J.A. Church, L. Clarke, Q. Dahe, P. Dasgupta, et al. *Climate change 2014: synthesis report. Contribution of Working Groups I, II and III to the fifth assessment report of the Intergovernmental Panel on Climate Change*. IPCC, 2014.

[7] M. Menon, S. Rousseva, N.P. Nikolaidis, P. van Gaans, P. Panagos, D.M. de Souza, K.V. Ragnarsdottir, G.J. Lair, L. Weng, J. Bloem, et al. SoilTrEC: a global initiative on critical zone research and integration. *Environmental Science and Pollution Research*, 21(4):3191–3195, 2014.

[8] S. Banwart, M. Menon, S.M. Bernasconi, J. Bloem, W.E. Blum, D.M. de Souza, B. Davidsdotir, C. Duffy, G.J. Lair, P. Kram, et al. Soil processes and functions across an international network of Critical Zone Observatories: Introduction to experimental methods and initial results. *Comptes Rendus Geoscience*, 344 (11-12):758–772, 2012.

[9] W. Bank. *The World Bank Annual Report 2017*. The World Bank, 2017.

[10] P. Smith, S.J. Davis, F. Creutzig, S. Fuss, J. Minx, B. Gabrielle, E. Kato, R.B. Jackson, A. Cowie, E. Kriegler, et al. Biophysical and economic limits to negative CO 2 emissions. *Nature Climate Change*, 6(1):42, 2016.

[11] J. Boardman and B. Sauser. System of Systems-the meaning of of. In *System of Systems Engineering, 2006 IEEE/SMC International Conference on*, pages 6–pp. IEEE, 2006.

[12] J. Simunek, M.T. Van Genuchten, and M. Sejna. The HYDRUS-1D software package for simulating the one-dimensional movement of water, heat, and multiple solutes in variably-saturated media. *University of California-Riverside Research Reports*, 3:1–240, 2005.

[13] F.E. Stamati, N.P. Nikolaidis, S. Banwart, and W.E. Blum. A coupled carbon, aggregation, and structure turnover (CAST) model for topsoils. *Geoderma*, 211:51–64, 2013.

[14] G. Giannakis, N. Nikolaidis, J. Valstar, E. Rowe, K. Moirogiorgou, M. Kotronakis, N. Paranychianakis, S. Rousseva, F. Stamati, and S. Banwart. Integrated critical zone model (1D-ICZ): a tool for dynamic simulation of soil functions and soil structure. In *Advances in Agronomy*, volume 142, pages 277–314. Elsevier, 2017.

[15] P. Renforth, P.P. von Strandmann, and G. Henderson. The dissolution of olivine added to soil: Implications for enhanced weathering. *Applied Geochemistry*, 61:109–118, 2015.

[16] L. Ljung. *System identification: theory for the user*. Prentice-Hall, 1987.

[17] T. Söderström and P. Stoica. System identification. 1989.

[18] S.A. Billings. *Nonlinear system identification: NARMAX methods in the time, frequency, and spatio-temporal domains*. John Wiley & Sons, 2013.

[19] S. Chen and S.A. Billings. Representations of non-linear systems: the NARMAX model. *International Journal of Control*, 49(3):1013–1032, 1989.

[20] S. Billings and W. Voon. Piecewise linear identification of non-linear systems. *International Journal of Control*, 46(1):215–235, 1987.

[21] S. Billings. Identification of nonlinear systems–a survey. In *IEE Proceedings D (Control Theory and Applications)*, volume 127, pages 272–285. IET, 1980.

[22] S.A. Billings and S. Fakhouri. Identification of systems containing linear dynamic and static nonlinear elements. *Automatica (Journal of IFAC)*, 18(1): 15–26, 1982.

[23] G. Palm. On representation and approximation of nonlinear systems. *Biological Cybernetics*, 34(1):49–52, 1979.

[24] T. Baldacchino, S.R. Anderson, and V. Kadirkamanathan. Structure detection and parameter estimation for NARX models in a unified EM framework. *Automatica*, 48(5):857–865, 2012.

[25] H. Akaike. A new look at the statistical model identification. *IEEE transactions on automatic control*, 19(6):716–723, 1974.

[26] G. Schwarz et al. Estimating the dimension of a model. *The annals of statistics*, 6(2):461–464, 1978.

[27] A.A. Neath and J.E. Cavanaugh. The bayesian information criterion: background, derivation, and applications. *Wiley Interdisciplinary Reviews: Computational Statistics*, 4(2):199–203, 2012.

[28] N.M. Mangan, J.N. Kutz, S.L. Brunton, and J.L. Proctor. Model selection for dynamical systems via sparse regression and information criteria. *Proc. R. Soc. A*, 473(2204):20170009, 2017.

[29] S.L. Brunton, J.L. Proctor, and J.N. Kutz. Discovering governing equations from data by sparse identification of nonlinear dynamical systems. *Proceedings of the National Academy of Sciences*, page 201517384, 2016.

[30] M. KORENBERG, S. Billings, Y. Liu, and P. McIlroy. Orthogonal parameter estimation algorithm for non-linear stochastic systems. *International Journal of Control*, 48(1):193–210, 1988.

[31] M. Farina and L. Piroddi. Identification of polynomial input/output recursive models with simulation error minimisation methods. *International Journal of Systems Science*, 43(2):319–333, 2012.

[32] Y. Guo, L. Guo, S.A. Billings, and H.L. Wei. An iterative orthogonal forward regression algorithm. *International Journal of Systems Science*, 46(5):776–789, 2015.

[33] T. Toni, D. Welch, N. Strelkowa, A. Ipsen, and M.P. Stumpf. Approximate Bayesian computation scheme for parameter inference and model selection

in dynamical systems. *Journal of the Royal Society Interface*, 6(31):187–202, 2009.

[34] A. Gelman, J.B. Carlin, H.S. Stern, and D.B. Rubin. *Bayesian data analysis*. Chapman and Hall/CRC, 1995.

[35] K. Krishnanathan, S.R. Anderson, S.A. Billings, and V. Kadirkamanathan. Computational system identification of continuous-time nonlinear systems using approximate Bayesian computation. *International Journal of Systems Science*, 47(15):3537–3544, 2016.

[36] T. Baldacchino, S.R. Anderson, and V. Kadirkamanathan. Computational system identification for bayesian NARMAX modelling. *Automatica*, 49(9): 2641–2651, 2013.

[37] A. Falsone, L. Piroddi, and M. Prandini. A randomized algorithm for nonlinear model structure selection. *Automatica*, 60:227–238, 2015.

[38] G.D. Reeves, S.K. Morley, R.H. Friedel, M.G. Henderson, T.E. Cayton, G. Cunningham, J.B. Blake, R.A. Christensen, and D. Thomsen. On the relationship between relativistic electron flux and solar wind velocity: Paulikas and blake revisited. *Journal of Geophysical Research: Space Physics*, 116(A2), 2011.

[39] M.A. Balikhin, R.J. Boynton, S.N. Walker, J.E. Borovsky, S.A. Billings, and H.L. Wei. Using the NARMAX approach to model the evolution of energetic electrons fluxes at geostationary orbit. *Geophysical Research Letters*, 38(18), 2011.

[40] R. Boynton, M. Balikhin, S. Billings, G. Reeves, N. Ganushkina, M. Gedalin, O. Amariutei, J. Borovsky, and S. Walker. The analysis of electron fluxes at geosynchronous orbit employing a NARMAX approach. *Journal of Geophysical Research: Space Physics*, 118(4):1500–1513, 2013.

[41] G.R. Bigg, H.L. Wei, D.J. Wilton, Y. Zhao, S.A. Billings, E. Hanna, and V. Kadirkamanathan. A century of variation in the dependence of Greenland iceberg calving on ice sheet surface mass balance and regional climate change. *Proc. R. Soc. A*, 470(2166):20130662, 2014.

[42] K. Krishnanathan, S.R. Anderson, S.A. Billings, and V. Kadirkamanathan. A data-driven framework for identifying nonlinear dynamic models of genetic parts. *ACS Synthetic Biology*, 1(8):375–384, 2012.

[43] J. Vieira, J. Føns, and G. Cecconi. Statistical and hydrodynamic models for the operational forecasting of floods in the Venice Lagoon. *Coastal Engineering*, 21(4):301–331, 1993.

[44] H. Wei and S. Billings. An efficient nonlinear cardinal b-spline model for high tide forecasts at the Venice Lagoon. *Nonlinear Processes in Geophysics*, 13(5):577–584, 2006.

[45] H. Wei, S. Billings, and M. Balikhin. Analysis of the geomagnetic activity of the D(st) index and self-affine fractals using wavelet transforms. *Nonlinear Processes in Geophysics*, 11(3):303–312, 2004.

[46] H.L. Wei, S.A. Billings, and M. Balikhin. Prediction of the Dst index using multiresolution wavelet models. *Journal of Geophysical Research: Space Physics*, 109(A7), 2004.

[47] H. Wei and S. Billings. Long term prediction of non-linear time series using multiresolution wavelet models. *International Journal of Control*, 79(06):569–580, 2006.

[48] F. Heiss and V. Winschel. Likelihood approximation by numerical integration on sparse grids. *Journal of Econometrics*, 144(1):62–80, 2008.

[49] J.K. Pritchard, M.T. Seielstad, A. Perez-Lezaun, and M.W. Feldman. Population growth of human Y chromosomes: a study of Y chromosome microsatellites. *Molecular Biology and Evolution*, 16(12):1791–1798, 1999.

[50] M.A. Beaumont, W. Zhang, and D.J. Balding. Approximate Bayesian computation in population genetics. *Genetics*, 162(4):2025–2035, 2002.

[51] S.A. Sisson, Y. Fan, and M.M. Tanaka. Sequential Monte Carlo without likelihoods. *Proceedings of the National Academy of Sciences*, 104(6):1760–1765, 2007.

[52] M.A. Beaumont. Approximate Bayesian computation in evolution and ecology. *Annual Review of Ecology, Evolution, and Systematics*, 41:379–406, 2010.

[53] P. Marjoram, J. Molitor, V. Plagnol, and S. Tavaré. Markov chain Monte Carlo without likelihoods. *Proceedings of the National Academy of Sciences*, 100(26): 15324–15328, 2003.

[54] A. Doucet, N. De Freitas, and N. Gordon. An introduction to sequential Monte Carlo methods. In *Sequential Monte Carlo methods in practice*, pages 3–14. Springer, 2001.

[55] P. Del Moral, A. Doucet, and A. Jasra. Sequential Monte Carlo samplers. *Journal of the Royal Statistical Society: Series B (Statistical Methodology)*, 68(3): 411–436, 2006.

[56] J. Liepe, C. Barnes, E. Cule, K. Erguler, P. Kirk, T. Toni, and M.P. Stumpf. ABC-SysBio-approximate Bayesian computation in Python with GPU support. *Bioinformatics*, 26(14):1797–1799, 2010.

[57] M.G. Blum and O. François. Non-linear regression models for Approximate Bayesian Computation. *Statistics and Computing*, 20(1):63–73, 2010.

[58] J. Li, D.J. Nott, Y. Fan, and S.A. Sisson. Extending approximate Bayesian computation methods to high dimensions via a Gaussian copula model. *Computational Statistics & Data Analysis*, 106:77–89, 2017.

[59] M.G. Blum, M.A. Nunes, D. Prangle, S.A. Sisson, et al. A comparative review of dimension reduction methods in approximate Bayesian computation. *Statistical Science*, 28(2):189–208, 2013.

[60] M. Creel and D. Kristensen. On selection of statistics for approximate Bayesian computing (or the method of simulated moments). *Computational Statistics & Data Analysis*, 100:99–114, 2016.

[61] E. Ruli, N. Sartori, and L. Ventura. Approximate Bayesian computation with composite score functions. *Statistics and Computing*, 26(3):679–692, 2016.

[62] P. Fearnhead and D. Prangle. Constructing summary statistics for approximate Bayesian computation: semi-automatic approximate Bayesian computation. *Journal of the Royal Statistical Society: Series B (Statistical Methodology)*, 74(3):419–474, 2012.

[63] J. Mitrovic, D. Sejdinovic, and Y.W. Teh. DR-ABC: Approximate Bayesian Computation with kernel-based distribution regression. *International Conference on Machine Learning*, 2016.

[64] J.U. Harrison and R.E. Baker. An automatic adaptive method to combine summary statistics in approximate Bayesian computation. *arXiv preprint arXiv:1703.02341*, 2017.

[65] X.L. Meng. Posterior predictive p-values. *The Annals of Statistics*, pages 1142–1160, 1994.

[66] L. Lemaire, F. Jay, I. Lee, K. Csilléry, M.G. Blum, et al. Goodness-of-fit statistics for approximate Bayesian computation. *arXiv preprint arXiv:1601.04096*, 2016.

[67] D.T. Frazier, G.M. Martin, C.P. Robert, and J. Rousseau. Asymptotic properties of approximate Bayesian computation. *arXiv preprint arXiv:1607.06903*, 2016.

[68] W. Li and P. Fearnhead. On the Asymptotic Efficiency of ABC Estimators. *arXiv preprint arXiv:1506.03481*, 2015.

[69] D. Wegmann, C. Leuenberger, and L. Excoffier. Efficient approximate Bayesian computation coupled with Markov chain Monte Carlo without likelihood. *Genetics*, 182(4):1207–1218, 2009.

[70] M. Chiachio, J.L. Beck, J. Chiachio, and G. Rus. Approximate Bayesian computation by subset simulation. *SIAM Journal on Scientific Computing*, 36(3): A1339–A1358, 2014.

[71] S.K. Au and J.L. Beck. Estimation of small failure probabilities in high dimensions by subset simulation. *Probabilistic Engineering Mechanics*, 16(4): 263–277, 2001.

[72] P. Del Moral, A. Doucet, and A. Jasra. An adaptive sequential Monte Carlo method for approximate Bayesian computation. *Statistics and Computing*, 22 (5):1009–1020, 2012.

[73] C. Leuenberger and D. Wegmann. Bayesian computation and model selection without likelihoods. *Genetics*, 2009.

[74] S. Filippi, C.P. Barnes, J. Cornebise, and M.P. Stumpf. On optimality of kernels for approximate Bayesian computation using sequential Monte Carlo. *Statistical Applications in Genetics and Molecular Biology*, 12(1):87–107, 2013.

[75] T. Guillemaud, M.A. Beaumont, M. Ciosi, J.M. Cornuet, and A. Estoup. Inferring introduction routes of invasive species using approximate Bayesian computation on microsatellite data. *Heredity*, 104(1):88, 2010.

[76] P.D. O?Neill. A tutorial introduction to Bayesian inference for stochastic epidemic models using Markov chain Monte Carlo methods. *Mathematical Biosciences*, 180(1-2):103–114, 2002.

[77] G.D. Brown, A.T. Porter, J.J. Oleson, and J.A. Hinman. Approximate Bayesian computation for spatial SEIR (S) epidemic models. *Spatial and Spatio-temporal Epidemiology*, 24:27–37, 2018.

[78] M. Tanaka, A. Francis, F. Luciani, and S. Sisson. Estimating tuberculosis transmission parameters from genotype data using approximate bayesian computation. *Genetics*, 2006.

[79] P. Haccou, P. Jagers, and V. Vatutin. Branching Processes in Biology: Variation, Growth and Extinction, 2005.

[80] A. Sottoriva and S. Tavaré. Integrating approximate Bayesian computation with complex agent-based models for cancer research. In *Proceedings of COMPSTAT'2010*, pages 57–66. Springer, 2010.

[81] R.J. Ross, R.E. Baker, A. Parker, M. Ford, R. Mort, and C. Yates. Using approximate bayesian computation to quantify cell–cell adhesion parameters in a cell migratory process. *NPJ Systems Biology and Applications*, 3(1):9, 2017.

[82] J. Liepe, P. Kirk, S. Filippi, T. Toni, C.P. Barnes, and M.P. Stumpf. A framework for parameter estimation and model selection from experimental data in systems biology using approximate Bayesian computation. *Nature Protocols*, 9(2):439, 2014.

[83] C. Piou, U. Berger, and V. Grimm. Proposing an information criterion for individual-based models developed in a pattern-oriented modelling framework. *Ecological Modelling*, 220(17):1957–1967, 2009.

[84] A.R. Solow and W.K. Smith. Estimating species number under an inconvenient abundance model. *Journal of Agricultural, Biological, and Environmental Statistics*, 14(2):242–252, 2009.

[85] F. Jabot and J. Chave. Inferring the parameters of the neutral theory of biodiversity using phylogenetic information and implications for tropical forests. *Ecology Letters*, 12(3):239–248, 2009.

[86] O.B. Ericok, A.T. Cemgil, and H. Erturk. Approximate Bayesian computation techniques for optical characterization of nanoparticle clusters. *JOSA A*, 35 (1):88–97, 2018.

[87] F. Technow, C.D. Messina, L.R. Totir, and M. Cooper. Integrating crop growth models with whole genome prediction through approximate Bayesian computation. *PloS one*, 10(6):e0130855, 2015.

[88] X. Rubio-Campillo. Model selection in historical research using approximate Bayesian computation. *PloS one*, 11(1):e0146491, 2016.

[89] E. Jennings and M. Madigan. astroABC: An Approximate Bayesian Computation Sequential Monte Carlo sampler for cosmological parameter estimation. *Astronomy and Computing*, 19:16–22, 2017.

[90] E. Crema, K. Edinborough, T. Kerig, and S. Shennan. An Approximate Bayesian Computation approach for inferring patterns of cultural evolutionary change. *Journal of Archaeological Science*, 50:160–170, 2014.

[91] M. Porčić and M. Nikolić. The approximate Bayesian Computation approach to reconstructing population dynamics and size from settlement data: demography of the mesolithic-neolithic transition at lepenski vir. *Archaeological and Anthropological Sciences*, 8(1):169–186, 2016.

[92] L. Kulakova, P. Angelikopoulos, P.E. Hadjidoukas, C. Papadimitriou, and P. Koumoutsakos. Approximate Bayesian computation for granular and molecular dynamics simulations. In *Proceedings of the Platform for Advanced Scientific Computing Conference*, page 4. ACM, 2016.

[93] X. Hong, R.J. Mitchell, S. Chen, C.J. Harris, K. Li, and G.W. Irwin. Model selection approaches for non-linear system identification: a review. *International Journal of Systems Science*, 39(10):925–946, 2008.

[94] M. Bonin, V. Seghezza, and L. Piroddi. NARX model selection based on simulation error minimisation and LASSO. *IET Control Theory & Applications*, 4(7):1157–1168, 2010.

[95] S. Billings, S. Chen, and M. Korenberg. Identification of MIMO non-linear systems using a forward-regression orthogonal estimator. *International Journal of Control*, 49(6):2157–2189, 1989.

[96] H.L. Wei and S.A. Billings. Model structure selection using an integrated forward orthogonal search algorithm assisted by squared correlation and mutual information. *International Journal of Modelling, Identification and Control*, 3(4):341–356, 2008.

[97] A. Gelman, D.B. Rubin, et al. Inference from iterative simulation using multiple sequences. *Statistical Science*, 7(4):457–472, 1992.

[98] I. Aselmann and P. Crutzen. Global distribution of natural freshwater wetlands and rice paddies, their net primary productivity, seasonality and possible methane emissions. *Journal of Atmospheric Chemistry*, 8(4):307–358, 1989.

[99] M. Cao, S. Marshall, and K. Gregson. Global carbon exchange and methane emissions from natural wetlands: Application of a process-based model. *Journal of Geophysical Research: Atmospheres*, 101(D9):14399–14414, 1996.

[100] S. Hu, Z. Niu, and Y. Chen. Global wetland datasets: a review. *Wetlands*, 37 (5):807–817, 2017.

[101] S. Hagemann and L. Duemenil. Comparison of two global-wetlands data sets. In *Earth Surface Remote Sensing*, volume 3222, pages 193–201. International Society for Optics and Photonics, 1997.

[102] C. Prigent, E. Matthews, F. Aires, and W.B. Rossow. Remote sensing of global wetland dynamics with multiple satellite data sets. *Geophysical Research Letters*, 28(24):4631–4634, 2001.

[103] C. Prigent, F. Papa, F. Aires, W. Rossow, and E. Matthews. Global inundation dynamics inferred from multiple satellite observations, 1993–2000. *Journal of Geophysical Research: Atmospheres*, 112(D12), 2007.

[104] T. Kleinen, V. Brovkin, and R. Schuldt. A dynamic model of wetland extent and peat accumulation: results for the Holocene. *Biogeosciences*, 9(1):235–248, 2012.

[105] K. Beven. Topmodel: a critique. *Hydrological Processes*, 11(9):1069–1085, 1997.

[106] T. Marthews, S. Dadson, B. Lehner, S. Abele, and N. Gedney. High-resolution global topographic index values for use in large-scale hydrological modelling. *Hydrology and Earth System Sciences*, 19(1):91–104, 2015.

[107] Z. Zhang, N.E. Zimmermann, J.O. Kaplan, and B. Poulter. Modeling spatiotemporal dynamics of global wetlands: comprehensive evaluation of a new sub-grid TOPMODEL parameterization and uncertainties. *Biogeosciences*, 13(5):1387–1408, 2016.

[108] T. Stacke and S. Hagemann. Using WEED to simulate the global wetland distribution in a ESM. In *EGU General Assembly Conference Abstracts*, volume 18, page 6231, 2016.

[109] R. Wania, J. Melton, E. Hodson, B. Poulter, B. Ringeval, R. Spahni, T. Bohn, C. Avis, G. Chen, A. Eliseev, et al. Present state of global wetland extent and wetland methane modelling: methodology of a model inter-comparison project (WETCHIMP). *Geoscientific Model Development*, 6(3):617–641, 2013.

[110] J. Melton, R. Wania, E. Hodson, B. Poulter, B. Ringeval, R. Spahni, T. Bohn, C. Avis, D. Beerling, G. Chen, et al. Present state of global wetland extent and wetland methane modelling: conclusions from a model intercomparison project (WETCHIMP). *Biogeosciences*, 10:753–788, 2013.

[111] P. Bergamaschi, C. Frankenberg, J. Meirink, M. Krol, F. Dentener, T. Wagner, U. Platt, J. Kaplan, S. Körner, M. Heimann, et al. Satellite chartography of atmospheric methane from SCIAMACHY on board ENVISAT: 2. evaluation based on inverse model simulations. *Journal of Geophysical Research: Atmospheres*, 112(D2), 2007.

[112] P.C. Young and K.J. Beven. Data-based mechanistic modelling and the rainfall-flow non-linearity. *Environmetrics*, 5(3):335–363, 1994.

[113] P. Young. Data-based mechanistic modelling of environmental, ecological, economic and engineering systems. *Environmental Modelling & Software*, 13 (2):105–122, 1998.

[114] C. Jothityangkoon, M. Sivapalan, and D. Farmer. Process controls of water balance variability in a large semi-arid catchment: downward approach to hydrological model development. *Journal of Hydrology*, 254(1-4):174–198, 2001.

[115] P. Young. Top-down and data-based mechanistic modelling of rainfall–flow dynamics at the catchment scale. *Hydrological processes*, 17(11):2195–2217, 2003.

[116] C.J. Taylor, D.J. Pedregal, P.C. Young, and W. Tych. Environmental time series analysis and forecasting with the captain toolbox. *Environmental Modelling & Software*, 22(6):797–814, 2007.

[117] K.E. Taylor, R.J. Stouffer, and G.A. Meehl. An overview of CMIP5 and the experiment design. *Bulletin of the American Meteorological Society*, 93(4):485–498, 2012.

[118] B. Poulter, P. Bousquet, J.G. Canadell, P. Ciais, A. Peregon, M. Saunois, V.K. Arora, D.J. Beerling, V. Brovkin, C.D. Jones, et al. Global wetland contribution to 2000–2012 atmospheric methane growth rate dynamics. *Environmental Research Letters*, 12(9):094013, 2017.

[119] A. Anupam, D.J. Wilton, S.R. Anderson, and V. Kadirkamanathan. A data-driven framework for identifying tropical wetland model. In *2018 UKACC*

12th International Conference on Control (CONTROL), pages 242–247. IEEE, 2018.

[120] J. Hartmann, N. Jansen, H.H. Dürr, S. Kempe, and P. Köhler. Global CO2-consumption by chemical weathering: What is the contribution of highly active weathering regions? *Global and Planetary Change*, 69(4):185–194, 2009.

[121] C. Rosenzweig, J. Elliott, D. Deryng, A.C. Ruane, C. Müller, A. Arneth, K.J. Boote, C. Folberth, M. Glotter, N. Khabarov, et al. Assessing agricultural risks of climate change in the 21st century in a global gridded crop model intercomparison. *Proceedings of the National Academy of Sciences*, 111(9):3268–3273, 2014.

[122] R. Amundson, A.A. Berhe, J.W. Hopmans, C. Olson, A.E. Sztein, and D.L. Sparks. Soil and human security in the 21st century. *Science*, 348(6235): 1261071, 2015.

[123] D.J. Beerling. Enhanced rock weathering: biological climate change mitigation with co-benefits for food security? *Biology Letters*, 2017.

[124] D.J. Beerling, J.R. Leake, S.P. Long, J.D. Scholes, J. Ton, P.N. Nelson, M. Bird, E. Kantzas, L.L. Taylor, B. Sarkar, et al. Farming with crops and rocks to address global climate, food and soil security. *Nature Plants*, page 1, 2018.

[125] J. Hartmann, A.J. West, P. Renforth, P. Köhler, L. Christina, D.A. Wolf-Gladrow, H.H. Dürr, and J. Scheffran. Enhanced chemical weathering as a geoengineering strategy to reduce atmospheric carbon dioxide, supply nutrients, and mitigate ocean acidification. *Reviews of Geophysics*, 51(2):113–149, 2013.

[126] J. Rogelj, M. Den Elzen, N. Höhne, T. Fransen, H. Fekete, H. Winkler, R. Schaeffer, F. Sha, K. Riahi, and M. Meinshausen. Paris Agreement climate proposals need a boost to keep warming well below 2 C. *Nature*, 534 (7609):631, 2016.

[127] T. Gasser, C. Guivarch, K. Tachiiri, C. Jones, and P. Ciais. Negative emissions physically needed to keep global warming below 2 C. *Nature Communications*, 6:7958, 2015.

[128] J. Rockström, O. Gaffney, J. Rogelj, M. Meinshausen, N. Nakicenovic, and H.J. Schellnhuber. A roadmap for rapid decarbonization. *Science*, 355(6331): 1269–1271, 2017.

[129] R. Schuiling and P. Krijgsman. Enhanced weathering: an effective and cheap tool to sequester CO 2. *Climatic Change*, 74(1-3):349–354, 2006.

[130] T.O. West and A.C. McBride. The contribution of agricultural lime to carbon dioxide emissions in the United States: dissolution, transport, and net emissions. *Agriculture, Ecosystems & Environment*, 108(2):145–154, 2005.

[131] L.L. Taylor, J. Quirk, R.M. Thorley, P.A. Kharecha, J. Hansen, A. Ridgwell, M.R. Lomas, S.A. Banwart, and D.J. Beerling. Enhanced weathering strategies for stabilizing climate and averting ocean acidification. *Nature Climate Change*, 6(4):402, 2016.

[132] P. Renforth. The potential of enhanced weathering in the UK. *International Journal of Greenhouse Gas Control*, 10:229–243, 2012.

[133] I.B. Kantola, M.D. Masters, D.J. Beerling, S.P. Long, and E.H. DeLucia. Potential of global croplands and bioenergy crops for climate change mitigation through deployment for enhanced weathering. *Biology Letters*, 13(4): 20160714, 2017.

[134] P. Barak, Y. Chen, and A. Singer. Ground basalt and tuff as iron fertilizers for calcareous soils. *Plant and soil*, 73(1):155–158, 1983.

[135] L. Taylor, J. Leake, J. Quirk, K. Hardy, S. Banwart, and D. Beerling. Biological weathering and the long-term carbon cycle: integrating mycorrhizal evolution and function into the current paradigm. *Geobiology*, 7(2):171–191, 2009.

[136] S.C. Peters, J.D. Blum, C.T. Driscoll, and G.E. Likens. Dissolution of wollastonite during the experimental manipulation of hubbard brook watershed 1. *Biogeochemistry*, 67(3):309–329, 2004.

[137] D.V.O. D?HOTMAN and O. Villiers. Soil rejuvenation with crushed basalt in mauritius. *Int sugar J*, 63:363–364, 1961.

[138] Y. Goddéris, L.M. François, A. Probst, J. Schott, D. Moncoulon, D. Labat, and D. Viville. Modelling weathering processes at the catchment scale: The WITCH numerical model. *Geochimica et Cosmochimica Acta*, 70(5):1128–1147, 2006.

[139] H. Sverdrup and P. Warfvinge. Critical loads of acidity for Swedish forest ecosystems. *Ecological Bulletins*, pages 75–89, 1995.

[140] P. Warfvinge and H. Sverdrup. Calculating critical loads of acid deposition with PROFILE-a steady-state soil chemistry model. *Water, Air, and Soil Pollution*, 63(1-2):119–143, 1992.

[141] P. Warfvinge, U. Falkengren-Grerup, H. Sverdrup, and B. Andersen. Modelling long-term cation supply in acidified forest stands. *Environmental Pollution*, 80(3):209–221, 1993.

[142] B. Cosby, R. Ferrier, A. Jenkins, and R. Wright. Modelling the effects of acid deposition: refinements, adjustments and inclusion of nitrogen dynamics in the MAGIC model. *Hydrology and Earth System Sciences Discussions*, 5(3): 499–518, 2001.

[143] B.A. Keating, P.S. Carberry, G.L. Hammer, M.E. Probert, M.J. Robertson, D. Holzworth, N.I. Huth, J.N. Hargreaves, H. Meinke, Z. Hochman, et al. An overview of APSIM, a model designed for farming systems simulation. *European Journal of Agronomy*, 18(3-4):267–288, 2003.

[144] P. Renforth, C.L. Washbourne, J. Taylder, and D. Manning. Silicate production and availability for mineral carbonation, 2011.

[145] N. Moosdorf, P. Renforth, and J. Hartmann. Carbon dioxide efficiency of terrestrial enhanced weathering. *Environmental Science & Technology*, 48(9): 4809–4816, 2014.

[146] D.P. Edwards, F. Lim, R.H. James, C.R. Pearce, J. Scholes, R.P. Freckleton, and D.J. Beerling. Climate change mitigation: potential benefits and pitfalls of enhanced rock weathering in tropical agriculture. *Biology Letters*, 13(4): 20160715, 2017.

[147] K. Coleman. ROTHC-26.3 a model for the turnover of carbon in soil-model description and windows users guide, november 1999 issue (modified april 2005). *http://www. rothamsted. bbsrc. ac. uk/aen/carbon/mod26_3_dos. pdf*, 2005.

[148] W.G. Hopkins et al. *Introduction to plant physiology.* Number Ed. 2. John Wiley and Sons, 1999.

[149] P.A. Finke and J.L. Hutson. Modelling soil genesis in calcareous loess. *Geoderma*, 145(3-4):462–479, 2008.

[150] D. Aguilera, P. Jourabchi, C. Spiteri, and P. Regnier. A knowledge-based reactive transport approach for the simulation of biogeochemical dynamics in Earth systems. *Geochemistry, Geophysics, Geosystems*, 6(7), 2005.

[151] P. Wallman, M.G. Svensson, H. Sverdrup, and S. Belyazid. ForSAFE-an integrated process-oriented forest model for long-term sustainability assessments. *Forest Ecology and Management*, 207(1-2):19–36, 2005.

[152] J.L. Palandri and Y.K. Kharaka. A compilation of rate parameters of water-mineral interaction kinetics for application to geochemical modeling. Technical report, Geological Survey Menlo Park CA, 2004.

[153] N.P. Nikolaidis, J. Valstar, E.C. Rowe, K. Moirogiorgou, E. Kotronakis, G.V. Giannakis, F.E. Stamati, and S.A. Banwart. Integrated Critical Zone Model (1D-ICZ Model) - A Tool for Dynamic Simulation of Soil Functions and Soil Structure: Technical Manual. (December):101, 2014.

[154] M. Kotronakis, G. Giannakis, N. Nikolaidis, E. Rowe, J. Valstar, N. Paranychianakis, and S. Banwart. Modeling the impact of carbon amendments on soil ecosystem functions using the 1D-ICZ model. In *Advances in Agronomy*, volume 142, pages 315–352. Elsevier, 2017.

[155] J. Dai, B. Bean, B. Brown, W. Bruening, J. Edwards, M. Flowers, R. Karow, C. Lee, G. Morgan, M. Ottman, et al. Harvest index and straw yield of five classes of wheat. *Biomass and Bioenergy*, 85:223–227, 2016.

[156] J. Lewin and B.E. Reimann. Silicon and plant growth. *Annual Review of Plant Physiology*, 20(1):289–304, 1969.

[157] G. Korndörfer and I. Lepsch. Effect of silicon on plant growth and crop yield. In *Studies in plant science*, volume 8, pages 133–147. Elsevier, 2001.